Numerical Reservoir Simulations of Multiphase Pump Operations on the Rütenbrock Sour Gas Field, Northwest-Germany

Vorgelegt von
Abdulmalik Abdullah Alwan
M.Sc. Reservoir Engineering & Management
aus dem Jemen

an der Fakultät VI
Planen Bauen Umwelt
der Technischen Universität Berlin

zur Erlangung des akademischen Grades
Doktor der Ingenieurwissenschaften
-Dr. -Ing.-
genehmigte Dissertation

Promotionsausschuss:
Vorsitzender: Prof. Dr. Gerhard Franz
Berichter: Prof. Dr. Wilhelm Dominik
Berichter: Prof. Dr.-Ing. Moh'd M. Amro
Berichter: Prof. Dr.-Ing. Paul Uwe Thamsen

Tag der wissenschaftlichen Aussprache: 04.Mai 2011

Berlin 2011

D 83

Kurzfassung

Die voranschreitende Entwicklung der Multiphasentechnologie macht den Einsatz von Multiphasen-Pumpen zu einem wichtigen Bestandteil vieler Produktionsszenarien in der Kohlenwasserstoffindustrie. Im Rahmen eines Forschungsprojektes wurde eine Multiphasen-Pumpe im weitgehend ausgeförderten Sauergasfeld Rütenbrock (Hauptdolomit) in Nord-West Deutschland installiert. Die vorliegende wissenschaftliche Untersuchung thematisiert erstmals den erhöhten Ausbeutefaktor, der durch den Einsatz der Multiphasentechnologie in einer Gaslagerstätte mit 40 Jahren Produktionsgeschichte erzielt werden kann.

Die Multiphasen-Pumpe wurde in den Jahren 2004 bis 2006 in der Förderung aus dem 30 Meter mächtigen geklüfteten Hauptdolomit im Zechstein (Perm) eingesetzt. Das erstellte duale Porositäts- /Permeabilitäts-Simulationsmodell enthält insgesamt 332.280 Zellen. Auf Basis der Daten wurde ein Wert von initiales Volumen von 2,5 x 10^9 m³ (Vn) Gas für das Hauptkompartment geschätzt, wohingegen sich unter Verwendung der Materialbilanz P/Z Analyse ein Wert von nur 1,9 x 10^9 m³ (Vn) ergab. Anschließend wurden dynamische Reservoirsimulationen vorgenommen, um ein möglichst präzises Ergebnis für das "History Matching" und die Produktionsprognosen zu erzielen. Beim "History Matching" wurden die wesentlichen Parameter so lange geändert, bis sich eine Übereinstimmung mit den Produktionsdaten ergab.

Im Anschluss daran wurde eine Produktionsprognose durchgeführt, die mehrere Szenarien umfasste, um den Einfluss der Multiphasentechnologie auf die Bohrung RB_Z10a sowie das Gesamtkompartment für verschiedene Produktionsperioden zu untersuchen. Die Ergebnisse bestätigen, dass der Einsatz der Multiphasen-Pumpe von 2004 bis 2006 die Produktion beschleunigte und die Gasausbeute aus dem Hauptdolomit erhöhte. Das Ergebnis der Simulation ergab für den kontinuierlichen Einsatz der Multiphasen-Pumpe insgesamt 17,37 x 10^6 Sm^3 Gas, was einer Steigerung von +5,33 % im Vergleich zur aktuell produzierten Gasmenge (16,49 x 10^6 Sm^3) entspricht. Die Prognose bei Verwendung des konventionellen Produktionssystems ergab ein kumuliertes Gasvolumen von lediglich 5,2 x 10^6 Sm^3, was einer Reduktion von -68,3 % im Vergleich zur aktuellen Produktion entspricht. Die Prognosen für einen früheren Einsatz der Multiphasen-Pumpe als 2004 zeigen eine mögliche Erhöhung der Gesamtgasausbeute für RB_Z10a (bis zu +3,77 %) und das Gesamtkompartment (bis zu +2,5 %). Zusätzlich wurde ersichtlich, dass durch den Einsatz der Multiphasentechnologie eine Beschleunigung der Produktion möglich ist.

Neben der generellen Erhöhung des Ausbeutefaktors und der Beschleunigung der Produktion konnten durch das intensive Studium der Produktionsdaten weitere Auswirkungen des Einsatzes der Multiphasen-Pumpe beobachtet werden: 1) die konventionellen Gasproduktionsraten der Bohrung RB_Z10a während der Einschließzeiten der Multiphasen-Pumpe wurden im Vergleich zur vorangehenden Produktionsphase (2002-2003) verbessert; 2) es wurde ein positiver Effekt auf die Produktion der benachbarten Bohrung OT_Z02 entdeckt. Die Multiphasen-Pumpe war in der Lage, Reservoirinhaltsstoffe aus dem gesamten Kompartment zu den Bohrungen im Scheitel der Gasfeldstruktur zu fördern. Durch die Entfernung des Wassers aus den Klüften und die Verbesserung der relativen Permeabilität für das Gas resultierte eine erhöhte Gasrate.

Abstract

Multiphase pumping technology has evolved to become a critical component in many production schemes. A multiphase pump (MPP) field site test was conducted in Rütenbrock sour gas field, a mature carbonate reservoir (Hauptdolomit) in north-western Germany. First time this scientific study investigated an optimized recovery effect which resulted from the deployment of multiphase pumping technology on an existing sour gas reservoir with 40 years of production history.

The Hauptdolomit reservoir represents a fractured dolomite of the Permian Zechstein (Ca2) with a thickness of about 30 meters. A static model with 71 x 39 x 60/60 grid cells was constructed and interactively improved by reservoir dynamic data. The final dual porosity/permeability simulation model contains 332,280 cells in total, 201,619 of which are active cells. The dual porosity/permeability model was constructed based on available reservoir properties, fluids data, and production history data. The volume of gas initially in place (GIIP) estimated on the basis of the reservoir and fluid data totalled 2.5×10^9 m³ (Vn) in the main compartment, whereas the calculated GIIP from material balance P/Z plot was around 1.9×10^9 m³ (Vn). Subsequently, dynamic simulations were performed for the purpose of history match and production forecast. The history matching process was performed by manually changing the most influential parameters in matching production data until the desired output was observed. The accurate adjustment of history match parameters, in combination with the presence of a tight zone, faults and flow barriers, ensured an excellent history match for most of the gas producers. After the completion of the history matching process, a production forecast that comprised various forecast scenarios was carried out in order to investigate the impact of the MPP operation on well RB_Z10a and the entire compartment performance, for the production period from 2004 to 2006. A second production forecast scenario was performed on the assumption that the MPP facility would utilize prior to 2004.

The study results confirmed that the use of multiphase pumping technology from 2004 to 2006 resulted in optimized gas recovery for the Hauptdolomit reservoir. A positive impact on field economics is confirmed through numerical simulation by improved gas recovery and production acceleration. Two forecast scenarios were carried out for the production period 01/2004-03/2006 using either continuous deployment of the MPP facility or the conventional compression production system. The MPP forecast simulation result for the production period 01/2004-03/2006 was a total of 17.37×10^6 Sm^3, representing an increase of +5.33 % over the volume of gas actually produced which was 16.49×10^6 Sm^3. In contrast, the forecast simulation result of

the conventional compression production system for the production period 01/2004-03/2006 was a cumulative gas volume of 5.2 x 10^6 Sm^3 which represents a reduction of -68.3 % compared to actual production. Based on the forecast results, gas producer RB_Z10a would come to the end of its production life in 09/2004 i.e., 9 months later, if the conventional compression production system was used continuously after 01/2004. The forecast results of the assumption that the MPP facility would utilize prior to 2004 show an improvement in the ultimate gas recovery of RB_Z10a and the entire compartment of up to +3.77 % and +2.5 %, respectively, if the MPP facility was operational prior to 2004. Additionally, production acceleration would be possible i.e., it may lead to a significant saving in operation costs.

Decline curve analysis techniques were used to evaluate and verify reserves, also the forecast simulation results of the analytical models to be compared with numerical reservoir simulation results. However, using all available methods will provide a comprehensive understanding and a greater degree of confidence if all techniques agree. Decline curve analysis confirmed the results and conclusions obtained from the numerical simulation.

Intensive analysis of production history data identified the following observable effects as results of the MPP test operations in RB_Z10a: 1) the conventional compression gas production rates of RB_Z10a during the down-time of the MPP between 01/2004 and 03/2006 were increased compared with the previous production phase (2002-2003). 2) RB_Z10a well operational availability was evaluated for the production periods 2002 – 2007 based on actual well operation hours, and RB_Z10a turned out to be more efficient (98 %) during MPP operations compared to the prior production period (88 %). 3) A positive production response was detected in the performance of the neighbouring well (OT_Z02), which located 1.5 km in the structure crest. The MPP facility was able to pull out the reservoir fluids from the entire compartment towards the crest structure wells by creating a bigger pressure difference between the drainage areas and the crest structure area. Removing the water from the fractures (flow conduits) enhanced the gas rate, i.e., it improved the relative permeability of the gas.

Acknowledgements

This thesis has been completed at the Department of Exploration Geology, Institute for Applied Geosciences, Technical University Berlin, under the supervision of **Prof. Dr. W. Dominik**.

I wish to express my deepest gratitude to my supervisor **Prof. Dr. W. Dominik**, without whom this work would never have been possible. I thank him for the guidance, encouragement, patience, advice, constant support, and ideas he has provided throughout my work. I would like to thank him making me and my family feel at home in Germany.

I am deeply grateful to **Prof. Dr.-Ing. Moh'd M. Amro**, Professor Geoströmungs-, Förder- und Speichertechnik, Institut für Bohrtechnik und Fluidbergbau, TU Bergakademie Freiberg, who accepted to be a member of the PhD committee. Also, I wish to express my special thanks to **Prof. Dr.-Ing. Paul Uwe Thamsen**, Leiter des Fachgebiets Fluidsystemdynamik - Strömungstechnik in Maschinen und Anlagen Hermann-Föttinger-Institut, Technische Universität Berlin, for accepting to be a member of the PhD committee. I wish to thank **Prof. Dr. Gerhard Franz** for accepting to be the chairman of the promotion committee.

I am particularly indebted to Dr. Andre Brall for his encouragement and support and for his continuous follow-up which were a real push to this work.

I wish to thank my project team colleagues, Dipl. Geol. Volker Lorenz and Dipl. Eng. Thomas Franzen for their assistance, support and useful suggestions during the work. Also, I am thankful to Dr. Gerhard Rosenthal for his assistance and worthy discussions. As well, I express my deep appreciation to all colleagues of the Exploration Geology Department.

Also, I would like to use this opportunity to express my grateful thanks to the MPT e. V., and the coordinator Prof. H.G. Schafstall and to the Federal Ministry of Education and Research (BMBF) for funding this work. As well, I wish to thank Wintershall Holding AG for providing the data used in this work.

Many thanks go to Mrs. Schroeder, the secretary, for her cooperation and sincere thanks to Mr. Thiel for his assistance with computer software.

Last but not least, my warmest thanks go to my family in Yemen, mother, brothers and sisters for their support and pray. Most of all, I thank my wife and kids, for their patience and tolerance of my frequent and long absences and support during these years of hard work.

Table of Contents

Kurzfassung .... **II**

Abstract .... **IV**

Acknowledgements .... **VI**

Table of Contents .... **VII**

List of Figures .... **IX**

List of Tables .... **XII**

CHAPTER I: Introduction **1**

1.1 Objectives of the Study 2

1.2 Methods of Investigation 3

1.3 Literature Review 5

1.3.1 Mature Gas Fields: Production Problems 5

1.3.2 Multiphase Pumping Technology 7

1.3.2.1 Types of Multiphase Pumping Technologies 8

1.3.2.2 Comparison of Multiphase Pump Technology Types 12

1.3.2.3 Multiphase Pumping Technology Advantages 13

1.3.2.4 Worldwide Multiphase Pump Technology Application 15

1.3.3 Naturally Fractured Reservoirs 17

1.3.3.1 Classification of Naturally Fractured Reservoirs 20

1.3.3.2 Fractures Properties 21

CHAPTER II: Rütenbrock Gas Field **23**

2.1 Geological Setting 23

2.2 Hauptdolomit Reservoir: Reserves and Produced Reserves 27

2.3 Hauptdolomit Reservoir: Production History 28

CHAPTER III: Verification of the Initial Gas in Place **34**

CHAPTER IV: Decline Curve Analysis **40**

4.1 Arp Decline Curve Analysis 40

4.2 Decline Type Curves 42
4.3 Production Decline Analysis of Well RB_Z10a 47
4.4 Production Decline Analysis of Well OT_Z02 54
CHAPTER V: Reservoir Dynamic Simulation 56
5.1 Data Validation & Evaluation 56
5.2 Dual Porosity/Permeability Simulation Model 70
5.3 Reservoir Model Initialization 74
5.4 History Matching 75
    5.4.1 History Matching Key Parameters 76
    5.4.2 History Match Results 84
5.5 Production Forecast 89
5.6 Forecast Simulation Results 90
CHAPTER VI: Multiphase Pump Evaluation Based on Actual Production Data 95
CHAPTER VII: 103
7.1 Conclusions 103
7.2 References 105
7.3 Appendix 114
    7.3.1 Appendix 1: Production History 114
    7.3.2 Appendix 2: Decline Curve Analysis 118
    7.3.3 Appendix 3: History Match Results 124
Nomenclature 130

List of Figures

Fig. 1.1: Reservoir simulation workflow 3
Fig. 1.2: Production profile of a typical gas well (production rate vs. time) 7
Fig. 1.3: Different types of multiphase pumping technologies currently used worldwide. 8
Fig. 1.4: Worldwide usage of various types of multiphase pumps until 2002. 9
Fig. 1.5: Schematic view of the twin-screw pump 10
Fig. 1.6: Distribution of twin-screw pumps worldwide.. 11
Fig. 1.7: Operational envelopes for commercial multiphase pumps. 12
Fig. 1.8: Multiphase pumps speed, power ranges. 13
Fig. 1.9: The potential of the multiphase pump. 14
Fig. 1.10: Production acceleration and cash flow. 14
Fig. 1.11: Schematic of subsea production using multiphase pumping. 15
Fig. 1.12: Idealization of a fractured system. 18
Fig. 1.13: Plot of fracture porosity and permeability for the four fractured reservoir types 21
Fig. 2.1: Location map of the Rütenbrock gas field 23
Fig. 2.2: Facies distribution in the southern Zechstein basin. 24
Fig. 2.3: Lithostratigraphy of the Zechstein series in Germany 26
Fig. 2.4: Facies distribution of the Hauptdolomit reservoir 27
Fig.2.6: Hauptdolomit production history (reservoir cumulative gas & production rate vs. time) 29
Fig. 2.7: Hauptdolomit observed water gas ratio vs. time. 30
Fig. 2.8: Main compartment observed gas production rate vs. time. 31
Fig. 2.9: Observed gas rates from the main compartment’s wells 32
Fig. 2.10: Observed water production (RB_Z05). 32
Fig. 3.1: Gas reservoir P/Z material balance diagnostics. 34
Fig. 3.2: Main compartment GIIP estimation (P/Z vs. observed cumulative gas production).. 35
Fig. 3.4: Hauptdolomit reservoir multiple tank model using MBAL program. 36
Fig. 3.5: Main compartment pressure measurements vs. simulated.. 36
Fig. 3.6: Drive mechanisms vs. production history time. 37
Fig. 3.7: Reservoir pressure measurements vs. simulated. 38
Fig. 3.8: Reservoir pressure measurements vs. simulated 38
Fig. 3.9: Drive mechanisms vs. production history time. 39
Fig. 4.1: Arp decline curves: exponential, harmonic and hyperbolic. 41
Fig. 4.2: Fetkvoich log-log type curve (production rate vs. time). 44
Fig. 4.3: Production history (RB_Z10a). 48
Fig. 4.4: Arp exponential plot (RB_Z10a) 49
Fig. 4.5: Fetkovich type curve matched with RB_Z10a production history data. 50

Fig. 4.6: RB_Z10a analytical radial model. 52
Fig. 4.7: Analytical radial model (RB_Z10a): CC forecast results (01/2004-03/2006). 53
Fig.4.8: Analytical radial model (RB_Z10a): MPP forecast results (01/2004-03/2006) 54
Fig. 4.9: Fetkovich type curve matched with OT_Z02 production history data.. 55
Fig. 5.1: Hauptdolomit reservoir core data: porosity/permeability correlation. 58
Fig. 5.2: Matrix initial water saturation (from logs) vs. matrix porosity (RB_Z10a). 59
Fig. 5.3: Illustration of the mechanism of low water saturation creation in porous media. 61
Fig. 5.4: Phase diagram of well RB_Z09. 63
Fig.5.5: Free Water Level (FWL) @ the main compartment from fluids pressure gradients. 64
Fig. 5.6: Chart to calculate the water content of natural gases 65
Fig. 5.7: Plot of flowing bottom hole pressure vs. depth (the best multiphase flow correlation) 67
Fig. 5.8: VFP/IPR matching (RB_Z10a: bottom hole pressure vs. gas rate).. 68
Fig.5.10: Well test data from well OT_Z02 (main compartment).. 69
Fig. 5.11: Well test data integration (date vs. bottom hole pressures& gas rate). 70
Fig. 5.12: Hauptdolomit 3D geological model. 71
Fig. 5.13: 3D view of the matrix porosity distribution in the main compartment. 71
Fig. 5.14: 3D view of the matrix permeability distribution in the main compartment. 72
Fig. 5.15: Hauptdolomit - Matrix relative permeability (Corey curves) for gas and water 72
Fig. 5.16: Hauptdolomit - Matrix relative permeability (Corey curves) for gas and water. 73
Fig. 5.17: Hauptdolomit - Fracture relative permeability (X-curve) for gas and water. 73
Fig. 5.18: Hauptdolomit capillary pressure curves: Matrix & fracture. 74
Fig. 5.19: Main compartment initialized model.. 75
Fig. 5.20: Hauptdolomit depth map: the tight zone introduction in the main compartment 78
Fig. 5.21: Hauptdolomit depth map: the supplementary faults and flow barriers 79
Fig 5.22: RB_Z05 bottom hole pressure measurements & gas rate vs. production history time 80
Fig. 5.23: A view of the fracture water saturation in the bottom of main compartment in 1980.. 82
Fig. 5.24: A view of the fracture water saturation in the crest of main compartment in 1999 82
Fig. 5.25: RB_Z10a - Reservoir water match using the fracture capillary pressure. 83
Fig. 5.26: Base case history match (RB_Z10a)-bottom hole pressures & gas rate vs.time 85
Fig. 5.27: Base case history match (RB_Z05) - bottom hole pressures & gas rate vs. time 86
Fig. 5.28: Base case history match (RB_Z06) - bottom hole pressures & gas rate vs. time 86
Fig. 5.29: Base case history match (RB_Z10a) - observed water production rate vs. simulated. 87
Fig. 5.30: Base case history match (RB_Z05) - observed water production rate vs. simulated. 87
Fig. 5.31: RB_Z10a tubing head pressure measurements vs. simulation between 1998 and 2009 88
Fig. 5.32: Zoom-in of RB_Z10a tubing head pressures vs.simulation (2002-2004) 88
Fig. 5.33: RB_Z10a production forecasts-Conventional compression production (CC) 90
Fig. 5.34: Main compartment cumulative gas & gas rate (observed vs.forecast MPP deployment) ... 93

Fig. 5.35: Zoom-in of the production period 1998 - 2009 93
Fig. 5.37: Forecast scenarios of the MPP deployment @ earlier dates. 94
Fig. 6.1: Well RB_Z10a historical gas production rate from 2001-2009. 95
Fig. 6.2: Log-log plot of the RB_Z10a production history (gas rate vs. time). 96
Fig. 6.3: RB_Z10a cumulative gas production (CC & MPP, 2004-2006) 97
Fig. 6.4: RB_Z10a gas production rates from the MPP& CC, 2004 -2006). 98
Fig. 6.5: RB_Z10a cumulative water production (CC & MPP, the production phase 2004 -2006). ... 98
Fig. 6.6: RB_Z10a operational availability during the production period 2002 – 2007. 99
Fig. 6.7: RB_Z10a conventional compression actual production phases from 2002 - 2007.............. 100
Fig. 6.8: RB_Z10a tubing head pressure vs. produced brine (2002 - 2006). 101
Fig. 6.9: Well OT_Z02 production history (gas rate vs. time). 102
Fig. 6.10: Log-log plot of the well OT_Z02 production history (gas rate vs. time)........................... 102

List of Tables

Table 1.1: Multiphase twin-screw pumps models 11

Table 1.2: Status of subsea multiphase pumping projects 16

Table 2.1: Hauptdolomit gas initial in place and produced reserves 28

Table 2.2: Well production data 30

Table 4.1: Reservoir and fluid properties 47

Table 4.2: RB_Z10a type curve analysis results 50

Table 4.3: OT_Z02 - type curve analysis results 55

Table 5.1: Hauptdolomit initial gas composition 62

Table 5.2: History match final parameters 84

Table 5.3: Comparison of RB_Z10a actual/ forecast production for the period 2004 - 2006 91

Table 5.4: forecast results; comparison of the CC with the earlier MPP deployment 92

Table 6.1: Excerpt of the Excel sheet calculations - RB_Z10a 97

CHAPTER I: Introduction

Due to the challenges in finding new reserves and the current high prices of hydrocarbons, the oil and gas industry has made efforts to increase the rate of recovery in mature fields. Sweeping the greatest possible quantity of the hydrocarbons in place in the reservoir is a key objective in order to improve the recovery factor. The use of enhanced oil/gas recovery (EOR/EGR) techniques can boost recovery rates. Also, multiphase pumping technology is an evolving EOR/EGR option for many fields worldwide in different production schemes.

In view of the increasing global demand for fossil fuels during the next decades, it is the task of the oil and gas exploration and production industry to develop innovative and cost effective technologies to substantially increase the rate of recovery from today's average of 35% to over 50% for oil and from about 70% to over 80% ultimate recovery for gas (Rückheim et al., 2005). Mature fields are oil and/or gas fields reaching the end of their productive life. Typically, mature fields have been producing for more than 30 years and are located in certain geographical areas for different historical and geopolitical reasons. These fields accounted for over 70 % of the world's oil and gas production (Lisigurski et al., 2006). Mature fields possess the advantage of an existing infrastructure, providing the least expensive means to increase reserves and production.

Despite the emergence of fields requiring new technological advances, the most powerful growth driver for the oil industry is the development of onshore and offshore resources. Experts believe that conventional fields still contain around 1 trillion barrels of oil, for original oil in place of 3.5 trillion barrels (International Energy Agency, 2004). Most of these fields, which have historically supplied the global oil market, are mature in other words their output is declining. Mature oil and gas fields worldwide have a typical problem related to the following conditions, e.g.: limited data quantity and quality, depleted reservoir with a high water cut, sand/scale problems, small fields in different area, and mostly having an old infrastructure. However, mature fields have strengths such as high asset value, committed gas markets, mostly onshore fields, and the fields are still under primary recovery. Moreover, there are some unexplored deep zones, shallow prospects, adjacent areas surrounding the existing fields. Hence, we tried to recover more oil from the existing fields with a new revitalization concept. A field revitalization could be remodelling (geology and/or reservoir), infill or step-out drilling, reopening, re-perforation, water shut-off, stimulation (acidizing, fracturing), optimizing artificial lift, developing new production technologies or combinations of these wellbore strategies (Aprilian et al., 2006). Although EOR/EGR techniques may be implemented at any stage of oil/gas field development, they continue to hold great potential for mature fields. Techniques such as air or steam injection,

injection of miscible or non-miscible gas, gravity injection of gas designed to dislodge oil from the tops of reservoirs, or addition of polymers to injection water, are capable of extending the economic life of reservoirs. These techniques emerged during the 1980s, and are the focus of renewed interest today. Applying EOR/EGR (enhanced oil/gas recovery) techniques to mature fields is a multidisciplinary process which must integrate the constraints associated with the existing installations. To this end, a methodology and screening tool which reflect not only the reservoir aspects but the well and production constraints specific to each field, now permit rapid selection of the type of EOR/EGR technique best suited to each particular field. Improving recovery of the mature oil and gas fields is one of the best places to look for additional reserves. As artificial lift options are limited, as is the case for subsea wells, it is quickly discovered that recoveries drop to among the lowest in the industry. Today, selection of an artificial lift technique plays an increasingly important role in determining ultimate recovery. In addition to the challenges posed by subsea/deepwater production, unconventional reservoirs also require new ideas to improve recovery. For example, steam operations used to produce from heavy-oil reservoirs require down hole and surface pumps to operate at temperatures well beyond our experience base. Unconventional gas reservoirs, such as coalbed methane and ultralow-permeability sand/shale, also present unique challenges. In these cases, operating companies must solve problems associated with lifting liquids to the surface i.e., liquid loading (Scott, 2007).

Multiphase pumping systems are considered a development option for many fields worldwide. Multiphase pumping provides unique opportunities to boost recovery and minimize the complexity and cost of surface facilities. Now this technology is being applied for compressing fluid with very high gas content of gas volume fraction (GVF) > 99 % (Scott, 2007). The challenge is to select the best candidates to take full advantage of this novel technology. Multiphase pumping is a quickly evolving technology that has gained acceptance as a best practice in fields around the world.

1.1 Objectives of the Study

The main objectives of this scientific study were: 1) to investigate the Hauptdolomit reservoir performance during the multiphase pump facility operations, applying: numerical reservoir simulation and decline curve analysis; 2) to evaluate and compare the RB_Z10a performance through various production phases during, prior to and after the MPP phase, including the conventional compression within the MPP phase based on actual production history data; 3) to identify the possible effects on the production performance of the neighbouring well (OT_Z02) and the ultimate recovery of the entire compartment during the MPP operations.

1.2 Methods of Investigation

To implement the goals, three software packages were utilized, Eclipse from Schlumberger, PROSPER, PVTp, MBAL programs from Petroleum Experts Ltd and FAST.RTA^{TM} from Fekete Associates Inc. Verification of the gas initial in place using MBAL and FAST RTA^{TM} programs was the first step. Second, the production decline curve analysis was performed to gain a better understanding of the individual well performance. Also, decline curve analysis used to gain some information about the reservoir and fracture system, to forecast the production base on actual data and finally the results to be compared with Eclipse numerical simulation results. Third, numerical reservoir simulation (Fig. 1.1) consisting of the process stages of initialization, history match and forecast was conducted.

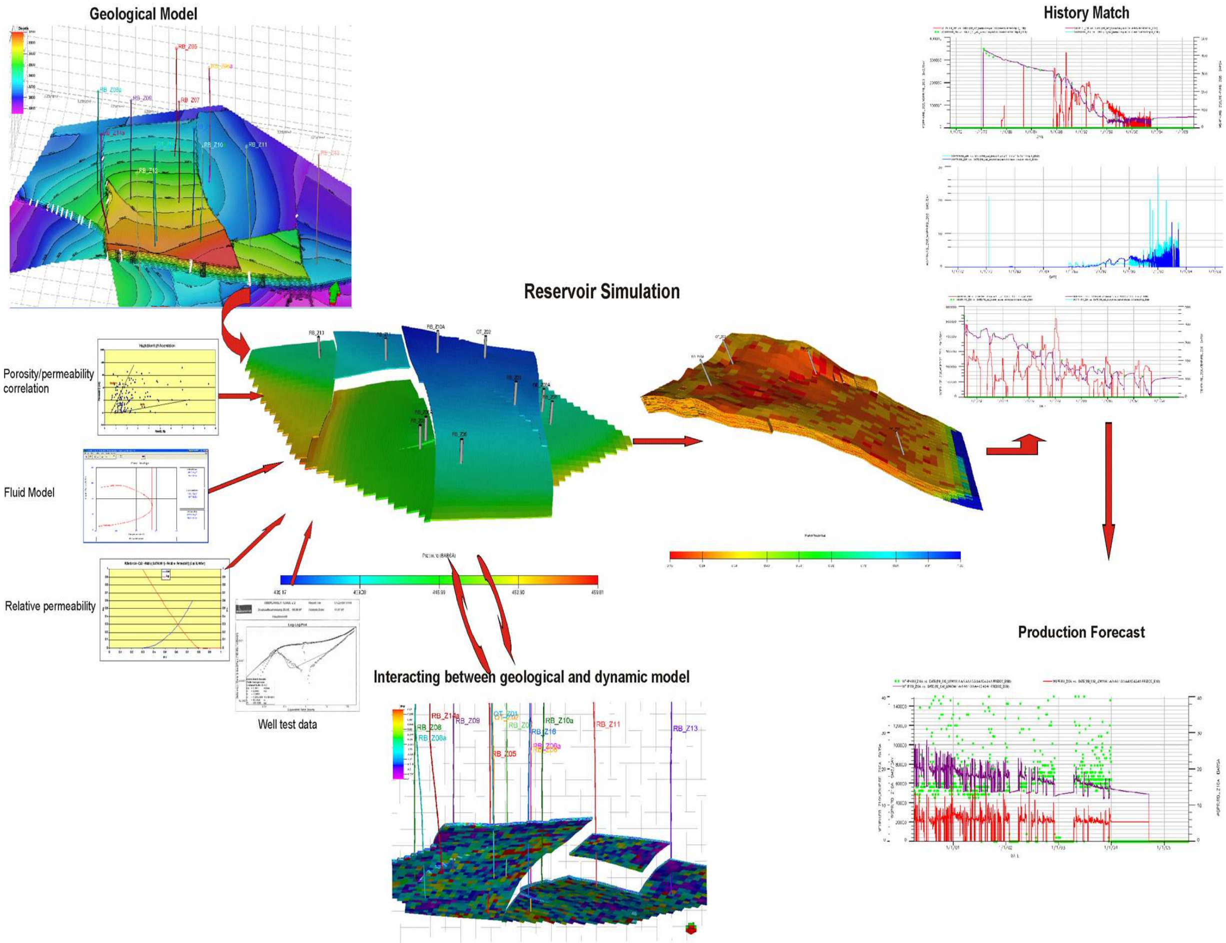
Geological Model
History Match
Reservoir Simulation
Porosity/permeability correlation
Fluid Model
Relative permeability
Well test data
Interacting between geological and dynamic model
Production Forecast

Fig. 1.1: Reservoir simulation workflow

The numerical reservoir simulation included the following steps: 1) review of all available engineering data to ensure that an adequate reservoir description and production history data is available; 2) development of a detailed fluid, flow and well models using PVTp, Eclips, PROSPER programs; 3) a black oil, dual porosity simulator was used to simulate the Hauptdolomit reservoir; 4) perform a history match using the dynamic data to acquire reasonable match; 5) run production forecast cases. The integration of multiphase pump functionality was achieved by setting the reduced flowing wellhead pressures in Eclipse program.

1.3 Literature Review

In the following paragraphs, there is a literature survey about the gas field's problems as well the multiphase pumping technology and the naturally fractured reservoirs.

1.3.1 Mature Gas Fields: Production Problems

Over the last decade, the oil and gas industry, apart from the need of replenishing reserves through exploration activities, has put increased efforts into the development of a variety of new technologies to unlock reserves in mature fields.

Gas wells problems may be categorized as limited production rate, high water production, and mechanical failures. However, high water production is more difficult to handle in producing gas wells. Generally, limited gas producing rate may be a result of (1) low reservoir pressure; (2) extreme low reservoir permeability; (3) formation damage; (4) well bore or tubing plugging; (5) excessive back pressure on formation; (7) liquid loading; (8) mechanical problems (Allen et al., 1982).

Low Reservoir Pressure

If reservoir pressure measurements have been carried out on a routine basis, reservoir pressure history should be well documented. The next step is to consider the dominant reservoir drives in a particular reservoir and how these drive mechanisms are associated with the real or apparent well problem being investigated (Allen et al., 1982).

Low Reservoir Permeability

Low reservoir permeability may be the overall characteristics of a reservoir, or it may be limited to a specific area. If low permeability has been proved as a cause of limited production, this problem should be considered along with other possible causes of low productivity. Characteristically, in a low permeability reservoir, well productivity declines rapidly as fluids near the wellbore are produced (Allen et al., 1982). If available geological and reservoir data do not readily prove low reservoir permeability, production tests and pressure build-up tests may aid in differentiating between low permeability and formation damage.

Formation Damage

Formation damage may be defined as any impairment of well productivity due to plugging within the wellbore, in perforations, in formation pores adjacent to the wellbore, or in fractures communicating with the wellbore. Formation damage may be determined by production tests, pressure build-up and drawdown tests, comparison with offset wells, and careful analysis of production history, including prior completion, workover, and well servicing operations (Bennion et al., 2000). A large majority of production problems with low permeability gas reservoirs, including fines migration, retrograde condensate dropout and solids precipitation are all associated with large pressure drops or flowrates associated with the low permeability nature of the reservoir (Bennion et al., 2000).

Back Pressure on Formation

Excessive back pressure can appreciably lower producing rates in wells producing from a reservoir near pressure depletion. Excessive formation back pressure may be due to limited or plugged perforation; partially plugged wellbore, tubing, or flowline; subsurface or surface chokes; undersized gas-oil separator, flowlines, tubing, or casing; or excessive back-pressure setting on casing head gas gathering system, or on gas-oil separator (Allen et al., 1982).

Liquid Loading on Gas Wells

As gas fields become mature worldwide, significant production losses are increasingly caused by liquid loading. Liquid loading of gas production wells reduces deliverability of gas wells (Guo et al., 2005). The reservoir energy is insufficient to transport liquid particles to the surface, liquid falls back and build up a hydrostatic column in the wellbore that balance-out with the reservoir pressure, killing the well and leaving significant reserves behind. An increasingly large number of producing gas wells are maturing. New problems that arise at tail-end production phase of the wells must be resolved, which will impact the total economics of their production. When a gas well’s driving force, i.e., reservoir pressure decreases, gas production rate also decreases and a change in flow regime can take place (Guo et al., 2005). Decrease in reservoir pressure can lead to additional fluid influx caused by condensation or an aquifer getting active (Werner et al., 2007).

A typical gas well production profile can be seen in Figure 1.2, where the onset of liquid loading, which is the onset of erratic gas production. Several measures can be taken to reduce the liquid loading problem in gas production wells. Using smaller tubing or creating a lower wellhead pressure sometimes can prolong mist flow. The loaded gas wells can be unloaded by gas lifting or pumping the liquids out of the wellbore. Foaming the liquid water can enable the gas to lift water from the well. Heating the wellbore can prevent condensation (Guo et al., 2005). The major challenge however, is to find a suitable artificial lifting technology, as most artificial lifting technologies work well with liquid, but cannot handle free gas.

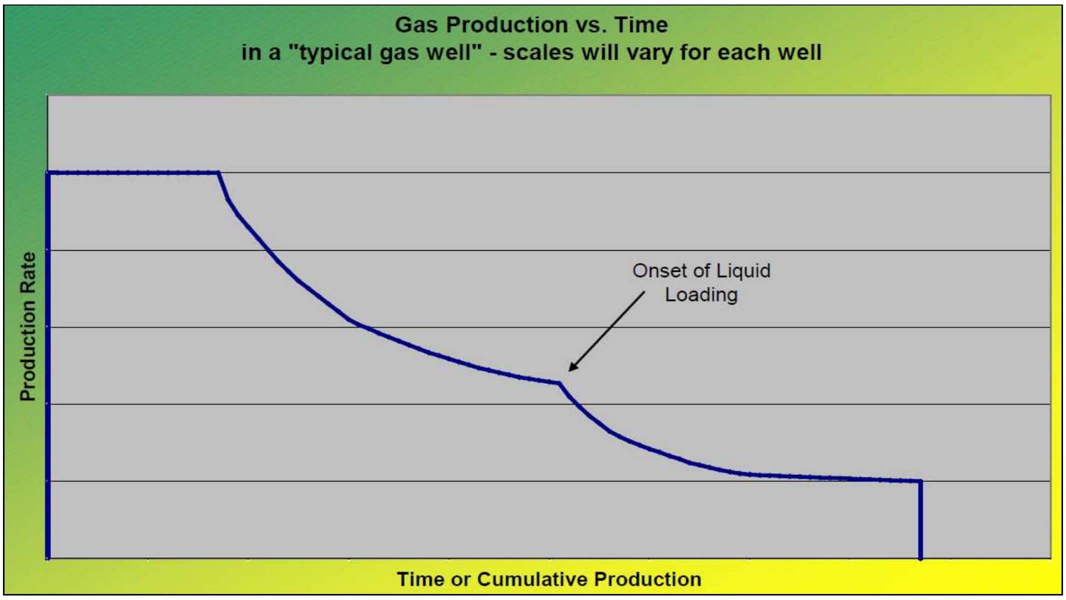

Fig. 1.2: Production profile of a typical gas well (production rate vs. time), showing two decline trends of the gas rate before and after the onset of liquid loading (after Werner et al., 2007).

Multiphase Pumps Solve Liquid Loading

The most common development in maturing gas wells is reduced bottom hole pressure and increased production of liquids, predominantly water. Abandoning a mature well was once an option, but with higher gas prices, producers are looking at new technologies such as multiphase pumping technology as options to maintain economical late-life production. Olson (2006) defined the multiphase pumping technology as one of the correct tool to solve the liquid loading problem. The successful selection of a multiphase pump for conventional gas wells depends on flow conditions, gas volume, and liquid flow, whether flow is water and/or hydrocarbons, temperature, presence of hydrogen sulphide and carbon dioxide, slugging and slug regime, inlet pressure, and required pressure boost (Olson et al., 2006).

1.3.2 Multiphase Pumping Technology

Multiphase pumping is fast becoming a standard component of the modern oil and gas production system and is being utilized to improve efficiency allowing longer production from the wells and better recovery factors, to provide cost saving and operational flexibility in applications. This section considers the multiphase pumping technology status, types, advantages and examples of applications worldwide. Following it’s emergence from research labs a decades ago, multiphase pumping has become a viable solution to a wide number of field development plans. While the technology is seen to be particularly beneficial in remote locations such as the deep water offshore fields in the Gulf of Mexico, pumps also have been deployed to a number of onshore locations ranging from Alaskan North Slope to Columbia and from West Africa to the Middle East (Scott et al., 2002). Multiphase production systems require the transportation of a mixture of oil, water and gas, often for many miles from the production well to a distant processing facility. This represents a significant departure from conventional production operations in which fluids are separated before being pumped and compressed through separate pipelines. By eliminating this equipment, the cost of a multiphase pumping facility is about 70 % that of a conventional facility (Dal Porto, 1996) and significantly greater savings can be realized if the need for an offshore structure is eliminated altogether.

1.3.2.1 Types of Multiphase Pumping Technologies

A variety of single phase pump technologies have been applied in oil and gas production operations (Scott, 2003). While most pump technologies can tolerate trace amounts of gas in the liquid stream, only a few can handle the higher gas volume fractions (GVF) found in today's oilfield. Figure 1.3 illustrates the established and commercial multiphase pump technologies that have been applied in pumping multiphase fluids.

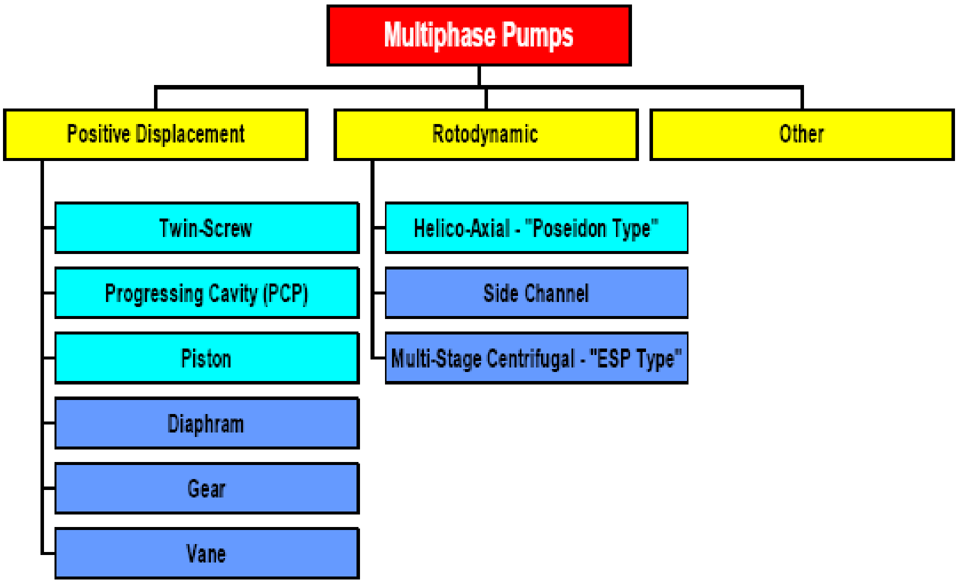
Multiphase Pumps
Positive Displacement
Rotodynamic
Other
Twin-Screw
Progressing Cavity (PCP)
Piston
Diaphram
Gear
Vane
Helico-Axial - "Poseidon Type"
Side Channel
Multi-Stage Centrifugal - "ESP Type"

Fig. 1.3: Different types of multiphase pumping technologies which are currently used worldwide (after Scott et al., 2004).

The positive displacement twin-screw, PCP and piston pump have emerged as successful multiphase pumping technologies in addition to the helicoaxial-rotodynamic pump (Scott, 2004). Each of these technologies has developed a range of applications that are best suited to its unique capabilities and to meet specific requirements. Figure 1.4 shows that the number of multiphase pump installations has increased rapidly over the past years (Scott et al., 2002).

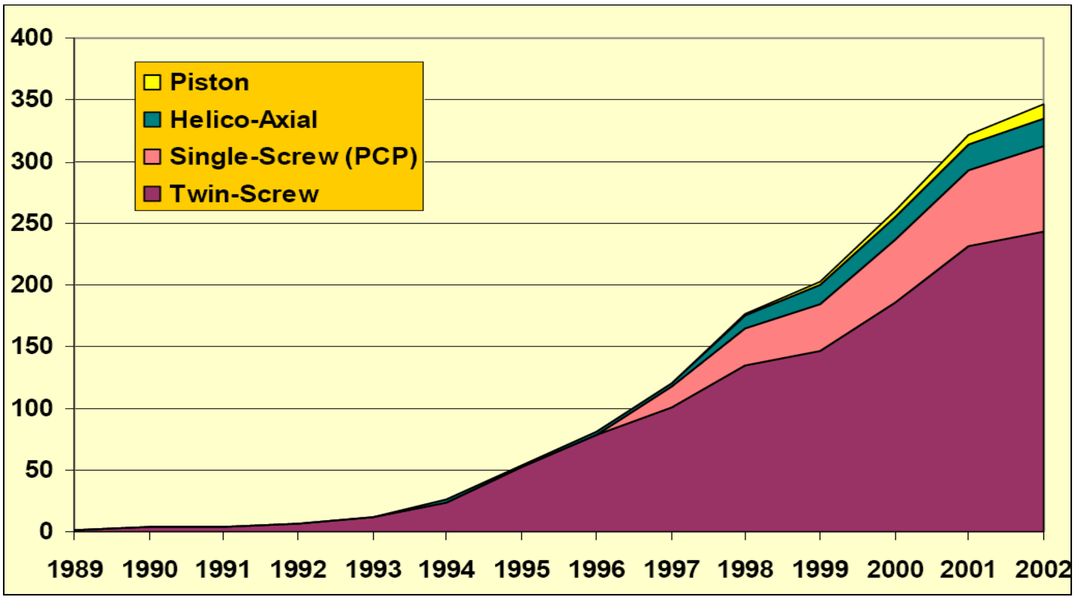

Fig. 1.4: Worldwide usage of various types of multiphase pumps until 2002. The twin-screw multiphase pump however, is by far the most popular in use (after Scott, 2002).

Positive Displacement Pumps

The type of multiphase pump that has been tested in the Hauptdolomit sour gas reservoir was a twin-screw pump from Bornemann, therefore it is obvious to describe the positive displacement technique multiphase pumps in detail. Positive displacement pumps operate on the principle that a definite amount of fluid is transferred through the pump based on the volume created by the pumping chamber and the speed at which this volume is moved. The amount of differential pressure that develops in the pump is a function of the resistance to flow downstream of the pump, that is, the pressure losses that must be overcome to deliver the fluid to a set pressure downstream of the pump (Scott et al., 2002). For any positive displacement pump, the interaction between the pump and the adjacent pipeline segments determines pump performance.

Twin-Screw Pumps

The twin-screw pump is by far the most popular multiphase pump in use and is manufactured by Bornemann (Fig. 1.5). Twin-screw pumps are particularly effective in handling high gas volume fraction (GVF) and fluctuating inlet conditions. These pumps remain functional even at GVF of more than 95 % and with recirculation systems can function at 100 % GVF for short periods of time (Scott et al., 2002). Figure 1.5 gives a schematic view of a twin-screw pump.

The multiphase mixture enters one end of the pump and is split into two flow streams that feed into inlets situated on the opposite side of the pump, a design that equalizes stresses associated with slugging. The flow then passes through a chamber, created by the dependent on the pitch and diameter of the screws and rotational speed (Fig. 1.5). As the gas is compressed, a small amount of liquid will slip back through the small gaps between the screws and the containment chamber wall resulting in a reduced volumetric efficiency (Scott et al., 2002).

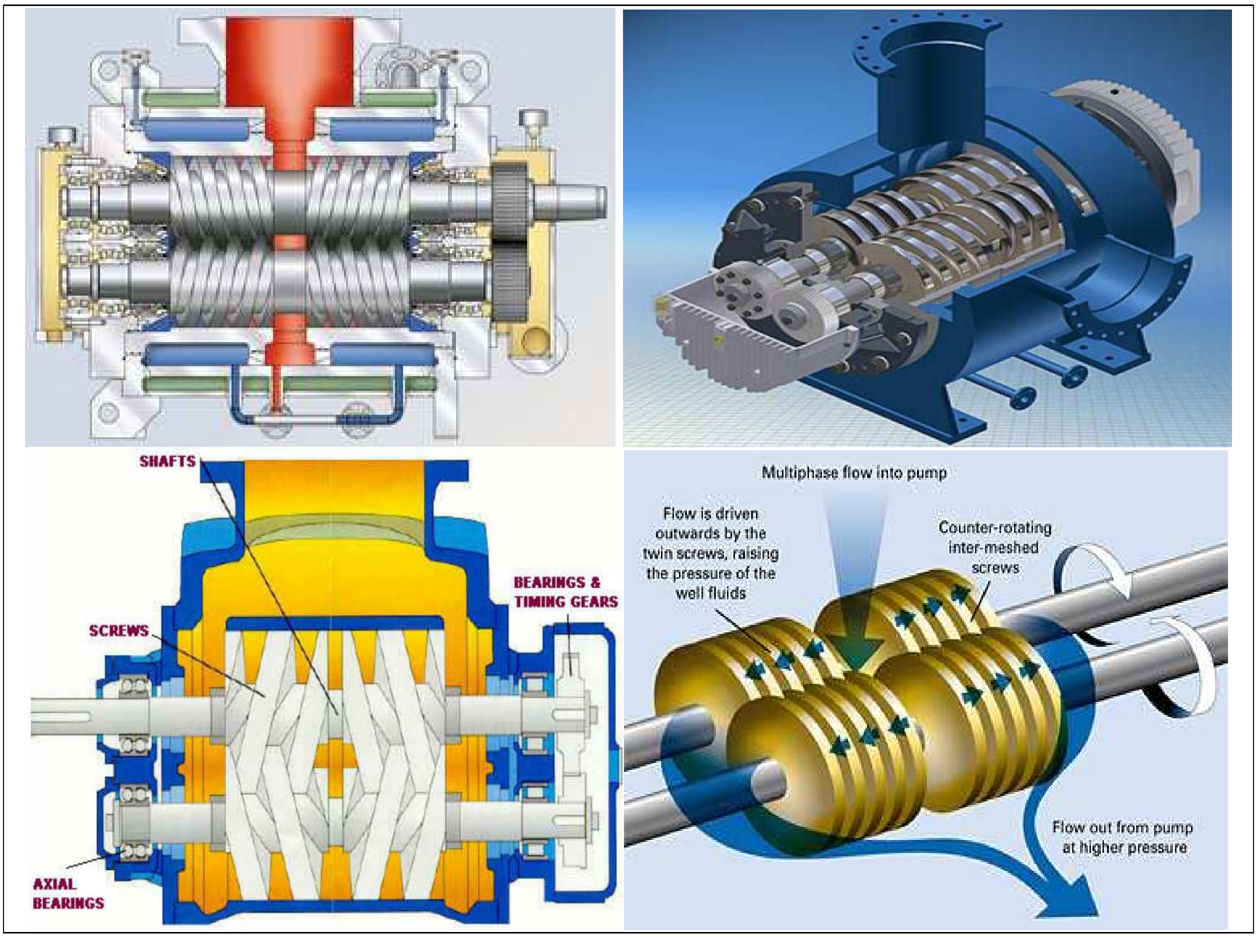
SHAFTS
BEARINGS &
TIMING GEARS
SCREWS
AXIAL
BEARINGS
Multiphase flow into pump
Flow is driven
outwards by the
twin screws, raising
the pressure of the
well fluids
Counter-rotating
inter-meshed
screws
Flow out from pump
at higher pressure

Fig. 1.5: Schematic view of the twin-screw pump, shown also the twin-screw pump elements and how the twin-screw pump works (after Bornemann, BP).

Twin-screw pumps are most often used in heavy oil applications, but are gaining acceptance for offshore and conventional oil/gas developments. The large volume capacity of these pumps tends to push them toward multi-well/cluster applications. Recently a number of models have been presented to describe the performance of twin-screw multiphase pumps. Table1.1 illustrates the various models that have been published. These published models represent a significant advance over the proprietary manufacturer models used (Devegowda et al., 2003). These new models allow examination of the assumptions used in the development of the pump performance predictions and allow for the comparison of pumps proposed by various manufacturers.

Table 1.1: Multiphase twin-screw pumps models (after Scott et al., 2004)

Model	Developer	Funded	Year	Capabilities	Comments
U. of Erlangen	Letter & Wincek	Leistritz	1993	mechanistic	requires detailed geometry and solution algorithm poorly defined
JNOC	Egashira, Shoda, Tochikawa and Furukawa	JNOC	1996	empirical	correlations for slip may not extend to other pumps
Texas A&M University	Martin & Scott	BP, ChevronTexaco, Marathon	2003	mechanistic	uses easy to obtain combine slip concept
Flowserve	Prang & Cooper	Flowserve	2004	mechanistic	requires detailed geometry
U. of Hannover	Rausch, Vauth, Brandt & Mewes	Bornemann / German Federal Ministry for Education & Research	2004	thermodynamic	neglects slip and requires detailed geometry

Figure 1.6 shows the worldwide distribution of twin-screw multiphase pumps.

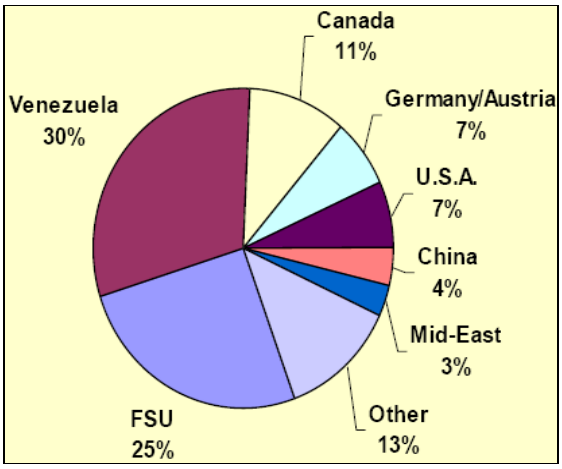

Fig. 1.6: Distribution of twin-screw pumps worldwide. It is shown that up to 2002, the applications in Venezuela heavy oil fields was 30% of the total number of twin-screw pumps (after Scott, 2002).

The twin-screw pump, which has been tested in Rütenbrock sour gas field, has the following characteristics:

- Pump type: UW-MPC
- Capacity: < 1400 Sm3/hr
- Gas volume fraction (GVF): 96 – 99.9%
- Inlet pressure: 0.5 – 20 barg
- Discharge pressure: < 40 barg
- Temperature: 40 °C
- Speed: variable rpm
- Shaft power: 700 kW

1.3.2.2 Comparison of Multiphase Pump Technology Types

Pump technologies can be compared in a number of ways. The number of possible comparisons increases dramatically for multiphase pumps as the presence of an additional phase introduces a new dimension for comparison.

Operational Ranges

Figure 1.7 shows a very general comparison based on the pressure boost and flow rates for the primary multiphase technologies. It should be noted that the limits shown on the plot are taken directly from pump manufacturers (Scott et al., 2004). In some cases other manufacturers have been able to exceed the operational limits shown.

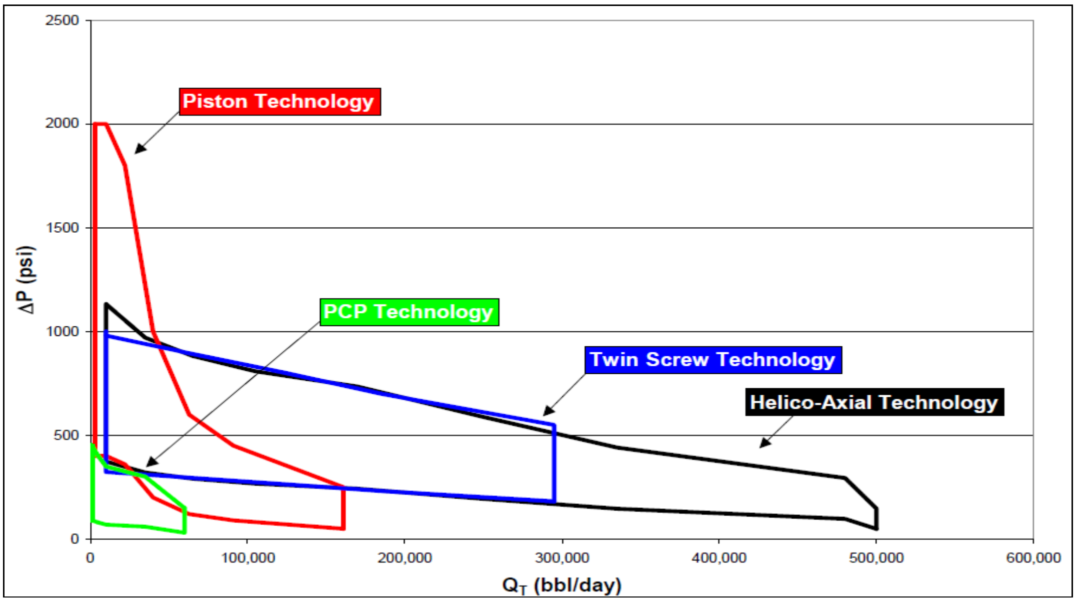

Fig. 1.7: Operational envelopes for commercial multiphase pumps. It should be noted that manufactures have combine up to six pumps in parallel to increase the volume capacity and have combine two pumps in series to increase the pressure boost provided (after Scott et al., 2004).

Figure 1.8 illustrates the range of multiphase pump speeds and horsepower for each of the multiphase technologies. Comparisons of the various pump technologies can also be made based on parameters such as GVF and liquid viscosity. Application specific issues such as their ability to handle sand or slugging or their size, shape and weight can also serve as a basis for comparison (Scott et al., 2004).

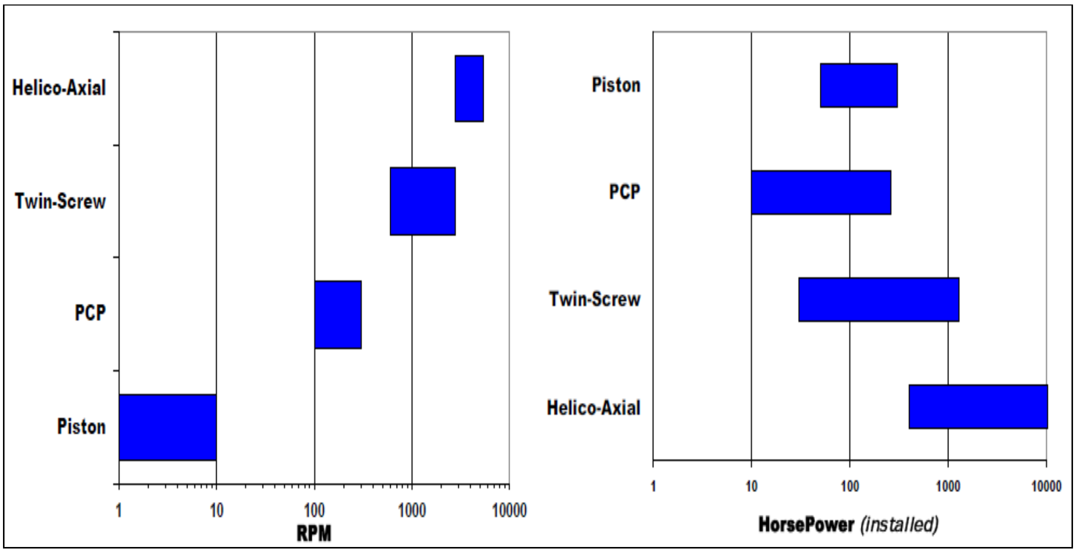

Fig. 1.8: Multiphase pumps speed, power ranges. According to the ranges in the figure, twin-screw pump is the best choose for onshore and offshore applications (Scott et al., 2004).

1.3.2.3 Multiphase Pumping Technology Advantages

Multiphase pumps have been available for a few decades for onshore and topside applications in the upstream petroleum industry. However, the numbers of field installations have been limited. Most of these applications are still considered pilot applications in the field in order to demonstrate the technology. The main advantages of multiphase pumping technology include the following: 1) the possibility to reduce the wellhead pressure in order to increase the hydrocarbon flowrate and simultaneously increase the discharge pressure to boost the fluids to central host (Fig. 1.9); 2) to accelerate the production rate, and improve field development economics i.e., leads to a significant operation cost saving (Fig. 1.10); 3) to enable production of low energy fields; 4) to produce low & medium pressure wells into a high pressure manifold/ separator; 5) to segregate production scheme of medium and low pressure wells by using MPP; 6) to allow longer subsea tiebacks by boosting the flowing wellhead pressure; 7) to boost remote fields to an existing or central host and eliminate the need for surface facilities in the field. Facilities reduction leads to reduce investment in equipment, reduction in maintenance costs and reduced operation costs. Figure 1.11 illustrates the benefits of a subsea twin screw multiphase pump installation in comparison to a satellite platform with conventional separation facilities; 8) to reduce likelihood of liquid slugging; 9) to eliminate the need for other competing technologies - gas lift, or water injection. This leads to a significant cost saving of approximately 30% of total costs; 10) an environmental advantage with the possibility to reduce the footprint of production plant and gas emission for marginal / satellite fields;

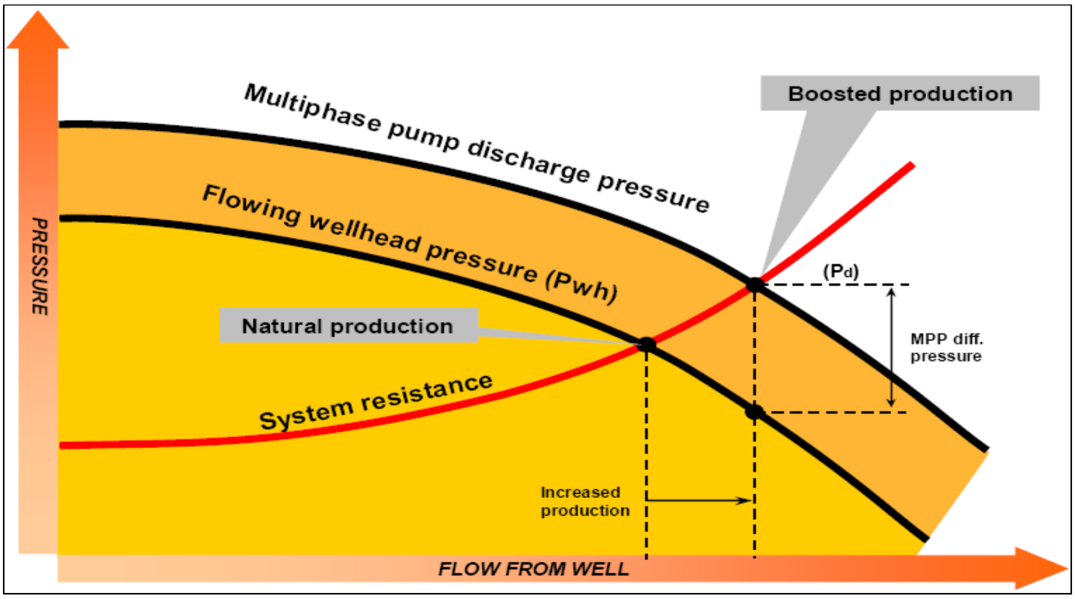
PRESSURE
Multiphase pump discharge pressure
Flowing wellhead pressure (Pwh)
Boosted production
(Pd)
MPP diff. pressure
Natural production
System resistance
Increased production
FLOW FROM WELL

Fig. 1.9: The potential of the multiphase pump. The reduction in the flowing tubing head pressure (inlet) by the pump resulted in increase of production and the increase in the discharge flowing head pressure (outlet) boost the production to a remote host platform (after Elde, 2005).

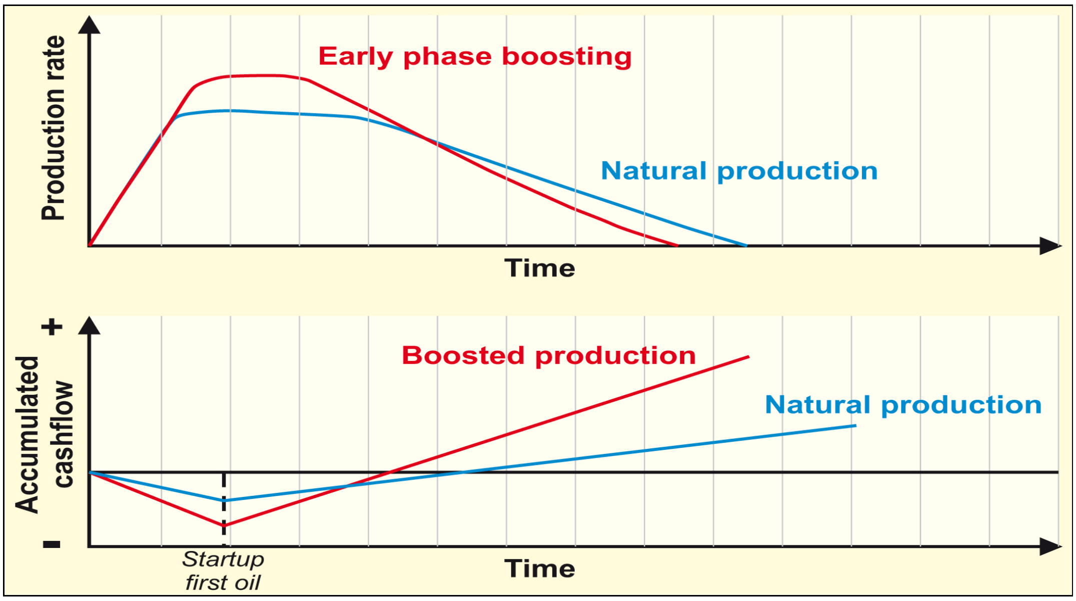

Fig. 1.10: Production acceleration and cash flow. The production acceleration (red line) leads to improve the field economics by increasing the hydrocarbon flowrates and saving costs of longer operation times.

11) to reduce unstable flow regimes in multiphase pipelines due to higher superficial velocities; 12) to eliminate gas flaring (gas emissions) and recover gas by boosting the unprocessed well stream to a separation plant.

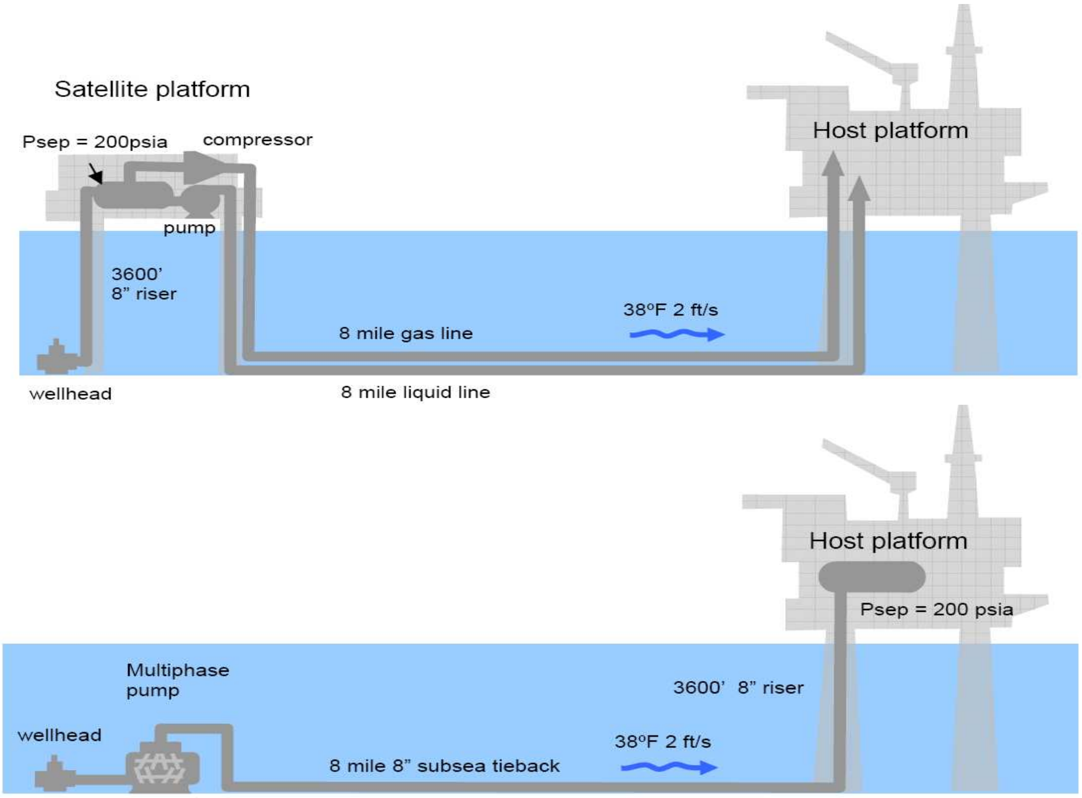
Satellite platform
Psep = 200psia
compressor
pump
3600'
8" riser
wellhead
8 mile gas line
8 mile liquid line
38ºF 2 ft/s
Host platform
Host platform
Psep = 200 psia
Multiphase
pump
wellhead
3600' 8" riser
38ºF 2 ft/s
8 mile 8" subsea tieback

Fig. 1.11: Schematic of subsea production using multiphase pumping. In the case of the subsea fields, conventional production system which consist of surface facilities to process the well fluids and boost them using two pipelines to the host platform, if the multiphase pump is used only one pipeline is needed to boost the unprocessed well fluids as mixture of oil, water and gas to the host platform (after Scott, 2002).

1.3.2.4 Worldwide Multiphase Pump Technology Application

The oil and gas industry has successfully applied multiphase pumping technology to solve a variety of operational problems. In the following sections examples of applications are discussed. These applications have been provided as case histories. This section describes several of the major multiphase pump installations operating around the world.

Onshore Heavy Oil Applications

Utilization of multiphase pumps in on-shore heavy oil applications has been the most common form. Engineers have had the opportunity to compare conventional production operations with the modern multiphase production approach. In most cases the multiphase approach was found to provide upfront capital cost savings that could be leverage across many production sites. Applications in Venezuela and Indonesia are among the best documented (Uvwo, 2004; Scott, 2004).

Conventional Onshore Oil and Gas Applications

Use of multiphase pumps in conventional oil and gas operations also has an established track record. The applications tend to involve only one multiphase pump and tend to address specific operational issues. The Priobskoye field is an example case. The multiphase pumps are installed in the part of the Priobskoye field extended on the right bank of the river Ob in western Siberia. The climate is rough (temperatures range from -55 °C to +35 °C). The area is swampy and difficult to access, being in the flood plain of the river Ob and environmentally sensitive. For these reasons and also because of a significant cost saving, the multiphase pump option was selected by the operator (Pershukov et al., 2001).

Offshore & Subsea Applications

Multiphase pumping has been utilized to address several interesting offshore operational challenges. Multiphase pumping represents the only commercial form of subsea processing techniques and represents the most basic type of subsea processing and hence the most achievable. A twin-screw pump was selected to boost a combined gas/liquid flow stream for Freeport (McMoRan Exploration Co.) after the loss of one of their single-phase export pipelines.

Table 1.2: Status of subsea multiphase pumping projects (after Scott et al., 2004)

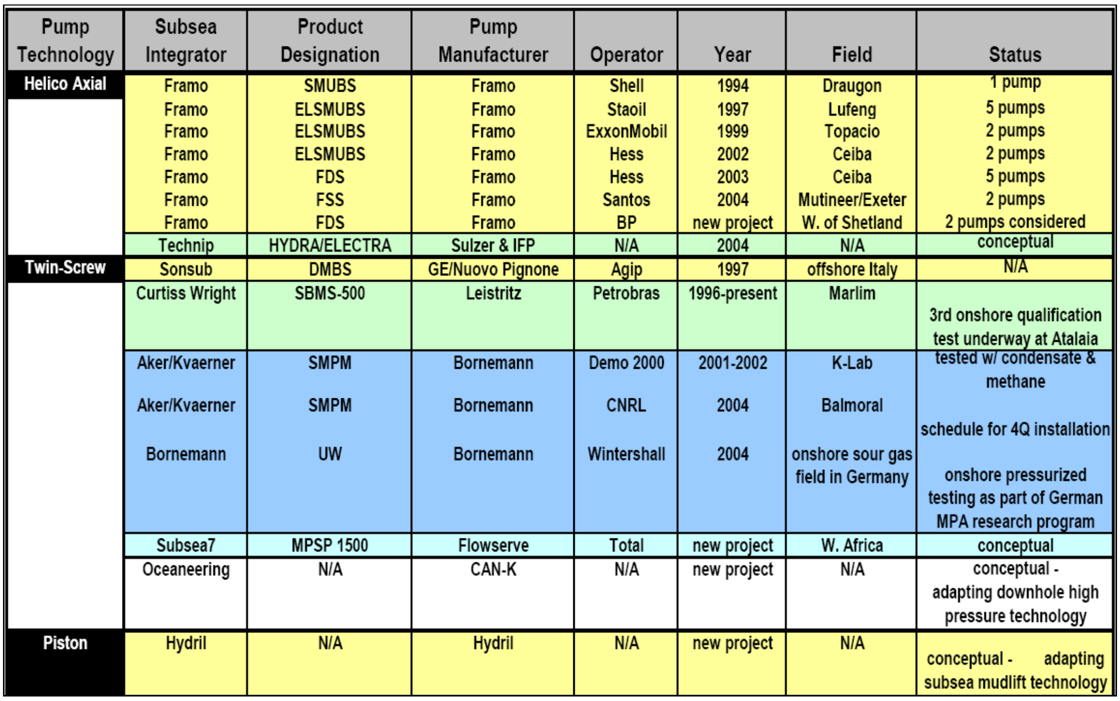

Pump Technology	Subsea Integrator	Product Designation	Pump Manufacturer	Operator	Year	Field	Status
Helico Axial	Framo	SMUBS	Framo	Shell	1994	Draugon	1 pump
	Framo	ELSMUBS	Framo	Staoil	1997	Lufeng	5 pumps
	Framo	ELSMUBS	Framo	ExxonMobil	1999	Topacio	2 pumps
	Framo	ELSMUBS	Framo	Hess	2002	Ceiba	2 pumps
	Framo	FDS	Framo	Hess	2003	Ceiba	5 pumps
	Framo	FSS	Framo	Santos	2004	Mutineer/Exeter	2 pumps
	Framo	FDS	Framo	BP	new project	W. of Shetland	2 pumps considered
	Technip	HYDRA/ELECTRA	Sulzer & IFP	N/A	2004	N/A	conceptual
Twin-Screw	Sonsub	DMBS	GE/Nuovo Pignone	Agip	1997	offshore Italy	N/A
	Curtiss Wright	SBMS-500	Leistritz	Petrobras	1996-present	Marlim	3rd onshore qualification test underway at Atalaia
	Aker/Kvaerner	SMPM	Bornemann	Demo 2000	2001-2002	K-Lab	tested w/ condensate & methane
	Aker/Kvaerner	SMPM	Bornemann	CNRL	2004	Balmoral	schedule for 4Q installation
	Bornemann	UW	Bornemann	Wintershall	2004	onshore sour gas field in Germany	onshore pressurized testing as part of German MPA research program
	Subsea7	MPSP 1500	Flowserve	Total	new project	W. Africa	conceptual
	Oceaneering	N/A	CAN-K	N/A	new project	N/A	conceptual - adapting downhole high pressure technology
Piston	Hydril	N/A	Hydril	N/A	new project	N/A	conceptual - adapting subsea mudlift technology

In addition, an offshore application of a twin screw pump was for BP (British Petroleum) in Trinidad (Scott et al., 2004). Multiphase pumps can also be used in conjunction with the other types of subsea processing schemes. Subsea multiphase pumping has established an impressive track record. A recent example of multiphase pumps application in subsea is the King Field in the Gulf of Mexico, originally came into production in 2001 through two subsea wells and is 90 kilometres from shore. BP is recovering more oil from one of this deepwater field through an ambitious subsea pumping project, opening up new opportunities for both the company and the wider industry. The multiphase pumps have been boosting production from the BP-operated King Field and are expected to recover 20 % more oil from the reservoir, extending the field's producing life and delivering many millions of barrels of additional oil (BP Publications). Table 1.2 shows a list of various subsea multiphase pump projects completed, underway or in the conceptual stage.

1.3.3 Naturally Fractured Reservoirs

Naturally fractured reservoirs have increasingly gained attention in the past two decades. Fractured petroleum reservoirs represent over 20 % of the world's oil and gas reserves, but they are among the most complicated class of reservoirs to produce efficiently (Cuong et al., 2009). It is undeniable that reservoir characterization, modelling and simulation of naturally fractured reservoirs present unique challenges that differentiate them from conventional, single porosity reservoirs. Not only do the intrinsic characteristics of the fractures, as well as the matrix, have to be characterized, but the interaction between matrix and fractures must also be modelled accurately. Many reservoirs, initially classified as classical matrix reservoirs, have been reclassified as fractured reservoirs during advanced stages of development carrying significant losses on recoverable reserves.

Naturally fractured reservoirs are heterogeneous porous media where the openings (fissures and fractures) vary in size. Fractures and openings of large size form vugs and interconnected channels, whereas the fine cracks form block systems which are the main body of the reservoir (Fig. 1.12).

The porous blocks store most of the fluid in the reservoir, and are often of low permeability, whereas the fractures have a low storage capacity and high permeability. Most of the fluid flow will occur through the fractures with the blocks acting as fluid sources. Even though the volumetric average permeability in a dual porosity system is low, such systems often exhibit an effective permeability which is higher than the block matrix permeability, and behave differently from ordinary homogeneous media.

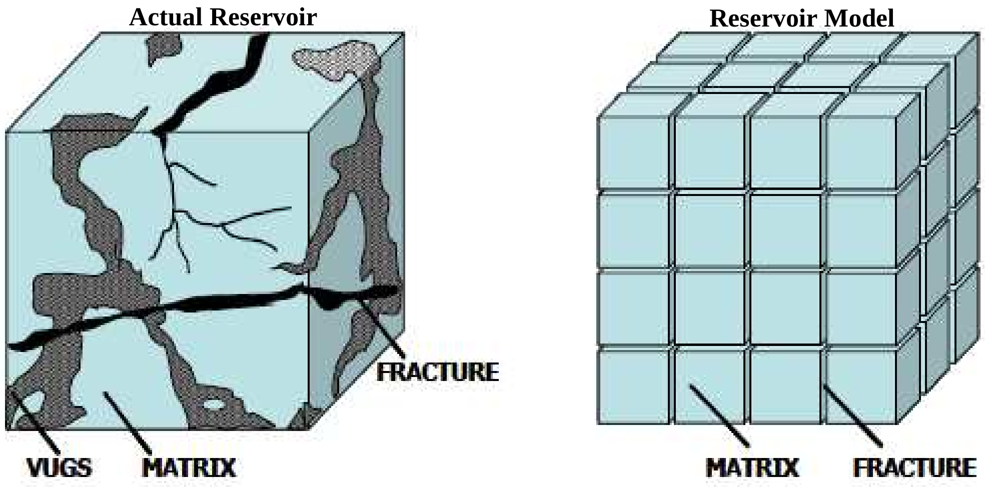

Fig. 1.12: Idealization of a fractured reservoir (dual porosity system). The actual reservoir is idealized to create model reservoir for the purpose of reservoir simulation (after Warren and Root, 1963).

Identifying the fractured nature of a reservoir at an early time stage is critical for an adequate reservoir management to maximize the economic benefit. Nelson (2001) defined fracture as a naturally macroscopic planar discontinuity in rock due to deformation or physical diagenesis. Fractures can be produced by brittle or ductile failure. The characteristics of fractures also differ depending on the creation process. Fractures can have positive or negative effects on fluid flow. Naturally fractured reservoirs are those reservoirs where fractures have any influence on reservoir performance. Nelson (2001) stressed the importance to collect information that allows identifying a reservoir as fractured in early stages of development. The solution is derived in the Laplace transform domain because it is considered a naturally fractured inner reservoir. The results are then numerically inverted to the time domain using the algorithm proposed by Stehfest (1970). The models differ in the way the matrix/fracture fluid transfer is handled. Warren and Root (1963) considered pseudo-steady-state matrix/fracture fluid transfer. The flow details within the matrix are not considered, and the matrix is treated as a time-dependent source term that feeds the fracture with strength dependent on the fracture pressure. The model presented by Kazemi (1969) considers transient flow in both matrix blocks and fractures.

Barenblatt et al., (1960) introduced the concept of dual porosity systems to quantify flow in naturally fractured reservoirs. According to this concept, a fractured reservoir consists of two interacting, overlapping continua: a low permeability and high storativity matrix, high permeability and low storativity fracture. Fluid flows from the matrix into the fractures and the fractures feed the fluid to the well. Numerous studies have been conducted on the basis of the above concept. For dual-porosity idealization and to represent the naturally fractured reservoir, Warren and Root (1963); Kazemi 1969 assumed the system as an idealized system formed by identical rock-matrix blocks, separated by an orthogonally fractures and that assumption was used to simulate the naturally fractured porous system (Fig. 1.12).

Dual Porosity Models

Dual porosity models refer to those models which have two media of different properties. The first is a fracture system that contains very little fluid (low storage capacity) and has most of the fluid transmissibility. The second system is the matrix system which has high storage capacity and low fluid transmissibility. These models are hypothetical models that are used to characterize naturally fractured reservoirs. There are many dual porosity models that are based on the same idea which is two porosity systems. The models differ from each other in two main things: the relation between the matrix and the fracture's flow systems and the shape of the building blocks of the matrix. The basic difference between dual porosity models is the type of interporosity flow, i.e. the type of the flow between the matrix blocks and the fracture system. There are two main types of interporosity flow. The first type is pseudo-steady-state interporosity flow in which the flow from the matrix blocks to the fracture system is assumed to be in the pseudo-steady-state. The second type of interporosity flow is the transient type (Sageev et al., 1985). The transient interporosity flow assumes that the flow in the matrix is governed by the transient flow theory.

Characterizing Dual Porosity Models

Dual porosity models are characterized by the usual parameters that are used to characterize homogeneous reservoirs in addition to two more parameters (λ and ω). The usual parameters are permeability, k, porosity, ϕ, formation thickness, h, fluid viscosity, μ, formation volume factor, B, and total compressibility, c_t. The interporosity flow coefficient (matrix fracture coupling factor), λ, determines the interrelation between matrix blocks and the fracture system. High λ value means the fluid easily moves from the matrix to the fracture system. The opposite is also true. The storativity ratio, ω, determines how much fluid is stored (exists) in the fracture system compared to the total fluid in the reservoir (matrix and fractures). These two parameters, λ and ω, are usually calculated from pressure transient analysis (Sageev et al., 1985). Their relations to the reservoir parameters are given by:

$$\lambda = \alpha \frac{k_m}{k} r_w^2 \quad \text{...} \quad (1.1)$$

Where α is a geometric factor that depends on the shape of the matrix blocks and has dimensions of length $^{-2}$. The subscripts m and f refer to matrix and fracture systems, respectively.

$$\omega = \frac{(\phi c_t)_f}{(\phi c_t)_f + (\phi c_t)_m} \quad \text{(1.2)}$$

1.3.3.1 Classification of Naturally Fractured Reservoirs

Based on Hubbert's and Willis's work (1955), Nelson (2001) proposed the following classification of fractured reservoirs based on the extent the fractures have altered the reservoir matrix porosity and permeability (Fig. 1.13):

- Fractures provide the essential reservoir porosity and permeability
- Fractures provide the essential reservoir permeability
- Fractures assist permeability in an already producible reservoir
- Fractures provide no additional porosity or permeability but create significant reservoir anisotropy (barriers).

In type 1 reservoirs, fractures provide the essential reservoir storage capacity and permeability. Typical type 1 naturally fractured reservoirs are the Amal field in Libya, Edison field California, and pre-Cambrian basement reservoirs in Eastern China (Tiab et al., 2006). All these fields are characterised by high fracture density. In type 2 naturally fractured reservoirs, fractures provide the essential permeability, and the matrix provides the essential porosity, such as in the Monterey fields of California, the Spraberry reservoirs of West Texas, and Agha Jari and Haft Kel oil fields of Iran (Tiab, et al., 2006). In type 3 naturally fractured reservoirs, the matrix has an already good primary permeability. As shown in Figure 1.12, the effect of fractures is of paramount importance for type 1 reservoirs, decreases for type 2 and so on. In the same way, the importance of proper characterization of porosity and permeability changes with reservoir type. The fractures add to the reservoir permeability and can result in considerable high flow rates, such as in Kirkuk field of Iraq, Gachsaran field of Iran, and Dukhan field of Qatar. Nelson (2001) includes Hassi Messaoud (HMD) field in this list. While indeed there are several low permeability zones in HMD that are fissured, in most zones however the evidence of fissures is not clear or it is unproven (Nelson, 2001).

Naturally fractured carbonate reservoirs are geological formations characterized by a heterogeneous distribution of porosity and permeability (Chilingarian et al., 1996). A common scenario is low porosity and permeability matrix blocks surrounded by a tortuous, high permeability fracture network. With the matrix blocks acting as the hydrocarbon source, the overall fluid flow of the reservoir is strongly dependent on the fluid flow properties of the fracture network.

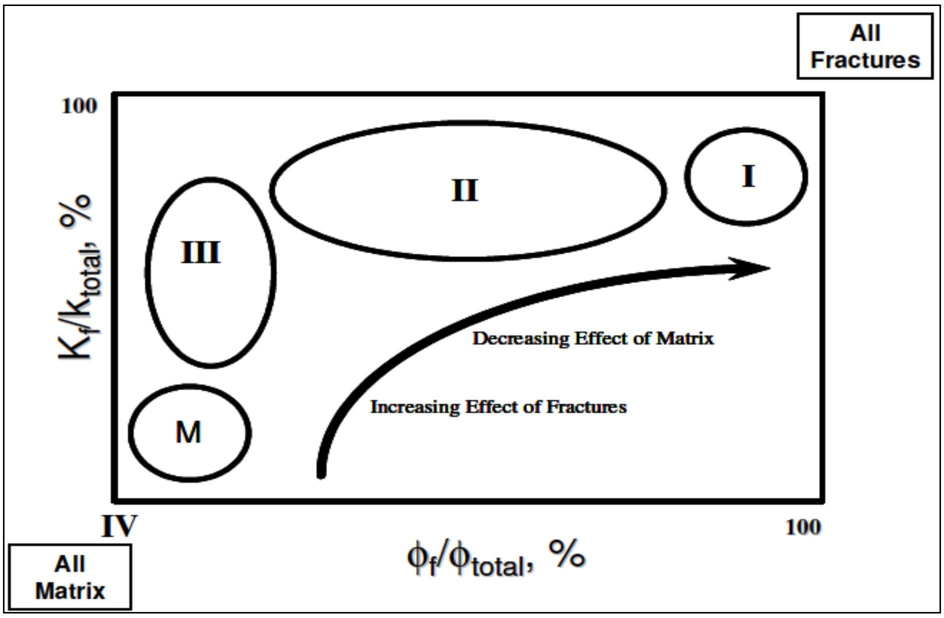

Fig. 1.13: Plot of fracture porosity and permeability percentage for the four fractured reservoir types (after Nelson, 2001).

1.3.3.2 Fractures Properties

According to Nelson (2001), the relevant properties of fractured reservoirs are: fracture porosity, fracture permeability, fluid saturations within fractures and expected recovery factor. Two major factors that govern permeability and porosity of fractures are fracture width and spacing. Fracture width is the distance between the two parallel surfaces that represent the fracture. Fracture spacing is the average distance between parallel regularly spaced fractures. Two significant fracture properties are described below: the fracture porosity and fracture permeability.

Fracture Porosity

Fracture porosity is a percentage of void space in fractures compared to the total volume of the system. As can be noticed from the expression, fracture porosity is very scale-dependent. The value of fracture porosity can be 100 % in a particular location of reservoir, but the value for the whole reservoir is generally less than 1 %. According to Nelson (2001), fracture porosity is always less than 2 %; in most reservoirs is less than 1 % with a general value of less than 0.5 %. An exception to these rules of thumb is vuggy fractures where porosity can vary from 0 to a very large value. The importance of fracture porosity in reservoir performance depends on the type of fractured reservoir. If the fracture system provides an essential porosity and permeability to the reservoir, then fracture porosity is a critical parameter to be determined in early stages of development. As contribution of matrix porosity to the whole system increases, the relevance of fracture porosity decreases. Fracture porosity is one of the fracture properties that are difficult to determine. The common sources of fracture porosity estimation are: 1) core data analysis; 2) porosity/permeability correlation; 3) Lab determinations; 4) Logs; and 5) well test.

Fracture Permeability

Permeability defines the ability of porous medium to transmit fluids. The presence of open fractures has a great impact in reservoir flow capacity. Therefore, fracture permeability is an important factor that determines reservoir quality and productivity. Darcy’s equation that is used to model fluid flow through porous media can not be used to represent flow through fractures. Thus, parallel plate theory was developed to model fluid flow in fractures. The parallel plate model is based on fracture width and spacing concepts (Nelson, 2001). Fractures do not always improve fluid flow in a reservoir. In some cases, partially or total filled fractures can act as flow barriers. The effect of fractures on permeability depends on several factors such as morphology, orientation, and others. Fracture width and permeability are difficult to determine from direct sources such as core data or laboratory test. Core data and well test analysis are the most common source of fracture permeability information. The fracture permeability of the Hauptdolomit was determined by manually adjusting until the production data was matched.

CHAPTER II: Rütenbrock Gas Field

The Rütenbrock sour gas field is located in the North West of Germany (Fig. 2.1). The field was discovered in 1959/1960 and developed in the years following. The gas field consists of two different formations, the Main Dolomite or Hauptdolomit within the Zechstein strata (Richter-Bernburg 1959) and the Rotliegend strata.

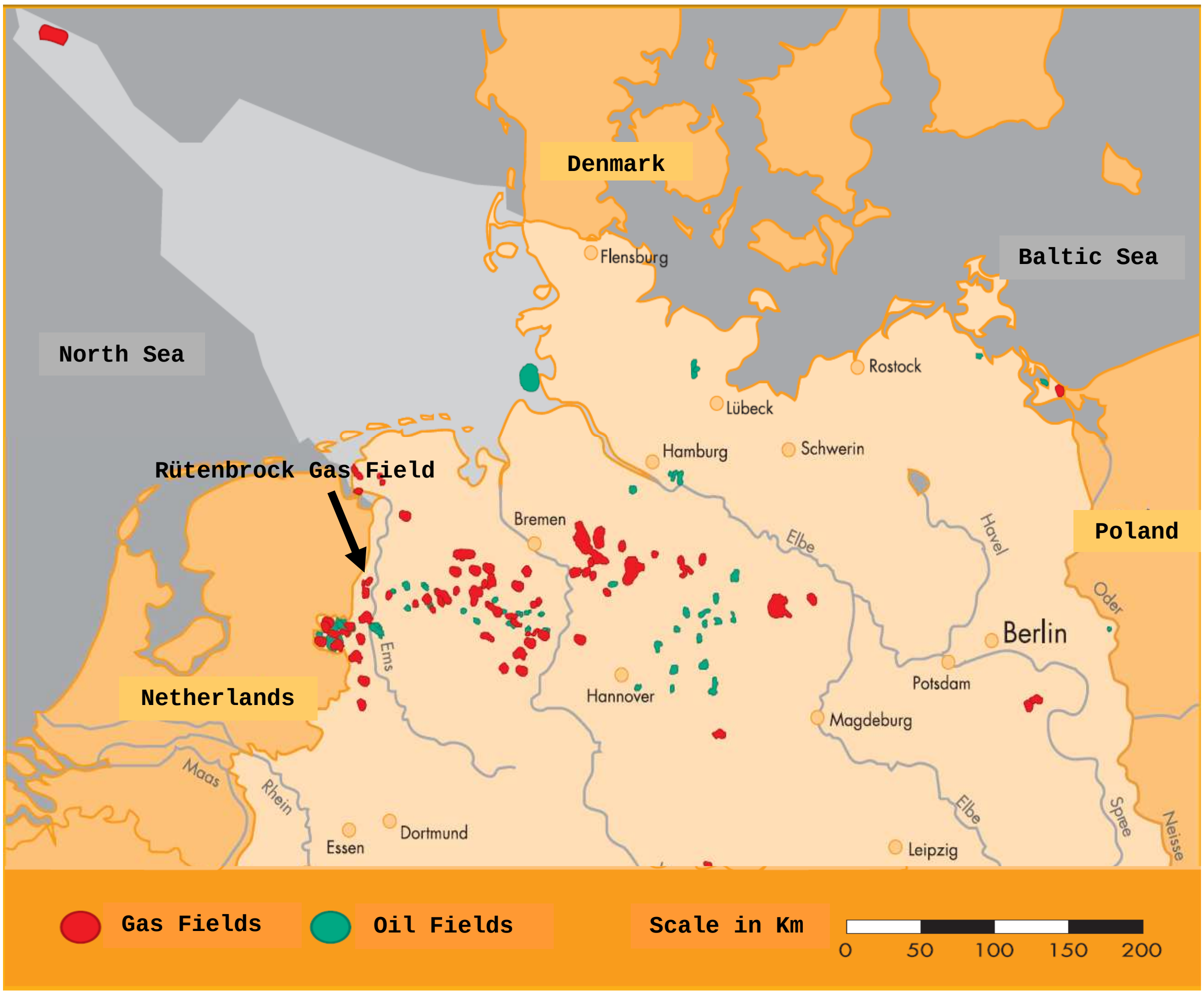
Denmark
Baltic Sea
North Sea
Flensburg
Rostock
Lübeck
Hamburg
Schwerin
Rütenbrock Gas Field
Bremen
Elbe
Havel
Poland
Oder
Berlin
Ems
Potsdam
Netherlands
Hannover
Magdeburg
Maas
Rhein
Elbe
Spree
Neisse
Essen
Dortmund
Leipzig
Gas Fields
Oil Fields
Scale in Km
0
50
100
150
200

Fig. 2.1: Location map of the Rütenbrock gas field (after W.E.G Der Wirtschaftsverband Erdöl- und Erdgasgewinnung e. V).

The Hauptdolomit consists of dolomite from the Late Permian age, and the Rotliegend of sandstone from the Early Permian. The Rotliegend reservoir is situated beneath the Hauptdolomit reservoir. The main focus of this study is the Hauptdolomit reservoir.

2.1 Geological Setting

The Zechstein is a complex of evaporates and carbonate rocks from the Late Permian age which underlies a substantial area of the North Sea and part of north-western Europe (Tayler, 1986). The most important reservoir rocks in this area are sandstones, which occur from the

Carboniferous into the Tertiary period. Carbonate reservoirs are of important in Upper Permian, Upper Jurassic, and in Eocene times (Warren, 2006). The Zechstein basin stretches from northern Britain, across the North Sea through The Netherlands, Denmark, Germany and Poland to the edge of the Hercynian massifs (Harz, Rhenish Massif and Bohemian mountains). During the Late Permian, an area of approximately 600,000 km^2 in northern Europe was covered by the waters of the epicontinental Zechstein Sea (Fig. 2.2). The sea was relatively shallow; its maximum basin centre depth is estimated to have been 300 meters in the early mesohaline stage, prior to complete isolation and evaporations (Brongersma-Sanders, 1972).

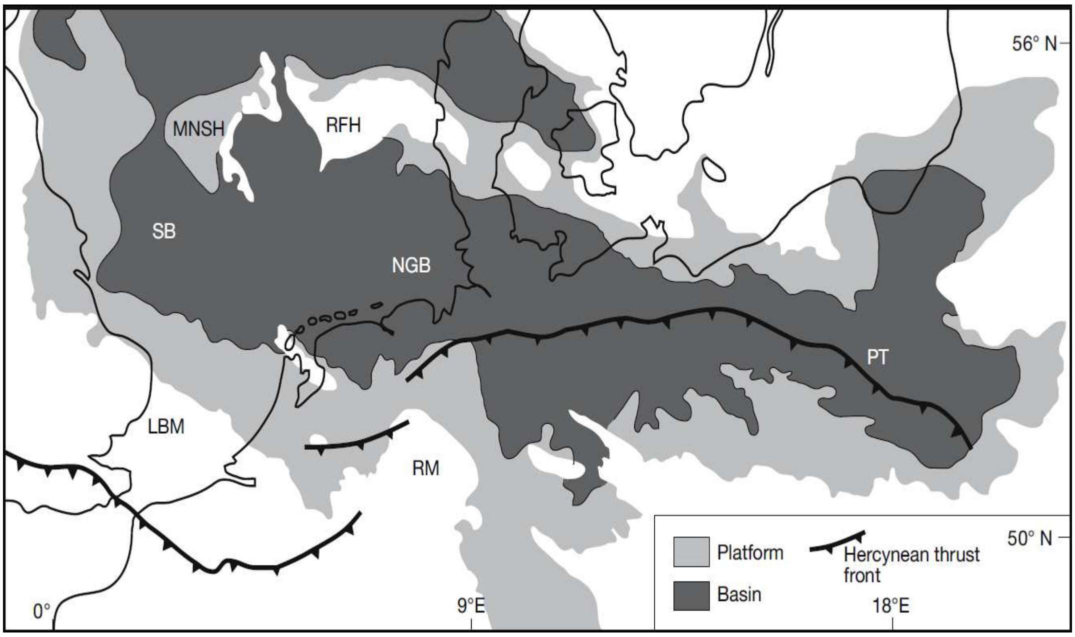

Fig. 2.2: Facies distribution in the southern Zechstein basin. In the Figure, the solid black line represents the location of the Variscan Thrust Front; MNSH: Mid-North Sea High; RFH: Ringkobing-Fyn High; SB: Silverpit Basin; LBM: London-Brabant Massif; RM: Rhenish Massif; NGB: North Germany Basin; PT: Polish Trough. (after Geluk, 2000).

The basin was subdivided into two main east-west oriented basins, called the Northern and Southern Permian Basins, which were separated by a sequence of palaeo-highs, the Mid-North Sea and Ringkobing-Fyn Highs. During the Late Permian, this part of northern Europe lay at a palaeolatitude of 25° N, within the Pangaean supercontinent. This coupled with restricted and at times marine-fed seepage supply of seawater from the Boreal Ocean to the North and the Tethys Ocean to the Southeast, resulting in the deposition of a thick sequence of bedded sulphate and halite evaporates, along with minor volumes of bittern salts (Warren, 2006). Prior to the onset of marine-fed seepage, the basin accumulated terrigenous sediments known as the Rotliegend/Wiessliegend Formation, in an arid continental playa/eolian/Wadi setting in a subsea level depression, created by the final stages of the Variscan Orogency (Carboniferous-Early Permian) (Warren, 2006). At that time, the region was characterized by the development of pull-apart rift basins that evolved into passive margins by the Middle Permian to Triassic period. This time frame encompasses the main stages of basin subsidence and is characterised by arid widespread evaporate deposition, including Zechstein evaporites in the Late Permian, followed by Muschelkalk salts in the Middle Triassic, and Keuper salts in the Late Triassic (Fig. 2.3). The Mesozoic age of NW Europe was also characterised by ongoing metasomatic and hydrothermal activity, as evident from multiphase, cross-cutting, intraformational veinlets. The following Rhaetian through the Lower Cretaceous period was marked by intensive faulting, rifting, and the initiation of large scale halokinesis through much of the basin, sourced by the Zechstein halites (Warren, 2006).

The Zechstein encompassed the last 5-7 million years of the Permian (Fig. 2.3). Most well intersections and sequence stratigraphic interpretations have been carried out in the Southern Permian basin (Warren, 2006). This region is associated with onshore hydrocarbon discoveries in the Zechstein of The Netherlands and Northern Germany, and is also a region where halite and potash salts have been mined for centuries. A Late Permian fill in the Southern Zechstein Basin constitutes a classic basin wide deposit, with circumbasinal transitions from an evaporate platform around the basin edge into a deeper-water centre dominated by laminitic shales (Fig. 2.3).

Traditionally, the Zechstein Group is divided by its mineralogy into evaporate cycles that reflect progressive evaporation from less saline to more saline salts. This method defines four main evaporates cycles (Z1-Z4) and rudimentary fifth and sixth cycles (Fig. 2.3). Figure 2.3 shows the classic Zechstein cycles (Z1-Z6) as published by Strohmenger et al., (1996a). An ideal Zechstein cycle starts with transgressive, non-evaporitic “shale”, followed by carbonates, and culminates in thick evaporates. Since most of the classic formation boundaries are chosen because they are maximum flooding surfaces (at base Z1: Coppershale or Kupferschiefer Member; base Z3: Grey Salt Clay member; base Z4: Red Salt Clay member), the lithostratigraphy of the Zechstein Group closely approaches that of units broken out using the concepts of genetic sequence stratigraphy (Warren, 2006). In the classic terminology, four main cycles (Z1-Werra Series, Z2-Stassfurt Series; Z3-Leine Series and Z4-Aller Series) and rudimentary fifth and sixth cycles are then precipitated (Fig. 2.3). The deposition of the Hauptdolomit reservoir rock took place during the Zechstein 2 cycle (Stassfurt-Carbonate, Ca2) in the Southern Permian basin (Fig. 2.4). The Hauptdolomit reservoir is approximately 30 meters thick and consists of fine-grained grainstones, packstones and mudstones.

German Zechstein		**Lithostratigraphy**			**Zechstein Sequence** **Tucker, 1991**
Late Permian	**Friesland** **252 Ma**	**Z6**	A6	Friesland Anhydrite	ZS7
			T6	Friesland Clay	
	Ohre	**Z5**	Na5	Ohre Salt	
			A5	Ohre Anhydrite	
			T5	Ohre Clay	
	Aller **253 Ma**	**Z4**	Na4	Aller Salt	
			A4	Pegmatite Anhydrite	ZS6
			T4	Red Salt Clay	
	Leine **254.5 Ma**	**Z3**	Na3	Leine Salt	ZS5
			A3	Main Anhydrite	
			Ca3	Platy Dolomite	ZS4
			T3	Gray salt clay	
	Stassfurt **256 Ma**	**Z2**	Na2	Stassfurt Salt	
			A2	Basal Anhydrite	
			Ca2	**Stassfurt Carbonate (Hauptdolomit)**	ZS3
	Werra **258 Ma**	**Z1**	A1	Werra Anhydrite	
			Ca1	Zechstein Limestone	ZS2
			T1	Kupferschiefer	ZS1
			T1Ca	Mutterflöze Carbonate	
			Z1C	Zechstein Conglom,	
Early Permian			**Rotliegendes/Late Carboniferous**		

Fig. 2.3: Lithostratigraphy of the Zechstein series in Germany (after Strohmenger et al. 1996a). Tucker (1991) published an earlier alternative to the classic Zechstein stratigraphy based on what he interpreted as third sequence ZS1-ZS7.

The shelf facies of the Hauptdolomit has provided commercial oil and gas reservoirs in Poland, Eastern and North-Western Germany, and The Netherlands, principally from oncolithic and oolitic beds in the barrier facies, from local highs on the fore-barrier and in the back-barrier lagoon.

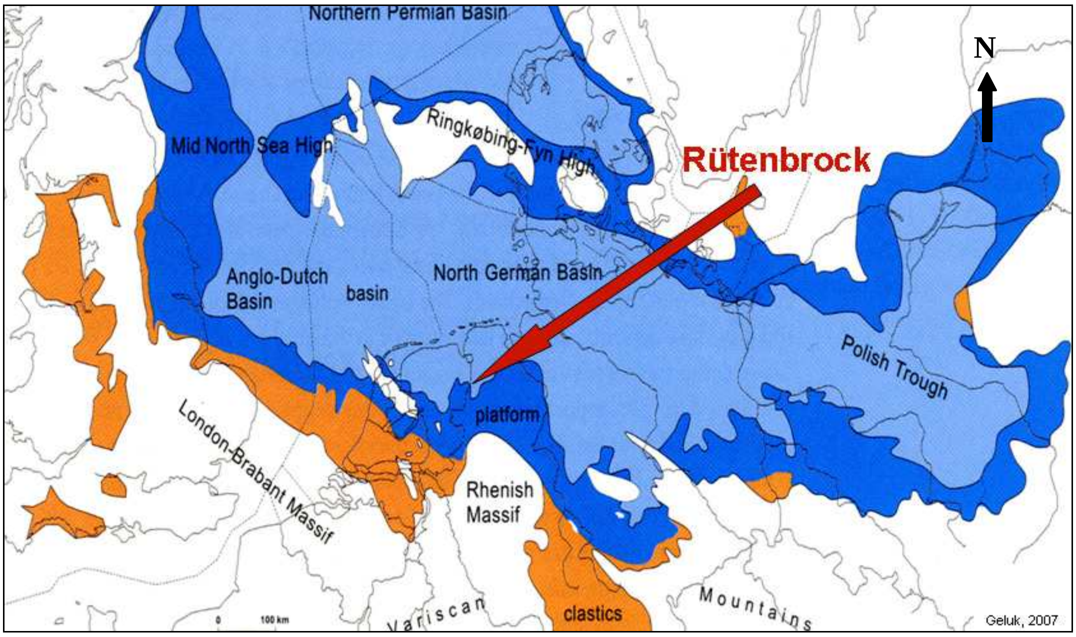
Northern Permian Basin
N
Mid North Sea High
Ringkøbing-Fyn High
Rütenbrock
Anglo-Dutch Basin
basin
North German Basin
Polish Trough
platform
London-Brabant Massif
Rhenish Massif
Variscan
clastics
Mountains
0
100 km
Geluk, 2007

Fig. 2.4: Facies distribution of the Hauptdolomit reservoir (after Geluk, 2007). The Stassfurt-Carbonate developed in the study area in a slope facies with transition to basin facies towards the North.

The Hauptdolomit reservoir consists of five compartments, separated by faults with an offset of up to several hundred meters (Fig. 2.5). Well RB_Z10a, where the multiphase pump has been tested, is located at the crest of the structure of the main compartment.

2.2 Hauptdolomit Reservoir: Reserves and Produced Reserves

The Hauptdolomit reservoir initially contained 3.570 x 10^9 m^3 (Vn), calculated using material balance. Until 10/2009 in excess of 2.778.1 x 10^9 m^3 (Vn) have been produced, representing a recovery factor of 77.8 %. Table 2.1 shows the gas initially in place (GIIP) and the cumulative gas volume produced from each compartment up to 10/2009. The calculated GIIP of the compartments and in particular the main compartment were verified using different methods and tools such as P/Z plot, MBAL program from Petroleum Experts and FAST.RTA^{TM} from Fekete Association Inc.

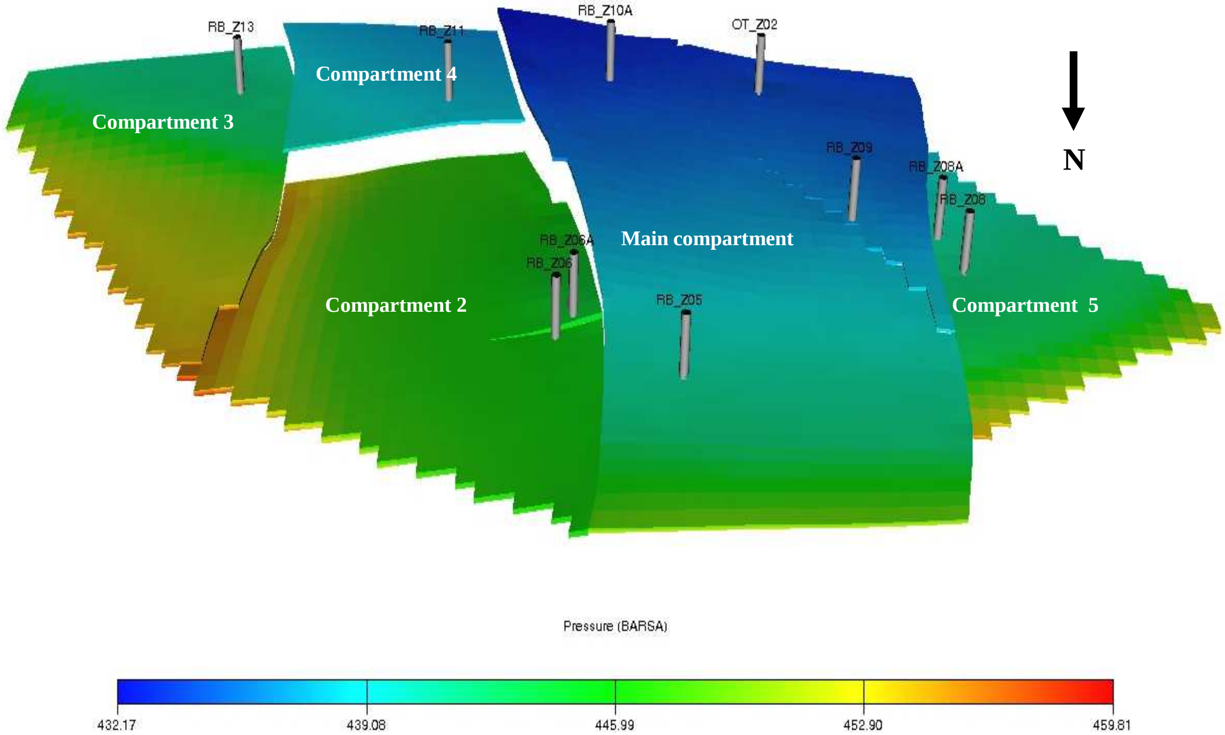
RB_Z13
RB_Z11
RB_Z10A
OT_Z02
Compartment 4
Compartment 3
N
RB_Z09
RB_Z08A
RB_Z08
RB_Z06A
RB_Z06
Main compartment
Compartment 2
RB_Z05
Compartment 5
Pressure (BARSA)
432.17
439.08
445.99
452.90
459.81

Fig. 2.5: Perspective view of the 3D Hauptdolomit compartmentalized structure which consists of five separate compartments by big faults, also shown the location of the gas producers in different compartments, the pressure distribution.

Table 2.1: Hauptdolomit gas initial in place and produced reserves

	Gas Producers	**Calculated GIIP, Mio m^3**	**Cum. Gas Prod. 10/2009, Mio. m^3**	**Recovery, %**
Main Compartment	RB_Z10a, RB_Z09, RB_Z05, OT_Z02	1930	1655.2	85.76
Compartment 2	RB_Z06, RB_Z06a	950	792	83.4
Compartment 3	RB_Z013	90	49.4	54.9
Compartment 4	RB_Z011	120	38.2	31.6
Compartment 5	RB_Z08, RB_Z08a	480	243.3	50.6
Sum		3570	2778.1	77.8

2.3 Hauptdolomit Reservoir: Production History

Production at the Hauptdolomit reservoir started in 1971 (Fig. 2.6) and continued at a number of wells up to 2010. Twelve wells were drilled on the structure and ten wells have been in production at the Hauptdolomit reservoir. Only 4 wells, including RB_Z10a have been produced at the main compartment. The field cumulative gas production (Fig. 2.6) shows that after 25 years of production, the field was approaching the tail end of the production phase with a steep decline in production rates.

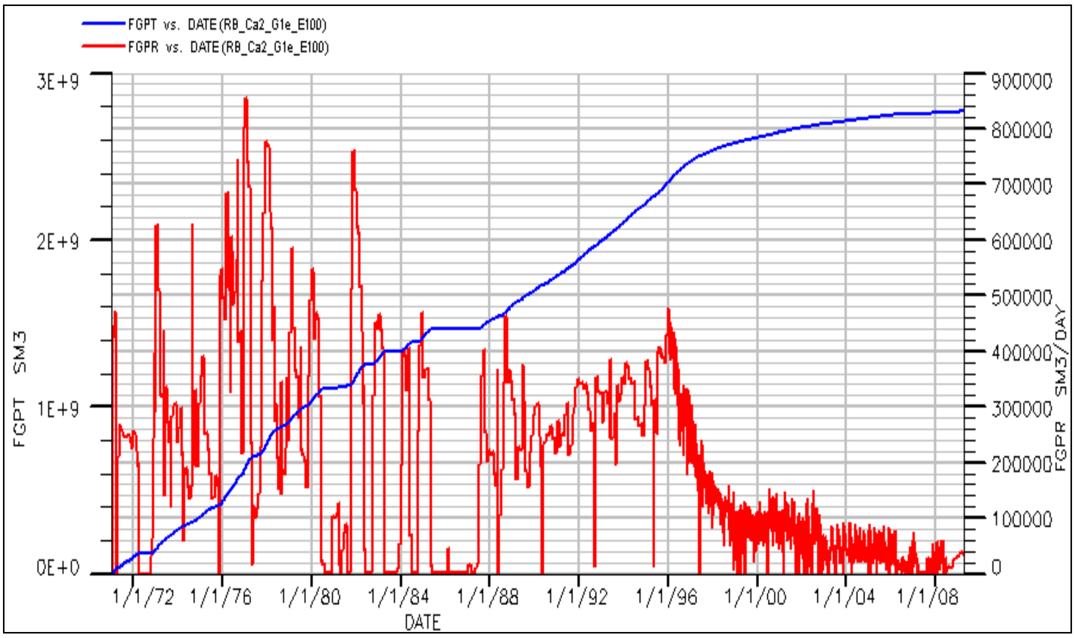

Fig.2.6: Hauptdolomit reservoir production history (reservoir cumulative gas "FGPT" & production rate "FGPR" vs. time). The red curve is the field gas rate which was strongly declined after 1996, blue curve represent the cumulative field gas production.

The ratio of produced water to produced gas (WGR) remained more or less around 10 L/1000 m^3 of gas for approximately 25 years and increased significantly to about 300 L/1000 m^3. This increase was primarily due to the encroachment of water towards wells RB_Z08a, RB_Z06a, and RB_Z05. Figure 2.7 shows that the decline in gas production associated with an increase in WGR is an indicator of the tail end production phase.

Well Production History

Production rates are available for gas and water from first gas in 01/1971 to 10/2009. Monthly production rates are available up to 1996 and daily production rates from 1996 to 2009. A summary of well production time, initial pressure and cumulative gas production from wells is provided in Table 2.2. Static bottom hole and wellhead pressure surveys were taken from the wells. Static pressure measurements have been converted to reference depth (3400 mNN in the main compartment).

Various initial static bottom hole pressures were observed between 434 and 446 bar which give an indication of the communication between the compartments through faults. Technical and mechanical failures as well as pipe collapse caused the abandonment of some wells which were replaced by implementing new deviated wells, e.g., RB_Z06a and RB_Z08a, to continue gas production from these regions. The cumulative gas production of two well (OT_Z02 and RB_Z06a) was smaller compared with the other gas producers because these wells started gas production at later production stage.

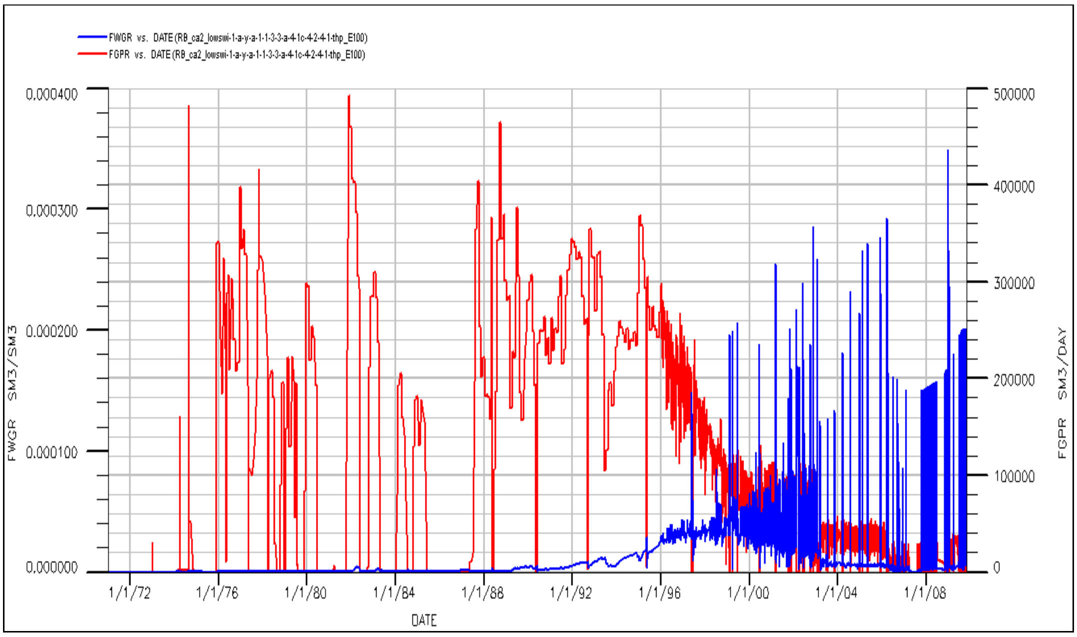

Fig. 2.7: Hauptdolomit observed water gas ratio “FWGR” vs. time. In the figure, the increase of water gas ratio (blue curve) caused the decline in the field gas rate (red curve).

Table 2.2: Well production data

Well Name	Production Period	Initial Press. bar	Observed Cumulative Production, 10/2009, Mio. Sm^3
RB_Z10a	1975 - 2009	438	929
RB_Z05	1976 – 2002	438	440
RB_Z09	1973 – 1998	435.5	100
OT_Z02	1994 - 2009	190	183.7
RB_Z06	1971 - 1985	446	720
RB_Z06a	1995 - 1997	121	72
RB_Z13	1978 - 1992	442	49
RB_Z11	1976 - 1980	434	38
RB_Z08	1973 - 1975	442.3	146
RB_Z08a	1993 - 2009	365.9	97.36

The focus of this scientific study was the main compartment, where the MPP facility has been tested at well RB_Z10a. A detailed description of the main compartment well production history therefore follows. The production from this compartment comes from wells RB_Z10a, RB_Z09, RB_Z05 and OT_Z02. Production began from RB_Z09 in 1973. The peak of gas production was achieved in 1981, reaching 500000 Sm^3/day followed a steep decline which began in 1996 (Fig. 2.8). The cumulative production of this compartment is 1.655.2 x 10^9 m^3 (Vn) to 10/2009, i.e. an 85.76 % recovery factor. The MPP production phase was from 01/2004 to 03/2006. The gas production from producer RB_Z10a began in 01/1974. Wells RB_Z05 and OT_Z02 started production in 05/1976 and 12/1994 respectively (Fig. 2.9). For many reasons, such as water encroachment to the wells and a high H_2S percentage, gas production from RB_Z09 and RB_Z05 was interrupted from the early 80's until 1987.

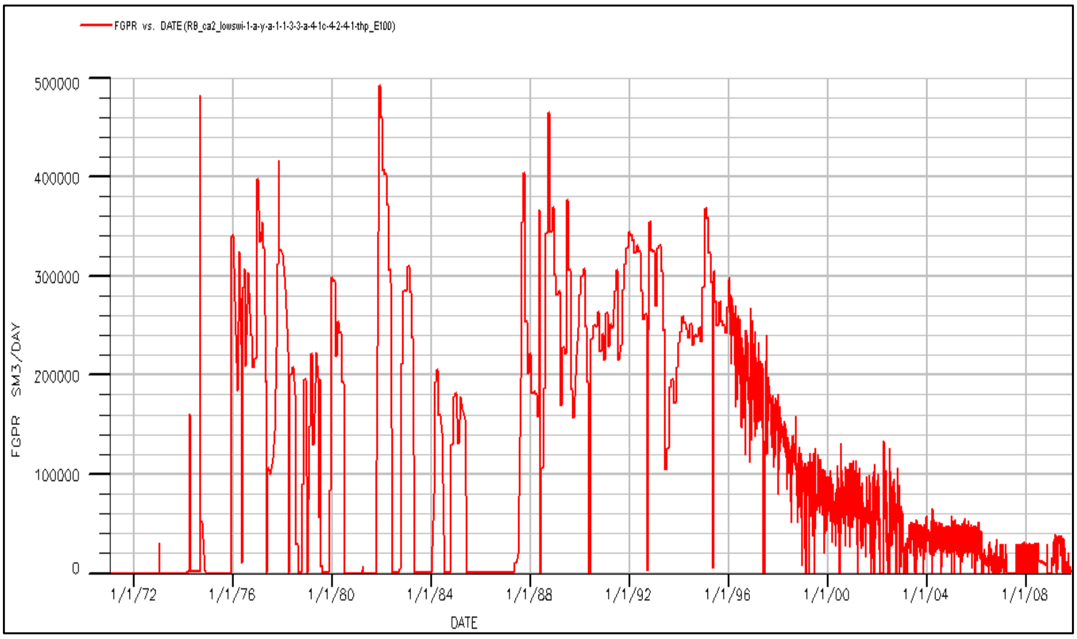

Fig. 2.8: Main compartment observed gas production rate “FGPR” vs. time. The gas production trend at later stage from 1996 forward was an indication of tail-end production phase.

RB_Z10a and RB_Z05 were recompleted in 02/1981 and 04/1986 respectively. After the MPP production phase (2004 – 2006), RB_Z10a has been intermittently productive at steadily decreasing rates. Figure 2.10 shows that in 1999 water production from RB_Z05 started to rise as a result of the water encroachment (weak influx).

The production history of the gas producers which located in the other compartments are provided in Appendix 1. The calculated GIIP of compartment 2 (well RB_Z06 and RB_Z06a) was originally about 950 x 10^6 m^3 (Vn). Cumulative gas production was 792 x 10^6 Sm^3, i.e. an 83.4 % recovery factor was achieved. Well RB_Z06 came on stream in 01/1971 and the deviated well RB_Z06a some 26 years later. RB_Z06 proved to be a prolific producer, reaching its peak of 500000 Sm^3/day in 01/1978, 7 years after coming on stream. Due to pipe failures RB_Z06 was shut-down in 05/1985. RB_Z06a came on stream in 1995 and was abandoned in 1998 because of high water production.

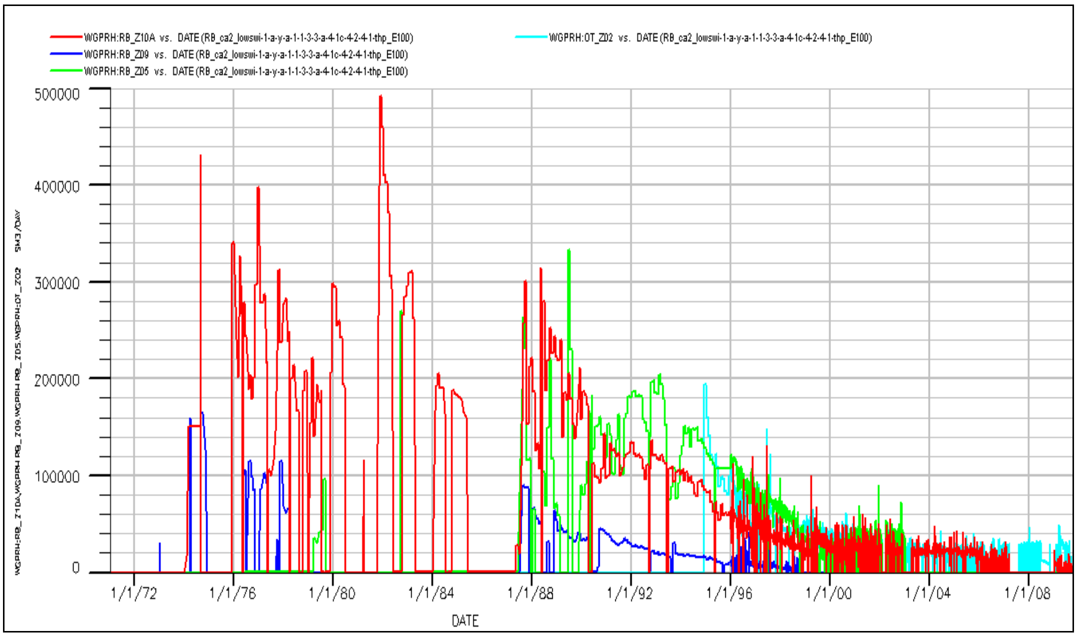

Fig. 2.9: Observed gas rates “WGPRH” from the main compartment’s wells (RB_Z10a, RB_Z05, RB_Z09 and OT_Z02). RB_Z10a was the main gas producer with a cumulative production of around 50% of the main compartment reserves.

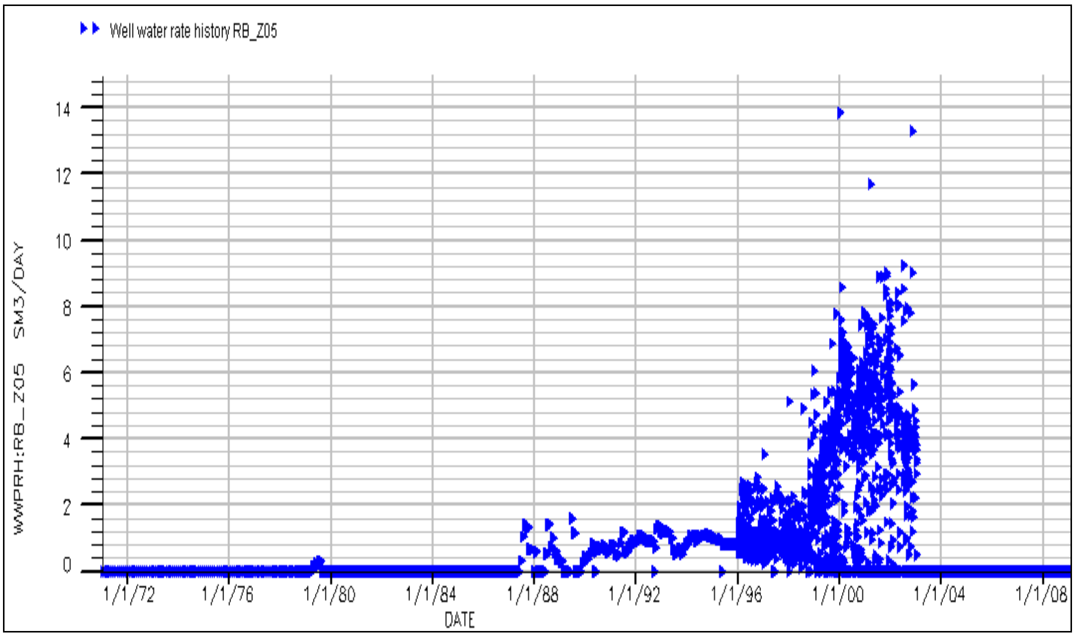

Fig. 2.10: Observed water production “WWPRH” (RB_Z05). The well was production for years with 1 - 2 m^3/ day and suddenly in 1999 increase the water production rate to 8 -10 m^3/day which was interpreted as water breakthrough or water encroachment towards the well RB_Z05 (the nearest to the gas water contact (GWC)).

Compartment 3 and 4 are to be found at the eastern end of the main compartment. Compartment 3 contains only one well, RB_Z13. RB_Z13 was productive from 1978 to 1992 and abandoned in 1992 because of water encroachment towards the wellbore. RB_Z13 was recompleted in 09/1992 in order to block the lower perforation interval to prevent water encroachment and improve production, but it was not successful. In compartment 4, only one well, RB_Z11, was drilled. It was producing for a few years from 1975 to 1980, after which RB_Z11 was watered out and shut-down in 1980. Wells RB_Z13 and RB_Z11 had recovery factors of 54.9% and 31.6% respectively. Compartment 5 is located to the west of the main compartment. The production from this compartment came from just one gas well, RB_Z08, between 1973 and 1975. The well was shut-down in 1975 because of a pipe collapse. In 1982, a new deviated well, RB_Z08a, was drilled on the site of RB_Z08. Production from RB_Z08a started in 1993.

CHAPTER III: Verification of the Initial Gas in Place

With sufficient production, material balance techniques offer a largely independent alternative method of estimating the original hydrocarbon in place to supplement direct volumetric calculation. A material balance of a pool's history can also help to identify the drive mechanism and the expected recovery factor range, since different drive mechanisms display different pressure behaviours for the same cumulative production. Figure 3.1 presents the different standard P/Z curve trends that result from different drive mechanisms.

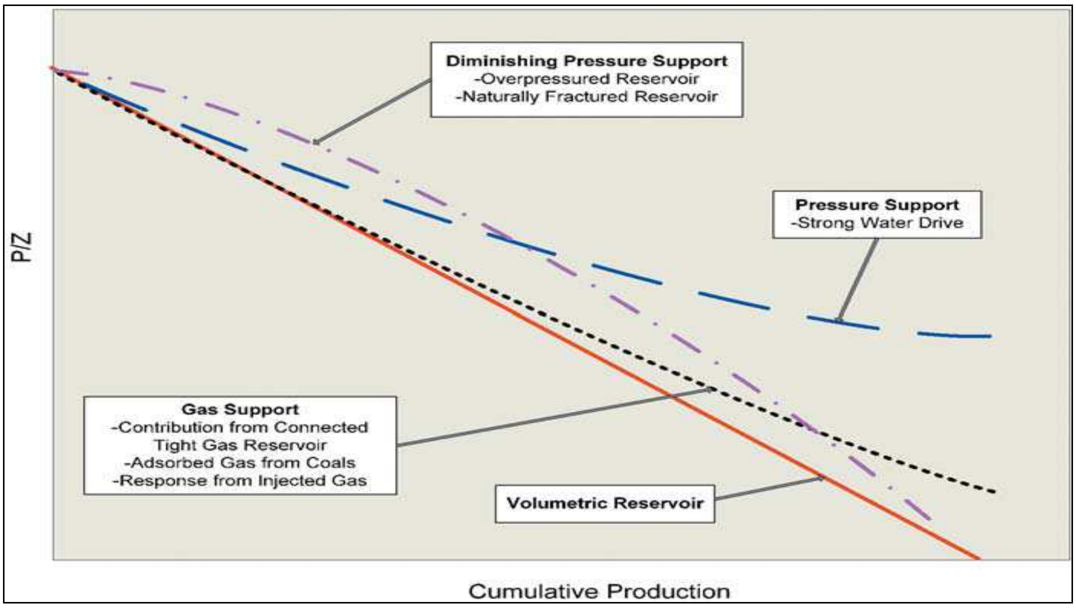

Fig. 3.1: Gas reservoir P/Z material balance diagnostics. Different drive mechanisms show different decline trends of P/Z curve (after Fekete).

Material balance calculations are commonly used to answer reservoir development questions, but the technique can also help with the interpretation of reservoir geometry. Geological and geophysical mapping will give an indication of a pool's shape and orientation, but typically the confidence in the in place volume is not high. Conversely, material balance can reveal a great deal about the volume of a reservoir but nothing about its shape or orientation. The combination of the two often greatly improves the understanding and interpretation of the pool parameters. Material balance uses actual reservoir performance data, and is therefore generally accepted as the most accurate procedure for estimating original gas in place. But a minimum of 10 to 20% of the in place volume must be produced before there is sufficient data to identify a trend and reliably extrapolate the original in place volume through material balance (Mireault et al., 2008). This is the case in this study. Also, the material balance procedure describes the expansion of oil, gas, water, and rock over time as a pool is exploited. When fluid is removed from a reservoir, reservoir pressure tends to decrease, and the remaining fluids expand to fill the original space.

From the geological model’s static data (the reservoir and fluid data), a volume of 2.5 x 10^9 m³ (Vn) was identified as total volume of gas initially in place (GIIP) in the main compartment whereas the GIIP calculated from material balance P/Z plot was approximately 1.910 x 10^9 m³ (Vn). The P/Z plot in figure 3.2 shows that, the main compartment is a volumetrically closed system.

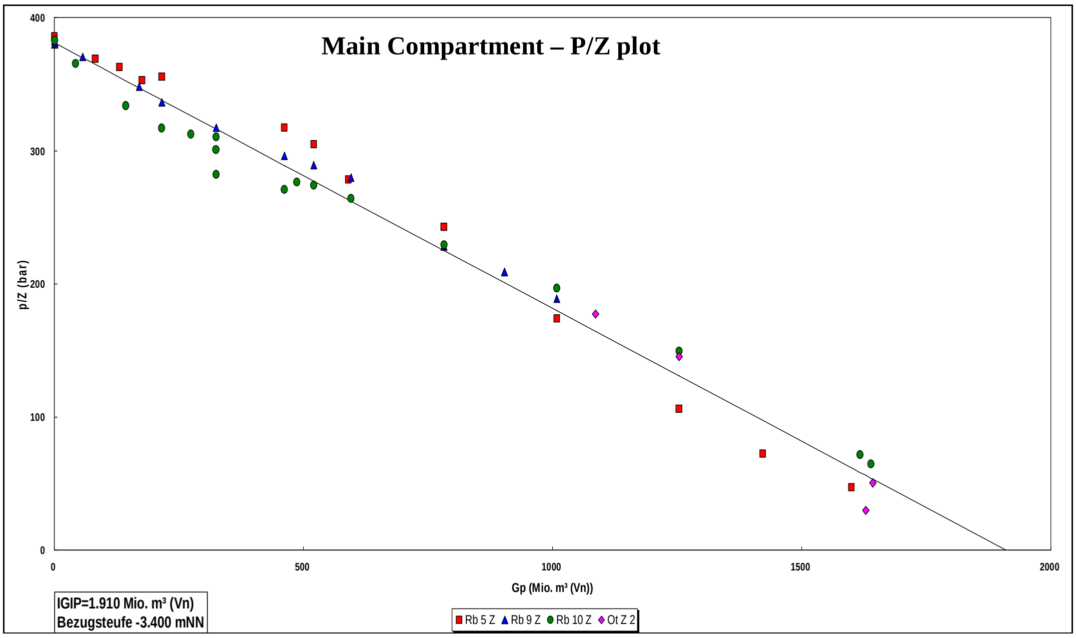

Fig. 3.2: Main compartment GIIP estimation (P/Z measurements vs. observed cumulative gas production “GP”). The pressure measurements “P/Z” were taken from the wellbores (RB_Z10a, RB_Z05, RB_Z09 and OT_Z02). The P/Z curve trend represented a volumetric (closed) compartment.

MBAL (material balance tool) program from Petroleum Experts software was used to verify the calculated GIIP based on pressure measurements. MBAL provides a better understanding of the reservoir behaviour prior to dynamic simulation and it has the following capabilities: 1) history matching to determine initial hydrocarbon in place and main drive mechanisms; 2) comparison simulations which compare accuracy of model to production history; 3) production of a single tank model and a multiple tank model which offers the possibility of connecting the tanks through transmissibility. The drive mechanisms have been evaluated and the possible flow communication between the compartments has been investigated. Because the Hauptdolomit reservoir has a compartmentalized structure, a multiple tank model was constructed to understand the reservoir behaviour, evaluate the reservoir drive mechanisms and the communication between the various regions. Figure 3.4 describes the multiple tank models and shows the gas producers which belong to each compartment. Each individual compartment is considered a separate tank with the possibility of communication with the other tanks by introducing transmissibility. The data required for the modelling of tanks, including the initial pressure, temperature, porosity, connate water saturation, GIIP, rock compressibility, relative permeability function, and production history, was entered into MBAL.

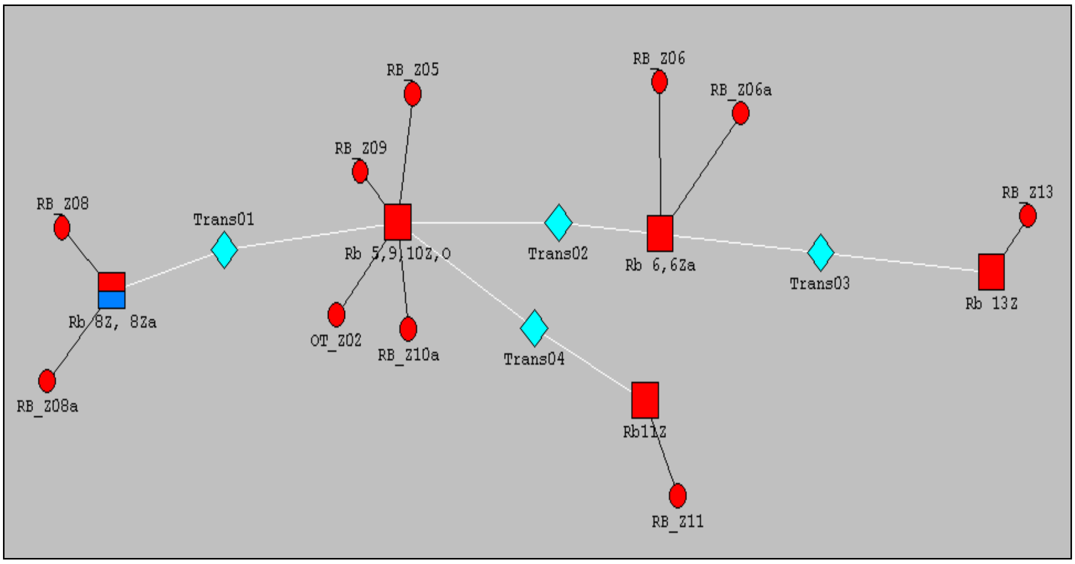
RB_Z05
RB_Z06
RB_Z06a
RB_Z09
RB_Z13
RB_Z08
Trans01
Rb 5,9,10Z,O
Trans02
Rb 6,6Za
Trans03
Rb 13Z
Rb 8Z, 8Za
OT_Z02
RB_Z10a
Trans04
RB_Z08a
Rb11Z
RB_Z11

Fig. 3.4: Hauptdolomit reservoir multiple tank model using MBAL program. Five tanks model represent the various compartments which associated with a transmissibility option to test the communication between them during the history match process.

History match runs were carried out to obtain the best match of static pressure measurements against simulated data. An excellent match of measured pressure vs. cumulative production was observed in four compartments (1, 2, 3 and 4) (Fig. 3.5).

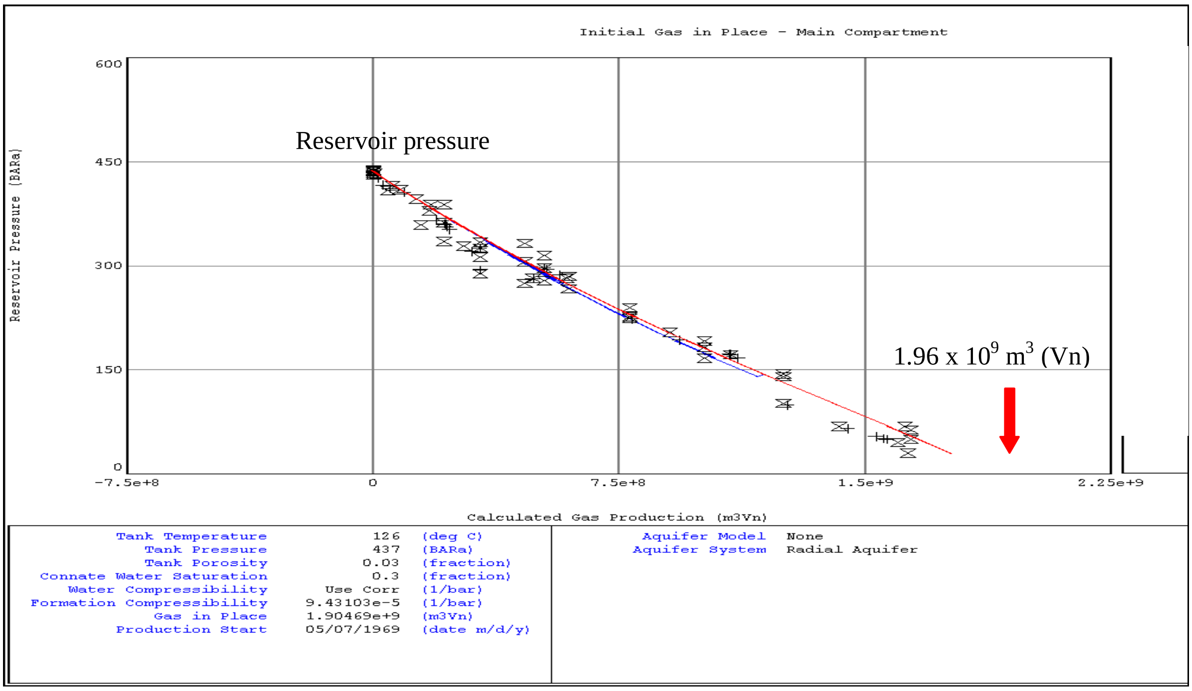

Tank Temperature	126	(deg C)
Tank Pressure	437	(BARa)
Tank Porosity	0.03	(fraction)
Connate Water Saturation	0.3	(fraction)
Water Compressibility	Use Corr	(1/bar)
Formation Compressibility	9.43103e-5	(1/bar)
Gas in Place	1.90469e+9	(m3Vn)
Production Start	05/07/1969	(date m/d/y)

Aquifer Model	None
Aquifer System	Radial Aquifer

Fig. 3.5: Main compartment pressure measurements (black marks) vs. simulated (red curve). The pressure decline trend confirmed that it is a volumetric compartment. The reservoir and fluids data are shown bottom of the figure.

The GIIP of the main compartment was calculated at around 1.96 x 10^9 m^3 (Vn). Several transmissibility values were introduced to examine communication between the regions, but simulation results which used no communications through the faults were excellent. Combinations of two types of drive mechanisms were acting in compartments 1, 2, 3 and 4: fluid expansion and pore volume compressibility. Fluid expansion is the main drive mechanism, representing more than 95 % (Fig. 3.6). The measured pressure trend in RB_Z08, showing a distinct pressure decline, indicates that an additional energy source such as an aquifer supported the reservoir pressure after the abandonment of RB_Z08 in 1975.

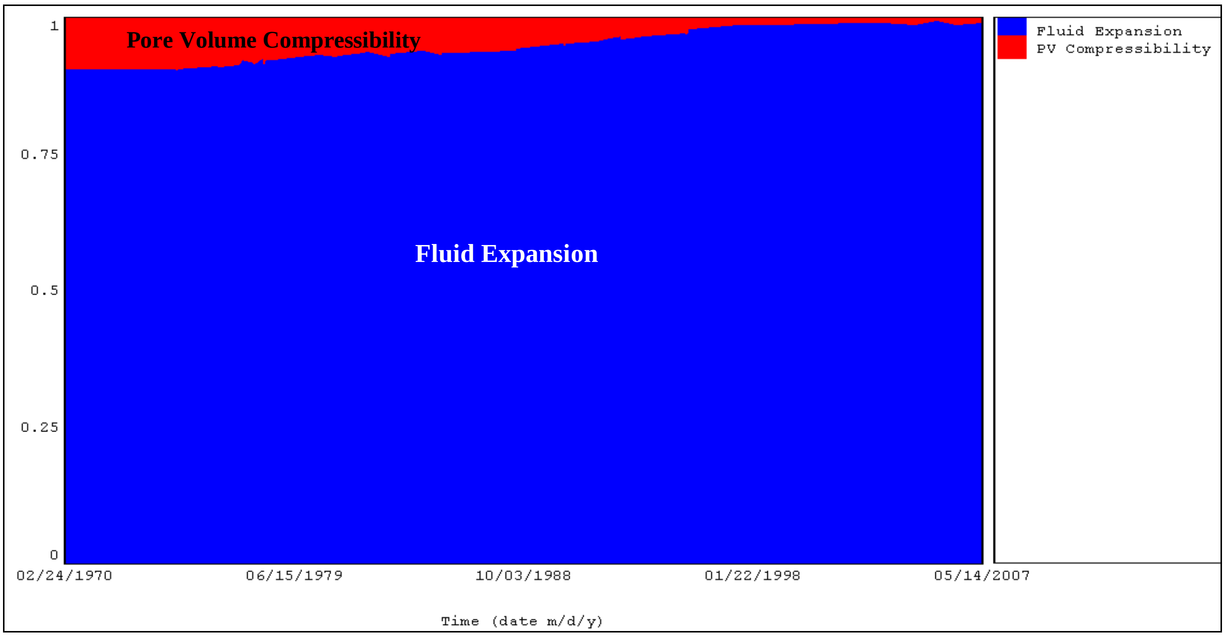

Fig. 3.6: Drive mechanisms vs. production history time. Fluid expansion (dark blue) and pore volume compressibility (red) are the drive mechanisms acting in the main compartment. The fluid expansion was the dominant drive mechanisms. The pore volume compressibility drive mechanism was disappeared as the reservoir pressure declined.

Figure 3.7 demonstrates the mismatch between the pressure measurements and simulated modeling (red trend line). The production history data shows a typical declining trend in pressure at the initiation of production from RB_Z08, which could be a sign of weak aquifer. Fetkovich semi-steady state aquifer was used to match the pressure trend, and the aquifer system used was a bottom drive aquifer. The estimated aquifer volume is 170 x 10^6 m^3 water. Figure 3.8 shows the match obtained by introducing an aquifer. Figure 3.9 shows the percentage of the relative contribution of drive mechanisms in compartment 5. At the beginning of production, the dominant drive mechanism was fluids expansion, while later the bottom drive water influx becomes the dominant drive mechanism.

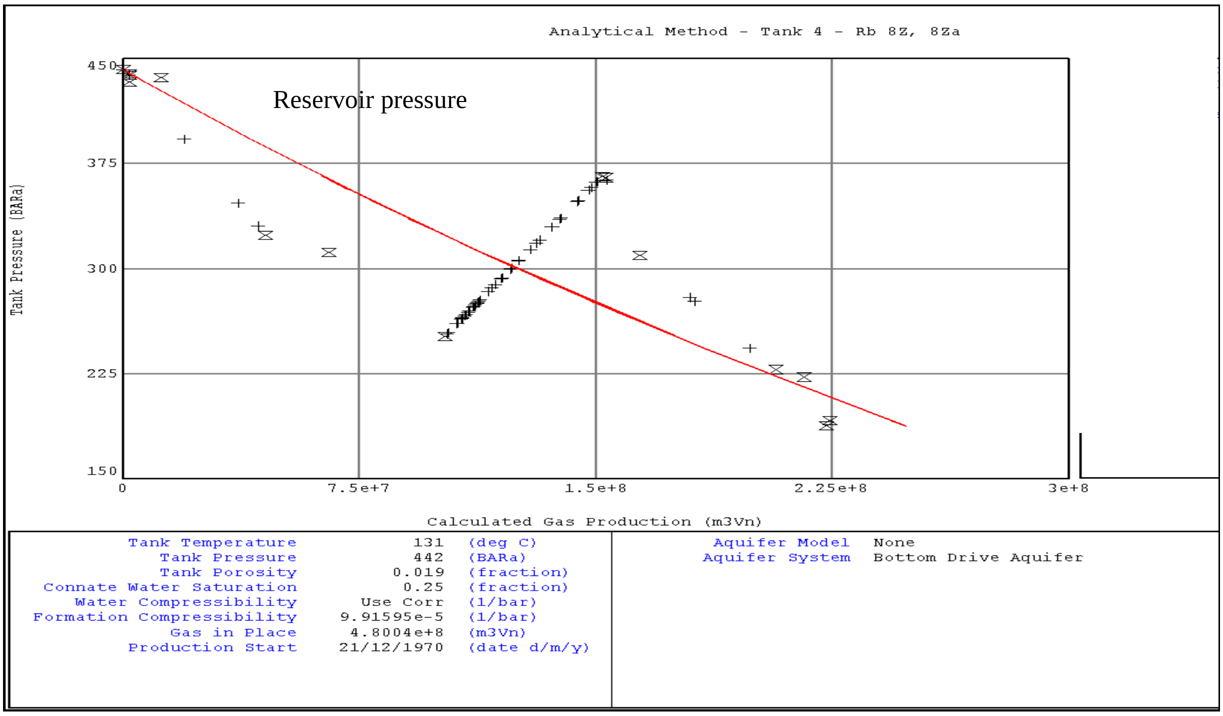

Tank Temperature	131	(deg C)
Tank Pressure	442	(BARa)
Tank Porosity	0.019	(fraction)
Connate Water Saturation	0.25	(fraction)
Water Compressibility	Use Corr	(1/bar)
Formation Compressibility	9.91595e-5	(1/bar)
Gas in Place	4.8004e+8	(m3Vn)
Production Start	21/12/1970	(date d/m/y)

Aquifer Model	None
Aquifer System	Bottom Drive Aquifer

Fig. 3.7: Reservoir pressure measurements (black marks) vs. simulated (red curve). No match was observed without introducing an aquifer (compartment 5). The reservoir and fluids data of the compartment are shown bottom of the figure.

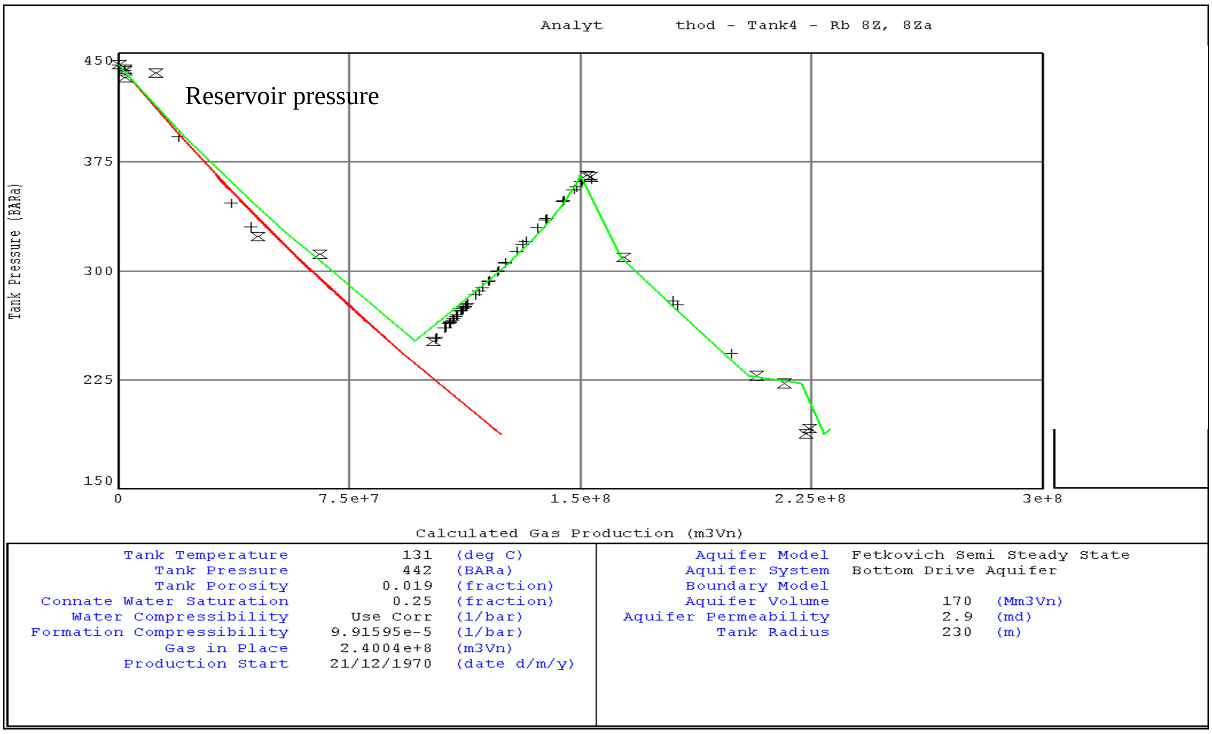

Tank Temperature	131	(deg C)
Tank Pressure	442	(BARa)
Tank Porosity	0.019	(fraction)
Connate Water Saturation	0.25	(fraction)
Water Compressibility	Use Corr	(1/bar)
Formation Compressibility	9.91595e-5	(1/bar)
Gas in Place	2.4004e+8	(m3Vn)
Production Start	21/12/1970	(date d/m/y)

Aquifer Model	Fetkovich Semi Steady State	
Aquifer System	Bottom Drive Aquifer	
Boundary Model		
Aquifer Volume	170	(Mm3Vn)
Aquifer Permeability	2.9	(md)
Tank Radius	230	(m)

Fig. 3.8: Reservoir pressure measurements (black marks) vs. simulated (green curve). A perfect match of the production history was achieved by introducing an aquifer (compartment 5). The red curve represents the early production stage without introducing an aquifer.

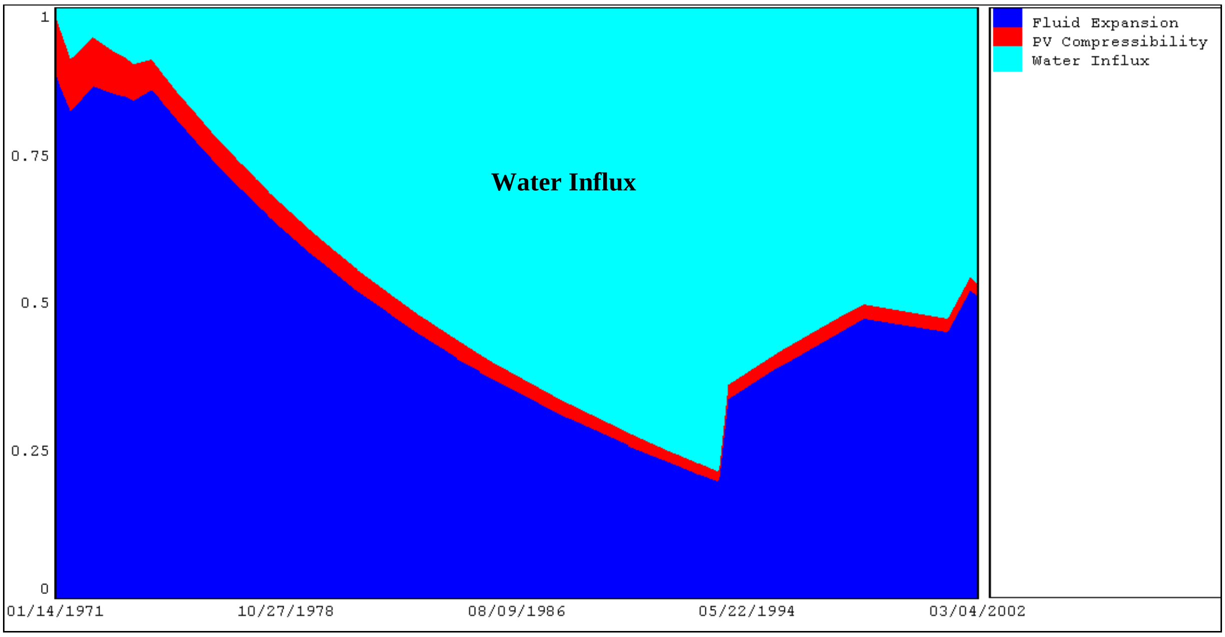

Fig. 3.9: Drive mechanisms vs. production history time. Fluid expansion (dark blue), pore volume compressibility (red) and water influx (light blue) are the drive mechanisms acting in the compartment 5. The fluid expansion drive mechanism was the dominant at the beginning for a short production time then the water influx became the dominant drive mechanism.

CHAPTER IV: Decline Curve Analysis

Decline curve analysis is one of several techniques used to estimate recoverable reserves and to predict future production performance from routinely available production data. Various techniques have been developed to accomplish this task. The techniques range from a simple decline curve analysis to the use of sophisticated multidimensional, multiphase reservoir simulators. Whether a simple or sophisticated technique is employed, the basic principle in predicting production rates is first to compute the rates and pressure measurements for a history production time.

Decline curve analysis is a graphical procedure used for analyzing declining production rates and forecasting the future performance of oil and gas wells. A curve fit of past production performance is carried out using certain standard curves. This curve fit is then extrapolated to predict potential future performance. Analyzing the production history and pressure data of a well can be an effective way to estimate the well and reservoir properties. Production data analysis approaches have advanced significantly over the past few years, and while there are many different methods published in the literature, there is no single method that always yields the most reliable answer (Al-Reshedan et al., 2009). However, using all available methods in combination will provide a comprehensive understanding and a greater degree of confidence if all techniques agree. Production data analysis begins by using methods for determining rate vs. time, decline curve analysis and type curve matching. The last two techniques are used to determine the characteristics of the reservoir and its fractures. FAST. RTA™, an advanced production analysis package, was used to perform production analysis. The production decline analysis includes a history match, and predictions start from 01/2004. The objectives are to confirm the calculated reserves, to estimate the recoverable reserves, to predict the future production performance of RB_Z10a with and without the use of MPP facility, and to compare the results with the conventional compression production system. Also, the analysis includes a study of the neighboring well OT_Z02, which was carried out by inspecting any production response. It thus covers the entire compartment. Actual production data, flowrates (gas and water) and flowing wellhead pressure data were used for this purpose.

4.1 Arp Decline Curve Analysis

The basis of decline curve analysis is to match past production performance histories or trends with a model, assuming that future production continues to follow past trends. These models can be used to estimate original gas in place and to predict ultimate gas reserves at some future reservoir. They can also be used to determine abandonment pressure, economic production rate, or even the remaining productive life of a well. Arp (1945) introduced the decline curve analysis method in 1940s using mathematical equations to determine the rate of decline of well production (Al-Reshedan et al., 2009). The method is a mathematical equation with no actual physical basis other than the fact that the equation shows a declining trend. The function introduced by Arp is characterized by three parameters: initial flow rate (q_i), initial decline rate (D_i), and decline exponent (b). When b=0, the decline is exponential (I). When b=1, the decline is harmonic (III). When 0 < b < 1, the decline is said to be hyperbolic (II) (Al-Reshedan et al., 2009).

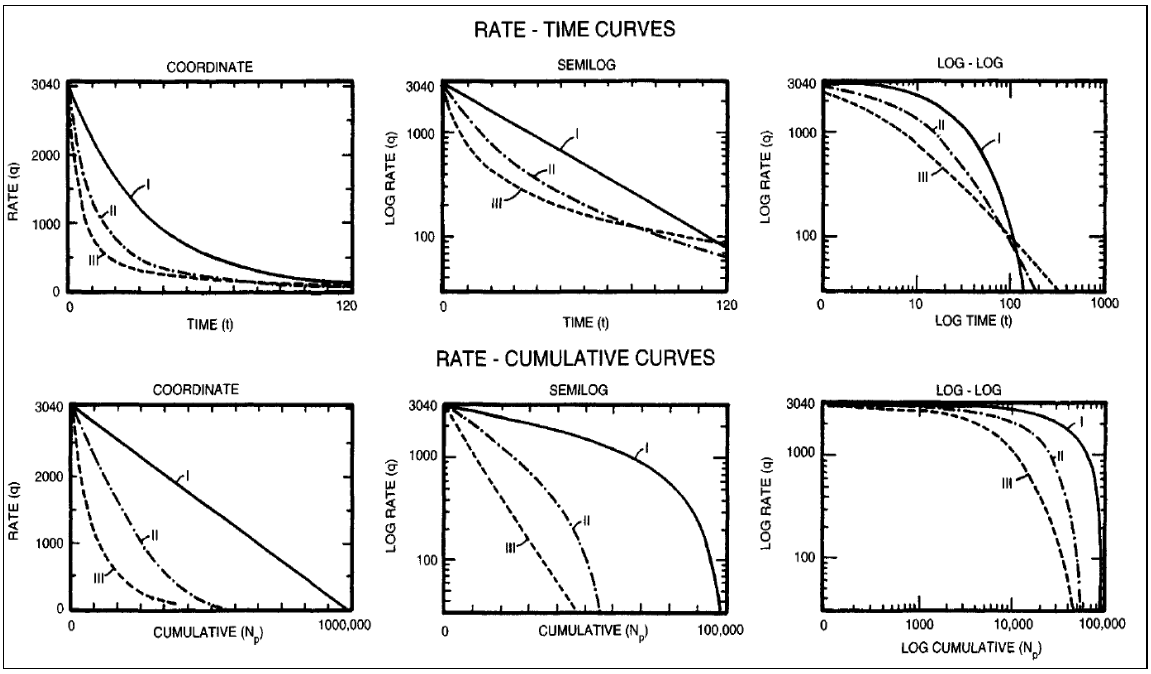

Fig. 4.1: Arp decline curves: exponential, harmonic and hyperbolic, which have different shapes on Cartesian, semi-log and log-log graphs (after Lyons, 2005).

Application of decline curve analysis techniques to gas reservoirs is most appropriate when more conventional volumetric or material balance methods are not accurate or when sufficient data are not available to justify complex reservoir simulation (Al-Reshedan et al., 2009). For example, material balance methods require estimates of stabilized shut-in bottom hole pressures; however, in low permeability reservoirs, where long times are needed for stabilization, accurate shut-in bottom hole pressure data is not available. Early attempts at decline-curve analysis required finding plotting techniques or functions which would linearize the production history. Because linear functions are simple to manipulate mathematically or graphically, the future performance could then be estimated fairly easily if it was assumed that the production trend remained linear for the remaining life of the well or reservoir (Al-Reshedan et al., 2009). Most conventional decline curve analyses are based on Arp empirical rate/time decline equation,

$$q(t) = \frac{q_i}{\left(1 + bD_i t\right)^{1/b}} \quad (4.1)$$

where,

$D_i = -\frac{dq(t)}{dt / q(t)}$ = initial decline rate, days^{-1}

Note that the units of gas flow rate, time, and initial decline rate in Eq. 4.1 must be consistent. Depending on the value of the decline exponent *b*, Eq. 4.1 has three different forms. Because it is an empirical method, it requires no knowledge of reservoir or well parameters. However it has its failings, the most important one being that it completely ignores flow pressure data. As a result, it can underestimate or overestimate reserves (Arp, 1945; Fetkvoich, 1980; Blasingame, 1993). Arp's method is still being used primarily because of its simplicity, and since it is an empirical method, it does not need any reservoir or well parameters.

4.2 Decline Type Curves

Type curve matching is essentially a graphical technique for matching production data visually using preplotted curves on a log-log paper. Type curves are plots of theoretical solutions to flow equations and can be generated for virtually any kind of reservoir model for which a general solution describing the flow behaviour is available. Theoretical assumptions, model applicability and data requirements limit each analysis technique (Mattar et al., 2003; Rushing et al., 2003). A systematic approach to production data analysis, using all the best methods available, enables the analyst to obtain a full picture of what is going on with regards to both reservoir and operations (Mattar et al., 2003). Decline curve analysis techniques offer alternatives to volumetric and material balance methods and history matching with reservoir simulation for estimating original gas in place and recoverable gas reserves. Decline type curve analysis is a widely used method for analyzing and predicting past and future performance of production wells, especially in low permeability gas reservoirs. For fractured low permeability gas wells, analysis of production data is the more practical method, due to the long time necessary to achieve pseudo radial flow (Cramer et al., 2004). A number of techniques have been developed by the petroleum industry for evaluating well performance. Unfortunately, no single methodology is perfect or capable of handling all data and reservoirs. Fetkvoich (1980) introduced the technique of decline curve analysis by way of type curves. Fetkovich (1980) was the first to extend the concept of using type curves to transient production. The Fetkovich methodology uses the same Arps depletion techniques for the analysis of boundary dominated flow and constant pressure type curves for transient production. Wattenbarger (1987) introduced a normalized time function that linearizes the rate of decline against normalized time for gas reservoirs producing at constant bottom hole pressures during boundary dominated flow. The calculation of the normalized times involves an iterative process. In 1993, Blasingame & Palacio addressed the issue of variable, non constant bottom hole pressures in gas wells. They introduced new methods, which use a modified time function for analyzing the performance of gas wells. They have also established a new algorithm, along with the modified time function, to compute gas in place, which together are capable of modelling the behaviour of production data for variable rate and/or variable pressure drop conditions. Like normalized time, the calculation of pseudo equivalent time is an iterative process. In 1998, Agarwal introduced new type curves, which represent advancement over the Palacio & Blasingame type curves because a clearer distinction can be made between transient and boundary dominated flow periods. Although decline curve analysis and type curve matching of gas well decline curves are still used widely, they all require bottom hole pressure data. Subjectivity of each either of these methods, along combined with the need for pressure data, calls for a new method which does not require pressure data and eliminates the subjectivity of the analysis. The primary differences between distinctive type curves are described below.

Fetkovich decline type curve: Fetkovich presented a new set of type curves that extended the Arps type curves into the transient flow region (Fig. 4.2). He recognized that Arp decline curve analysis was applicable only during the time period when production was in boundary dominated flow; i.e., during the depletion phase. This meant that the early production life of a well was not analyzable by conventional decline curve methods. A well producing at constant pressure will follow one of these curves. One reason for the success of Fetkovich type-curves is that most oil wells are produced under wide-open conditions, i.e., at the constant lowest possible pressure. Combining the Fetkovich transient curves with the Arp decline curves, and blending them where the two sets of curves meet; results in the Fetkovich decline type curves shown below (Fig. 4.2). Fetkovich (1980) used analytical flow equations to generate type curves for transient flow, and he combined them with the Arp empirical decline curve equations. Accordingly, the Fetkovich type curves are made up of two regions which are blended into a continuous whole and thereby encompass the entire production life from early stages (transient flow) to late stages (boundary dominated flow).

Blasingame type curve: the production decline analysis techniques of Arp and Fetkovich are limited insofar as they do not account for variations in bottom hole flowing pressure in the transient regime or changing PVT properties with reservoir pressure in gas wells. Blasingame,

(1993) however, has developed a production decline method that accounts for these phenomena. This method uses a form of superposition time function that only requires one depletion stem for type curve matching, the harmonic stem. One important advantage of this method is that the type curves used for matching are identical to those used for Fetkovich decline analysis, without the empirical depletion stems. When the type curves are plotted using Blasingame's superposition time function the analytical exponential stem of the Fetkovich type curve becomes harmonic (FAST.RTA Manual).

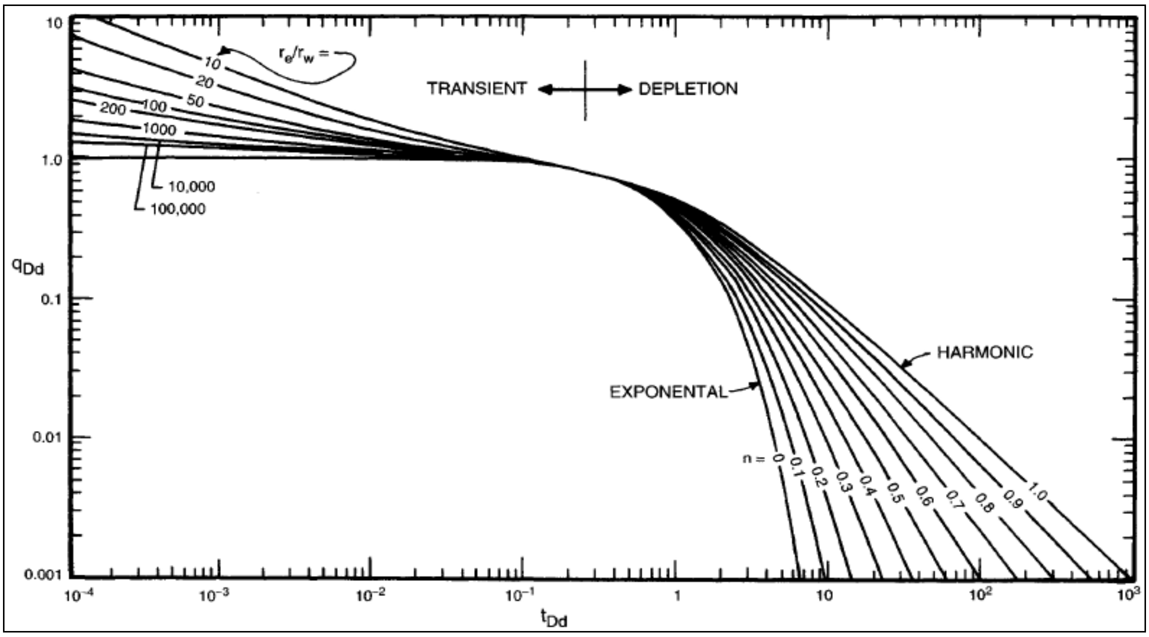

Fig. 4.2: Fetkovich log-log type curve (production rate vs. time). The early production life is identified as transient flow and the boundary-dominated flow which is represented by the Arp decline types (after Lee et al., 1996).

Agarwal-Gardner type curve: Agarwal and Gardner (1998) compiled and presented new decline type curves for analyzing production data. Their methods build upon the work of both Fetkovich and Palacio-Blasingame, utilizing concepts of the equivalence of constant rate and constant pressure solutions. Agarwal and Gardner present new type curves with dimensionless variables based on the conventional well test definitions, as opposed to the Fetkovich dimensionless definitions used by Blasingame et al., (1993). They also include primary and semi-log pressure derivative plots (in inverse format for decline analysis). Moreover, they present their decline curves in distinct formats in addition to the standard normalized rate vs. time plot. These include the rate vs. cumulative and cumulative vs. time analysis plots (FAST.RTA Manual).

Flowing Material Balance: The Flowing Material Balance technique uses the principle of stabilized or pseudo-steady-state flow to evaluate total in-place fluid volumes. In a conventional material-balance calculation, reservoir pressure is measured or extrapolated based on stabilized shut-in pressures at the well. In a flowing situation, the average reservoir pressure clearly cannot be measured. However, in a stabilized flow situation, there is a very close connection between well flowing pressures (which can be measured) and the average reservoir pressure. The diagram below shows how these pressures are related (FAST.RTA Manual).

Normalized Pressure Integral (NPI)*:* The Normalized Pressure Integral was initially developed by Blasingame in 1989 (*Type-Curve Analysis Using the Pressure Integral Method*, Blasingame et al., 1989). The objective of the method was to present a robust diagnostic method for drawdowns that did not suffer from noise and data scatter, as is typical of the standard well test derivative. The solution involves using a pressure integral curve as the base curve for noisy drawdown analysis.

Transient Type curve Analysis: The transient type curve analysis technique is not a new method of data analysis. Rather, it provides an alternative perspective that is ideal for the analysis of very short (early) production periods, and/or the analysis of very low permeability reservoirs. In the Blasingame (1993), Agarwal-Gardner (1998) and NPI presentations, the type curves are scaled such that there is convergence onto a single boundary dominated stem (unit slope). This is achieved through the use of a dimensionless time that is based on area (t_{DA} or t_{Dd}). One consequence of this type of scaling is that there are numerous transient stems. If a dimensionless time based on well radius (t_D) is chosen instead, there will be a single transient stem with a series of boundary dominated curves.

Wattenbarger type curve Analysis**:** Long linear flows have been observed in many gas wells. These wells are usually in very tight gas reservoirs with hydraulic fractures designed to extend to or nearly to the drainage boundary of the well. Wattenbarger et al. (1998) presented new type curves to analyze the production data of these gas wells. Two features of modern analysis that improve upon the traditional techniques are: 1) normalizing rates using flowing pressure, which enables the effects of back pressure changes to be accommodated in the reservoir analysis; 2) handling the changing compressibility of gas with pressure using pseudo-time, as the time function enables the gas material balance to be handled rigorously as the reservoir pressure decreases with time.

Type curve analysis is useful for estimating reservoir parameters such as permeability, skin and original gas in place (OGIP). Furthermore, there is important diagnostic value in type curve analysis. Some practical diagnostics include: identifying skin damage; qualifying fracture effectiveness; identifying a transition between transient and boundary dominated flow;

identifying liquid loading; identifying pressure support; characterizing over-pressured reservoirs; identifying interference.

FAST.RTA™ is a decline analysis tool that analyses production rates and flowing pressures. Methods include traditional decline analysis, Fetkovich, Blasingame, Agarwal-Gardner, NPI, Transient and Wattenbarger type curves, specialized analysis and flowing material balance. Reservoir models include volumetric and water drive types. Well models include horizontal, vertical, and hydraulically fractured well types. FAST.RTA™ analyses production data, yielding hydrocarbons in place (OIIP), expected ultimate recovery (EUR), drainage area, permeability, skin and fractures half length and aquifer strength. It allows the evaluation of infill potential, characterization of the reservoir, and estimation of reserves with ease and efficiency. There are a number of conventional analysis techniques incorporated within the FAST.RTA™ and are used for production data analysis, including: 1) Arp decline analysis (exponential, hyperbolic and harmonic); 2) Fetkovich type curve analysis; 3) Blasingame type curve analysis; 4) Agarwal-Gardner type curve analysis; 5) Normalized Pressure Integral (NPI) type curves; 6) Flowing Material Balance; 7) Wattenbarger; 8) Analytical & Numerical Modelling. The analytical and numerical modelling options allow you to create your own reservoir models, in order to either confirm results from the conventional analysis techniques (Fetkovich, Blasingame, Agarwal-Gardner, NPI), or to construct more complicated reservoir/well geometries which cannot be handled by conventional analysis. FAST.RTA™ offers the unique capacity to simulate pressure from production history, or simulate rates and cumulative production from pressure history, or both simultaneously. The non-linear regression allows history matching, minimizing the error in terms of pressures, rates and cumulative production. The Analytical models are Radial, Fracture, Horizontal, Water Drive, Composite and Multilayer reservoir models.

After the achievement of history matching, a production forecast for any analytical or numerical model can be run based on anticipated producing pressure. The productivity index's sensitivity to improvement can also be simulated. A review of literature on type-curve analysis of gas reservoirs reveals that there is no specific attention paid to type curves of naturally fractured gas reservoirs. Due to the double porosity behaviour in a naturally fractured gas reservoir and the importance of fracture and matrix compressibilities, the evaluation of type-curve analysis components such as average reservoir pressure, total compressibility, pseudo-time, and pseudo material balance time requires special attention. Warren and Root (1963) characterized the naturally fractured porous medium in terms of two parameters: storativity ratio, ω and interporosity flow parameter (matrix-fracture-coupling) λ. The parameter ω is a dimensionless quantity relating the fluid capacitance of the fractures to that of the combined system. The parameter λ is proportional to the ratio of matrix permeability to fracture permeability. Typical values of λ range from 10^{-3} to 10^{-9} where low values of λ indicate low fluid transfer between matrix and fractures. A homogeneously distributed porosity is considered to be the limiting case in the model. This happens when $\omega = 1$ or $\lambda = \infty$. FAST.RTA™ is capable of analyzing the dual porosity models by introducing the dual porosity parameters, interporosity flow parameter and storativity ratio.

4.3 Production Decline Analysis of Well RB_Z10a

The RB_Z10a production gas rates and well head flowing pressures were loaded into FAST. RTA™. The real production data is shown in figure 4.3, while Table 4.1 shows fluid and reservoir properties.

Table 4.1: Reservoir and fluid properties

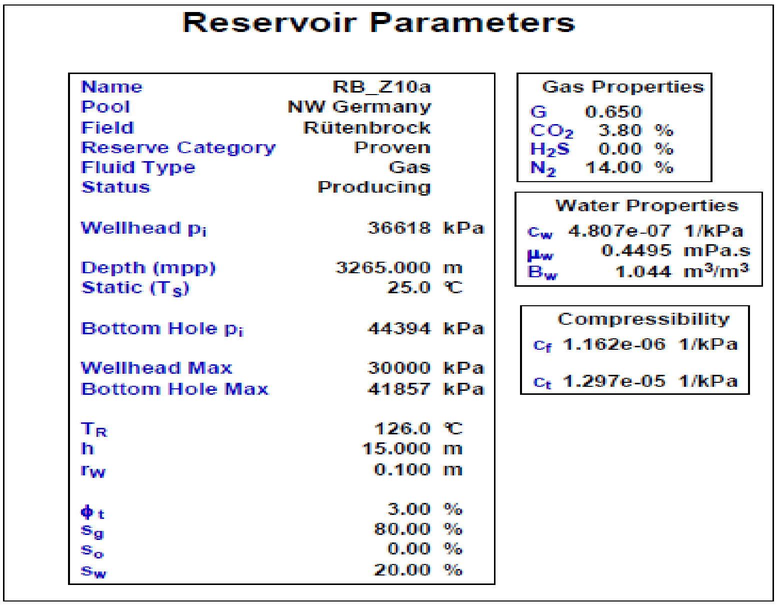

Reservoir Parameters

Name	RB_Z10a	
Pool	NW Germany	
Field	Rütenbrock	
Reserve Category	Proven	
Fluid Type	Gas	
Status	Producing	
Wellhead p_i	36618	kPa
Depth (mpp)	3265.000	m
Static (T_S)	25.0	℃
Bottom Hole p_i	44394	kPa
Wellhead Max	30000	kPa
Bottom Hole Max	41857	kPa
T_R	126.0	℃
h	15.000	m
r_w	0.100	m
ϕ_t	3.00	%
S_g	80.00	%
S_o	0.00	%
S_w	20.00	%

Gas Properties		
G	0.650	
CO_2	3.80	%
H_2S	0.00	%
N_2	14.00	%

Water Properties		
c_w	4.807e-07	1/kPa
μ_w	0.4495	mPa.s
B_w	1.044	m^3/m^3

Compressibility		
c_f	1.162e-06	1/kPa
c_t	1.297e-05	1/kPa

Using FAST.RTA™, the observed tubing head pressures were converted to bottom hole pressures at a depth of 3265m using the existing pressure loss correlations incorporated within FAST.RTA™. The calculated pressure difference between the bottom hole flowing pressure and the tubing head flowing pressure, by the existing pressure loss correlation, did not exceed 8 to 10 bar. To justify that, the pressure loss correlations handle the flow stream as a single phase (gas) while water was being there in the well flow column as vapour or second phase. It was concluded from the well modelling software Prosper that the difference between the flowing tubing head and flowing bottom hole pressure at RB_Z10a must between 15 and 30 bar, particularly in the tail-end phase. An excess pressure drop of 30 bar was therefore added to represent the water content in the gas or the hydrostatic loss from a suspected column of liquid at the bottom of the wellbore.

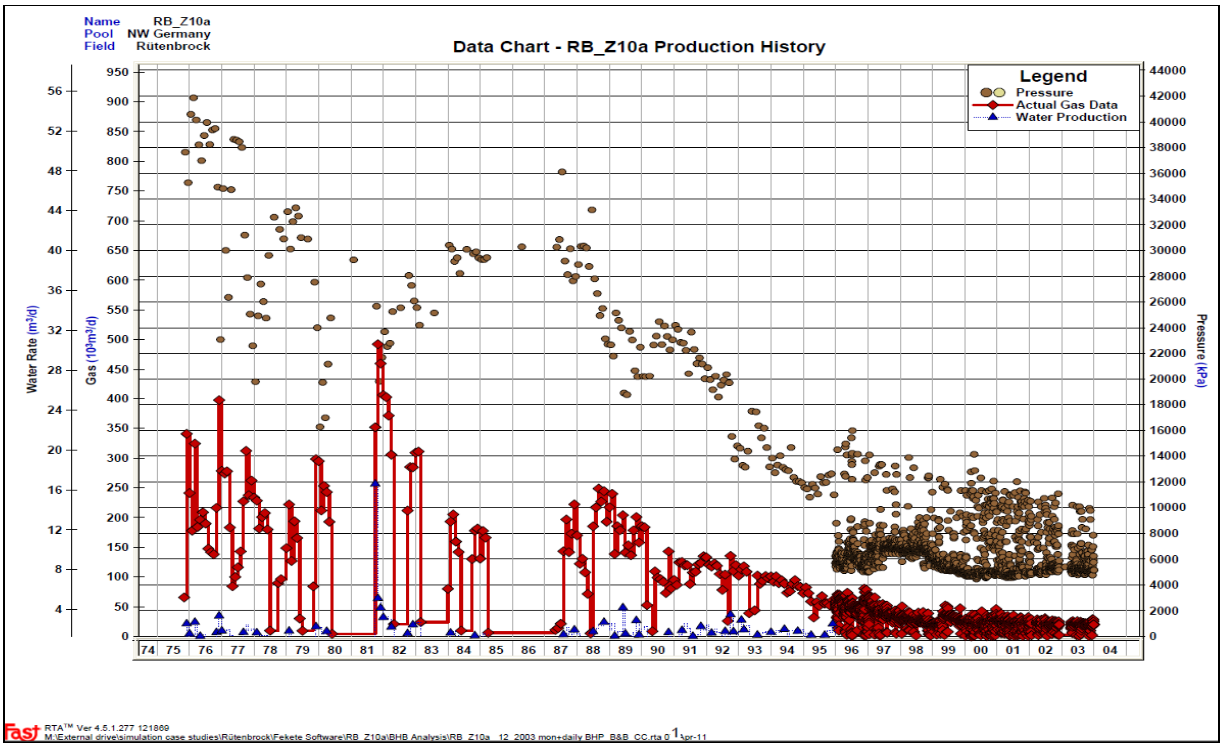

Fig. 4.3: Production history (RB_Z10a). Shown in this figure are the flowing bottom hole pressures (brown dots) which have been converted from the observed tubing head pressures & observed production rates (red curve) vs. time.

Results and Discussion

Figure 4.4 shows Arp exponential plot indicating reserves of approximately 1164 x10^6 m^3 and expected gas recovery of 960 x10^6 m^3. Arp decline analysis is an adequate technique to estimate the reserves assuming that the bottom hole flowing pressure is relatively constant with respect to time, especially at the tail-end of the production phase (2000 - 2004). The left side of Figure 4.4 demonstrates decline type and output parameters such as EUR (expected ultimate recovery), RR (remaining reserves) and (OGIP) Reserves. During the type curve analysis, RB_Z10a is assumed to be a hydraulically fractured well in the centre of a rectangular reservoir. In Wattenbarger type curve analysis, the fractures are assumed to extend to the drainage boundary of the well or the boundaries of the compartment.

Figure 4.5 and Appendix 2 show the production history using various type curve techniques including, Blasingame, Fetkovich, Agarwal and Gardner, Normalized Pressure Integral and Wattenbarger. The data plotted in the Blasingame plot uses Normalized rate integral and a derivative function to reduce the noise level. From the Blasingame and Fetkovich type analysis shown in figure 4.5 and Appendix 2, it is obvious that the production response consists of two distinct flow periods, a transient production followed by a pseudo-steady state (boundary dominated).

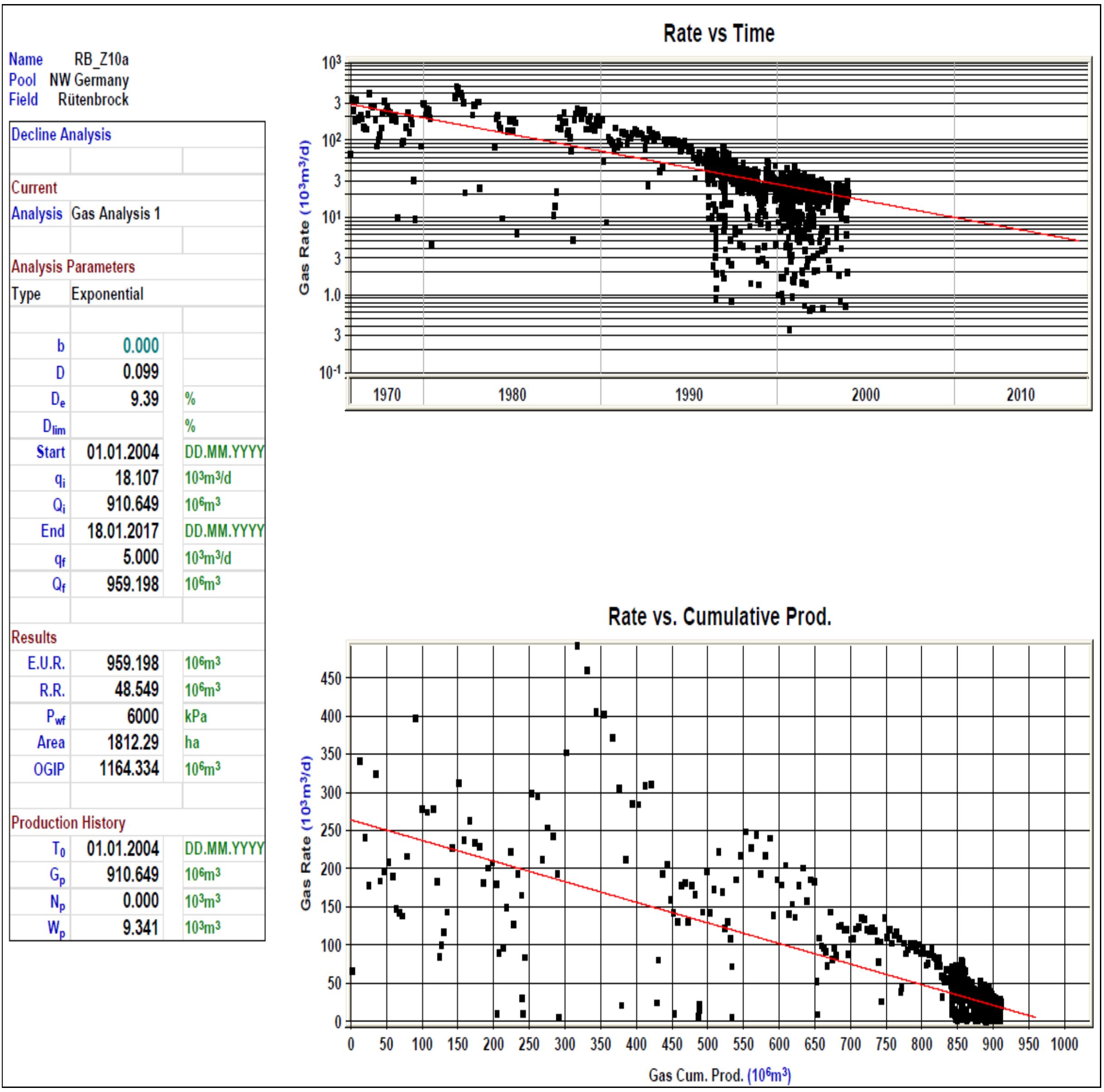

Name RB_Z10a
Pool NW Germany
Field Rütenbrock

Decline Analysis		
Current		
Analysis	Gas Analysis 1	
Analysis Parameters		
Type	Exponential	
b	0.000	
D	0.099	
D_e	9.39	%
D_{lim}		%
Start	01.01.2004	DD.MM.YYYY
q_i	18.107	$10^3m^3/d$
Q_i	910.649	10^6m^3
End	18.01.2017	DD.MM.YYYY
q_f	5.000	$10^3m^3/d$
Q_f	959.198	10^6m^3
Results		
E.U.R.	959.198	10^6m^3
R.R.	48.549	10^6m^3
P_{wf}	6000	kPa
Area	1812.29	ha
OGIP	1164.334	10^6m^3
Production History		
T_0	01.01.2004	DD.MM.YYYY
G_p	910.649	10^6m^3
N_p	0.000	10^3m^3
W_p	9.341	10^3m^3

Rate vs Time
Gas Rate (10³m³/d)
10³
3
10²
3
10¹
3
1.0
3
10⁻¹
1970
1980
1990
2000
2010
Rate vs. Cumulative Prod.
Gas Rate (10³m³/d)
450
400
350
300
250
200
150
100
50
0
0 50 100 150 200 250 300 350 400 450 500 550 600 650 700 750 800 850 900 950 1000
Gas Cum. Prod. (10⁶m³)

Fig. 4.4: Arp exponential plot (RB_Z10a): a semi log plot of rate vs. time and a Cartesian plot of rate vs. gas cumulative. In the left-hand side of the figure are the inputs and output parameters from Arp decline analysis. The outputs are the well reserves, expected ultimate recovery and rest recoverable reserves.

Commonly, in this production response sequence of a transient production followed by pseudo-steady state, different types of reservoir information can be obtained from each flow period. The transient flow period can provide information on the permeability thickness product of the well's drainage volume, an estimate of the wellbore skin factor, and an estimate of the drainage radius.

The pseudo-steady state period can be used to identify the onset of interference and forecast a production schedule and remaining reserves. From the Fetkovich plot (Fig. 4.5), there are two sets of curves that converge in the centre. Matching data on the left side provides information about the transient behaviour of the system while the right side provides information about the boundary dominated behaviour of the reservoir (reserves, area). Furthermore, from the early stages in the Blasingame plot (Appendix 2), the fracture properties are estimated. Table 4.2 gives a result summary of the various type curves match.

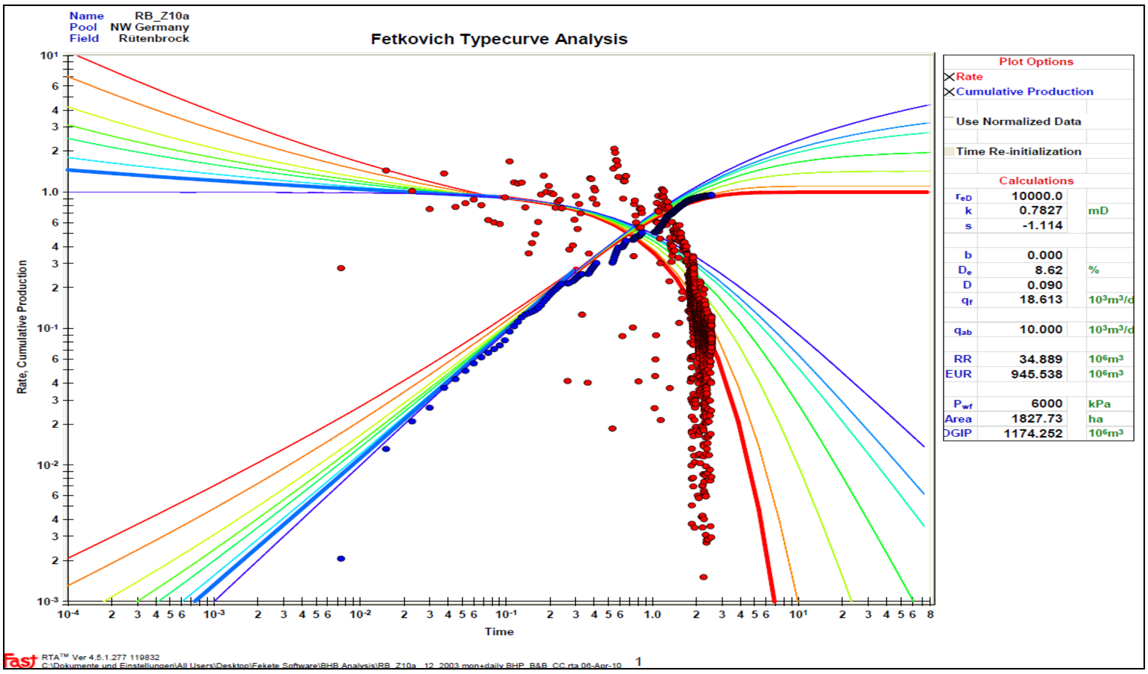

Plot Options

☒ Rate

☒ Cumulative Production

☐ Use Normalized Data

☐ Time Re-initialization

Calculations

r_{eD}	10000.0	
k	0.7827	mD
s	-1.114	
b	0.000	
D_e	8.62	%
D	0.090	
q_f	18.613	$10^3m^3/d$
q_{ab}	10.000	$10^3m^3/d$
RR	34.889	10^6m^3
EUR	945.538	10^6m^3
P_{wf}	6000	kPa
Area	1827.73	ha
OGIP	1174.252	10^6m^3

Fig. 4.5: Fetkovich type curve matched with RB_Z10a production history data. Two sets of data are shown, the well observed gas rate (red dots) and well observed cumulative gas (blue dots) vs. time. The production history data were fitted to one of the preplotted curves (red & blue curves). The results are in the right-hand side of the figure.

Table 4.2: RB_Z10a type curve analysis results from the application of various type curves.

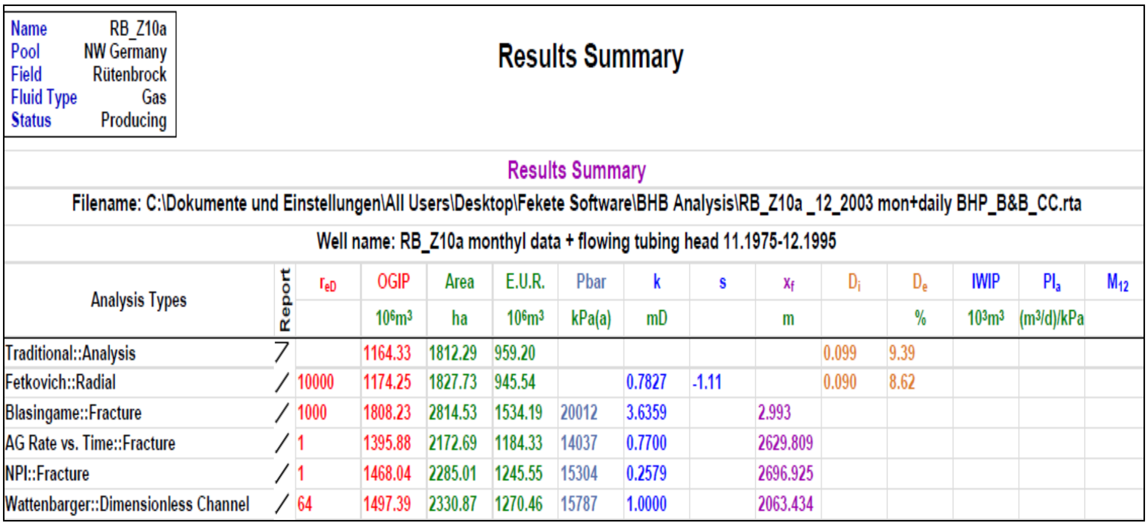

Name RB_Z10a
Pool NW Germany
Field Rütenbrock
Fluid Type Gas
Status Producing

Results Summary

Results Summary

Filename: C:\Dokumente und Einstellungen\All Users\Desktop\Fekete Software\BHB Analysis\RB_Z10a _12_2003 mon+daily BHP_B&B_CC.rta

Well name: RB_Z10a monthyl data + flowing tubing head 11.1975-12.1995

Analysis Types	Report	r_{eD}	OGIP	Area	E.U.R.	Pbar	k	s	x_f	D_i	D_e	IWIP	PI_a	M_{12}
			10^6m^3	ha	10^6m^3	kPa(a)	mD		m		%	10^3m^3	$(m^3/d)/kPa$	
Traditional::Analysis	☑		1164.33	1812.29	959.20					0.099	9.39			
Fetkovich::Radial	☑	10000	1174.25	1827.73	945.54		0.7827	-1.11		0.090	8.62			
Blasingame::Fracture	☑	1000	1808.23	2814.53	1534.19	20012	3.6359		2.993					
AG Rate vs. Time::Fracture	☑	1	1395.88	2172.69	1184.33	14037	0.7700		2629.809					
NPI::Fracture	☑	1	1468.04	2285.01	1245.55	15304	0.2579		2696.925					
Wattenbarger::Dimensionless Channel	☑	64	1497.39	2330.87	1270.46	15787	1.0000		2063.434					

The estimated parameters from various type curves are quite distinct, especially the reserves. The variations in the result were due to: a) decline curve analysis and the fact that type curve matching of gas well decline curves requires observed data from the wellbore (bottom hole pressure) whereas the available pressure data was flowing tubing head pressures. Accordingly, there were uncertainties in the calculated bottom hole pressure from tubing head pressures; b) the complexity of the naturally fractured reservoir is another possible cause, and thus the reservoir complication of a naturally fractured reservoir cannot be handled by a conventional type curve analysis.

RB_Z10a Analytical Model

Since there was a dissimilarity of the output from the conventional analysis, such as the reserves which were overestimated, there are other modelling alternatives available in FAST.RTA™ for such a complicated reservoir, for instance the analytical models option. The analytical model allows the creation of your own reservoir models, which cannot be handled by the conventional analysis, which represent the actual reservoir and which can be matched with the historical data. History is matched by creating a pressure match and a future forecast of rates at any specified pressure. Three analytical models were selected, supposed to be the best representative models of RB_Z10a's naturally fractured drainage area, the radial model, fracture model and composite model. The dual porosity model option was used during the pressure history match process. Matrix-fracture coupling factor of 1E-05 was used. The storativity ratio was calculated using Equation 4.2. The average matrix and fracture porosities were assumed to be 2.5 % and 0.5% respectively. The total compressibility of 1.2 e-5 bar^{-1} was evaluated by the existing correlation within FAST.RTA^{TM} software. The storativity value is 0.166.

$$\omega = \frac{(\phi.C_t.h)_1}{(\phi.C_t.h)_1 + (\phi.C_t.h)_2} \quad \ldots\ldots\ldots\ldots\ldots\ldots\ldots\ldots\ldots\ldots\ldots\ldots\ldots \quad (4.2)$$

where,

ω = storativity
$\phi_{1,2}$= matrix & fracture porosity
C_t = total compressibility
h = net pay thickness

The uncertainty parameters used to provide a match include initial reservoir pressure, reserves, reservoir parameters, fluid properties, well data and dual porosity parameters. With the exception of original gas in place, most of the required parameters were known either from reservoir and fluids data, well tests or reservoir simulation match results. From the pressure match, the production history was categorised into three phases, early phase, middle phase and tail-end phase which represent the production periods from 1975-1980, 1981-1994 and 1995-2003 respectively. In the bottom of the figure there is a zoom-in of the tail-end production phase pressure match. Figures 4.6 and Appendix 2 show that in the early and tail-end production phases, a good pressure match was obtained with the historical data, while a mismatch in the middle production phase was observed.

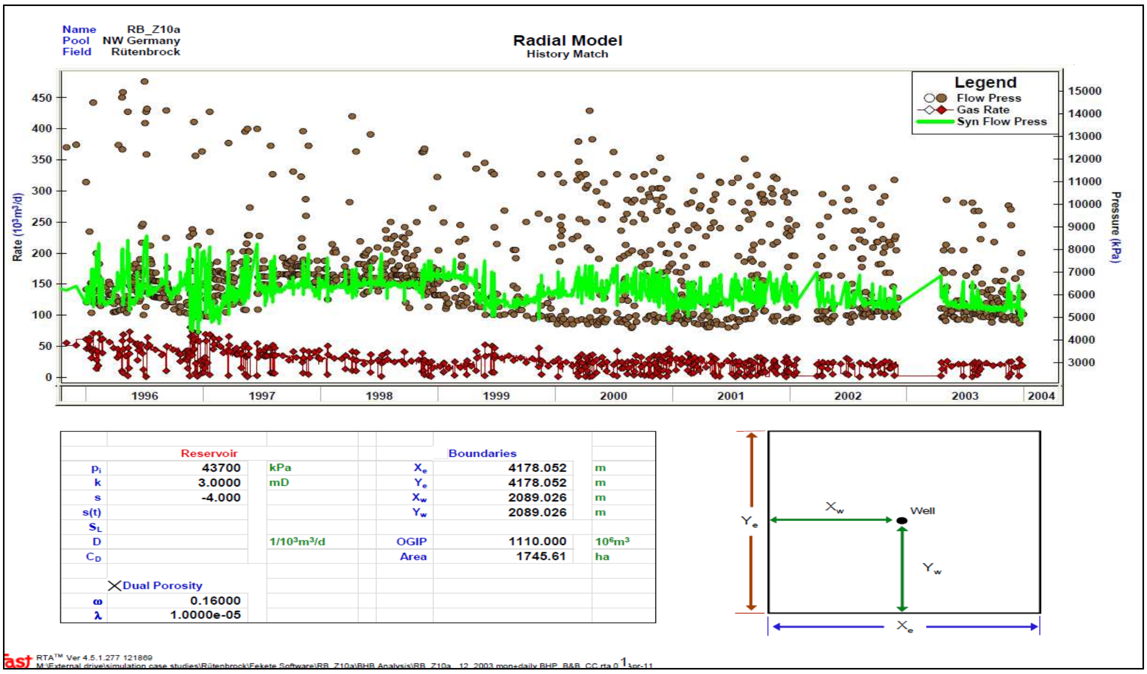

	Reservoir			Boundaries	
p_i	43700	kPa	X_e	4178.052	m
k	3.0000	mD	Y_e	4178.052	m
s	-4.000		X_w	2089.026	m
s(t)			Y_w	2089.026	m
S_L					
D		1/10³m³/d	OGIP	1110.000	10⁶m³
C_D			Area	1745.61	ha
	☒ Dual Porosity				
ω	0.16000				
λ	1.0000e-05				

Fig. 4.6: RB_Z10a analytical radial model. A zoom in of the RB_Z10a`s tail-end production phase, also shown a good pressure match between the pressure measurements and simulated pressure over the production period from 1996 to 2003. In bottom of the figure are the reservoir and dual porosity match parameters. Also

The production data may not plot on a single trend due to perturbation in field operations or other reasons, including 1) production turbulence due to the occurrence of several wells producing from same compartment and same times; 2) the fact that wellbore damage or recompletions lead to production response and well productivity alteration; 3) uncertainties regarding the bottom hole pressures that are converted from the well head pressure. Figure 4.6 and Appendix 2 demonstrate that the given well reserves (OGIP) of 1100 x 10^6 m^3 resulted in a good pressure match in early and tail-end production phases in the radial, fracture and composite analytical models. The significant production phase for identifying the well potential and forecast the future production is the tail-end phase. Pressure match parameters of reservoir, dual porosity, fractures and well data are shown at the bottom of the figure.

Production Forecasts Based on the well RB_Z10a Analytical Model

FAST.RTA™ is able to forecast the well potential. The observed cumulative gas production from RB_Z10a until 12/2003 was 910 x 10^6 Sm^3. Two production forecast scenarios were applied to investigate the multiphase pump impact on the performance of the well RB_Z10a: continuous application of conventional compression production system (CC) and multiphase pump (MPP) over the production time 01/2004 to 03/2006 using an abandonment gas rate of 20000 Sm^3/day. The final flowing bottom hole pressure measurement at the end of 2003 was 51 bar. To perform a production forecast, the bottom hole pressure for CC scenario was adjusted to 48 bar (flowing bottom hole pressure) which is equivalent to 13 bar (the minimum reduction limit of the well head pressure).

For MPP scenario 35 bar (flowing bottom hole pressure) was used for approximately 2 bar at the wellhead. The forecast results illustrate that RB_Z10a is able to produce cumulative gas of 5 x 10^6 Sm^3 from a continuous CC production system and 20 x 10^6 Sm^3 from continuous application of MPP. Well RB_Z10a actual cumulative gas production (MPP+CC) from 01/2004 to 03/2006 was 16.49 x 10^6 Sm^3. If the forecast results were compared with the actual production for the production period 2004 -2006, a reduction of -70 % if CC forecast scenario was applied (Fig. 4.7 & Appendix 2). In contrast, an increase in cumulative gas production as results of the MPP utilize in the forecast simulations (Fig. 4.8 & Appendix 2).

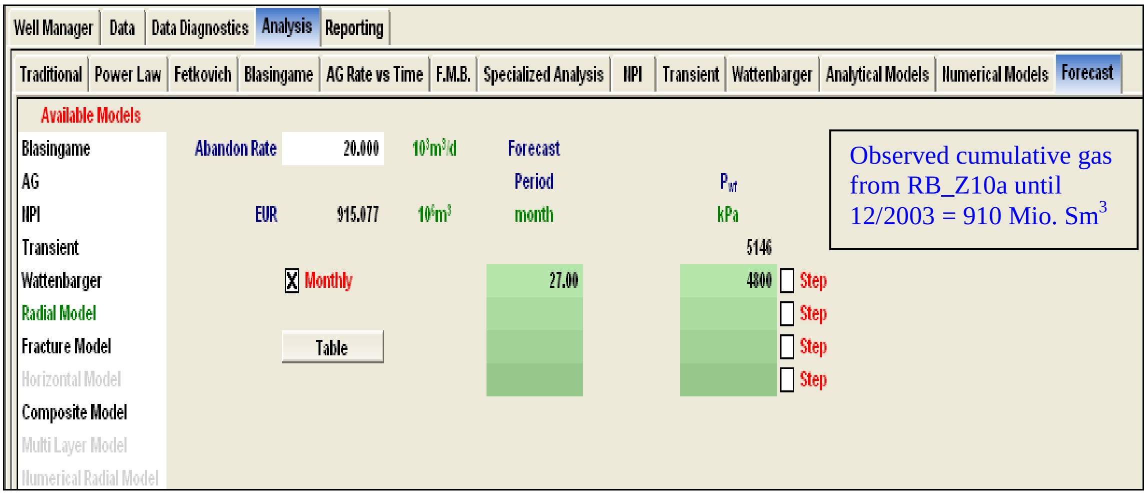
Well Manager
Data
Data Diagnostics
Analysis
Reporting
Traditional
Power Law
Fetkovich
Blasingame
AG Rate vs Time
F.M.B.
Specialized Analysis
NPI
Transient
Wattenbarger
Analytical Models
Numerical Models
Forecast
Available Models
Blasingame
AG
NPI
Transient
Wattenbarger
Radial Model
Fracture Model
Horizontal Model
Composite Model
Multi Layer Model
Numerical Radial Model
Table

Abandon Rate 20.000 $10^3m^3/d$

EUR 915.077 10^6m^3

☒ Monthly

Forecast Period month: 27.00

P_{wf} kPa: 5146

4800 ☐ Step

☐ Step

☐ Step

☐ Step

Observed cumulative gas from RB_Z10a until 12/2003 = 910 Mio. Sm^3

Fig. 4.7: Analytical radial model (RB_Z10a): CC forecast results (01/2004-03/2006). A 70% reduction of the gas cumulative as a result of the CC use compared with the actual cumulative gas, also the RB_Z10a would shut-down in 2004. **) EUR = expected ultimate recovery; Pwf= flowing bottom hole pressure.*

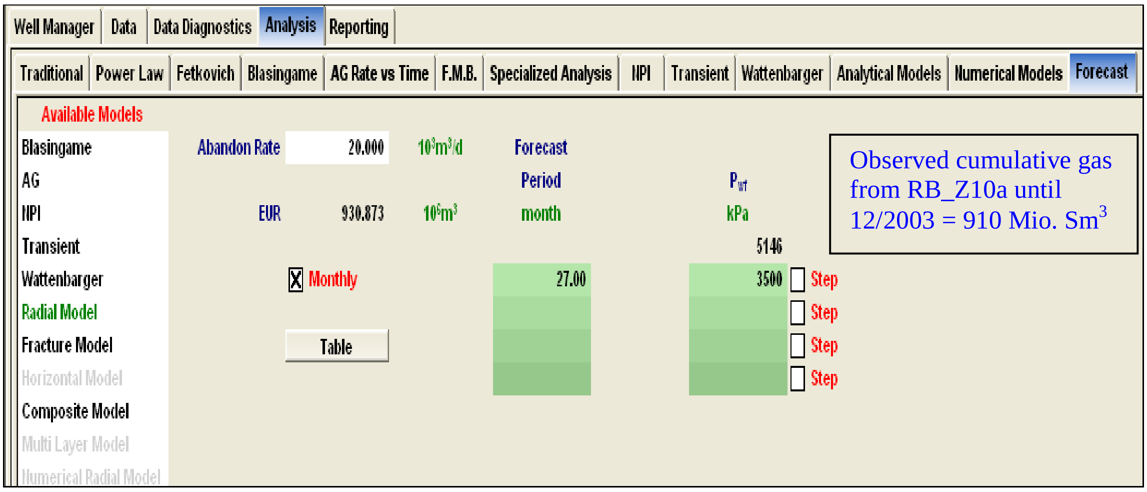
Well Manager
Data
Data Diagnostics
Analysis
Reporting
Traditional
Power Law
Fetkovich
Blasingame
AG Rate vs Time
F.M.B.
Specialized Analysis
NPI
Transient
Wattenbarger
Analytical Models
Numerical Models
Forecast
Available Models
Blasingame
AG
NPI
Transient
Wattenbarger
Radial Model
Fracture Model
Horizontal Model
Composite Model
Multi Layer Model
Numerical Radial Model
Table
☐ Step
☐ Step
☐ Step
☐ Step

Abandon Rate 20.000 $10^3 m^3/d$

EUR 930.873 $10^6 m^3$

☒ Monthly

Forecast Period month: 27.00

P_{wf} kPa: 5146; 3500

Observed cumulative gas from RB_Z10a until 12/2003 = 910 Mio. Sm^3

Fig.4.8: Analytical radial model (RB_Z10a): MPP forecast results (01/2004-03/2006) - The application of MPP resulted of a cumulative gas higher than that from the actual production history until 03/2006.
**) EUR = expected ultimate recovery; Pwf= flowing bottom hole pressure.*

4.4 Production Decline Analysis of Well OT_Z02

Production decline analysis was carried out for well OT_Z02 because of its location at the crest of the structure adjacent to RB_Z10a. OT_Z02 was also producing during the MPP phase 01/2004 – 03/2006. The production analysis for OT_Z02, prior to MPP phase and up to the end of 2003, is significant for the investigation of the MPP effect on neighbouring wells and also on the entire compartment. The decline curve analysis was performed using FAST.RTA™ for the inquiry of possible negative or positive production response at well OT_Z02. Production history data from1994 to 2003 has been loaded into FAST.RTA™. The actual cumulative gas production measurements from OT_Z02 until 12/003 and 10/2009 were 160 x 10^6 Sm^3 and 190 x 10^6 Sm^3 respectively. Historical production data matches with the various type curve method are shown in Figure 4.9 and Appendix 2.

The estimated reserves and expected gas recovery can be obtained from the type curves match shown on the right hand side of the figures. The comparison of the match results indicated the presence of production interference. The summary of type curve match results from the production period up to 12/2003 is shown in Table 4.3. The maximum estimated well reserve is 223 x 10^6 m^3, while the EUR maximum value was 180 x 10^6 m^3 i.e. 10 x 10^6 m^3 a reduced amount compared with the actual cumulative gas production of 190 x 10^6 m^3 up to 10/2009. The MPP operations in RB_Z10a had a positive impact on the performance of OT_Z02. These results demonstrate that the multiphase pumping facility had a positive impact on OT_Z02 gas recovery. A decline curve analysis was also performed for the well RB_Z05 and the estimated gas in place of RB_Z05 is estimated to be 550 x 10^6 m^3.

The cumulative reserves of all wells located in the main compartment are approximately 1.96 x 10^9 m^3.

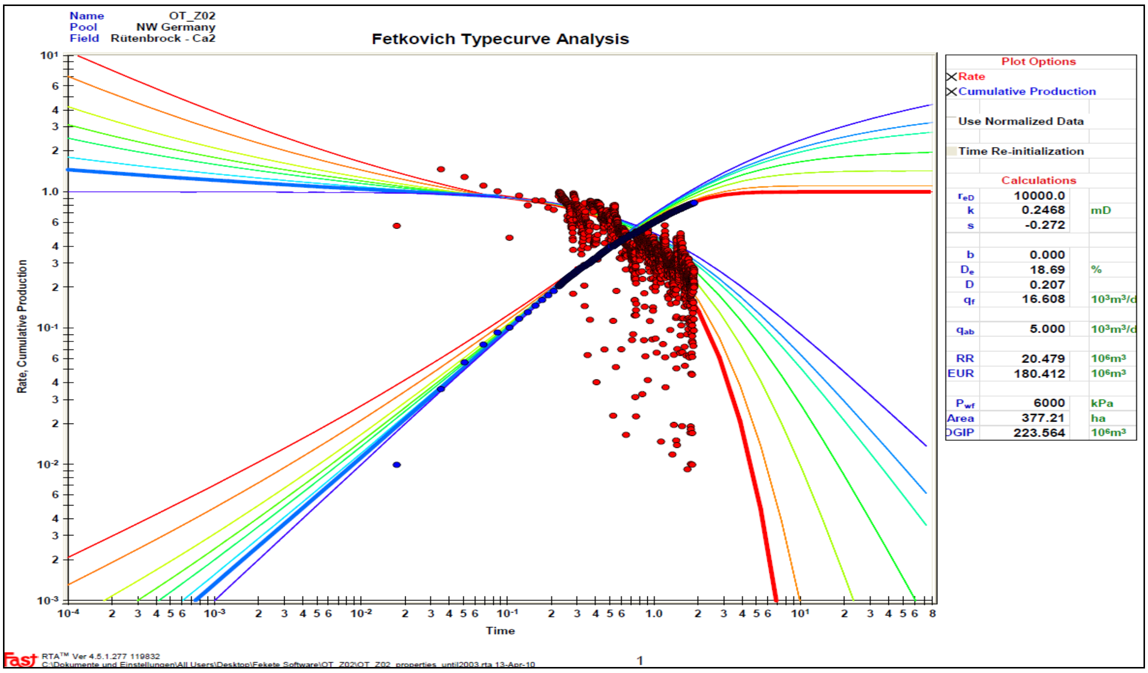

Calculations

r_{eD}	10000.0	
k	0.2468	mD
s	-0.272	
b	0.000	
D_e	18.69	%
D	0.207	
q_f	16.608	10³m³/d
q_{ab}	5.000	10³m³/d
RR	20.479	10⁶m³
EUR	180.412	10⁶m³
P_{wf}	6000	kPa
Area	377.21	ha
OGIP	223.564	10⁶m³

Fig. 4.9: Fetkovich type curve matched with OT_Z02 production history data. Two sets of data are shown, the well observed gas rate (red dots) and well observed cumulative gas (blue dots) vs. time. The production history data were fitted to one of the preplotted curves (red & blue curves). The results are in the right-hand side of the figure.

Table 4.3: OT_Z02 - type curve analysis results from various type curves.

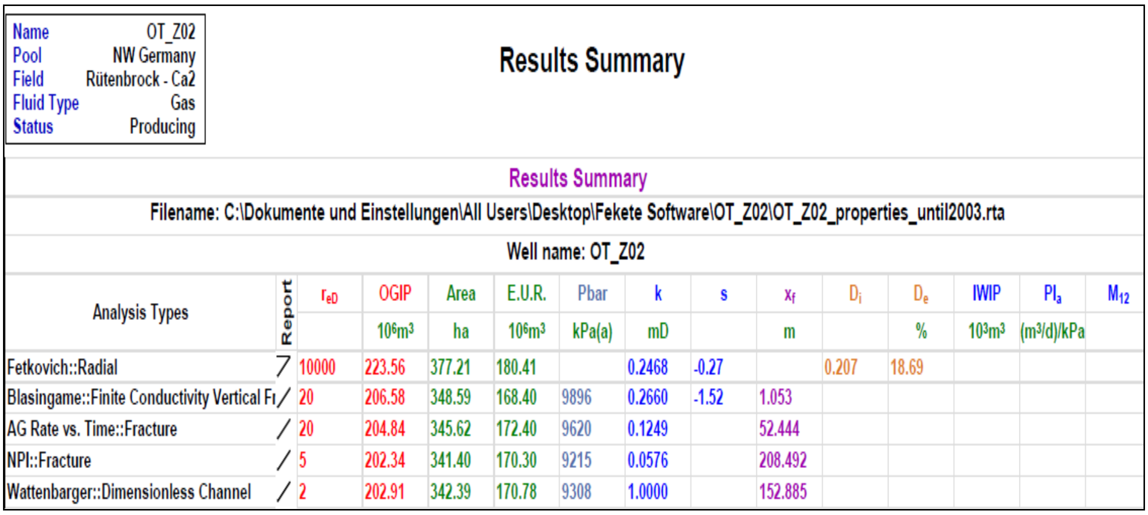

Name	OT_Z02
Pool	NW Germany
Field	Rütenbrock - Ca2
Fluid Type	Gas
Status	Producing

Results Summary

Results Summary

Filename: C:\Dokumente und Einstellungen\All Users\Desktop\Fekete Software\OT_Z02\OT_Z02_properties_until2003.rta

Well name: OT_Z02

Analysis Types	Report	r_{eD}	OGIP	Area	E.U.R.	Pbar	k	s	x_f	D_i	D_e	IWIP	PI_a	M_{12}
			10⁶m³	ha	10⁶m³	kPa(a)	mD		m		%	10³m³	(m³/d)/kPa	
Fetkovich::Radial	✓	10000	223.56	377.21	180.41		0.2468	-0.27		0.207	18.69			
Blasingame::Finite Conductivity Vertical Fı	✓	20	206.58	348.59	168.40	9896	0.2660	-1.52	1.053					
AG Rate vs. Time::Fracture	✓	20	204.84	345.62	172.40	9620	0.1249		52.444					
NPI::Fracture	✓	5	202.34	341.40	170.30	9215	0.0576		208.492					
Wattenbarger::Dimensionless Channel	✓	2	202.91	342.39	170.78	9308	1.0000		152.885					

CHAPTER V: Reservoir Dynamic Simulation

Simulation is one of the most powerful tools for guiding reservoir management decisions. From planning early production wells and designing surface facilities, to diagnosing problems with enhanced recovery techniques, reservoir simulations allow engineers to predict and visualize fluid flow more efficiently than ever before. Reservoir simulation in the oil and gas industry has become the standard practice for solving reservoir engineering problems. Simulators have been developed for various recovery processes and continue to be developed for new oil and gas recovery processes. Reservoir simulation is the art of combining physics, mathematics, reservoir engineering, and computer programming to develop tools for predicting hydrocarbon reservoir performance under various operating conditions.

The function of a reservoir simulation is helping engineers to understand the production pressure behaviour of a reservoir and consequently to predict future performance (production rates) as a function of time. The future production schedule, when expressed in terms of revenues and compared with costs and investments, helps managers determine both economically recoverable reserves and the limits of profitable production. Once the goal of simulation is determined, the next step is to describe the reservoir in terms of the volume of hydrocarbons, the amount that is recoverable and the rate at which it will be recovered. To estimate recoverable reserves, a model of the reservoir framework, including faults and layers and their associated properties, must be constructed.

To perform the numerical reservoir simulation, Eclipse program was used. Eclipse is the Schlumberger reservoir simulator for black oil and compositional and it is widely used in the industry. The geological 3D model has been constructed by the geologist in the team and was a simplified representation, based on the existing data, of relatively complex natural bodies. The dynamic model was created by integrating the rock, fluid properties, flow functions and production history data on the basis of the Hauptdolomit 3D geological model.

5.1 Data Validation & Evaluation

The accurate and efficient simulation of subsurface conditions requires a blend of physical modelling of subsurface processes and careful numerical implementation. Dynamic data typically available for any study consists of engineering information (production history from all wells, PVT data, pressure build-up analysis tests, SCAL data, and well completions for all production wells). For the description of the Hauptdolomit rock/fluid properties and production history, the collected dynamic data was included historical gas & water flow rates, static/flowing bottom hole and tubing head pressure measurements, gas & water compositions, a number of pressure build-up tests, and well completion data (depths and tubing/casing details, deviation surveys). The available dynamic data was filtered, screened and validated.

Porosity/Permeability Correlation

The porosity and permeability of Stassfurt-Carbonate (Ca2) are generally poor (Taylor, 1986). Clark (1980; 1984) has studied the reservoir potential of the slope facies and determined that a good primary porosity is often reduced by cementation, especially by anhydrite or halite, but is locally enhanced by the creation of a secondary solution (porosity) by late diagenetic process. A number of thin sections were collected from the main compartment and have been analysed by the team geologist, who demonstrated that primary matrix porosity is filled with cement to a nearly zero percent value. But, during the late diagenetic process, the primary porosity was enhanced by the creation of the secondary porosity as a series of narrow extended laterally channels. The channels are short and well connected in laterally. The vertical communications between the lateral layers are ensured by the fracture system. Also observed from the thin section, the fractures were partially cemented which indicates the reduction in fracture permeability of the Hauptdolomit reservoir compared to the standard fracture permeability.

Porosity and permeability values were obtained from wire line logs and core data respectively. The available log and core data were combined for comparison and in order to compensate for the depth shift between the holes before core-log data integration to develop porosity - permeability correlation. As logging depths are known to be accurate, the depths of recovered cores were adjusted to the down hole logging depth by graphically correlating obvious peaks and troughs in the porosity - depth profile.

The Hauptdolomit reservoir represents a naturally fractured dolomite formation, i.e. dual porosity/permeability system according to the evaluation of core data and thin section analysis. Figure 5.1 demonstrates that two trends can be identified: a trend of high permeability & low porosity (fractures) and a trend of low permeability & high porosity (matrix). The evaluation of core data proves that only for a matrix system, porosity/ permeability correlation can be derived. The following empirical formula was obtained from the core data for the calculation of matrix permeability:

$$K_m = 0.0184 * e^{0.538 * \phi} \quad \ldots\ldots\ldots\ldots\ldots\ldots\ldots\ldots\ldots\ldots\ldots\ldots (5.1)$$

Because of the wide range of variation in the core samples' fracture permeability measurements, no accurate empirical correlation of fracture permeability could be derived due to the suspicion that breaks in the core plugs might occur during the coring process.

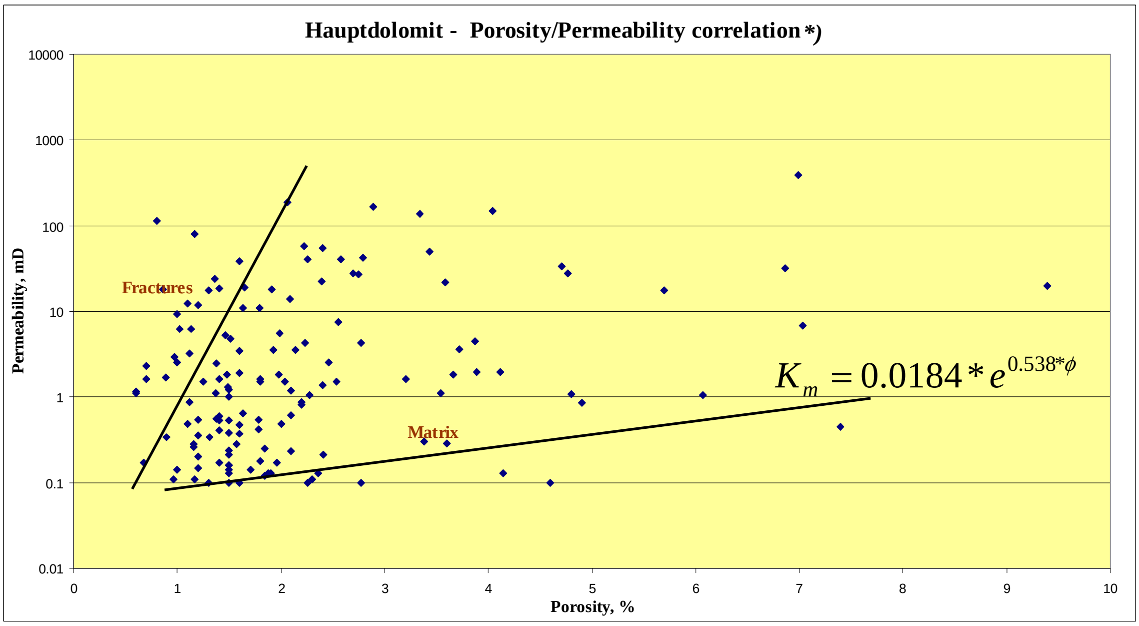

Fig. 5.1: Hauptdolomit reservoir core data. Semi log plot (porosity vs. permeability) was used for the purpose of the derivation of porosity/permeability correlation. Two trends were identified which represent a dual porosity system. **) The evaluation of the Poro/Perm correlation is based on the study of Thomas Franzen (member of the MPT project)*

Therefore, fracture permeability has been treated as a history match parameter and is expected to be low due to cementation, as concluded from the thin section analysis. Following Nelson (2001), the fracture porosity was supposed to be in the low range (0.3 - 0.5 %) due to the compaction effect resulted from the high reservoir depth (3200 - 3700 m).

Initial Water Saturation Evaluation

Generally, the initial water saturation S_{wi} is determined from logs and compared with the Lab measurements (core analysis). Due to the fact that a few values of initial water saturation were obtained from Lab measurements, the initial water saturation was also calculated from the logs for comparison and verification. Field experience worldwide suggests that the lower the porosity, the higher the water saturation, and vice versa (Archie, G. E. 1950). The standard corrections to sonic porosity values and formation water resistivity were applied and initial water saturation has been calculated from the resistivity and sonic logs according to Simandoux (1963):

$$S_w = \left(\frac{0.4 R_w}{\phi^2}\right)\left[\sqrt{\left(\frac{V_{sh}}{R_{sh}}\right)}^{2} + \frac{5\phi^2}{R_t R_w} - \frac{V_{sh}}{R_{sh}}\right] \quad \ldots\ldots\ldots\ldots\ldots\ldots\ldots\ldots\ldots \text{(5.2)}$$

where,

S_w : Water saturation, fraction
R_w : Formation water resistivity, ohm-m
ϕ : Porosity, fraction
V_{sh} : Shale volume, %
R_t : True formation resistivity, ohm-m
R_{sh} : Shale resistivity, ohm-m

Figure 5.2 is a cross-plot of matrix initial water saturation versus matrix porosity of well RB_Z10a which was selected as a reference well because its porosity values cover approximately the porosity range of the Hauptdolomit reservoir. According to Archie (1952), high porosity contains low water saturation and vice versa. This principle is demonstrated in figure 5.2.

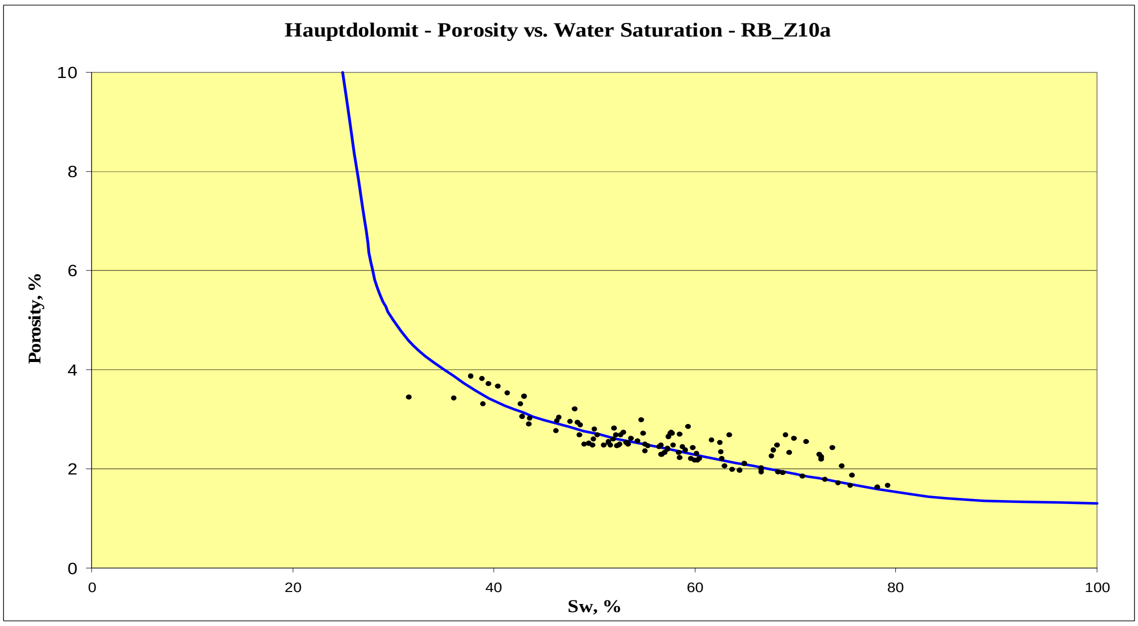

Fig. 5.2: Matrix initial water saturation (from logs) vs. matrix porosity (RB_Z10a). High water saturation is observed between 40 - 80%. There is uncertainty in the calculated water saturation from logs due to the limited availability of accurate electrical property data.

As shown in Figure 5.2, high initial water saturation was calculated in this way, whereas low initial water saturation values between 15 and 30 percent were measured in the laboratory. By comparing the calculated Sw_i from logs with those from the available Lab measurements, the average initial water saturations from well logs and laboratory measurements had values of 50 and 20 percent respectively. Initial water saturation calculated from logs is sometimes inaccurate due to the limited availability of accurate "a", "m" and "n" electrical property data to calibrate field resistivity logs and a concentration effect on the dissolved solids present in solution in the remaining low water saturation.

Establishment of Low Initial Water Saturations in Low Matrix Porosity /Permeability Media

The establishment of low initial water saturations in low matrix permeability/porosity porous media was due to:

1) With respect to the thin section analysis, as the internal pore surface area is related to irreducible (initial) water saturation, a small internal pore surface area was observed and illustrated by the thin sections. Consequently, small internal pore surface area was able to contain a small amount of water i.e., low initial water saturation
2) Bennion et al., (2000; 2002; 2004) introduced a number of theories for the establishment mechanism of subnormal saturation conditions in low permeability porous media, all of which have a common initial progression sequence that includes: a) deposition of the original reservoir sediments in some type of marine (100 % water saturated) environment (Fig. 5.3a); b) initial influx of hydrocarbon gas into the pay zone, resulting in displacement of the water saturation down to the initial ‘irreducible’ level, as governed by the capillary equilibrium of the system at that time (Fig. 5.3b); c) physical disconnection of the reservoir sediments from active capillary equilibrium with a free water/aquifer recharge source. Possible events would include faulting and tectonics, upheaval erosion and reburial, macro fracturing resulting in large capillary disconnected fault blocks or regional drainage of the initial contacting aquifer (Fig. 5.3c).

Divergent theories exist as to the next transitional phase, which results in the removal of all, or a portion of, the remaining trapped/bound water in the rock to result in an ultimate subnormal saturated condition. They include; 1) ultra high capillary pressure motivated hygroscopic extraction of the water saturation into highly hydratable associated shales in contact with the formation (Bennion et al., 2002); 2) diagenetic and pore system changes associated with increased overburden pressure, compression, mineral formation (cementation and overgrowths) as well as long-term formation of authigenic pore filling clays resulting in a reduction of apparent reservoir quality (and increase in capillary potential), in the absence of recharge from an active water source (Bennion et al., 2002); 3) dehydration (evaporation) of the water saturation by transfer into a non-equilibrium gas phase over extended geological time due to extensive regional migration of undersaturated gas through the sediments of interest (Fig.5.3d) (Bennion et al., 2002).

The theory with the greatest degree of physical support from both a laboratory and field perspective is that of desiccation effects caused by long term regional migration of undersaturated gas from source rock to the ultimate gas producing intervals resulting in gradual transfer of water saturation from liquid to gas phase that resulted in current reservoir environment of low permeability combined with low initial water saturation (Bennion et al., 2002).

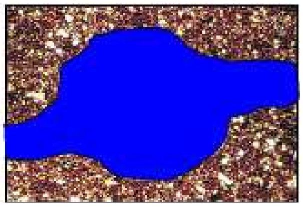

Fig. 5.3a: Original deposition of sediments inmMarine environment

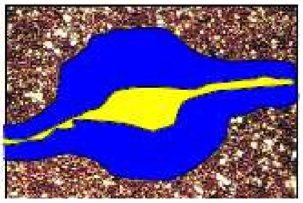

Fig. 5.3b: Primary gas influx and displacement to capillary Swirr

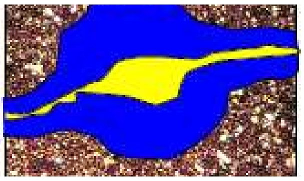

Fig. 5.3c: Hydraulic disconnection from active water recharge/contact

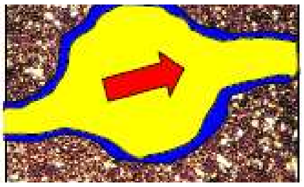

Fig. 5.3d: Long-term regional gas migration dehydrates water saturation to capillary Swirr subnormal level

Fig. 5.3: Illustration of the mechanism of low water saturation creation in porous media (after Bennion et al 2002).

The high initial water saturations obtained from logs is a consequence of the resistivity of the formation water, resulting from the unknown composition of the formation water in the reservoir. This process can be seen to have a concentration effect on the dissolved solids present in solution in the remaining trapped water. For example, assuming that deposition of the sediments with a salinity of approximately 50,000 ppm and if desiccation occurs as a result of the regional gas long term migration, reducing the water saturation from an average initial value of 50 % to 15 %. This will result in a concentration of the soluble salts in the brine into the remaining water saturation, and an increase in the salinity of the remaining brine saturation to 200,000 ppm. This obviously causes a significant reduction in the apparent resistivity of the formation water, resulting in the prediction of much higher water saturation than is, in reality, present in the reservoir (using conventional log parameters).

Based on the above, the low initial water saturations from laboratory measurements which varied between 15 and 30 % were used in the dynamic simulation. To obtain reasonable initial water saturation distribution and accomplish a realistic description of flow, different methods such as average value, grouping or in normalized form have been considered. The distribution of matrix initial water saturation by grouping based on porosity groups was selected due to its suitability in the corresponding simulation history match results. Initial water saturation of the fractures was determined to be between 2 - 4 % (Crain, 2000).

Fluid Properties (PVT model)

The fluid model[*)] was generated using PR – EOS (Peng-Robinson equation of state). The EOS determines fluid properties at different fluid pressure, temperature and composition. PVT analysis of fluid samples from all gas wells was evaluated to generate a representative PVT model. The gas composition is illustrated in Table 5.1.

Table 5.1: Hauptdolomit initial gas composition

Compartment	He vol%	N_2 vol%	CO_2 vol%	H_2S vol%	C1 vol%	C2 vol%	C3 vol%	nC4 vol%	iC4 vol%	nC5 vol%	iC5 vol%
Compartment 1 (RB_Z09)	0.12	14	3.8	0.004	81.6	0.39	0.04	0.02	0.01	0.01	0.006
Compartment 2 (RB_Z06)	0.07	4.05	4.57	0.00042	90.88	0.33	0.04	0.02	0.01	0.01	0.019
Compartment 3 (RB_Z13)	0.17	34	6.29	0.0004	58.78	0.27	0.04	0.02	0.01	0.01	0.019
Compartment 4 (RB_Z09)	0.12	14	3.8	0.004	81.6	0.39	0.04	0.02	0.01	0.01	0.006
Compartment 5 (RB_Z08)	0.07	19.25	4.58	0.0006	75.76	0.29	0.02	0.01	0.01	0.009	

The PVTp program from Petroleum Experts software was used for fluid modelling. Different PVT tables were generated due to the dissimilarity in the main gas composition components (Methane, N_2, and CO_2). Well RB_Z09 was the representative PVT data in the main compartment because of its location. Also, RB_Z09 was used to represent compartment 4 due to identical gas composition and depth of both compartments. No Lab measurement data was available to match the generated PVT model. The laboratory evaluation of the fluids showed Hauptdolomit reservoir gas to be dry gas at its initial pressure and was considered a sour gas because there was initially more than 4 ppm of H_2S content in the initial gas composition. Dry gases are predominantly composed of methane and non-hydrocarbons such as nitrogen and carbon dioxide. Figure 5.4 shows the phase envelope plot of the reservoir dry gas. The phase envelope is relatively tight and mostly located below ambient temperature. Note that the gas did not remain single phase from the reservoir to the separator conditions due to the condensed water and associated produced reservoir water. Water, however, condensed at the well and in surface conditions due to the change in pressure and temperature. Reservoir water properties were entered into the simulator.

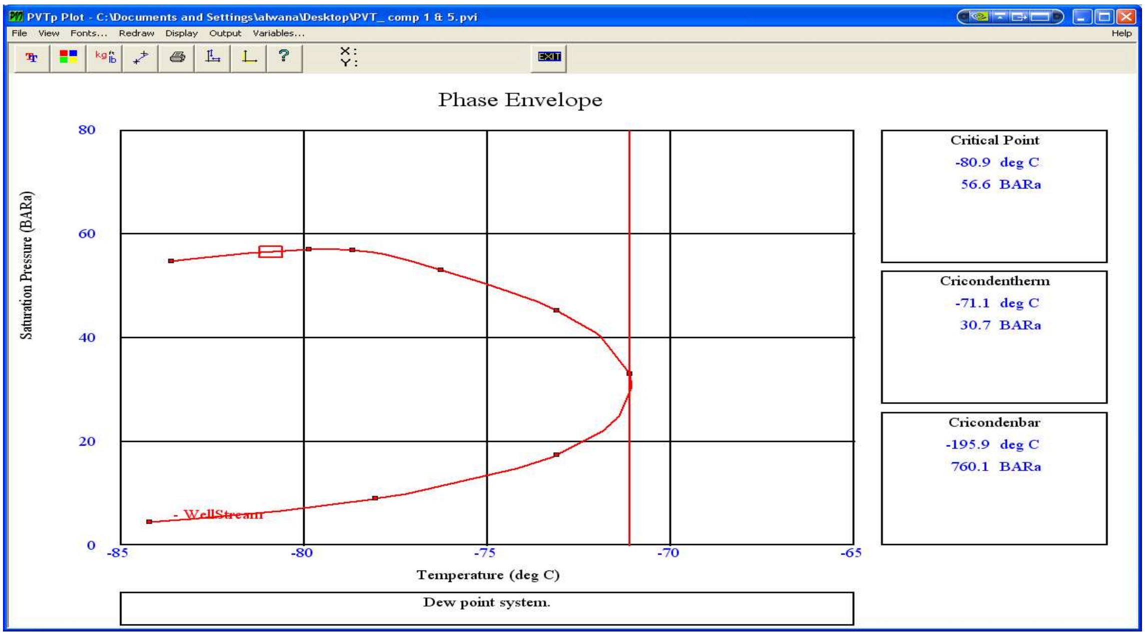

Critical Point
-80.9 deg C
56.6 BARa

Cricondentherm
-71.1 deg C
30.7 BARa

Cricondenbar
-195.9 deg C
760.1 BARa

Dew point system.

Fig. 5.4: Phase diagram of well RB_Z09. *) *The validation of the PVT model is based on the study of Thomas Franzen (member of the MPT project)*

Free Water Level (FWL) Estimation

The manner in which the fluid contacts in general can be located requires knowledge of fluid pressure regimes in the reservoir. No observations of the level at which gas water contact (GWC) could be located, thus they were primarily based on pressure gradient analysis. FWL at the main compartment was estimated from the calculation of the gas and water pressure gradients versus depth using different water salinities. PVTp program from Petroleum Experts software was used to calculate the compositional gradient of gas aligned with depth. The compositional gradient calculates the changes in composition (gas density) with depth, and consequently gas pressure gradient. The intersection of the gradients provides the free water level at 3722 mNN depth in the main compartment (Fig. 5.5).

The GWC depth in various compartments was treated as a history matching parameter. Using the pressure gradient means of evaluation, the FWL at compartments 2 & 5 were at depths of 3855 and 3637 mNN respectively. Non unique GWC depth for the various compartments and different estimated GWC depths indicated isolated compartments created by tectonic movements.

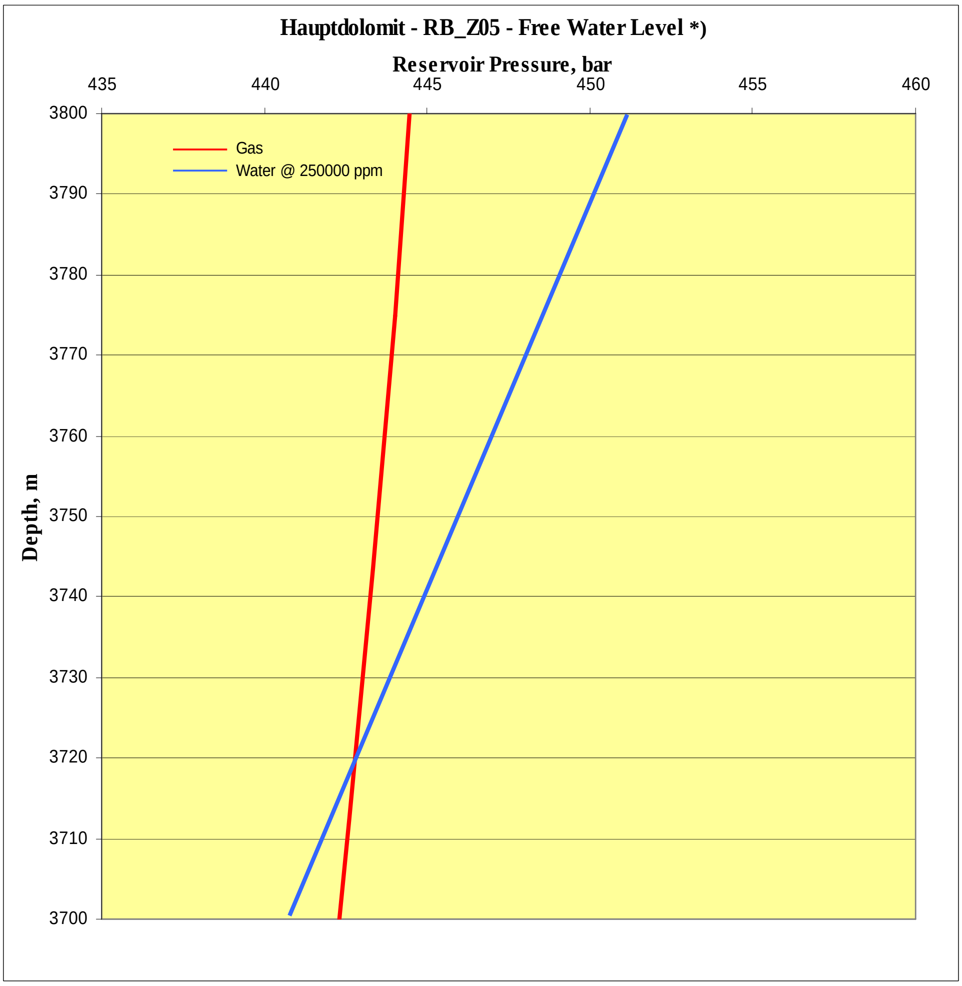

Fig.5.5: Free Water Level (FWL) @ the main compartment based on the gas and water pressure gradients. The red line is the gas pressure gradient; the blue is water pressure gradient. The FWL is where the gas and water pressure gradients are equals. **) The evaluation of the FWL is based on the study of Thomas Franzen (member of the MPT project)*

Water Content of Natural Gas

Natural gas reservoirs always have water associated with them, thus gas in the reservoir is water saturated. When gas is produced, water is produced as well. Some of this water is produced from the reservoir directly. Other water produced with the gas is formed by condensation due to the changes in pressure and temperature during production. Water vapour is the most common contaminant in natural gas. The water content of a gas is a function of pressure, temperature, composition, and the salt content of the free water. During the history match simulations the condensed water might a mismatch cause between the historical production data and the simulation output, therefore water content of natural gas*) was calculated and removed from the natural gas before starting the simulation. To calculate the water contents of natural gases with corrections for salinity and density, the correlation after McKetta and Wehe (1958) was used.

Mcketta et al., (1958) proposed a correlation to estimate the water content of natural gas based on experimental data available.

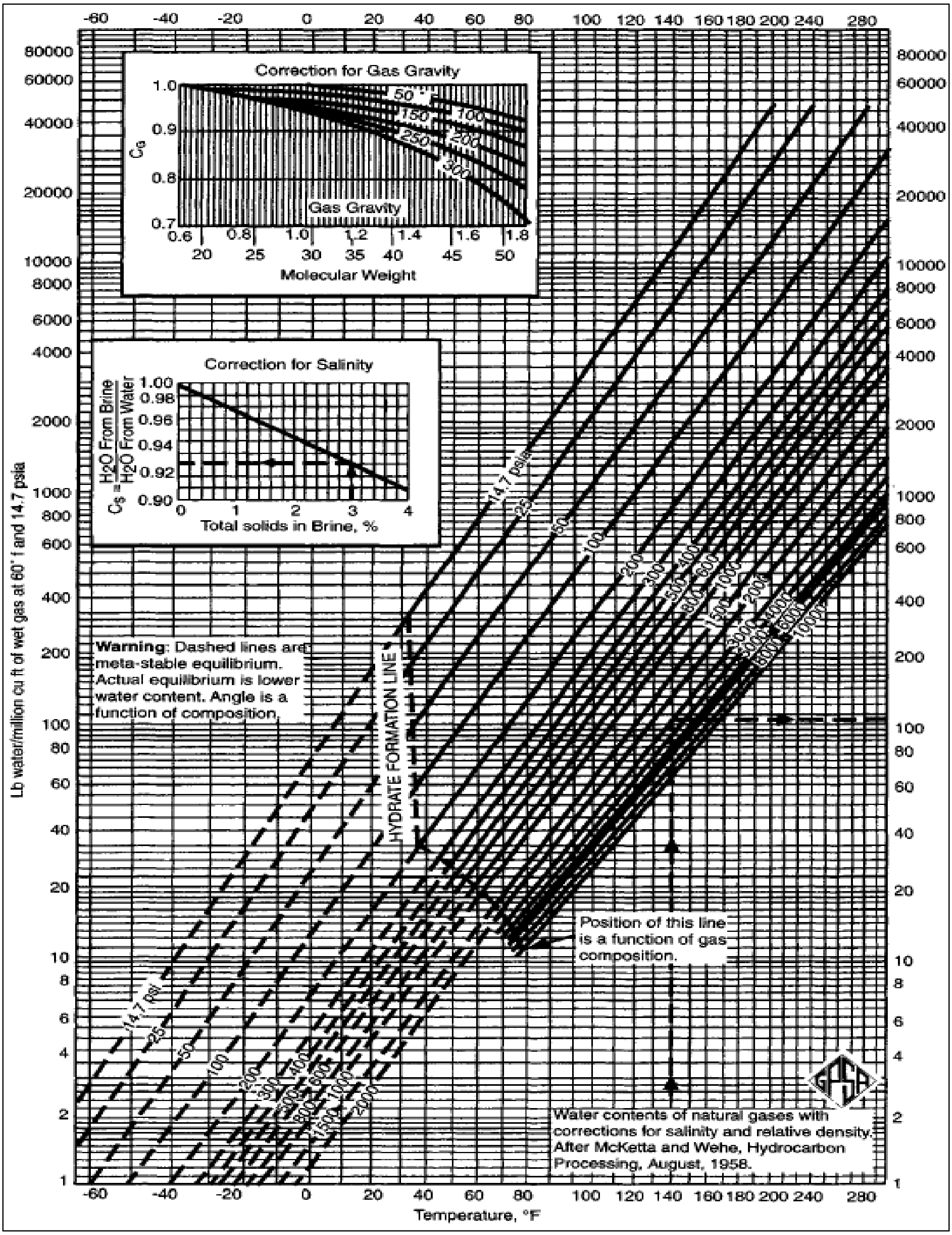

Warning: Dashed lines are meta-stable equilibrium. Actual equilibrium is lower water content. Angle is a function of composition.

Position of this line is a function of gas composition.

Water contents of natural gases with corrections for salinity and relative density. After McKetta and Wehe, Hydrocarbon Processing, August, 1958.

Fig. 5.6: Chart to calculate the water content of natural gases (after William C. Lyons et al. 2005). The salinity and gas gravity should be corrected before the estimation of the water content of the natural gas. **) The evaluation of the water content is based on the study of Thomas Franzen (member of the MPT project)*

Figure 5.6 shows a chart of water content in standard conditions and temperature at different pressure ranges with salinity and density correction. Once natural gas pressure and temperature are known, the corresponding water content of the gas can be read from the chart (Fig. 5.6) or by using the equation 5.3 (William et al., 2005).

$$W = \frac{A}{P} + B * C_G * C_s \quad \text{If SGg >0.6} \quad \text{……………………..……...…………} \quad (5.3)$$

Where,

W : Water content, g/m^3 C_s : Correction factor for salinity,
A, B: constants (equal to 1893 and 4.1) according to temperature table (William C. Lyons et al., 2005)
SG$_g$: Specific gravity of gas C_G : Correction factor for gas gravity
P: gas pressure in atmosphere

Equation (5.4) used to subtract the calculated condensed water from the total amount of water.

$$V_{wT}.\rho_{wT} = V_{wR}.\rho_{wR} + V_{wC}.\rho_{wC} \quad \text{…………….………………………………….…………} \quad (5.4)$$

where,

V_{wT} : total produced water, m^3 ρ_{wT} : density of total produced water, kg/m^3
V_{wR} : reservoir water, m^3 ρ_{wR} : density of reservoir water, kg/m^3
V_{wC} : condensed water, m^3 ρ_{wC} : density of condensed water, kg/m^3

Vertical Flow Performance Tables (VFP)

Vertical flow performance (VFP) tables are necessary data for 3D simulation. VFP curves supply the simulator with the necessary data to define bottom hole flowing and tubing head pressures as a function of various parameters such as flow rate, water gas ratio, and condensate gas ratio. PROSPER program from Petroleum Experts software is designed to allow building of reliable and consistent well models, with the ability to address each aspect of well bore modelling, PVT (fluid characterisation), VFP correlations (for calculation of flow line and tubing pressure loss) and IPR (reservoir inflow). VFP tables for gas producers consist of an array of bottom hole pressures (inflow pressures) produced by well modelling software (PROSPER) for a given tubing size at different combinations of flow parameters, namely flow rate, pressure at well head, water gas ratio, and condensate gas ratio. The data required for creating the VFP curves is imported to Prosper. This includes well completions data (depths and tubing/casing details, deviation survey), PVT data, reservoir characteristics, reservoir pressure and temperature. The reservoir deliverability or inflow performance (IPR) is the first component necessary to build a system model.

VLP curve generated for each well defines the pressure and temperature changes with depth for a particular completion string under a set of flow parameters, PVT conditions, flowing wellhead pressure and tubing restrictions. It is essential to have some measurement of pressure well tests to examine the best VFP correlation and to compute the matching of VFP/IPR. Well test data provides the required input data to implement a match. Well tests were available from three wells RB_Z10a, RB_Z05, and OT_Z02. Ensuring that a VFP correlation is accurate across the entire range of rates is the most important step when calculating the VFP tables. The VFP has to match the best fit correlation to ensure the accuracy of the input data and model quality.

Figure 5.7 shows the best fit correlation of Petroleum Experts 4 “PETEX 4”. The matching of VFP/IPR is essential, because the multiphase flow correlation will be finetuned in order to match bottom pressure, and the IPR will be finetuned so that the intersection of VFP/IPR matches the production rate of the well test. Input of the VFP array allows the simulator to determine the operating (solution) point of any well for the particular completion design at all stages of the field’s life.

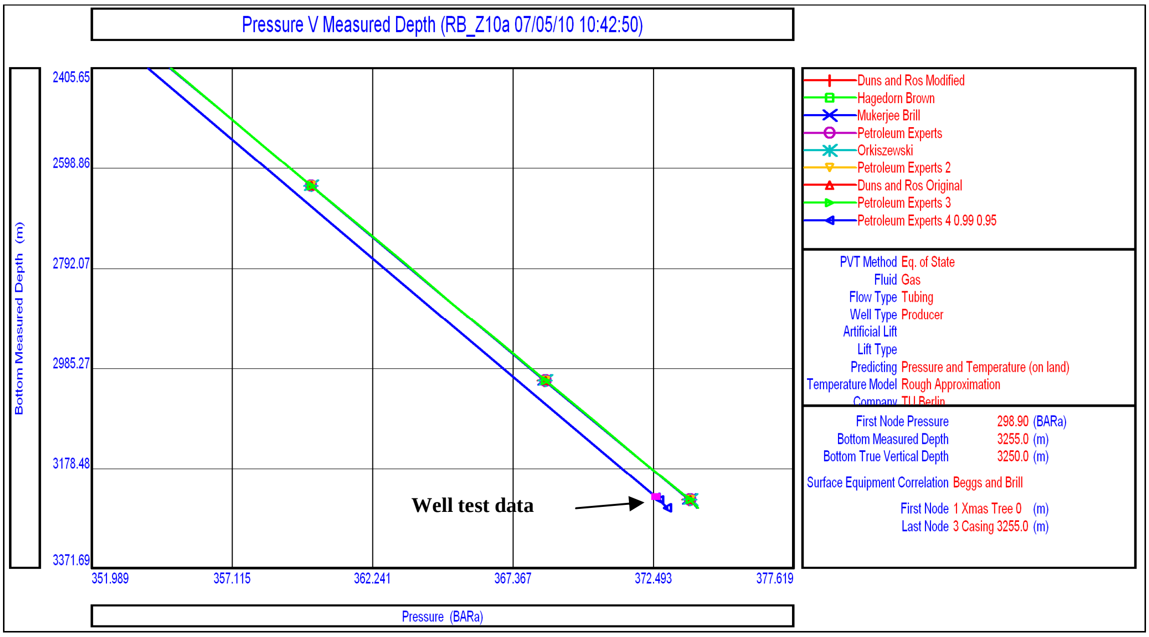

Fig. 5.7: Plot of flowing bottom hole pressure vs. measured depth to select the best fit multiphase flow correlation for the calculation of VFP tables (RB_Z10a) using well test data (pink spot). The multiphase flow correlation PETEX4 was the best fit (dark blue line).

Figure 5.8 illustrates the VFP/IPR matching with less than 10 % difference between the calculated and the actual test data from RB_Z10a. The intersection between the inflow and outflow curves is the operating point of the well.

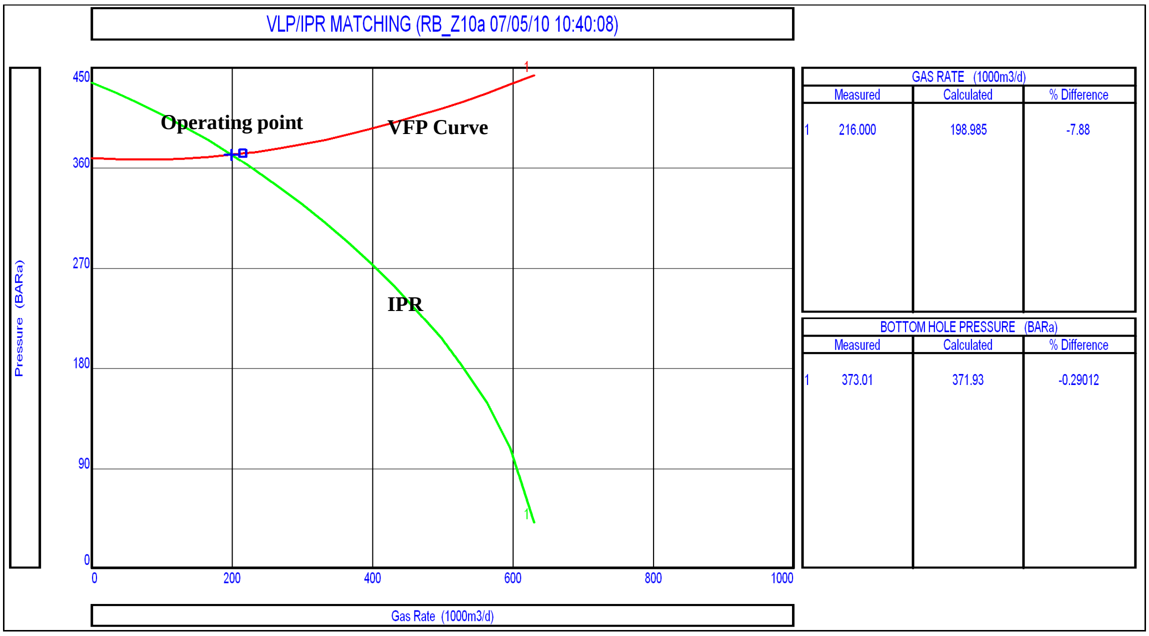

GAS RATE (1000m3/d)

	Measured	Calculated	% Difference
1	216.000	198.985	-7.88

BOTTOM HOLE PRESSURE (BARa)

	Measured	Calculated	% Difference
1	373.01	371.93	-0.29012

Fig. 5.8: VFP/IPR matching (RB_Z10a: bottom hole pressure vs. gas rate). The computing of the matching of VFP/IPR was to check the model quality. The intersection of the two curves is the operating point; in the right side of the figure are the measured data and the calculated data.

Well Test Data Integration

Well test results are incorporated and integrated into the reservoir numerical simulation for the verification of dual porosity/permeability history match process. Bourdet et al., (1984) introduced the use of pressure derivative type curves in well test interpretation. For natural fractured reservoirs, they considered both pseudo-steady-state and transient flow. They also included the effects of wellbore storage and skin. The pressure responses show different behaviour. For pseudo-steady-state flow, the derivative curve shows a **V** shape over the transition time. Figure 5.9 presents an example of Bourdet type curves for fractured reservoirs. The example data has been interpreted with a dual porosity model (Jourde et al., 2002).

Effective permeability and average reservoir pressure are two parameters which are commonly estimated from well test data and later incorporated into simulation models as input data. From well test reports, using the example of well OT_Z02 (Fig. 5.10), a similar shape was observed in the derivative curve to that standard derivative pressure curve of Bourdet curve, confirming that the system is a dual porosity/permeability system. Well test data (green dots in figure 5.11) was used as a calibration tool to adjust the reservoir parameters by matching the pressure response from the model simulation with actual well test pressure response (Fig. 5.11). The gas rate is the red curve while the bottom hole pressure is the indigo curve.

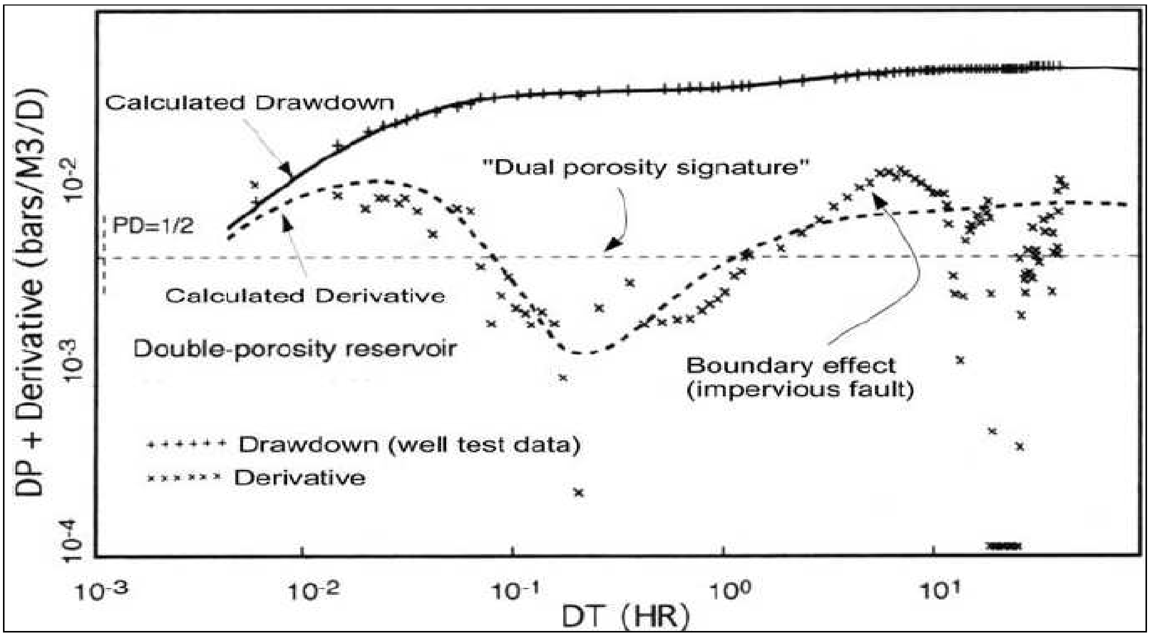

Fig.5.9: Well test data of a well, example of Bourdet Derivative type curve. Data have been interpreted with a dual porosity reservoir in proximity to a small fault (after Jourde et al., 2002).

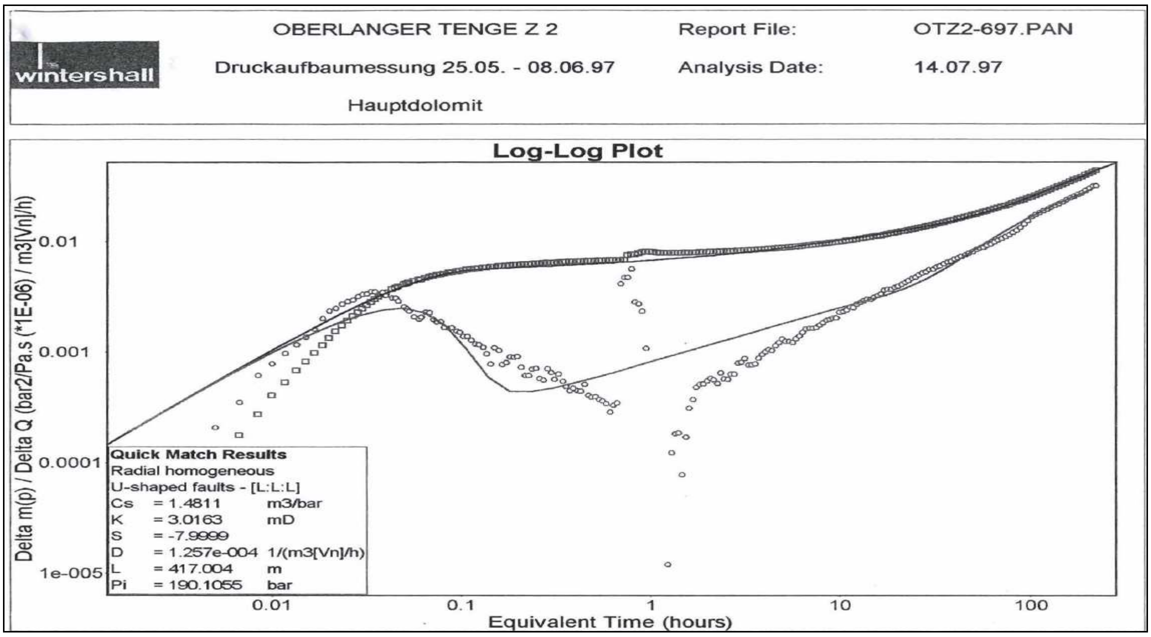

OBERLANGER TENGE Z 2
Druckaufbaumessung 25.05. - 08.06.97
Hauptdolomit

Report File: OTZ2-697.PAN
Analysis Date: 14.07.97

Quick Match Results
Radial homogeneous
U-shaped faults - [L:L:L]
Cs = 1.4811 m3/bar
K = 3.0163 mD
S = -7.9999
D = 1.257e-004 1/(m3[Vn]/h)
L = 417.004 m
Pi = 190.1055 bar

Fig.5.10: Well test data from well OT_Z02 (main compartment). The interpretation of such a Derivative type curve was that the system is a dual porosity system (fracture + matrix) and faults existing nearby OT_Z02.

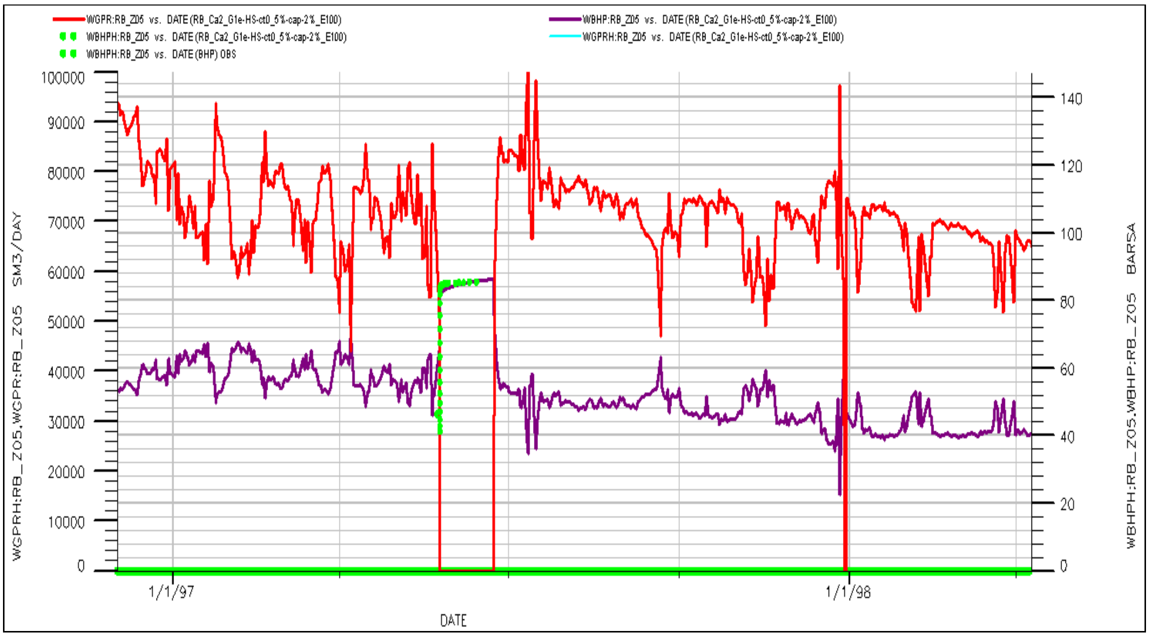

Fig. 5.11: Well test data integration (date vs. bottom hole pressures& gas rate). Match of the well test data (build-up tests: the green dots) from RB_Z05 vs. simulated pressure (indigo curve). The well test data were integrated and used as calibration tool to achieve a realistic pressure model response..

5.2 Dual Porosity/Permeability Simulation Model

A three dimensional, two phase (gas and water), reservoir simulator Eclipse100 (black oil model) was utilized to simulate the Hauptdolomit reservoir by matching the production history and predict reservoir performance with respect to different production scenarios. The dual porosity/permeability porous media was confirmed using a core and well test data evaluation. A detailed static geological model was created, taking into consideration geophysical as well as petrophysical data, improving interactively with dynamic reservoir data. The geological model was constructed by the team geologist using the Petrel program.

The Hauptdolomit geological model was formed from 60 layers and was exported to Eclipse (Fig. 5.12). The reservoir dynamic model comprises a total of 71 x 39 x 60 matrix grid cells and an identical number of grid cells for the fracture system on the basis of all available information. The model consists of 332,280 grid cells in total, with 201,619 active cells, each cell being 150 m on the X direction and 150 m on the Y direction. The model is approximately 30 meters thick. The grid cells were assigned by their respective porosity and permeability values (Fig. 5.13 & 5.14). The permeability along the X direction was assumed to be equal to the permeability value on the Y direction, stating isotropic permeability in the horizontal direction. Vertical permeability is one tenth of horizontal permeability. All essential data for instance faults data, PVT, SCAL, VFP and production history data were integrated into the model.

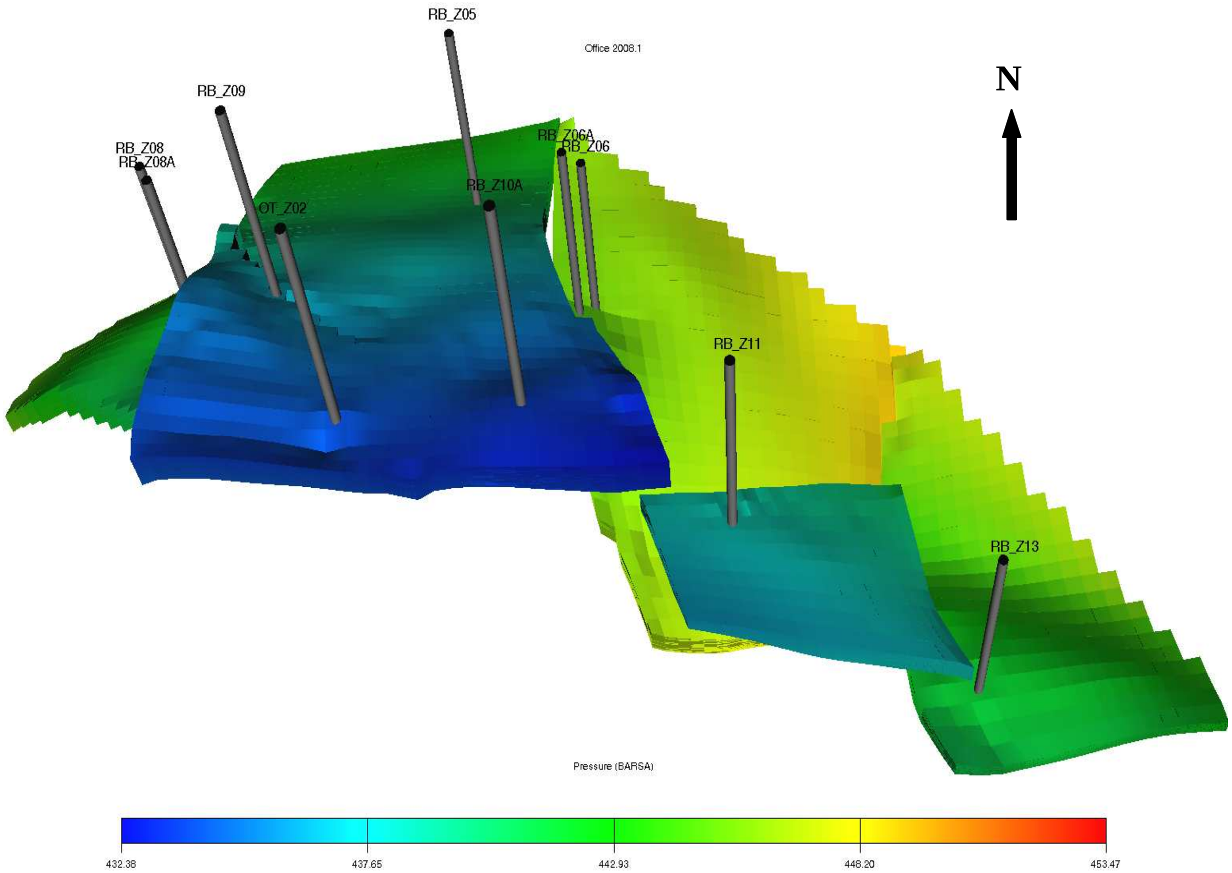
RB_Z05
Office 2008.1
N
RB_Z09
RB_Z08
RB_Z08A
RB_Z06A
RB_Z06
RB_Z10A
OT_Z02
RB_Z11
RB_Z13
Pressure (BARSA)
432.38
437.65
442.93
448.20
453.47

Fig. 5.12: Hauptdolomit 3D geological model. The compartmentalized reservoir structure is shown, well locations and the matrix pressure distribution in all compartments.

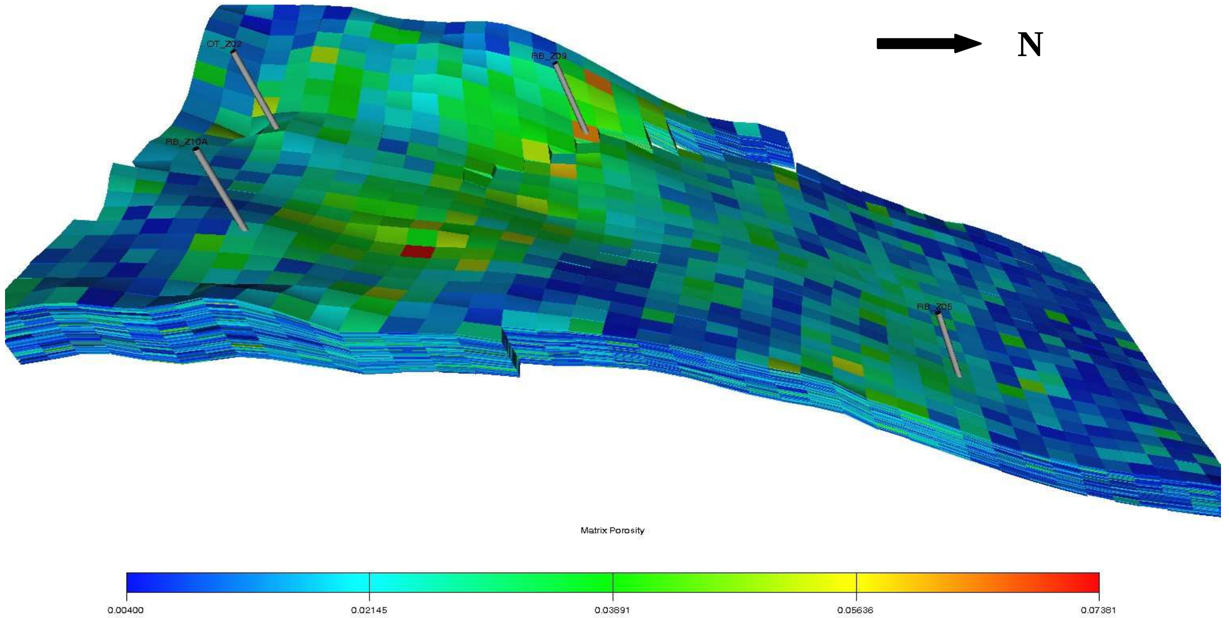
N
OT_Z02
RB_Z09
RB_Z10A
RB_Z05
Matrix Porosity
0.00400
0.02145
0.03891
0.05636
0.07381

Fig. 5.13: 3D view of the matrix porosity distribution in the main compartment. An average of 2.5% matrix porosity means that it is a very poor reservoir. Near the structure crest there is anomaly of the porosity values compared to the rest areas in the main compartment.

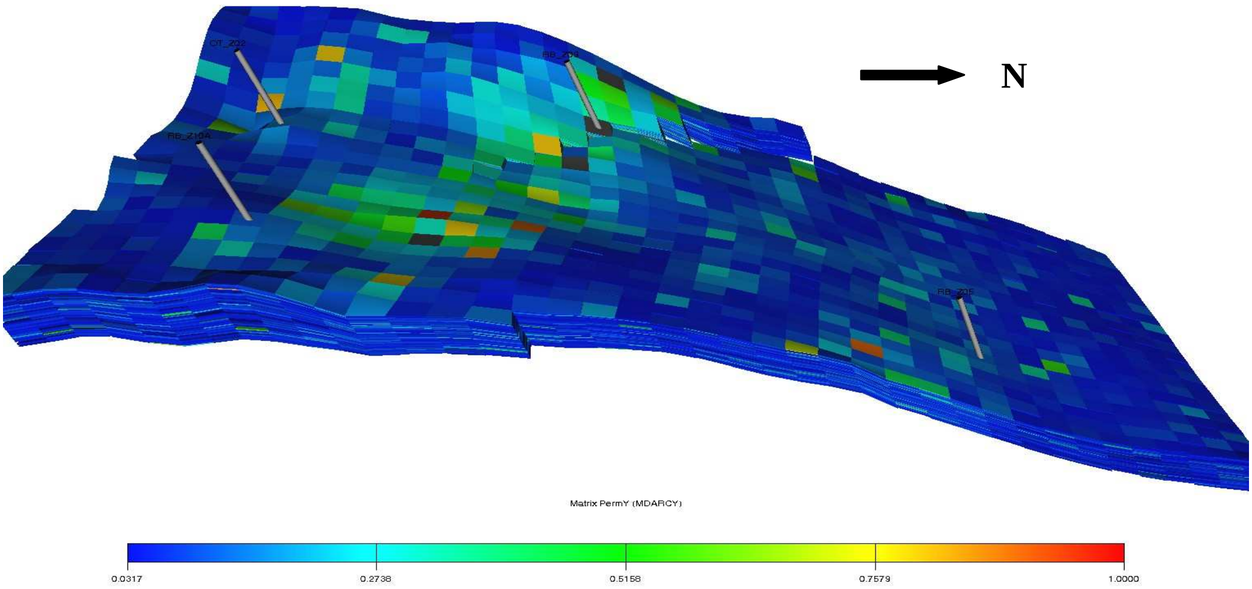

Fig. 5.14: 3D view of the matrix permeability distribution in the main compartment. The reservoir is poor reservoir with less than 1 mDarcy matrix permeability. The permeability values are higher near the structure crest.

Relative Permeability & Capillary Pressure Functions

Saturation dependent functions, such as relative permeability (k_r) and capillary pressure (P_c), are key factors for the assessment and prediction of gas production from a reservoir. Representative values are preferentially obtained through Special Core Analysis (SCAL). Since Special Core Analysis results were not accessible, capillary pressure data was obtained from published data (Reitenbach V., Pusch G., 2006).

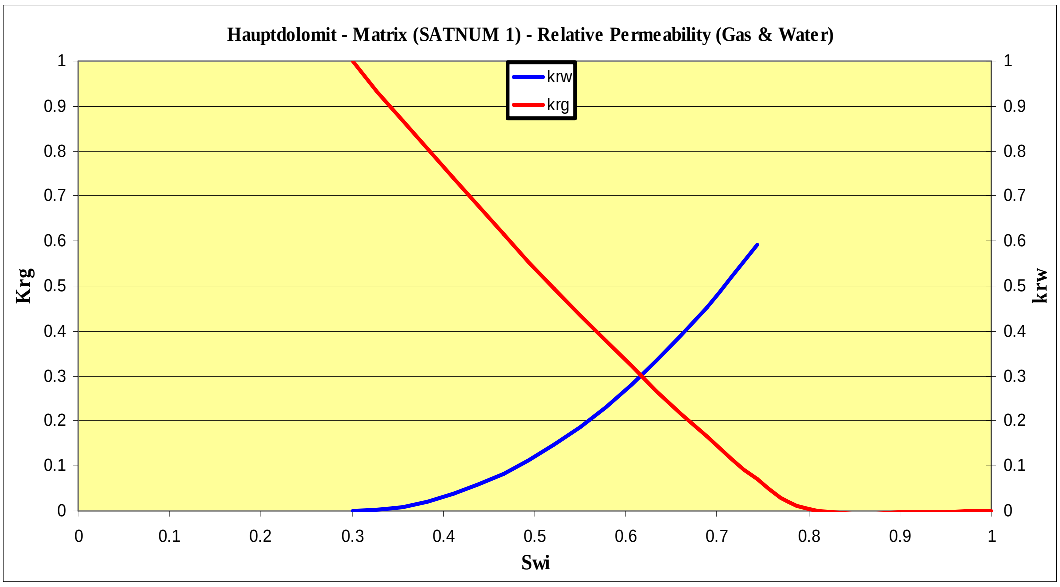

Fig. 5.15: Hauptdolomit - Matrix relative permeability (Corey curves) for gas (red curve) and water (blue curve).

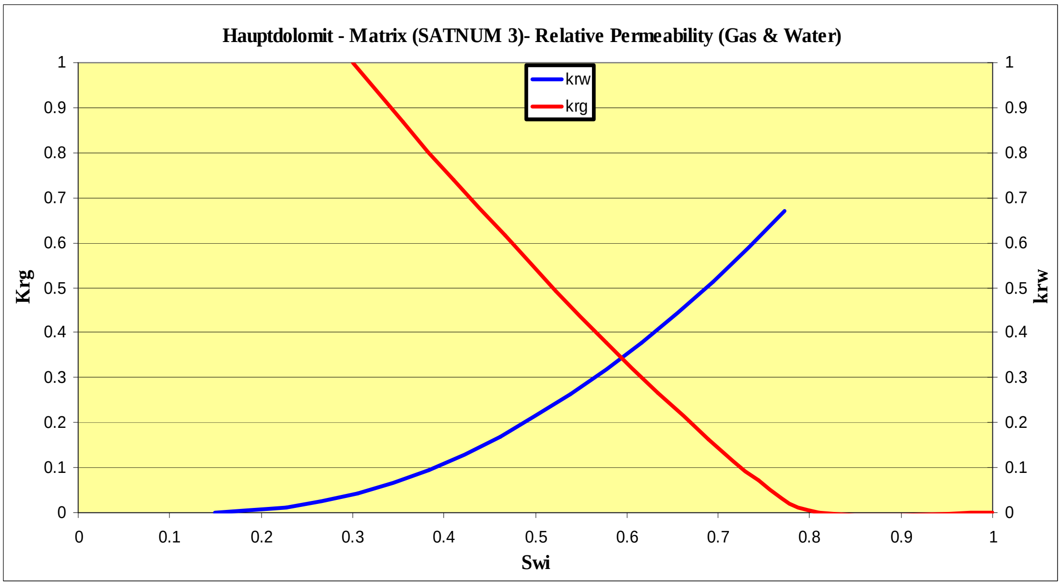

Fig. 5.16: Hauptdolomit - Matrix relative permeability (Corey curves) for gas (red curve) and water (blue curve).

Gas and water relative permeability were calculated using the existing Corey correlation, incorporated within Eclipse, to create the required tables. The saturation functions were assigned according to the predefined matrix porosity groups as follows: If ϕ < 2.3 then Sw_i = 30 % (*Satnum1*); if ϕ (2.3 – 5 %) then Sw_i = 22 % (*Satnum2*); and if ϕ> 5 % then Sw_i = 15 % (*Satnum3*). For fracture system the saturation function number is *Satnum4*. Figures 5.15 through 5.18 illustrate the relative permeability and capillary pressure used in the history match base case.

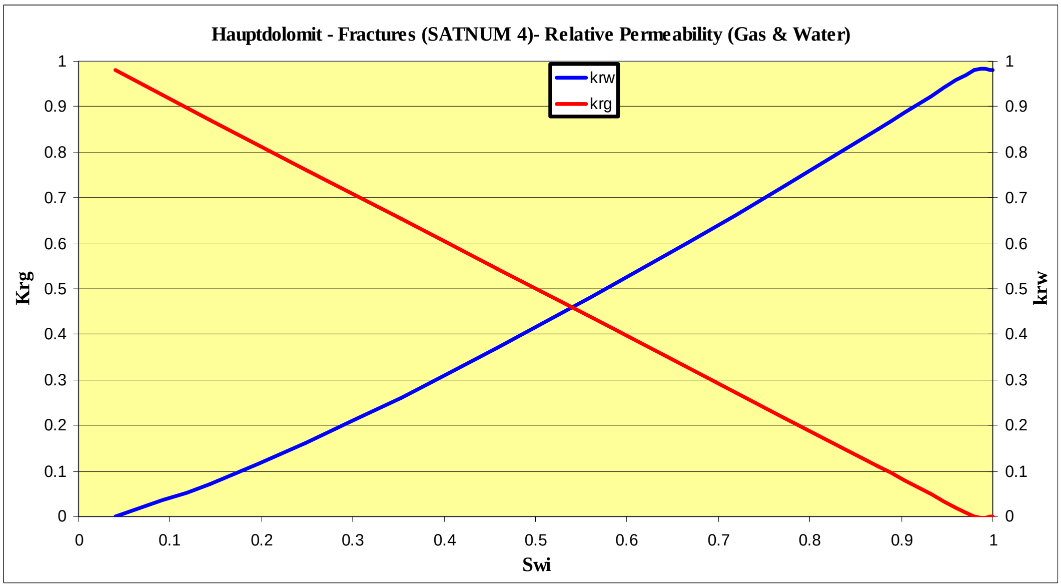

Fig. 5.17: Hauptdolomit - Fracture relative permeability for gas (red curve) and water (blue curve). X-curve type is usually used for the fracture system.

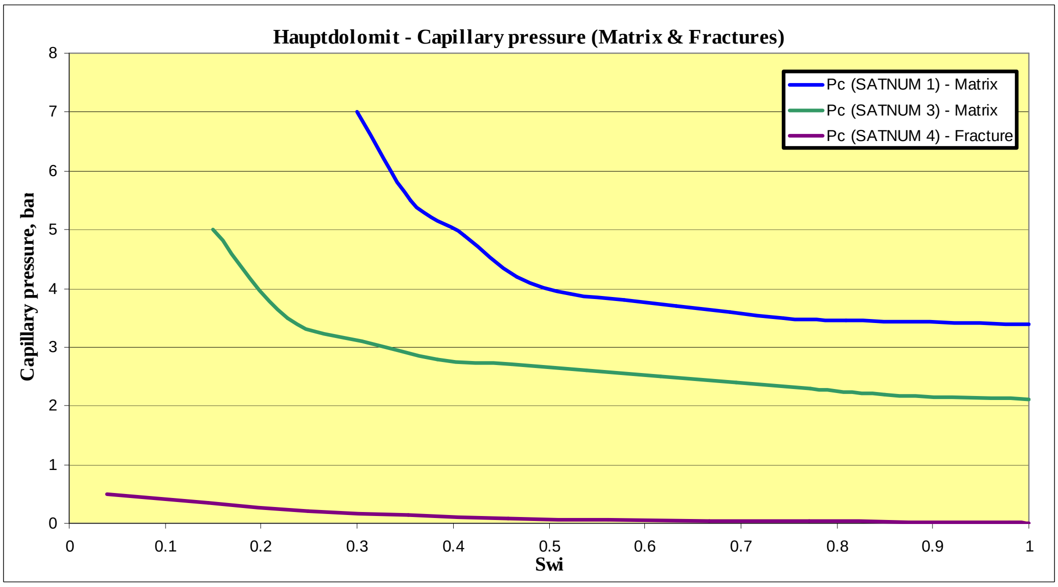

Fig. 5.18: Hauptdolomit capillary pressure curves: Matrix (blue & green curves) & fracture (brown curve).

Production History Data Validation

The Schedule program, incorporated in Eclipse software, was used for preparing, validating and integrating production and completion data for use in the Eclipse simulation. Required production and completion history data was imported into Eclipse.

5.3 Reservoir Model Initialization

The initialization process consists of the reservoir model validation by way of the calculation of the original fluid in place volumes, and allows establishing the initial fluid saturation and the pressure distribution within the reservoir. The process of initialization is the most important step in the screening of the created porosity models. The essential selection criterion during the initialization of the models was to verify the calculated gas initially in place (GIIP) of the main compartment from the material balance P/Z plot.

The geological 3D model was initialized with a total GIIP of approximately 2.5 x 10^9 m^3 gas Fig. 5.19). As mentioned previously (see chapter III), two types of GIIP were determined from the material balance P/Z plot and from the reservoir and fluid properties. Therefore, to determine the calculated GIIP from P/Z plot, the reduction multiplier factors on matrix porosity were applied to remove the extra gas share. A reduction multiplier factor of 0.8 was applied to matrix porosity values. The dynamic model was initialized using initial pressure versus reference depths, for example at main compartment 437 bar at 3400 mNN, and equilibration data specifications for the initial water saturation (Fig. 5.19).

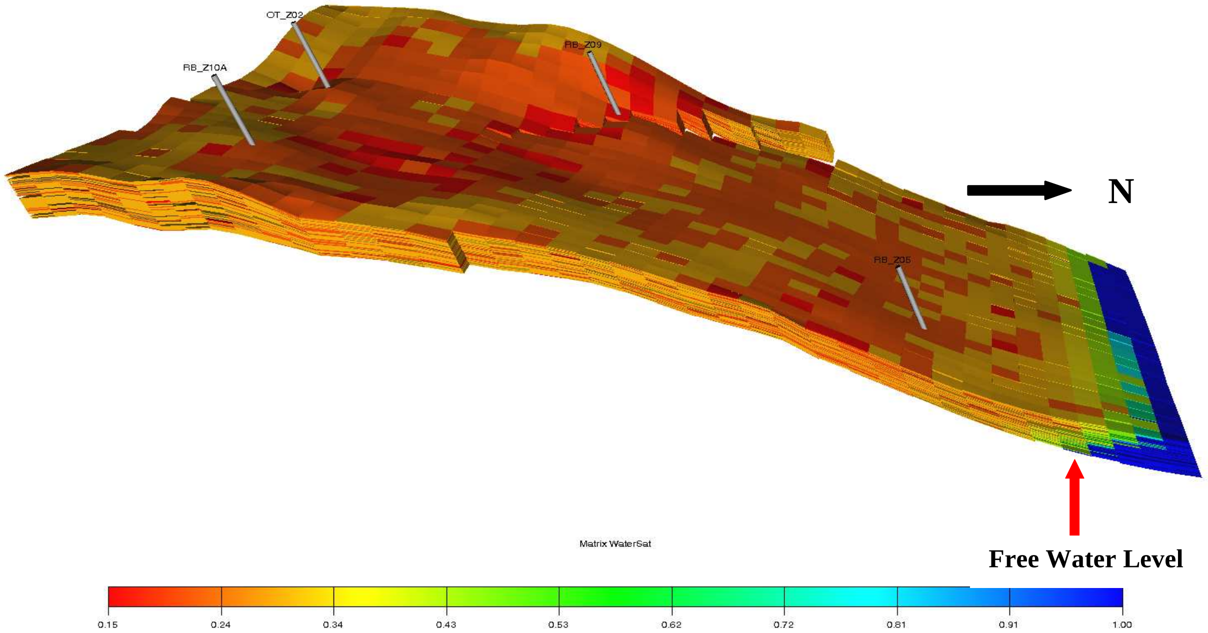

Fig. 5.19: Main compartment initialized model. Shown also the matrix water saturation distribution (15 - 30%), FWL (Sw_i=100 %) @ 3722mNN and the four gas producers in the main compartment.

Various reference depths were introduced due to fact that different initial pressures were initially measured at the reservoir compartments. Accordingly, that indicates the separation of each compartment i.e., no communication between the compartments. Many matrix porosity realisations have been created, but only seven models were selected and tested in Eclipse. The final realisation porosity model was chosen because of the suitability of the history match simulation results.

5.4 History Matching

The aim of history matching is to find a model which displays a minimal difference between the performance of the model and the production history of a reservoir. The history match process is iterative and validates the hydrocarbon volume present in the reservoir. Traditionally, this is done by hand, but the task of varying the parameters of a reservoir description by hand until a satisfactory match is obtained is extremely onerous and time-consuming. History matching involved matching simulated production volumes, static/flowing bottom hole/wellhead pressures and also cumulative reservoir production. History matching of naturally fractured reservoirs is especially challenging, particularly when these models represent a structurally compartmentalized reservoir. In structurally complex reservoirs, history matching can be a time consuming and frustrating process due to the large number of parameters affecting performance. Indeed, history matches are inevitably non-unique and therefore best efforts should be made to ensure that all input parameters are physically/geologically realistic.

During the history match the uniqueness problem arises from many factors. The most noteworthy factors are unreliable or limited field data, interpretation errors, and numerical effects. Data limitations are more difficult to resolve because there is not enough available data to ensure that the final solution is the correct one. It is recognized that the spatial heterogeneity and limited information about formation can lead to uncertainties in the process of reservoir characterization. In turn, the uncertainties create a degree of randomness in the model parameters and render the equations governing flow and transport in the media stochastic. Numerical reservoir simulation is subject to uncertainties, which may stem from inaccurate and imprecise measurements or inadequate characterization of spatially or temporally varying medium properties (Heng et al., 2009). Numerical reservoir simulation is based on the numerical approximation of solutions to the equation systems described by mass conservation and Darcy’s law. Computational complexity arises from the high spatial heterogeneity of multi-scale porous media. This heterogeneity, together with measurement limitations, leads to uncertainties in simulation. As a result, numerically approximating subsurface phenomena are an intricate problem, which is critical to the industry for accurate predictions of costly projects (Lu Bo et al., 2007).

For naturally fractured reservoirs, history matching requires that both the matrix and fractures are properly characterized. Generally, for naturally fractured reservoirs, geological models which are derived from static data alone fail to reproduce the field production history (Gang T. et al., 2006). This can be ascribed to the insufficient consideration of fracture effects on flow and insufficient dynamic characterization of the distribution of the fracture system. In other words, the hydrodynamic properties of the fractures system needs to be characterized using the production data, such as, in this case study, gas rate, WGR and bottom hole flow pressure, etc. The focus of the history match was to match gas producers in the main compartment with the wells produced from the other compartments that also had pressure measurements.

5.4.1 History Matching Key Parameters

The real challenge was to match a group of wells simultaneously with respect to production from the same compartment, which can generate production interference between the wells. Regarding the communication between reservoir compartments, it is obvious that applying sealing faults between the compartments ensures a better match. The influence of compaction on the pore volume is negligible in gas reservoirs because gas compressibility exceeds the rock compressibility in magnitudes of order (Voigt, 1979).

In this scientific study, the Hauptdolomit geological model was improved interactively by way of reservoir dynamic simulation. The history matching procedure was carried out by manually changing the parameters which have the main effects on matching the production data, until the desired field output was obtained. The key matching parameters were fracture permeability, the presence of a tight zone, faults & flow barriers and water encroachment into the reservoir. The combination of the above mentioned uncertainties with reservoir and fluid properties parameters, such as fault transmissibility, relative permeability & capillary pressure functions and dual porosity matrix-fracture coupling factor, ensured an excellent match.

Fracture Permeability

Gas flow mainly occurs through the fracture network, while a rock matrix contains the majority of fluid storage and provides fluid drainage from the fractures. Therefore, fracture permeability (especially in the presence of permeability contrast between matrix and fracture) represents a first order effect in matching the production data. Field experience suggests that it is very difficult to quantify fracture permeability without matching production data using the information gained from core data, well tests, decline analysis results and thin section analysis. All these data sources, used to determine the fracture permeability of Rütenbrock/Hauptdolomit reservoir, indicate low fracture permeability. The fractures were partially cemented according to the thin section analysis, collected from the main compartment gas producers. Cementation was the cause of low fracture permeability. To verify the accuracy of fracture permeability values, the procedure involves a trial and error method, where fracture permeabilities are adjusted manually to match the production data. The simulation results show that this method is reliable and efficient for naturally fractured reservoir history matching. It has been observed that low horizontal and vertical fracture permeability (less than 10 mDarcy) represent a better match of the well production history. To simplify the simulation and due to limited available data concerning fracture distribution, uniform fracture permeability was applied, excluding the tight zone area.

The Presence of Tight Zones

There was an observed mismatch with the historical data from the initial simulation results when a clean model without tight zone was used. The distribution of fractures became a significant step because fluid flow characteristics in the naturally fractured reservoirs are largely controlled by the distribution, orientation, and interconnectivity of the fracture system (T. Gang et al., 2006). The distribution of fractures in this study is a means of demonstrating the existence of a tight zone. The priority was therefore to investigate the presence of a tight zone with “strongly low fracture permeability areas" and its location within the main compartment. An indication of a tight zone was found in the production reports. A formation tester at a depth of 3430 and 3424.5 m on well RB_Z07 was performed and negative results were observed (Fig. 5.20). The RB_Z07 well was determined to be too poor for economical production and permanently abandoned. Similarly negative results were provided for well RB_Z16.

Based on thin section analysis collected from one of these wells (RB_Z07) which has been analysed by the geologist in the team, no Dolomitization process took place in this area. Dolomitization is a process by which limestone is altered into dolomite. When limestone comes into contact with magnesium-rich water, the mineral dolomite, calcium and magnesium carbonate, $CaMg(CO_3)_2$, replaces the calcite (calcium carbonate, $CaCO_3$) in the rock, volume for volume, generally generating secondary porosity. Accordingly, the fluid, that usually causes the Dolomitization process, did not have the access or the flow paths to enter this area through the flow conduits (fractures). In an exception from the rest of the areas in the main compartment, the fractures in this area around RB_Z07 are fully cemented. It can be concluded that the area around RB_Z07, including RB_Z16, might be a tight zone area, i.e., having strongly reduce fractured permeabilities, confirmed by the history match simulations. The boundary of this zone was inspected during history match simulations until a reasonable match of all wells located in the main compartment was achieved.

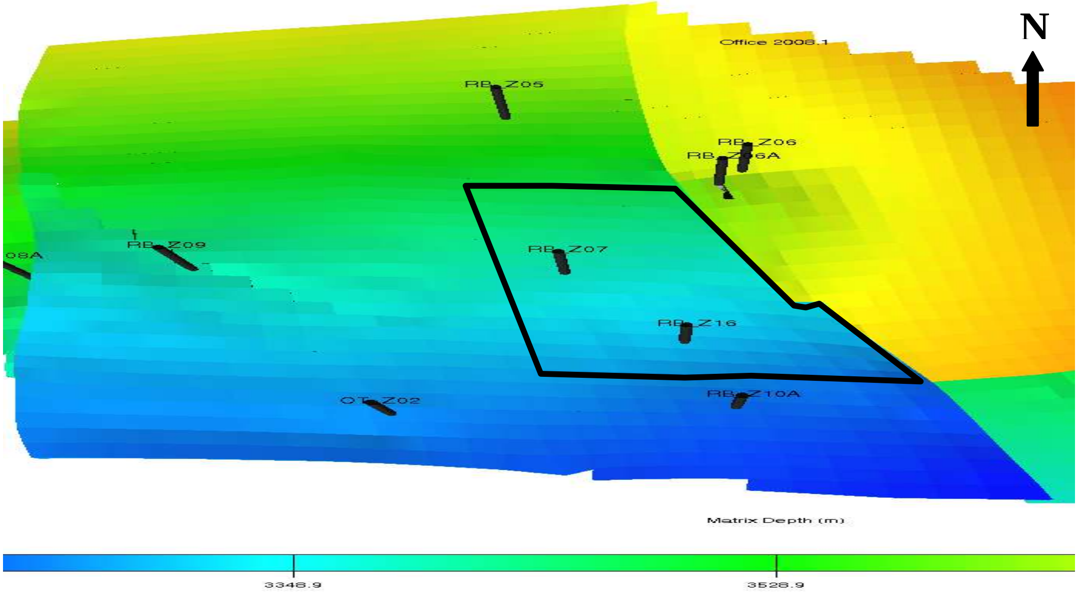

Fig. 5.20: Hauptdolomit depth map. The tight zone was introduced in the main compartment and its extent includes the two dry holes RB_Z07& RB_Z16.

The fracture porosity and fracture permeability in this zone were strongly reduced and approximately zero. This region in the main compartment only communicates with other parts through the matrix system.

Faults & Flow Barriers and Gas Volume Placement

Faults can act both as barriers and as conduits to fluid flow, and are normally included in reservoir simulation models. Fault transmissibility multipliers should be limited to the interval [0, 1] where a numerical value of 0 reflects a complete flow barrier and a value of 1 characterizes an open flow. Anything in between 0 and 1 corresponds to a partial barrier to fluid flow. For example, two supplementary faults were detected from the well tests in the main compartment. An extended north-south fault is situated between well OT_Z02 and RB_Z10a and an east-west fault between RB_Z10a and RB_Z16 (Fig. 5.21). As well in compartments, 2, 3 and 4, applying additional faults were introduced to match production history data (Fig. 5.21).

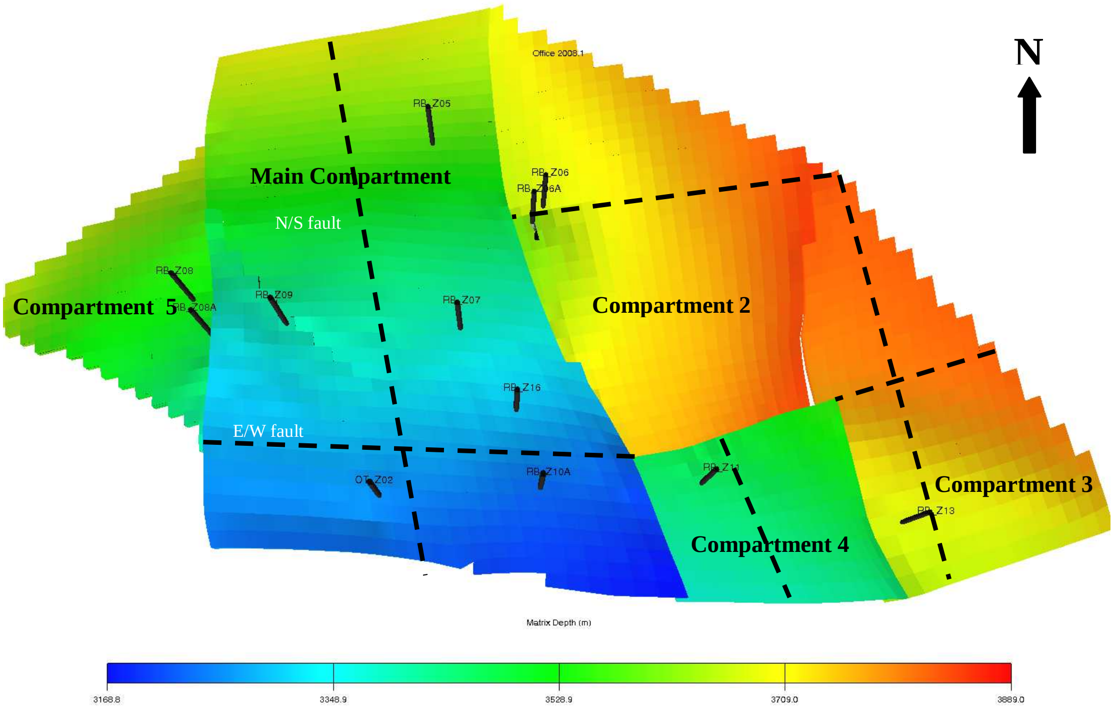
Office 2008.1
N
RB_Z05
Main Compartment
N/S fault
RB_Z06
RB_Z06A
RB_Z08
Compartment 5
RB_Z08A
RB_Z09
RB_Z07
Compartment 2
RB_Z16
E/W fault
OT_Z02
RB_Z10A
RB_Z11
Compartment 3
RB_Z13
Compartment 4
Matrix Depth (m)
3168.8
3348.9
3528.9
3709.0
3889.0

Fig. 5.21: Hauptdolomit depth map. The supplementary faults and flow barriers (dashed lines) over the entire structure are shown. The new faults and flow barriers are parallel to the main faults in the direction of the north/south or east/west.

The simulation results confirmed the existence of these faults and flow barriers, and to ensure a precise match the faults were either partially sealed (transmissibility multipliers varied between 0.005 - 0.02) or completely sealed. In compartments 2, 3, 4 and 5, several supplementary flow barriers were specified as shown in figure 5.21 which ensured excellent matches in pressure, gas rate and water wise. The volume placement of the initial gas in place in matrix or fracture system was important to reproduce the well's observed production behaviour. In this study, 15 % of the total initial gas in place was in the fracture system to obtain an excellent history match.

Dual Porosity Matrix-Fracture Coupling (SIGMA)

In dual porosity/dual permeability models, SIGMA is used to specify a multiplier to be used in the construction of the matrix-fracture coupling transmissibilities. It acts as a multiplier on the matrix-fracture coupling and may simply be treated as a history matching parameter. The precise match was achieved by applying SIGMA 1E-5.

Fault Zones as Flow Paths

Static pressure measurements of RB_Z05 show a decline while only RB_Z10a was producing, which indicates the presence of communication path between the crest and the deep part of the main compartment (Fig. 5.22). Fault zones are characterized by intensive fractures, and in particular dolomite tends to be wider and have higher fracture densities (Dinwiddie et al., 2006). Fractures surrounding a sub-vertical fault act as flow conduits. Open fractures in fault zones have a relatively high permeability and they preferentially promote flow (Bauer et al., 2010).

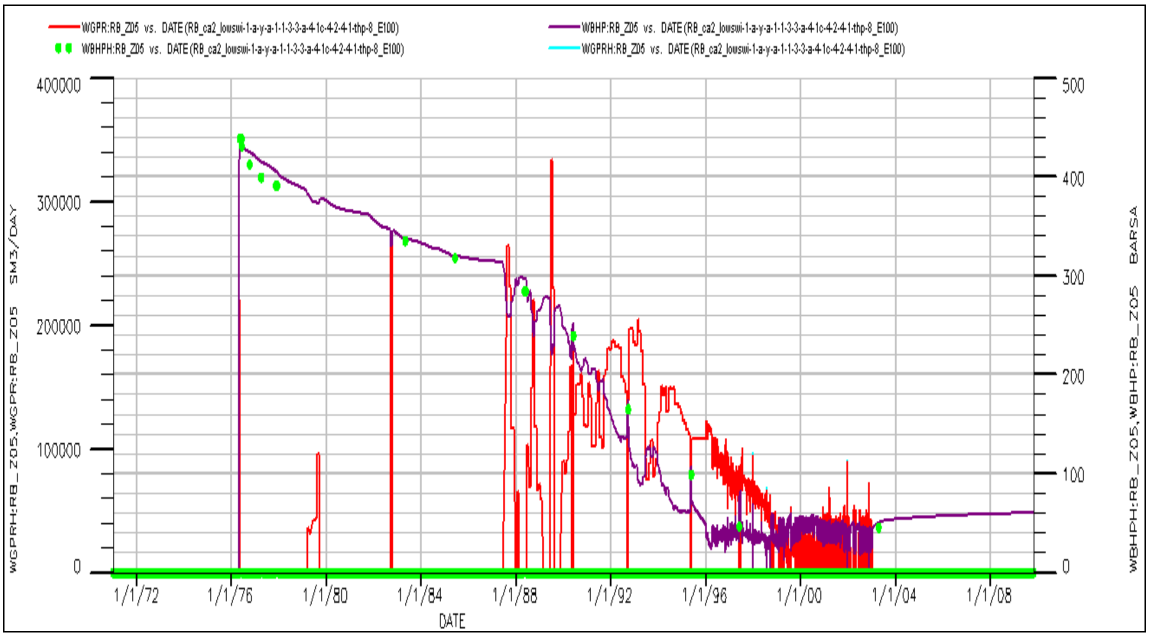

Fig 5.22: RB_Z05 bottom hole pressure measurements ("WBHPH" green dots) & gas rate ("WGPR" red curve) vs. production history time (date). The pressure decline at the early production stage when there was no production from this well indicate the communication between the top and bottom main compartment structure.

A number of assumptions were examined to find the proper communication path location between the crest and the deep part of the structure through a relatively higher permeability flow path. The communication path, which promotes an excellent match between RB_Z10a and RB_Z05, especially in the early production history phase, is between the tight zone and the N-S fault. Areas of fault intersections act as drains in the northern section of the main compartment and also as conduits for flowing gas.

At the beginning of 1992, it was difficult to match the tail end phase pressure measurements of RB_Z05, which indicates that the communication between the crest and deep part structure became poorer over production time. As the fractures are the flow conduits of gas and water, the water moved mainly through the flow pathways (fractures), partially filling and sealing them. The water proceeded through fractures from the bottom of the structure and as a consequence the communication between the crest and the deeper part of the structure became worse over production time. The history simulation match shows that the fault zones and fault intersections are contributing factors in the gas flow within the compartment.

Water Encroachment into the Hauptdolomit Reservoir

Water encroachment into a fractured reservoir, which governs the gas productivity, was investigated in previous studies by way of numerical simulation. Two gas trapping models are made possible by water encroachment in low permeability gas reservoirs: 1) a strong imbibition capillary pressure causes gas trapping, if the reservoir has very low matrix permeability, and water encroachment into the matrix permeability can therefore be significant (Holtz et al., 2002). As water moves into an area filled with gas, the displacement of the gas by water is not complete. The water fills pores and pore throats, causing capillary pressure and relative permeability effects to stop the flow of gas and allow only water to pass through the rock volume. This stoppage results in gas being trapped behind the encroaching waterfront as residual gas; 2) water bypasses the matrix gas through fractures (Hamon et al., 1991). The water invasion occurs in the reservoir's fracture network, bypassing the gas in the matrix. As a result the water can easily recede in the fractures, with limited water withdrawal in particular if the water influx is weak.

RB_Z05 is a well located in the deep part of the main compartment structure. Observed water production increased considerably from 1 to 8 m^3/day in 2001 and gas productivity at this well was simultaneously declining. Well RB_Z05 watered out a few years later in 2003. A series of runs were conducted and it was not possible to reproduce the actual history of some wells like RB_Z05 without changing certain properties, giving indications for the time dependency of certain parameters or temporally varying medium properties. As gas production starts from the wells, water encroachment into a reservoir is time dependent and the alteration of some properties such as gas relative permeability took place. For the investigation of these two gas trapping models by numerical simulation, the matrix and fracture transmissibility adjustment over production life was implemented. Starting from the production year 1999, the fracture transmissibility of the area between the GWC and well RB_Z05 was reduced by 0.1 and 0.08 multipliers on the X and Y direction directions respectively.

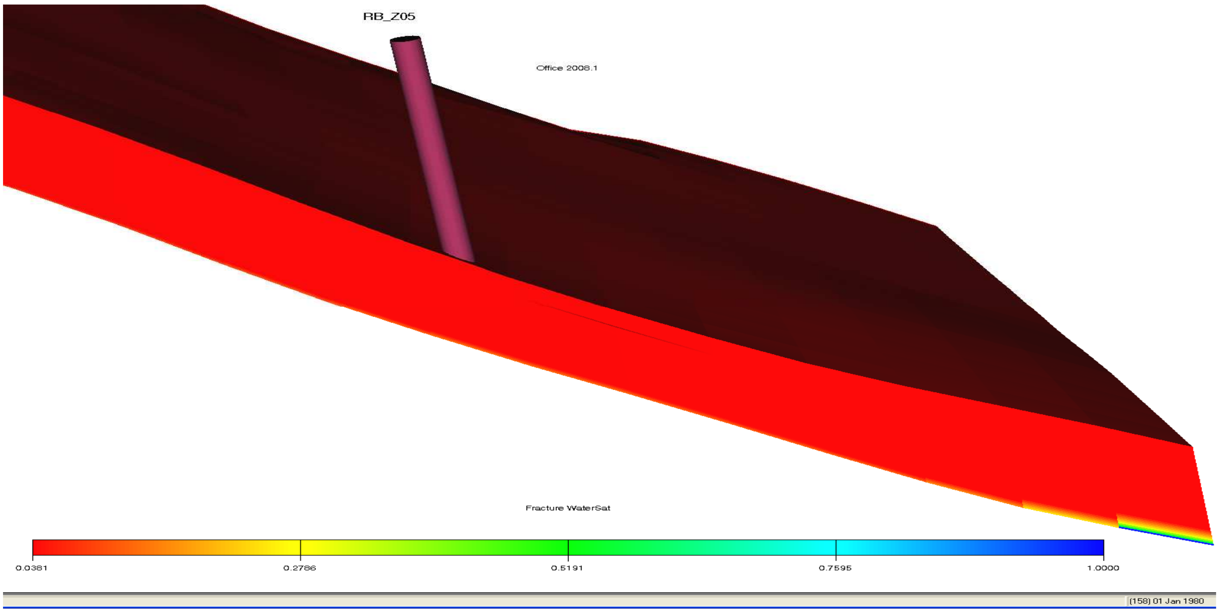
RB_Z05
Office 2008.1
Fracture WaterSat
0.0381
0.2786
0.5191
0.7595
1.0000
(158) 01 Jan 1980

Fig. 5.23: A view of the fracture water saturation in the deep structure part of main compartment in the production history year 1980. The red colour represents 96% gas saturation and blue represents 100 % water saturation.

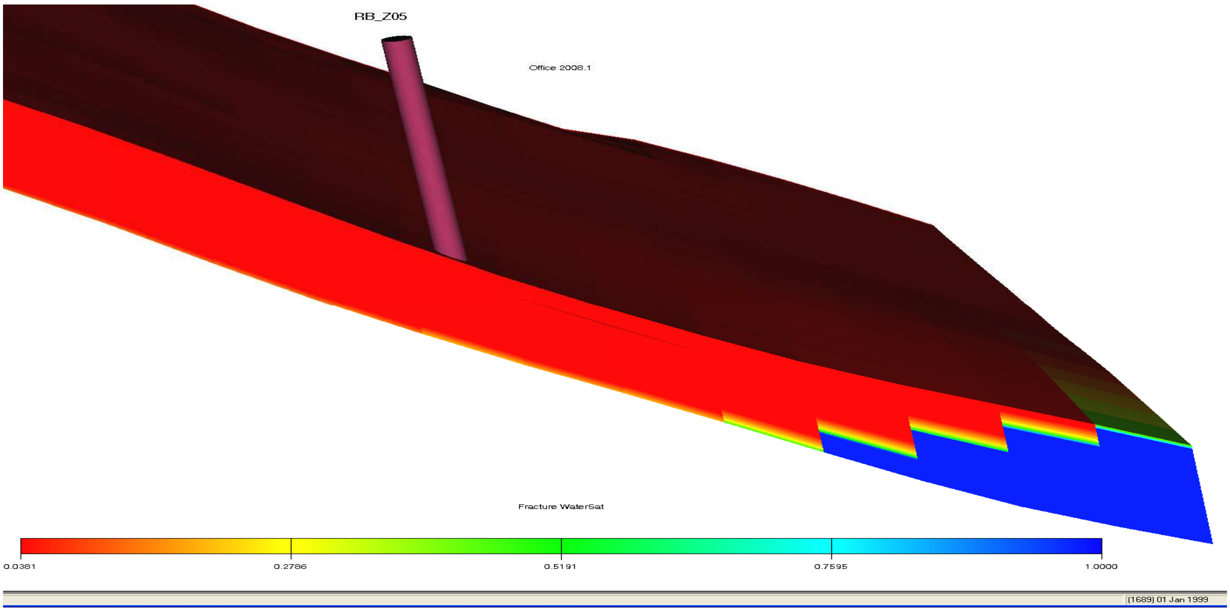
RB_Z05
Office 2008.1
Fracture WaterSat
0.0381
0.2786
0.5191
0.7595
1.0000
(1689) 01 Jan 1999

Fig. 5.24: A view of the fracture water saturation in the deep structure part of main compartment in the production history year 1999. From 1980 to 1999, the water encroachment occurred towards the bottom structure well RB_Z05 through the fracture system as a result of gas production.

The modification of the fracture transmissibility over time assured a precise match for the wells at the crest and at the deeper part of the structure. The gas can only be recovered if the water is removed from the fracture system, allowing the gas to flow from the matrix into the fracture system. It is concluded from simulation results that the bypassing of matrix gas was a result of the water encroachment through fractures (Fig. 5.23 & 5.24).

Capillary Pressure Continuity

It is important to understand the physical processes which take place during the interaction and fluid transfer between matrix and fracture, in order to improve models of multiphase fluid flow in fractured porous media (Gautam and Mohanty, 2004). The matrix flow for an ensemble of blocks will ultimately depend on the hydraulic connection of individual matrix blocks across fractures (Glass et al., 1995). Horie et al., (1990), Labastie (1990) and Stones et al., (1992) studied the capillary pressure continuity in stacked matrix blocks. They investigated the properties of materials present in the fracture, the effect of the overburden pressure and the permeability, and how this affected capillary continuity. The capillary continuity as a recovery mechanism may provide fluid communication between partially or completed isolated matrix blocks, thus increasing the recovery by gravity drainage or viscous displacement (Fernø, 2008).

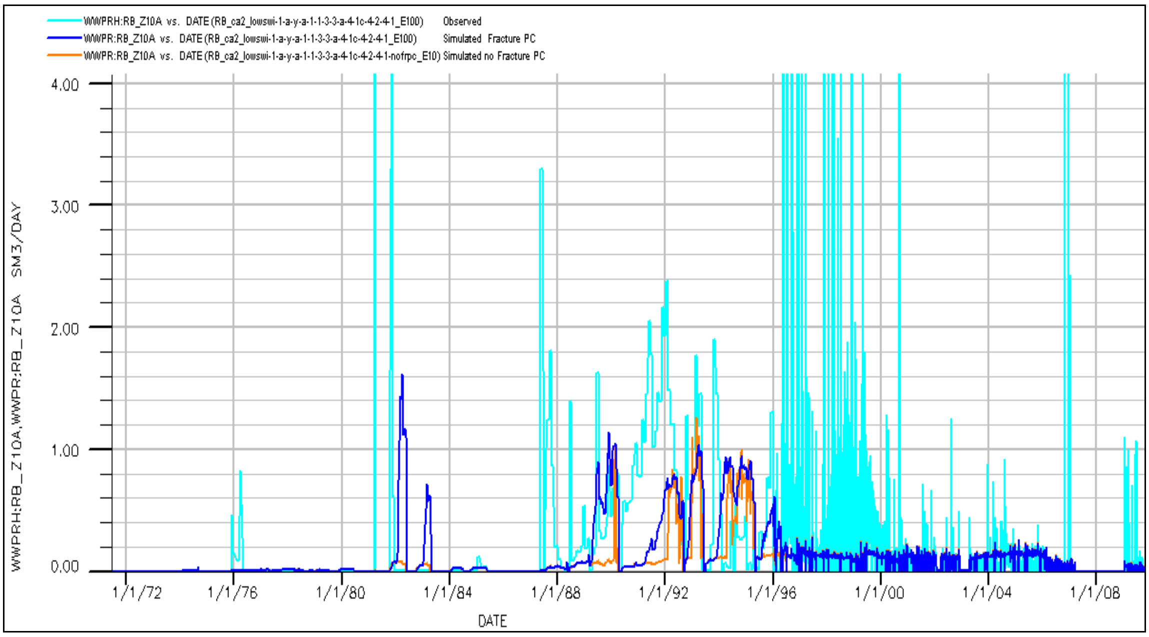

Fig. 5.25: RB_Z10a - Reservoir water match using the fracture capillary pressure. Observed water rate ("WWPRH" light blue) vs. simulated "WWPR". A better match was achieved if a fracture capillary was applied (dark blue curve).

The initial representation of the fracture network consisted of zero capillary pressure and relative permeabilities as linear functions of saturation, with slight irreducible water saturation. Applying zero fracture capillary pressure provided an acceptable match. This result discarded the assumption of a zero fracture Pc, as it was plausible that matrix contact points could have formed during assembly of the various matrix blocks. Applying slight fracture capillary pressure (0.5 - 0.01 bar @ Free water level), varied until a good match with water rate was found, particularly in the water slugs in the earlier production phase of well RB_Z10a (Fig. 5.25). The fracture capillary pressure curve was several orders of magnitude weaker than the matrix capillary pressure. These results illustrate the importance of understanding the effect that the presence of a small scale phenomenon like fracture capillary pressure has on matrix flow.

5.4.2 History Match Results

Despite limited field geology and engineering data, a reasonable history match for 8 gas producers producing from the Hauptdolomit reservoir was achieved by accurately adjusting the key parameters, in combination with relative permeability & capillary pressure functions, dual porosity matrix-fracture coupling factor and faults transmissibilities. Table 5.2 shows parameter values of the reservoir model obtained by history matching as final match parameters.

Table 5.2: History match final parameters

Main Compartment - initial gas in place (GIIP)	1.96 x 10^9 m^3 (Vn)
Matrix porosity	Avg. 2.5 %
Matrix permeability	$K = 0.0184 * e^{0.538 * \phi}$
Fracture permeability, XYZ	7 mDarcy
Fracture porosity	0.3 %
Tight zone - fracture porosity	0.0015%
Tight zone - fracture permeability	0.0001 mDarcy
Matrix initial water saturation groups	15, 22, 30%
Fracture initial water saturation	4 %
Matrix water relative permeability	Corey 2
Fracture water relative permeability	Corey 1.2
Matrix gas relative permeability	Linear
Fracture gas relative permeability	Linear
FWL @ main compartment	3722 m NN
GWC @ main compartment	3660 m

Figures 5.26 through 5.28 show the best case bottom hole pressure and gas flowrate matches of three wells which are located in different compartments: RB_Z10a, RB_Z05 in the main compartment and RB_Z06 in compartment 2. The history match results as figures for the wells, RB_Z09, RB_Z08, RB_Z11, RB_Z13 and OT_Z02 are provided in Appendix 3. No observed pressure measurements from RB_Z06a and RB_Z08a were available; therefore these wells were not considered in the history match process. In addition, the gas composition analysis reports pointed out that well RB_Z08a was producing simultaneously from both formations, the Hauptdolomit and Rotliegend. For all the history match graphs, the green dots are the shut-in and flowing bottom hole pressure measurements whereas the indigo curve is the simulated bottom hole pressure. The red curve is the simulated gas rate. The pressure measurements match with the simulated pressure was acceptable to excellent almost in all wells with the exception of a few points, e.g., in well OT_Z02 where the difference between the simulated and observed pressure is less than 10 bar.

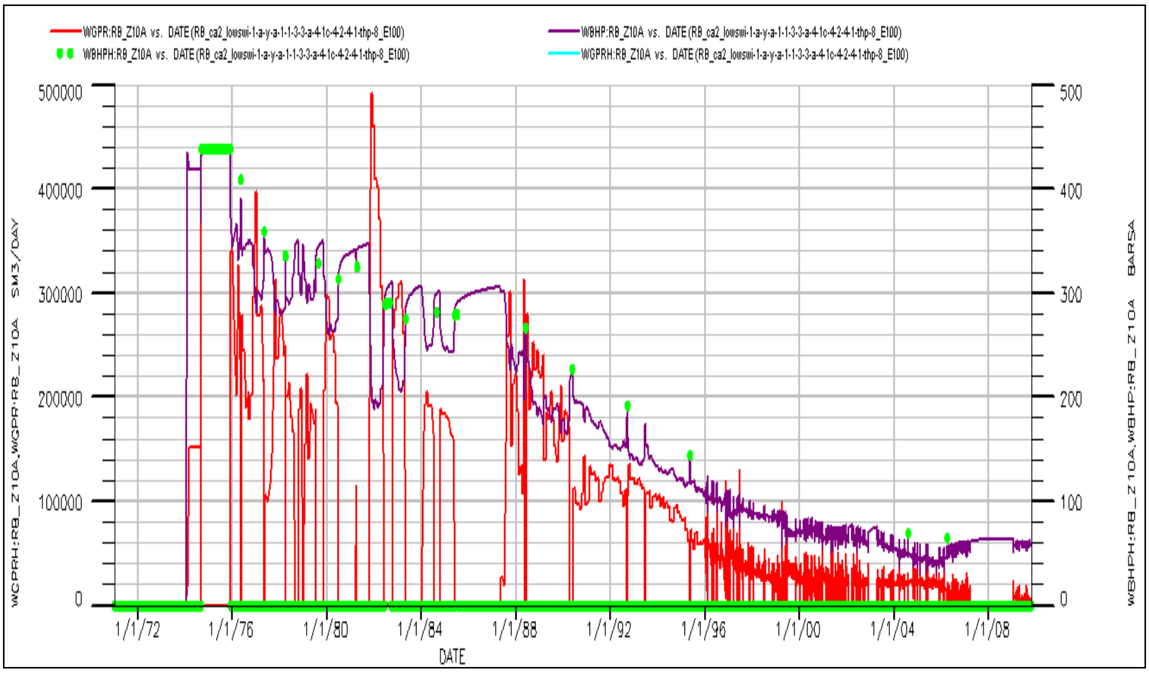

Fig. 5.26: Base case history match (RB_Z10a) - bottom hole pressures & gas rate vs. production history time (date). Bottom hole pressures measurements "WBHPH": green dots; the simulated pressure "WBHP": indigo curve; gas rate "WGPR": red curve.

Water production match is provided in Figures 5.29 and 5.30 as well in Appendix 3. The light blue curve represents observed water rate, and dark blue the simulated water. The amount of condensed water has been calculated and removed from the total produced water and only the observed reservoir water was used in the simulations.

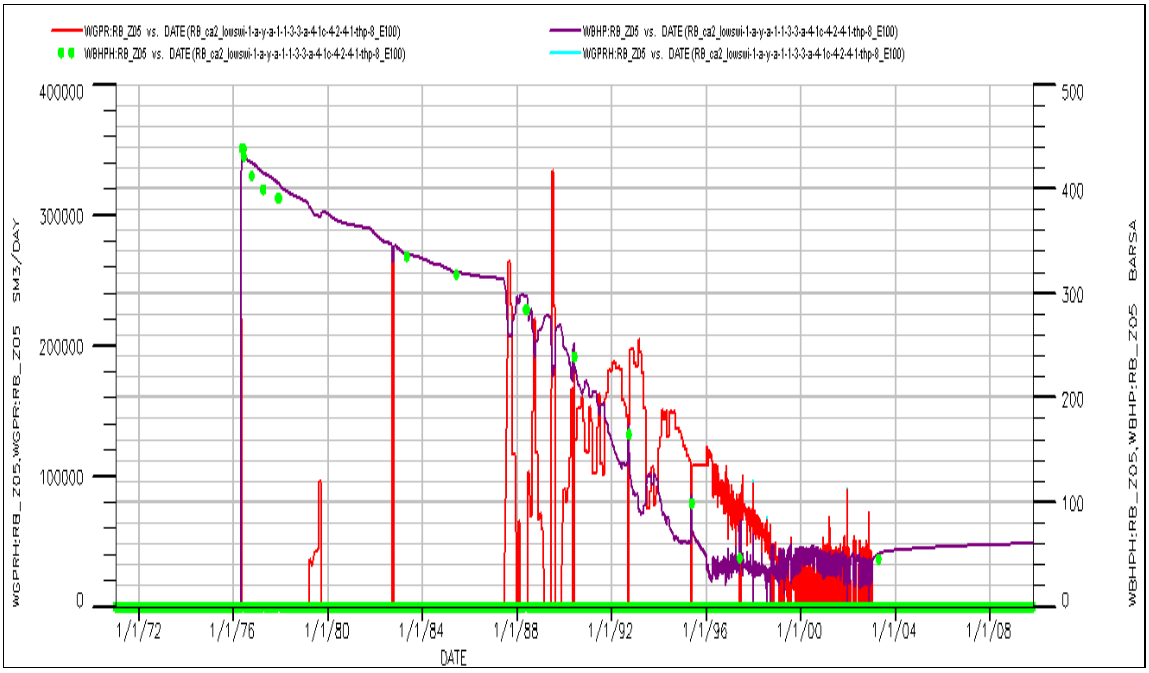

Fig. 5.27: Base case history match (RB_Z05) - bottom hole pressures & gas rate vs. production history time (date). Bottom hole pressures measurements "WBHPH": green dots; the simulated pressure "WBHP": indigo curve; gas rate "WGPR": red curve.

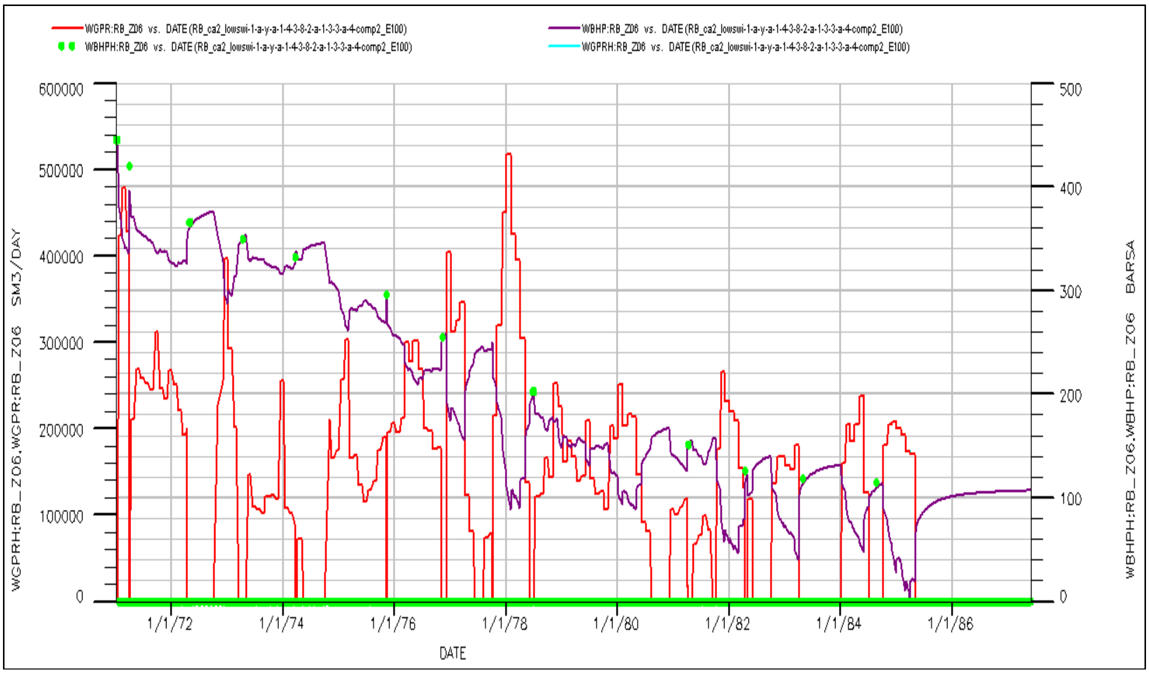

Fig. 5.28: Base case history match (RB_Z06) - bottom hole pressures & gas rate vs. production history time (date). Bottom hole pressures measurements "WBHPH": green dots; the simulated pressure "WBHP": indigo curve; gas rate "WGPR": red curve.

The water production in well RB_Z05 increased gradually and approached the well slowly due to weak water influx. Despite the extremely low quantities of produced reservoir water, the simulation model was able to pull out a little water and a satisfactory match of the water rate was obtained.

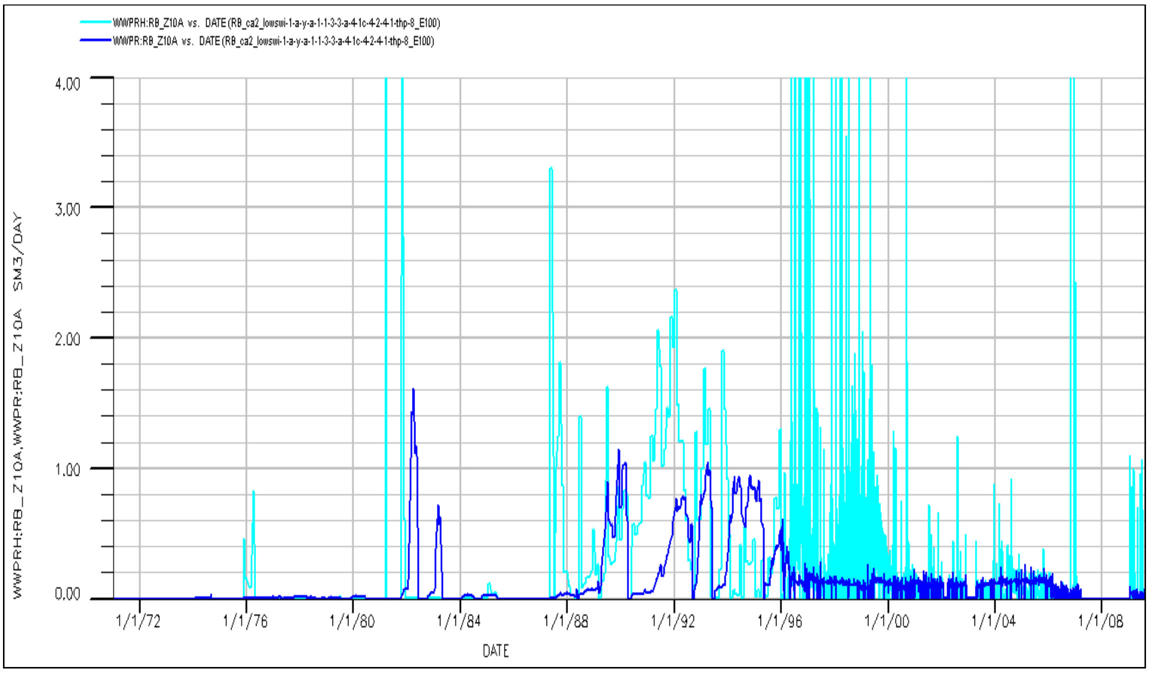

Fig. 5.29: Base case history match (RB_Z10a @ crest of the main compartment structure) - observed water production rate ("WWPRH" light blue) vs. simulated ("WWPR" dark blue).

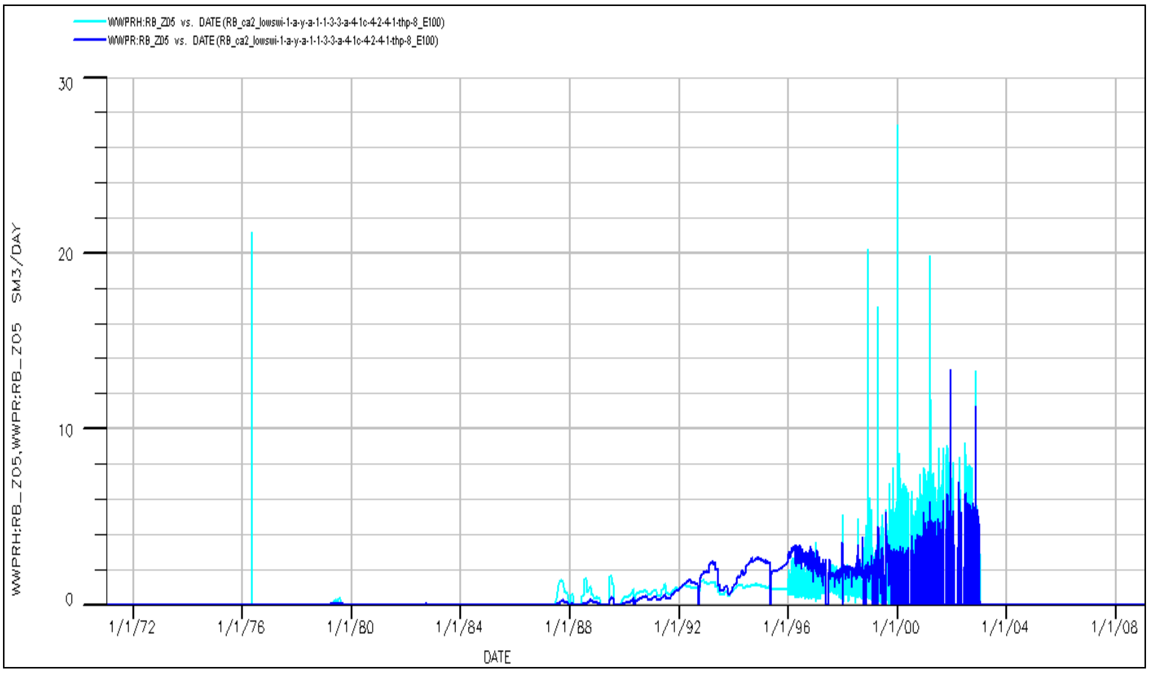

Fig. 5.30: Base case history match (RB_Z05 @ bottom of the main compartment structure) - observed water production rate ("WWPRH" light blue) vs. simulated ("WWPR" dark blue).

Wellhead Pressure Match

In order to perform a production forecast, RB_Z10a flowing well (tubing) head pressure has to match the historical pressure measurements. The various available multiphase flow correlations within the Prosper program were used to achieve a best match, especially at the tail-end production phase. The best match results were obtained using multiphase flow correlation (PETEX 4) with a mismatch of only 2 - 3 bar between the simulated and observed pressure data in the tail-end production phase, before the multiphase pump facility test. Figures 5.31 and 5.32 demonstrate the tubing head pressure history match of the tail-end production phase. The green dots represent historical flowing and shut-in tubing head pressure measurements and the indigo curve corresponds to the simulated flowing tubing head pressure.

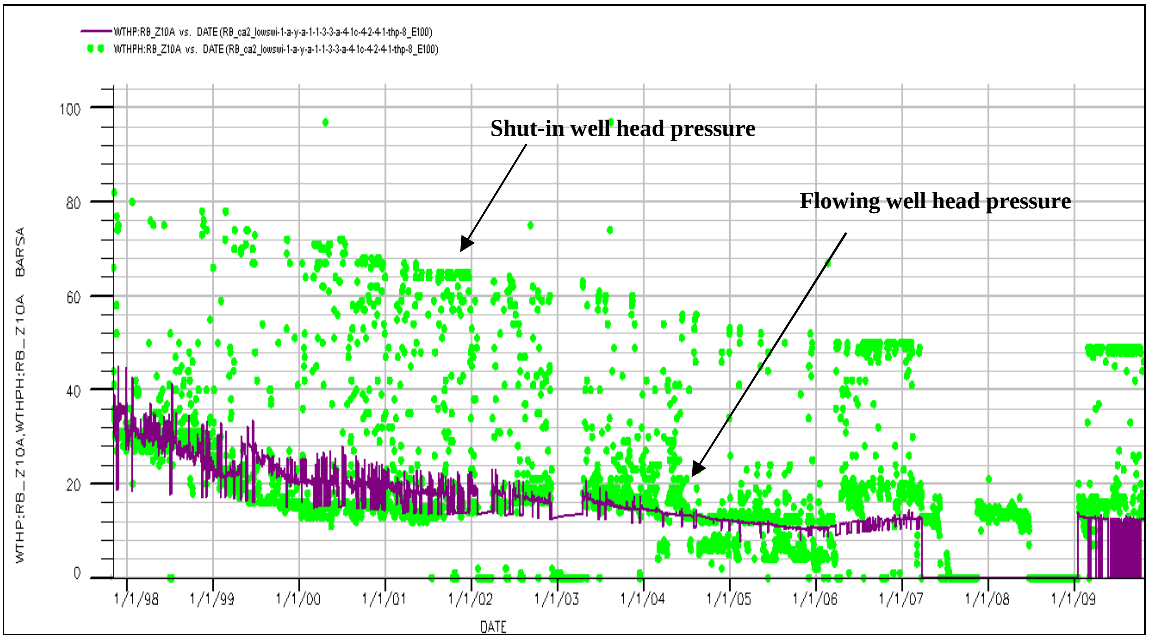

Fig. 5.31: RB_Z10a tubing head flowing & shut-in pressure measurements ("WTHPH" green dots) vs. simulation ("WTHP" indigo curve) between 1998 and 2009.

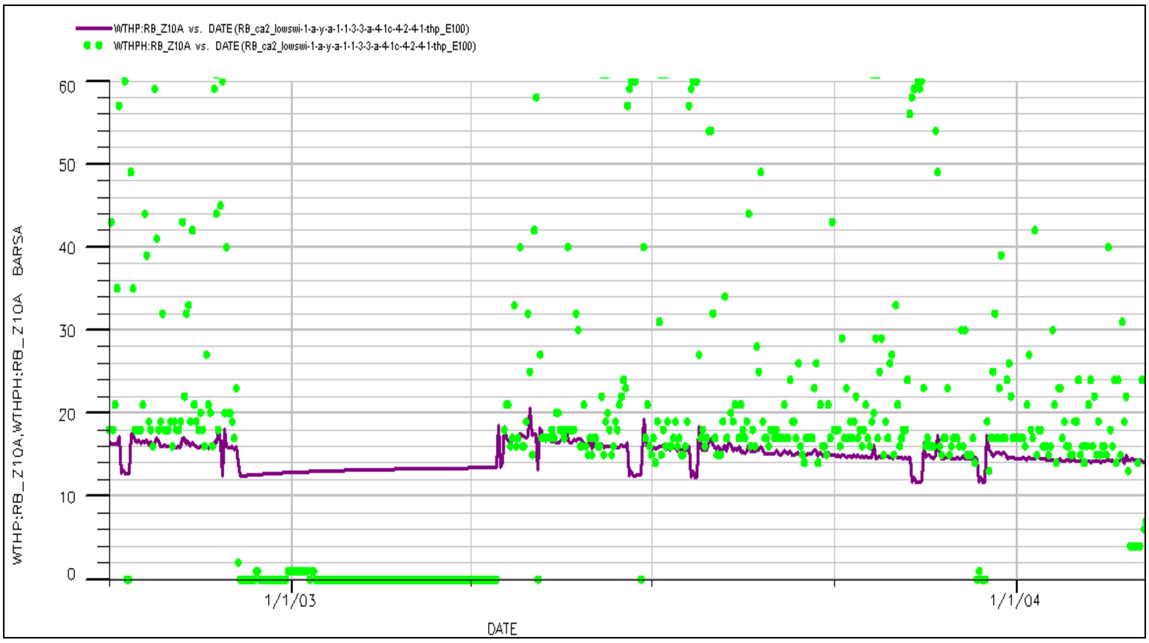

Fig. 5.32: A zoom-in of the RB_Z10a tubing head flowing & shut-in pressure measurements ("WTHPH" green dots) vs. simulation "WTHP" (10/2002-02/2004).

5.5 Production Forecast

A model was used to perform production forecasts to explore the MPP facility effects by means of several scenarios. A production forecast must be presented from production 01/2004 on, when only wells at the crest of the main compartment were producing. During the forecast simulation scenarios, OT_Z02 production history data was used. The first scenario was to consider what would happen if the MPP facility or the conventional compression (CC) production systems were deployed continuously from 01/2004 to 03/2006 and compare the results with the actual production history. The second scenario was to investigate what the various effects would be, e.g., on the gas recovery of RB_Z10a and the entire compartment, if the MPP facility were deployed prior to 01/2004.

Prediction Scenario (1)

Two optimised production forecast runs were performed for the period from 01/2004 to 03/2006 using continuous production by MPP and CC production systems. Average gas rates of 22000, 20000 Sm^3/day were assumed for the MPP and CC scenarios respectively. The minimum wellhead pressure reduction limit in the case of CC predictions was set to 13 bar, whereas for MPP predictions to 2 bar. The prediction results of CC and MPP scenarios were compared with actual historical production data (Table 5.3).

Prediction Scenario (2)

Assuming that the MPP facility would use a date prior to 2004, for instance 1998, several prediction runs were carried out. The maximum flow capacity of the MPP facility is 1400 Sm^3/hr, i.e., 33600 Sm^3/day. The maximum gas rate used during the predictions was the MPP facility's full capacity or less, starting from the deployment date. During the forecasts, the gas production rate was optimized between 25000 and 33000 Sm^3/day to achieve reasonable results. The minimum well head pressure limit reached during MPP facility prediction scenarios is 2 bar. The cumulative gas of the RB_Z10a and entire compartment of the forecast earlier MPP use was compared with the CC continuous forecast scenario and the actual production history. During predictions, OT_Z02 was produced using its historical production data in the MPP forecasts but not in the CC forecasts because it represented the stimulus effect caused by the MPP deployment. Actual production data and prediction results of well OT_Z02 were included for the entire compartment recovery calculations.

5.6 Forecast Simulation Results

From forecast results of prediction scenario 1, the positive impact of the MPP is confirmed by numerical simulations. The forecast simulation on RB_Z10a for the production period 01/2004 to 03/2006 integrating the MPP continuously resulted in a cumulative gas volume of 17.37 x 10^6 Sm^3, representing an increase of 5.33 % compared to the actual produced total gas of 16.49 x 10^6 Sm^3 (MPP facility and CC production) for the same production period. The actual cumulative gas through the production phase 2004 - 2006 was a result of 11322 operating hours of the MPP facility operations (10.33 x 10^6 Sm^3) and 6864 hours of CC (6.16 x 10^6 Sm^3) during the down-time of the MPP facility. The forecast simulation of only CC illustrates that the tubing head pressure reached the minimum limit (13 bar) after only 9 months of production at 09/2004 (Fig. 5.33). In contrast to the MPP cumulative gas volume, the forecast simulation for the CC resulted in a cumulative gas volume of 5.22 x 10^6 Sm^3 with only one third (-68.3 %) of the actual gas volume production (Table 5.3). It can be concluded that, without using the MPP facility, RB_Z10a would come to the end of its production life in 2004 and the actual cumulative gas of 16.49 x 10^6 Sm^3 by the means of the MPP facilities would not have been produced.

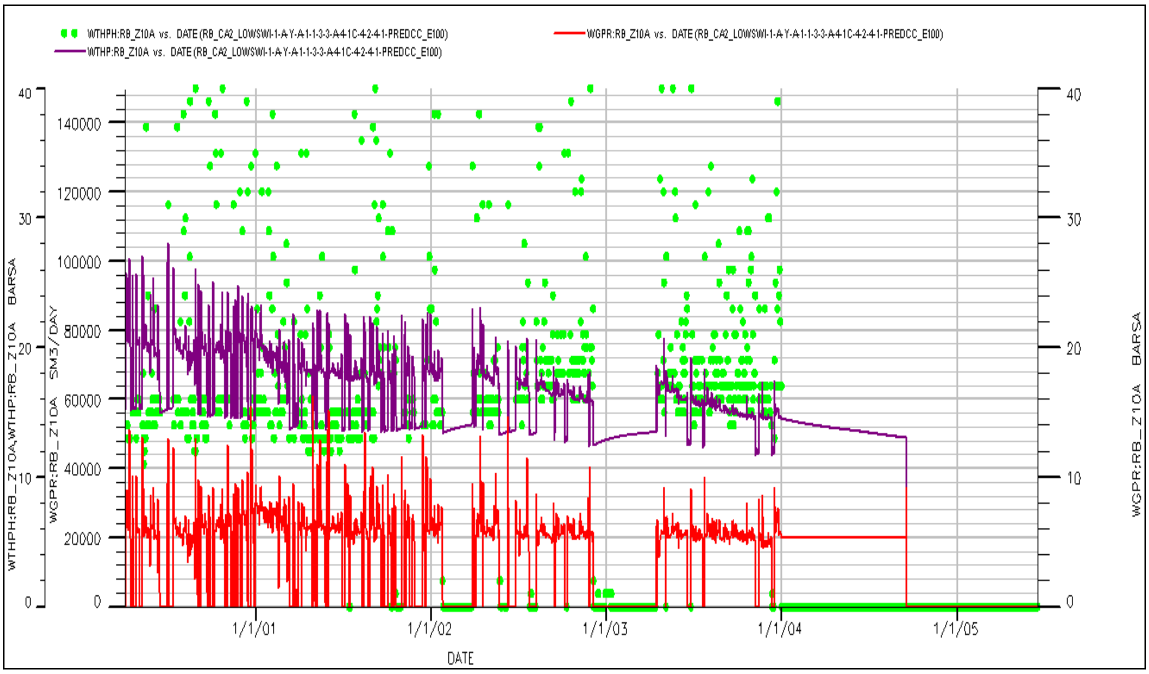

Fig. 5.33: RB_Z10a production forecast scenario - CC prediction (simulated and observed tubing head pressure & gas flow rate vs. time). The RB_Z10a as shown in the figure died after 9 months, (in 09/2004), if the production forecast scenario of the application conventional compression production system was used.

The recovery factors of RB_Z10a and the entire compartment resulting from the CC continuous forecast were compared with the actual production history and the simulated forecast of an earlier MPP deployment for the years 1998 to 2003. The forecast results of scenario 2 show that a considerable improvement of the ultimate gas recovery of the RB_Z10a and the entire compartment could be achieved by an earlier MPP installation (Table 5.4). Also, production acceleration at RB_Z10a could be achieved, representing up to 4.5 years savings of operations time and corresponding cost savings, possibly to save extended shut-in times (Table 5.4).

Table 5.3: Comparison of RB_Z10a actual/ forecast production for the period 01/2004 - 03/2006

Simulation/Actual Production	**Gas rate [Sm^3/day]**	**THP (reduction limit) [bar]**	**Cum. Gas Mio Sm^3 (01/2004 - 03/2006)**	**Difference [%]**
Actual Production (CC + MPP)	22000 (average)	17 - 2	16.49	-
Forecast Continuous CC	20000	13	5.22	**- 68.3%**
Forecast Continuous MPP	22000	2	17.37	**+ 5.33%**

*) CC = conventional compression; MPP = multiphase pump; THP = flowing tubing head pressure

The actual production data demonstrate that the production life of RB_Z10a was extended until 03/2006 by the use of the MPP. Figures 5.34 and 5.35 illustrate the incremental gas production improved by the MPP facility deployment at an earlier date, compared with actual history production data. The forecast results illustrate that a shorter production period was required to produce the same actual cumulative gas compared with historical production if the MPP facility was utilized prior to 2004. The green curve is the production history; the red curve is the forecast scenario of the MPP deployment in 1998.

Table 5.4: Prediction results (scenario 2); comparison of the continuous CC with an earlier MPP deployment forecasts (1998-2003)

Case	RB_Z10a Cum. Gas Mio. Sm^3	RB_Z10a Ultimate Recovery Improvement %	Main Compartment Cum. Gas Mio. Sm^3	Main Compartment Additional Gas Mio. Sm^3	Main Comp. Ultimate Recovery Improvement %
Forecast - Continuous CC (2004)	***915.5*** *(09/2004)*	-	***1633.1*** *(06/2006)*	-	-
Actual History Production (CC + MPP) (2004)	*929.4*	***+1.52***	*1655.2* *(10/2009)*	*22.1*	***+ 1.35***
Forecast - Earlier Deployment of MPP @ 2003	*932.4*	***+1.84***	*1656.8* *(10/2009)*	*23.7*	***+1.45***
Forecast - Earlier Deployment of MPP @ 2002	*936.6*	***+2.3***	*1661.5* *(10/2009)*	*28.4*	***+1.74***
Forecast - Earlier Deployment of MPP @ 2001	*940*	***+2.67***	*1663* *(10/2009)*	*29.9*	***+1.86***
Forecast - Earlier Deployment of MPP @ 2000	*941*	***+2.78***	*1664* *(10/2009)*	*30.9*	***+1.89***
Forecast - Earlier Deployment of MPP @ 1999	*943*	***+3***	*1667* *(10/2009)*	*33.9*	***+2.07***
Forecast Earlier Deployment of MPP @ 1998	*950*	***+3.77***	*1674* *(10/2009)*	*40.9*	***+2.5***

*) MPP = multiphase pump; CC = conventional compression

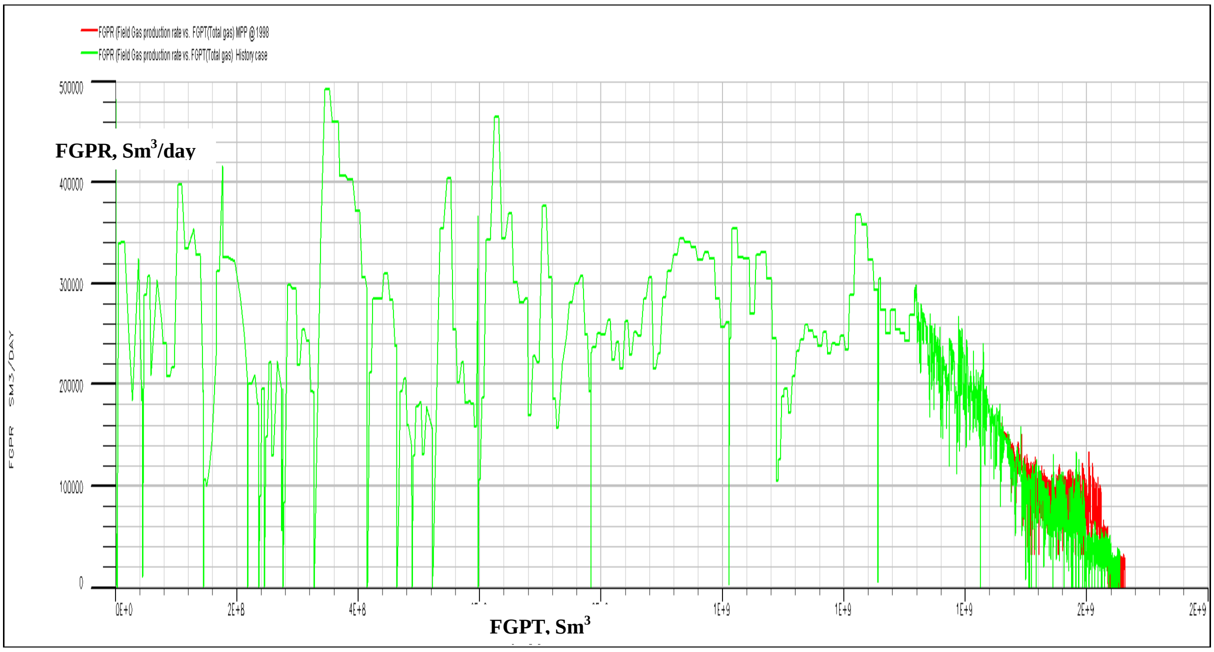

Fig. 5.34: Main compartment cumulative gas & gas rate (observed (green curve) vs. forecast (red curve) of MPP deployment @ 1998). **) FGPR= reservoir gad production rate; FGPT= total reservoir gas production*

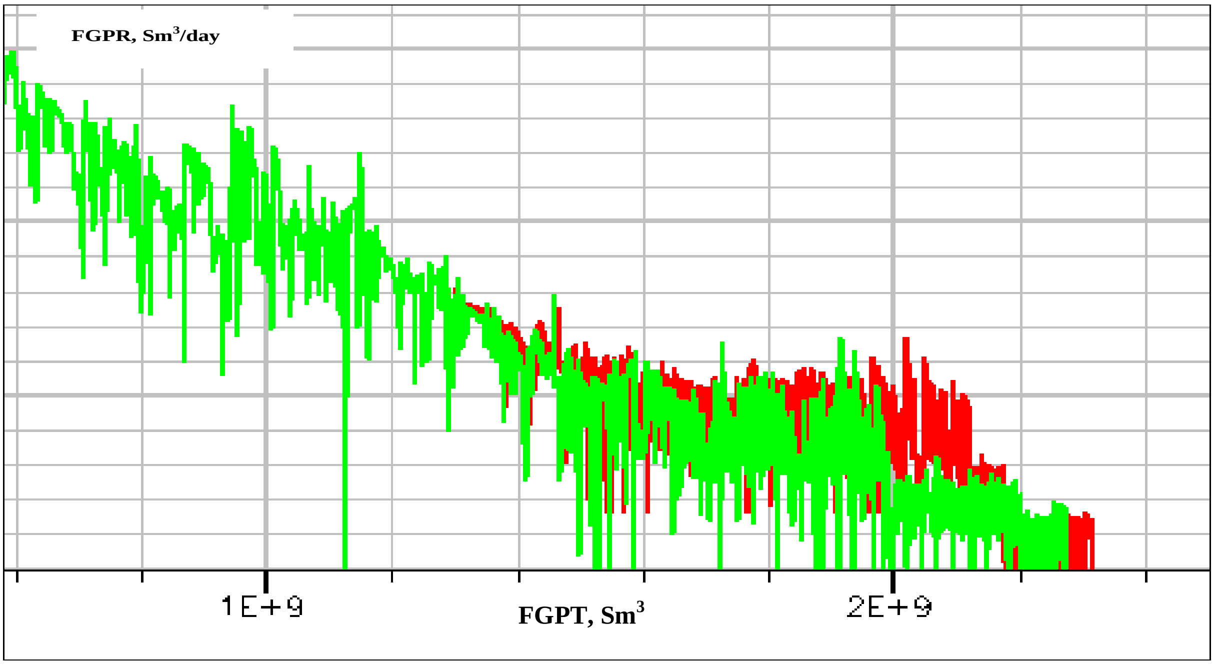

Fig. 5.35: Zoom-in of the production period 1998 – 2009, showing the improvement (red curve) of the main compartment's ultimate recovery by MPP if the MPP would use @ 1998.

The earlier the date of MPP deployment the higher the improvement of the main compartment ultimate recovery would be as shown in the forecast simulation results (Fig. 5.36 & Fig. 5.37), giving evidence of notable economic benefits. Optimally 1998 would be the preferred date to start using the MPP facility because of the highest incremental gas volumes to be produced and ensured production acceleration.

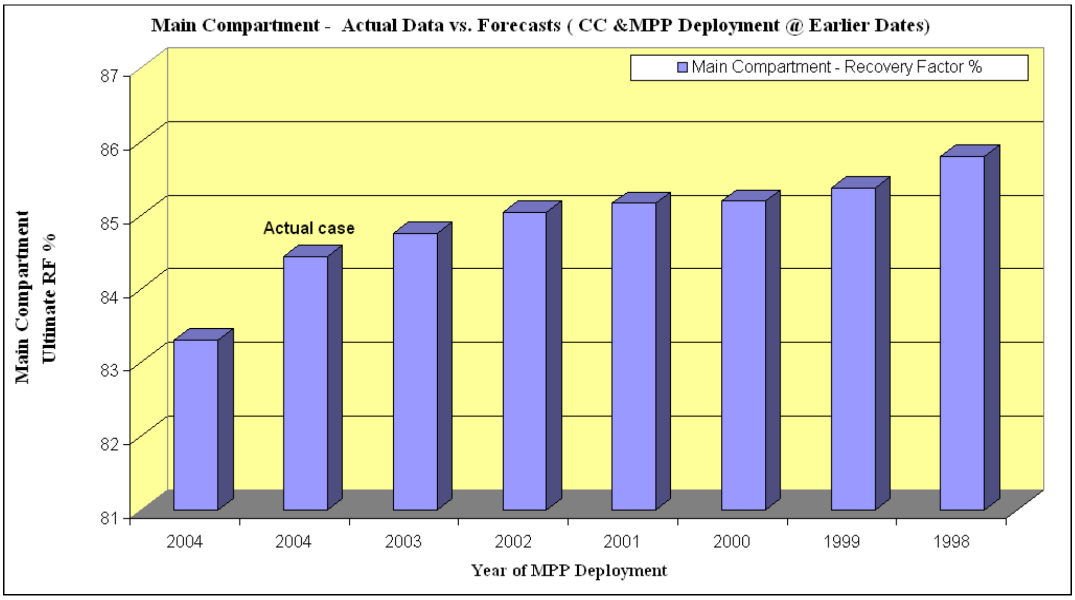

Fig. 5.36: Forecast results; Main compartment recovery factor (RF%) from actual data and MPP deployment at earlier dates forecast.

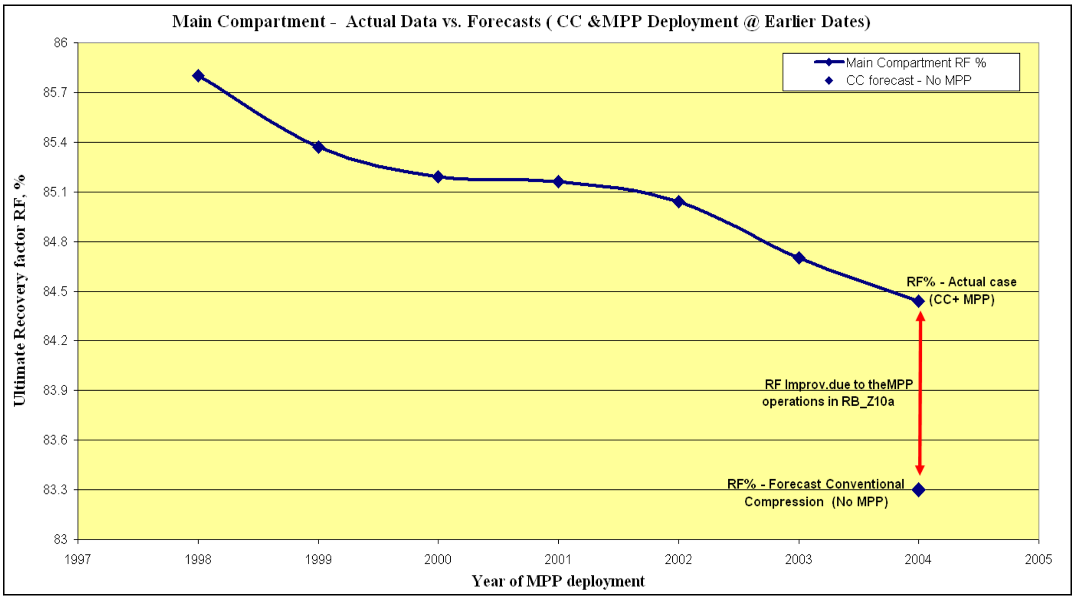

Fig. 5.37: Forecast scenarios of the MPP deployment @ earlier dates. Shown also the well RB_Z10a & main compartment recovery improvements by the early utilize of the MPP. The earlier the date of MPP deployment the more the main compartment ultimate recovery improvement would be.

CHAPTER VI: Multiphase Pump Evaluation Based on Actual Production Data

Analysis and evaluation of the production history data is an important step in understanding the influence of the MPP facility on well behaviour. Figure 6.1 illustrates the historical gas rates of the conventional compression (CC) and MPP facility production systems from 06/2001 to 03/2007 which are used on a continuous daily basis (starting in 2004 without taking into consideration the shut-in periods). The declining trend of the gas production rate of conventional compression phase prior to the MPP facility test changed at the beginning of 2004 (Fig. 6.1). After the MPP phase the subsequent CC phases in 2006 and 2009 demonstrate the steep decline in production towards the final field depletion. The RB_Z10a`s production life would never extend to 2006 without the use of MPP facility.

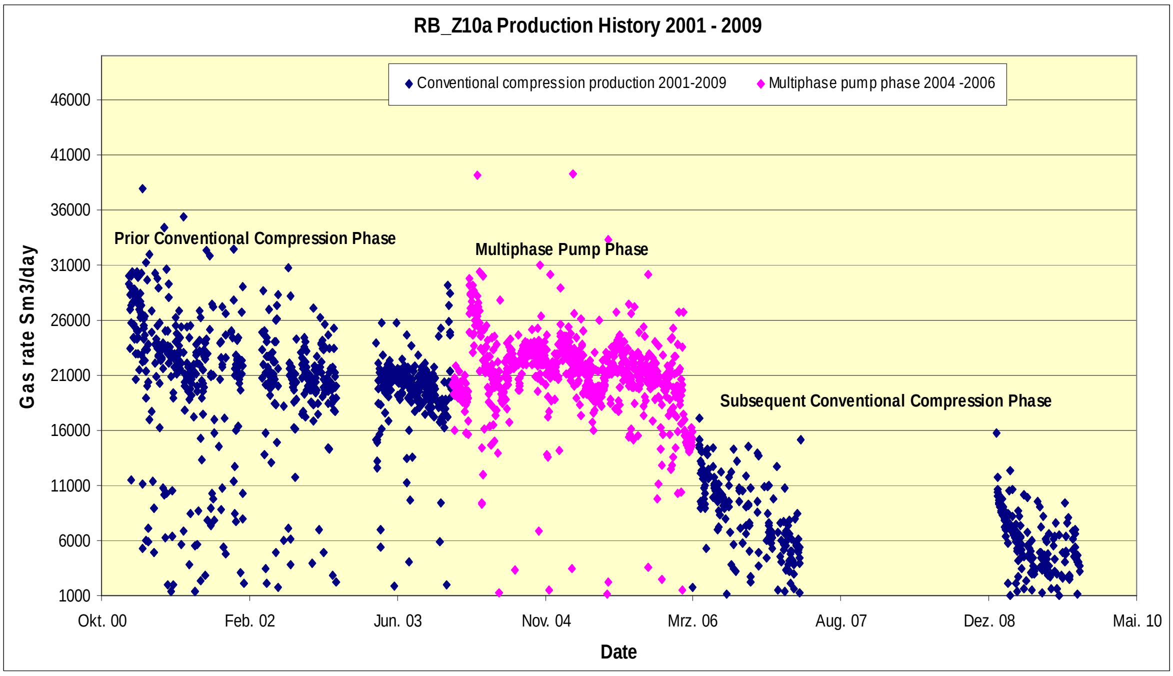

Fig. 6.1: Well RB_Z10a historical gas production rate from 2001-2009. Three production phase could be identified, during (pink dots), after and prior to the multiphase pump operations (2004-2006). In the production phase 2001-2003, the gas rate trend had a tendency to decline several times and the operator used a shut-in periods to keep on the production from the well. When the MPP started to operate the gas rate was enhanced for almost more than two years.

Fluid rate versus time plots are commonly used to diagnose well and reservoir performance. The log-log plot (Fig. 6.2) presents the RB_Z10a gas producer with a linear “straight line” trend for much of its production life. But at several times from 2002 and 2003 the actual performance was considerably below the expected decline rate and the well’s remaining production life appears to be short, unless there is interference in the well gas rate and well performance. The RB_Z10a gas rate was maintained during the production period from 2004 -2006 (6886 -7606 days) by the multiphase pump utilized as shown in Figure 6.2. An analysis of RB_Z10a's daily production data from 2004 to 2006 shows an average increase of gas rate by 15 Sm^3/hr during MPP operation hours compared to the CC production periods. Analysis based on cumulative gas volumes using the operating hours of the CC and MPP (Table 6.1), through the period 01/2004 to 03/2006, shows a clear difference between the two production systems.

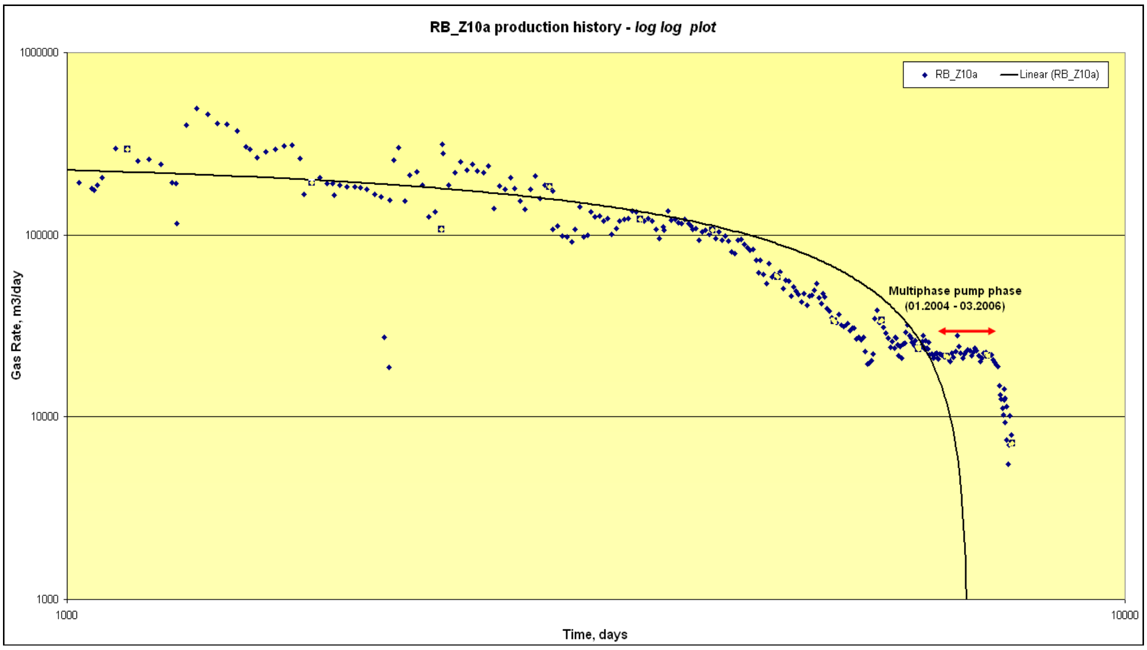

Fig. 6.2: Log-log plot of the RB_Z10a production history (gas rate vs. time). The linear function relation shows that the well would die in 2004 if the MPP was not used. Also shown, the gas rate trend was changed from declining at the production period prior to 2004 to enhancement (2004-2006).

The 11,322 MPP operation hours were scaled down to the 6,864 hours of the CC phase during the production period 2004 - 2006 for the purpose of comparison and evaluation. The MPP facility was not in operation all the time but alternated between phases of MPP and CC production. Before the MPP test, the well head flowing pressure measured at 17 bar. During the operation of MPP, the flowing well head pressure was measured at different reduction intervals between 13 and 2 bar. CC cumulative gas production was 6.16 x 10^6 Sm^3 from 6,864 well operating hours whereas 10.33 x10^6 Sm^3 was the cumulative gas production from 11,322 MPP operating hours. 6,864 MPP facility operation hours resulted in cumulative gas of 6.63 x 10^6 Sm^3, i.e., an increase of 7% compared with the CC production phase (Fig. 6.3). The comparison includes gas and water production. Calculating the gas rate from the cumulative gas over the operating hours of each production type shows an improvement in gas rate of MPP of 7% compared to the CC gas production rate (Fig. 6.4).

Table 6.1: Excerpt of the Excel sheet calculations - RB_Z10a

Date	**Daily gas rate** [m^3]	**Hrs/day** [h]	**Actual gas rate** [m^3/h]	**Cum. Hrs** [h]	**Cum. Gas** m^3	**Calculated gas rate** cum Gas/cum hrs [m^3/hr]
17.12.2003	29142	24	1214	24	29142	1214
18.12.2003	25850	23	1124	47	54992	1170
25.02.2004	24866	24	1036	71	79858	1125
26.02.2004	26609	24	1109	95	106467	1121
27.02.2004	29827	24	1243	119	136294	1145
28.02.2004	29196	24	1217	143	165490	1157
29.02.2004	28306	24	1179	167	193796	1160

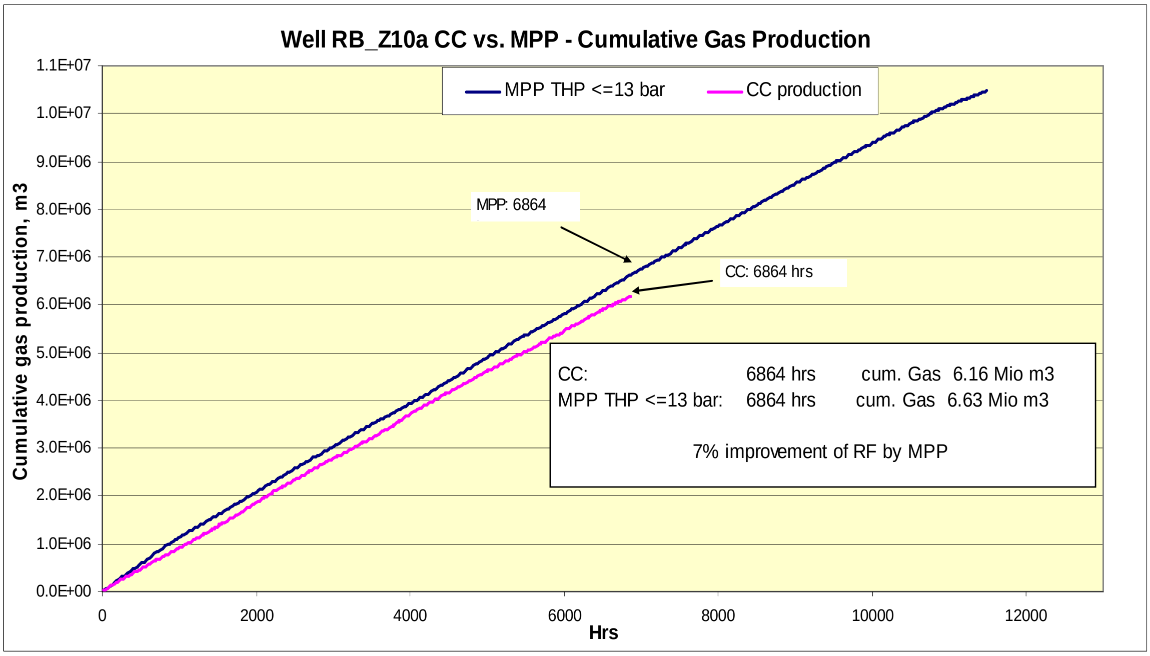

Fig. 6.3: RB_Z10a cumulative gas production (conventional compression (pink line) & MPP (blue line) during the production period 2004 -2006) vs. cumulative operation hours. Higher amounts of gas were accumulated by the use of the MPP compared with that from the conventional compression production system.

Higher amounts of water were produced as the MPP was in operation, compared to the CC system (Fig. 6.5). Consequently, the cumulative water production during the use of the MPP was three times higher than that from the CC production system (Fig. 6.6).

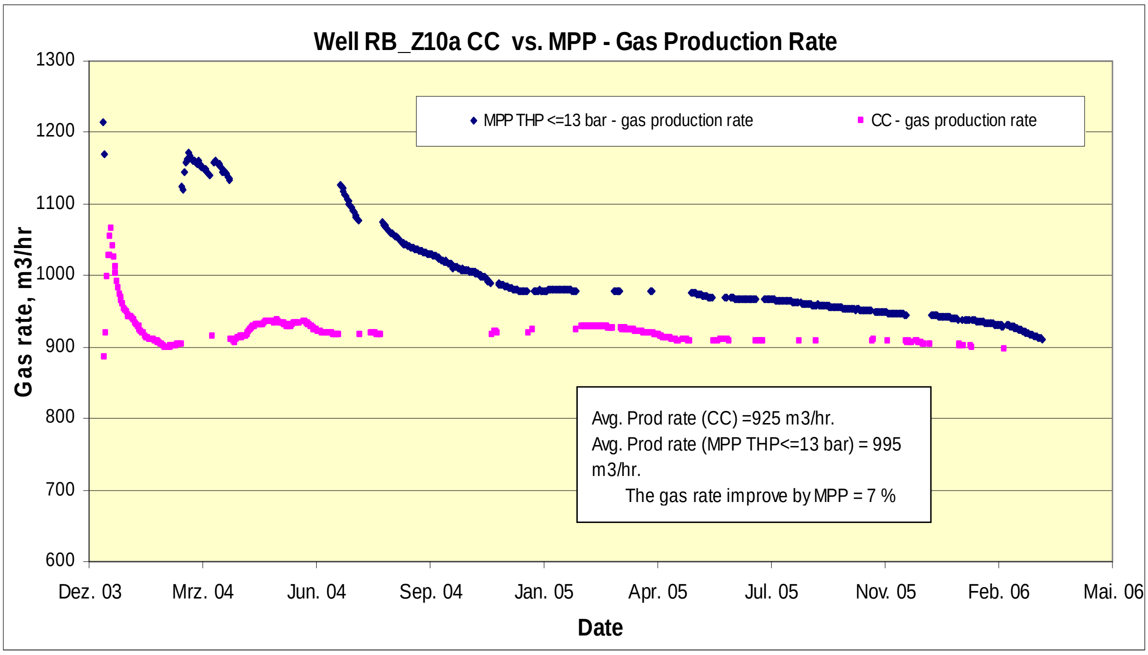

Fig. 6.4: RB_Z10a history gas production rates from the MPP& conventional compression during the production phase (2004 -2006).

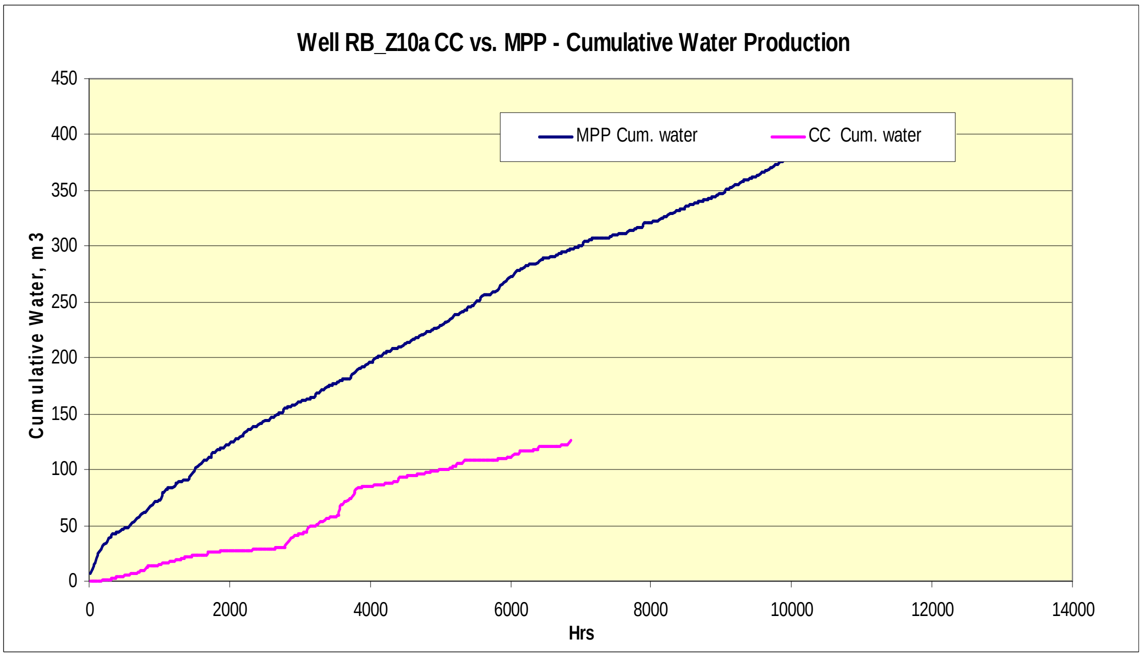

Fig. 6.5: RB_Z10a cumulative water production from the conventional compression & MPP during the production phase (2004 -2006). Higher amount of water was produced by the MPP i.e., the MPP was cleaning-up the water accumulated in the wellbore vicinity and the water resided in the fracture network. This clean-up of the water improve the gas flow towards the well.

Well Operational Availability

At well RB_Z10a, actual production operating hours during the production phases from 01/2002 to 03/2007, the well had an operational availability of 98% as a result of the MPP operations test between 01/2004 and 03/2006.

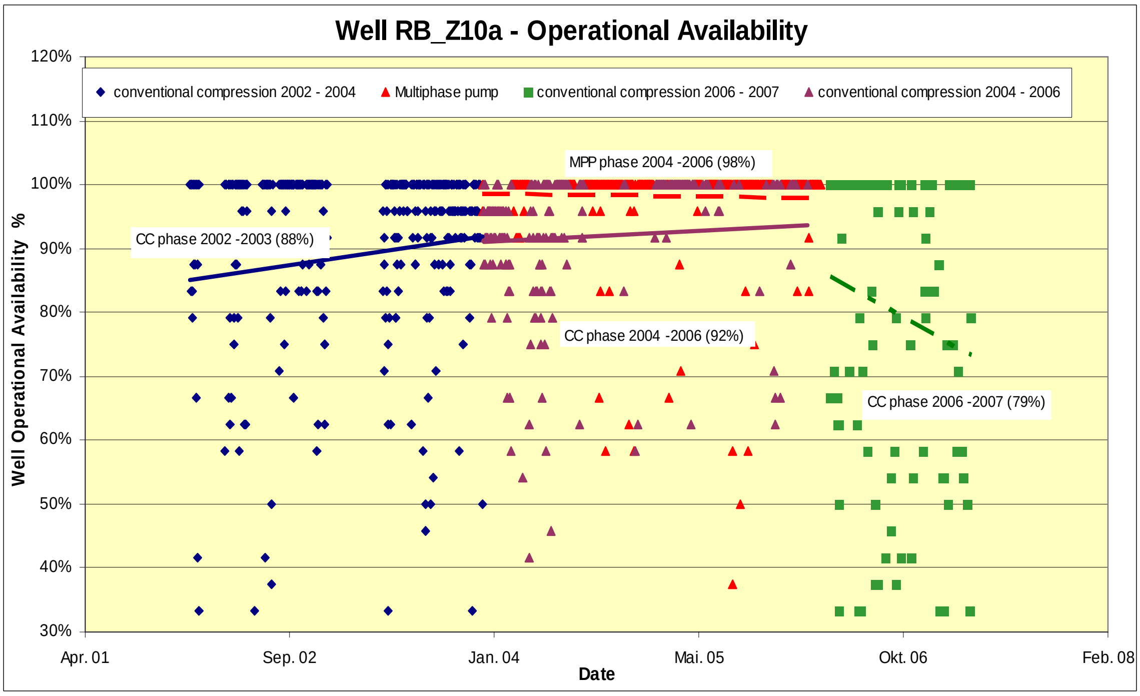

Fig. 6.6: RB_Z10a operational availability during the production period 2002 – 2007.

This was compared to 88% from the CC phase between 01/2002 and 12/2003 excluding shut-in periods, and 55% including shut-in periods (Fig. 6.6). Various factors cause the well to be shut-in, for instance fluctuating gas demand, mechanical failures, build the reservoir pressure pushing the gas up past water in the vicinity of the well, and finally a shut-in might be necessary to carry out other maintenance or construction work on the well site. Well RB_Z10a turned out to be more efficient with the deployment of the MPP.

Stimulus Effect

The conventional compression gas rate during the down-time of the MPP was markedly higher compared to the prior CC production phase in 2002 - 2003 (Fig. 6.7). The mathematical linear function drawn by the Excel program illustrates two different trends for the CC actual gas rates during MPP production phase (2004-2006) and the prior production phase (2002-2003). Observable facts can be interpreted as stimuli for the entire compartment by the MPP facility, as a result of lowering the flowing bottom hole pressure in RB_Z10a. Also, this phenomenon was observed in the neighbouring well, OT_Z02's production history behaviour. The positive production response (stimulus effect) was induced by the MPP test on RB_Z10a, increasing the pressure difference between the crest structure wells and the drainage areas, i.e., pulling out the water and gas from the far drainage areas towards the crest of the structure.

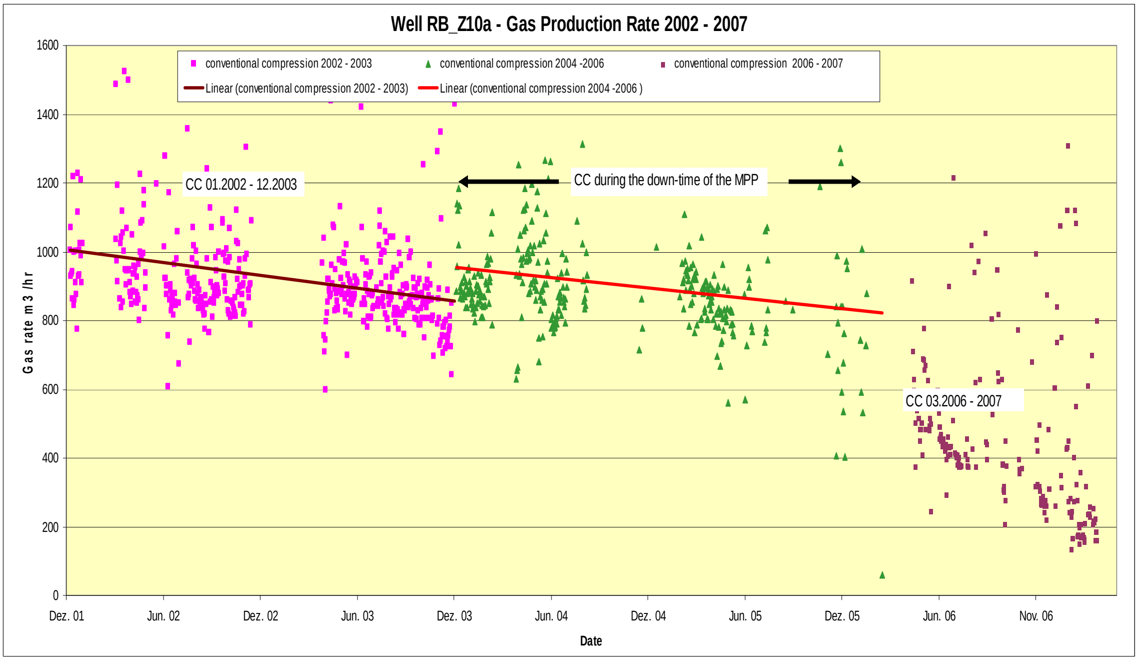

Fig. 6.7: RB_Z10a conventional compression actual production phases from 2002 - 2007. The linear function trend lines show that the conventional compression gas rates during the MPP phase were higher compared with the prior and following phases.

The removal of water from the fractures by the MPP through the reduction of the flowing tubing head pressure improved the reservoir performance. Consequently, there was an increase in the gas relative permeability by removing water from the fractures flow conduits (Fig. 6.8).

Figure 6.9 shows the OT_Z02 production history phases which includes: the production phase prior to the MPP phase (01/2002 -12/2003), during the MPP phase (01/2004-03/2006) and after the MPP phase (04/2006 – 03/2007. The observed conventional compression production rates of OT_Z02 through the production period from 2002-2003 had decline trend; however from 01/2004 to 03/2006 the production rates stabilized at certain range and even increased (Fig. 6.9). The change in the gas production rate of well OT_Z02 was happened when the MPP was operated in RB_Z10a which indicate that the positive impact on OT_Z02 performance was caused by the MPP operations in RB_Z10a. Figure 6.9 demonstrates how the observed gas rates of OT_Z02 fall down immediately after the MPP production phase. The log-log plot (Fig. 6.10) of the OT_Z02 production history data demonstrate that gas rate declining trend towards an end of production life of OT_Z02 would occur earlier and the actual ultimate recovery would not obtain without the MPP operations in RB_Z10a.

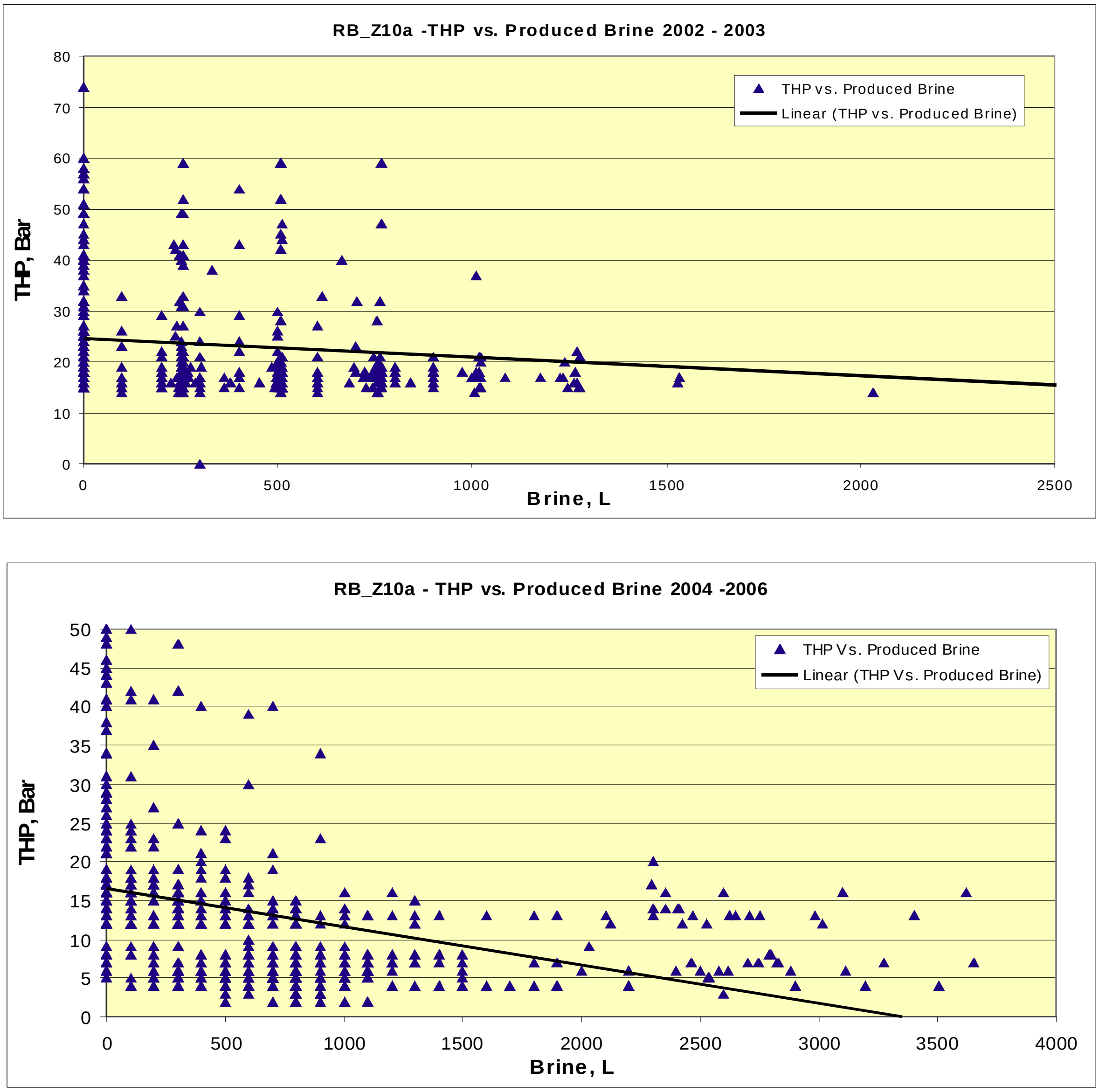

Fig. 6.8: RB_Z10a tubing head pressure vs. produced brine (2002 - 2006). The higher the reduction of tubing head pressure by the MPP operations, the higher the produced amounts of brine.

The numerical simulations were also used to investigate the impact of the MPP operations in RB_Z10a on the neighbouring well OT_Z02. Conventional compression forecast was carried out, eliminating the production history data of OT_Z02 and using minimum flowing tubing head pressure of 13 bar and a gas rate of 20,000 Sm^3/day. The forecast simulation shows that due to the stimulus effect by MPP, an additional gas volume of 8 Mio Sm^3 was gained from OT_Z02.

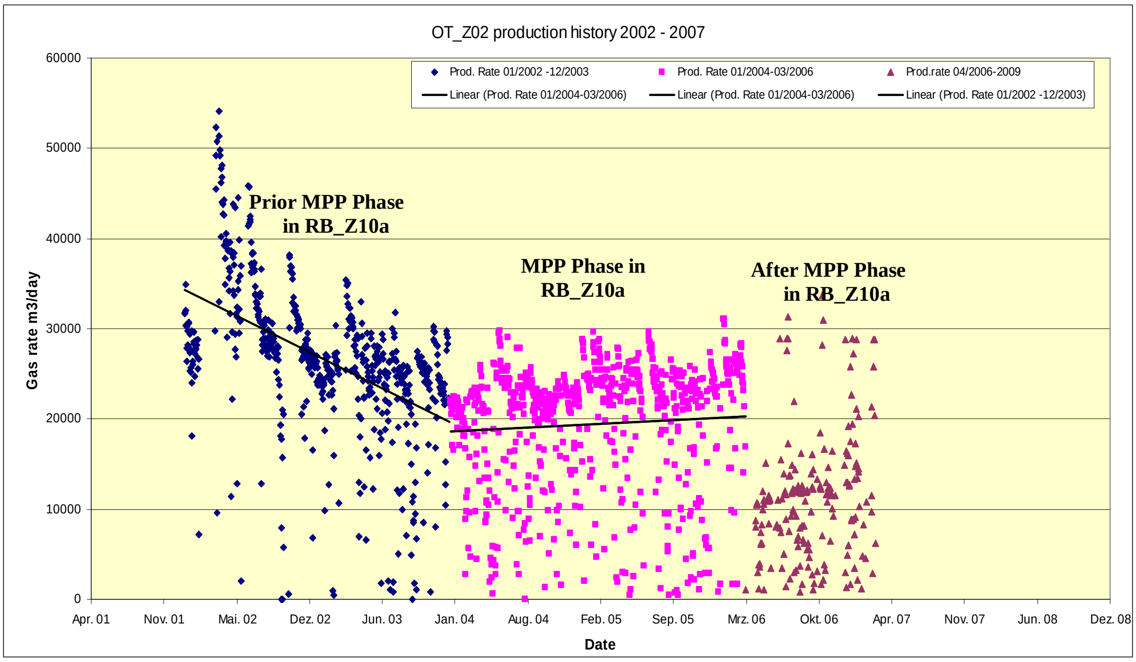

Fig. 6.9: Well OT_Z02 production history (gas rate vs. time). The OT_Z02 gas rate decline trend during the production phase 2002 – 2003 was changed to be a maintained rate trend and even with higher rates when the MPP was operated at the well RB_Z10a. As the MPP operations were stopped in 03/2006 in RB_Z10a, the OT_Z02 gas rates fall down.

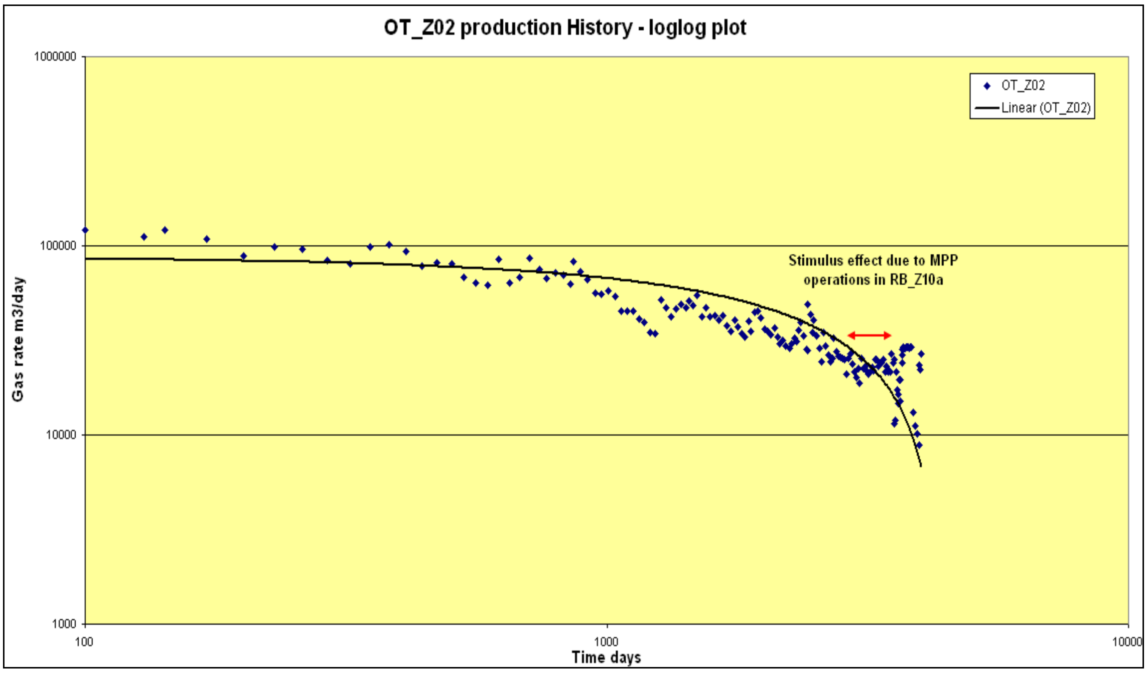

Fig. 6.10: Log-log plot of the well OT_Z02 production history (gas rate vs. time).

CHAPTER VII:

7.1 Conclusions

The reservoir simulation based on field reservoir production history for the 10 wells in the Hauptdolomit reservoir model was the ideal methodology for the investigation of reservoir performance during multiphase pump operations.

Despite data limitations, the geological model was interactively improved by dynamic reservoir data, a perfect history match was achieved, with the key parameters being fracture permeability, identification of tight zone, implementation of supplementary faults and flow barriers which were major contributing factors in the gas flow and pressure distribution.

The observed reservoir performance of the Rütenbrock-Hauptdolomit reservoir during multiphase pump operations brought the following conclusions:

- The forecasts simulation results during the production period 01/2004-03/2006 demonstrated that the continuous operation of the MPP had a positive impact on the optimised gas recovery of well RB_Z10a.
- Deploying the MPP facility prior to the production year 2004 would have ensured an improvement of the ultimate gas recovery of the entire compartment and well RB_Z10a and production acceleration, subsequently improved field economics.
- Numerical reservoir simulation and decline curve analysis agree that without the use of MPP, well RB_Z10a would go to the end of its production life in 2004 i.e. the RB_Z10a well’s production life was extended by the deployment of the multiphase pump.
- Analysis of the available historical production data concludes the following observable facts: 1) RB_Z10a turned out to be operationally more efficient by the deployment of the MPP between 01/2004 and 03/2006 compared to the prior production phase from 2001 to 2003; 2) The stimulus effect over the entire compartment as a consequence of the use of MPP was positive, observed in the conventional compression gas rate periods during the down-time of the MPP facility. Also, this effect was observed at the neighbouring gas producer OT_Z02 which located approximately at distance of 1.5 km from RB_Z10a.

Due to water produced by the MPP, compared with the conventional production system during its operations, there is a clean-up of the residual water from the fracture network, resulting in improvement of the gas relative permeability flow to the crest structure wellbores and an enhanced gas rate.

A field test of the MPP in a mature carbonate sour gas reservoir demonstrated that this technology can be used, due to the fact that the well responded to reduced wellhead pressure and additional gas production was recorded. By reducing the back pressure on the well head, multiphase pumping technology is able to extend the well/reservoir production life and produce incremental gas, also allowing the reservoir to accelerate production and as a result to delay the abandonment of the gas producers. In summary, the multiphase pumping technology can make marginal fields more economical, increase field life and gas recovery.

7.2 References

Al-Reshedan, F. S., Saudi Aramco, Gawish, A, Hazim, D. N., Petroleum and Natural Gas Engineering Dept. King Saud University(2009): *Evaluation the Methodologies of Analyzing production and Pressure data of Hydraulic Fractured Wells in Low Permeability Gas Reservoirs*, Oil and Gas Business, 2009.

Allen, T. O, Roberts, P. A. (1982): *Production Operations*, Volume2 Oil & Gas Consultants International, Inc. Tulsa 1982.

Aprilian, S.S. and Kurnely, K. Pertamina EP, (2006): *Improving the Value-Risk Management on Revitalizing Mature Oil Fields in One Company's Operating Area*, SPE Annual Technical Conference and Exhibition, 24-27 September 2006, San Antonio, Texas, USA.

Arps, J.J., (1945): *Analysis of Decline Curve,* Trans., AIME (1945), pp. 228-247.

Agarwal, R.G., Gardner, D.C., Kleinsteiber, S.W., and Fussell, D.D., (1998): *Analyzing Well Production Data Using Combined Type Curve and Decline Curve Concepts*, Paper SPE 57916 presented at the 1998 SPE Annual Technical Conference and Exhibition, New Orleans, September 27-30.

Archie, G.E. (1950): *Introduction to Petrophyscis of Reservoir Rocks*, Bull. Armer. Assoc. Petrol. Geol., Vol: 34, Nr: 5.

Archie, G. F. Housten Texas, (1952): *Classification of Carbonate Reservoirs Rocks and Petrophysical Consideration*, Bulletin of AAPG, Vol 36, No 2, PP. 278-298.

Barenblatt, G.I., Zheltov, I.P., and Kochina, I.N., (1960): *Basic Concepts in the Theory of Seepage of Homogeneous Liquids in Fissured Rocks*: Journal of Applied Mathematics, v. 24, 1286-1303.

Bauer, H., Decker, K, University of Vienna (2010): *Fault Architecture, Fault Rocks and Fault Rock Properties in Carbonate Rocks*, Geophysical Research Abstracts Vol. 12, EGU2010-5112, 2010, EGU General Assembly 2010.

Bennion, D. B. Thomas, F. B. Schulmeister, B. E. M. Sumani, Hycal Energy Research Laboratories Ltd (2004): *Determination of True Effective In Situ Gas Permeability in Subnormally Water-Saturated Tight Gas Reservoirs*, Journal of Canadian Petroleum Technology, Volume 43, Number 10, October 2004.

Bennion, D. B. Thomas, F. B. Schulmeister, B. E. Hycal Energy Research Laboratories Ltd.; J. Rushing, Anadarko Petroleum Corporation (2002): *Laboratory and Field Validation of the Mechanism of Establishment of Very Low Initial Water Saturations in Ultra-Low Permeability Porous Media*, Canadian International Petroleum Conference, Jun 11 - 13, 2002 , Calgary, Alberta.

Bennion, D. B. Thomas, F. B. D. Imer, T. Ma, Hycal Energy Research Laboratories Ltd. (2000): *Low Permeability Gas Reservoirs and Formation Damage -Tricks and Traps*, SPE/CERI Gas Technology Symposium, 3-5 April 2000, Calgary, Alberta, Canada.

Bennion, D. B. Thomas, F. B. and T. Ma, Hycal Energy Research Laboratories Ltd.(2000): *Formation Damage Processes Reducing Productivity of Low Permeability Gas Reservoirs*, SPE Rocky Mountain Regional/Low-Permeability Reservoirs Symposium and Exhibition, 12-15 March 2000, Denver, Colorado.

Blasingame, T.A., Johnston, J.L., and Lee, W.J. (1989): *Type-Curve Analysis Using the Pressure Integral Method*, Paper SPE 18799 presented at the SPE California Regional Meeting held in Bakersfield, April 5-7, 1989.

Blasingame, T.A, McCray, T.L., and Lee, W.J. (1991): *Decline Curve Analysis for Variable Pressure Drop/Variable Flowrate System*, Paper SPE 21513 presented at the SPE Gas Technology Symposium, January 23-24, 1991.

Blasingame, T.A. and Palacio, J.C. (1993): *Decline-Curve Analysis Using Type Curves - Analysis of Gas Well Production Data*, paper SPE 25909 presented at the 1993 SPE Rocky Mountain Regional Meeting/Low Permeability Reservoirs Symposium, Denver, 26-28 April.

Boigk, H., (1981): *Erdöl und Erdölgas in der Bundesrepublik Deutschland*. Enke Verlag, Stuttgart. 313 pp.

Bourdet, D., Ayoub J., Whittle, T., Pirard, Y., and Kniazeff V. (1983): *Interpreting Well Tests in Fractured Reservoirs*, World Oil (October 1983) 77.

Bourdet D., Whittle T., Douglas A. and Pirard Y. (1984): *New Type Curves Aid Analysis of Fissured Zone Well Tests*, World Oil (April 1984) 111.

BP Publication Magazine Issue 21, Subsea King Field, www.bp.com.

Bradley, H.B (1987): *Petroleum Engineering Handbook, Society of Petroleum Engineers*, Richardson, TX, USA.

Brongersma, M., (1972): *Hydrological Conditions Leading to the Development of Bituminous in the Pre-Evaporite Phase: in Geology of Saline Deposits*. Unesco Earth Sci, Ser. No.

Chilingarian, G. V.; Mazzullo, S. J.; Rieke, H. H. (1996): *Carbonate Reservoir Characterization - A Geologic-Engineering Analysis*, Part II, Elsevier, 1996.

Chilingarian, G.V., Eremenko, N.A., Gorfunkel, M.V. (2005): *Geology and Geochemistry of Oil and Gas*, Developments in Petroleum Science 52, New York, Heidelberg, u. a.: Elsevier. 2005.

Christensen, M. (2001): *Petrozuata`s Experience with Multiphase Pumps in Heavy Oil, Gas, Water and Sand Service*, presentation given at the 3rd Annual Texas A&M Multiphase Pump User Roundtable (MPUR), Houston (May 3, 2001).

Cimic, M (2006): *Russian Mature Fields Redevelopment*, SPE 102123, Russian Oil and Gas Technical Conference and Exhibition, 3-6 October 2006, Moscow, Russia.

Clark, D.N. (1980): *The Sedimentology of the Zechstein 2 Carbonate Formation of Eastern Drenthe, the Netherlands*. In: H. Füchtbauer and T. Peryt, Editors, the Zechstein Basin with Emphasis on Carbonate Sequences Contrib. Sedimentology 9 (1980), pp. 131–165.

Corless, R. (2001): *Multiphase Pumps Replace Conventional Heavy Oil Facilities*, Oil & Gas J. (Sept. 24, 2001).

Collins, A. Gene (1975): *Geochemistry of Oilfield Waters, Amsterdam*; New York: Elsevier Scientific Pub. Co. 1975.

Crain, E. R. (2000): *Petrophysical Handbook*, 3rd-Millennium Edition, Version 3.10 Online at *www.spec2000.net*.

Cramer, D., (2003): *Evaluating Well Performance and Completion Effectiveness in Hydraulically Fractured Low-Permeability Gas Wells*, Paper SPE 84214 presented at the 2003 SPE Annual Technical Conference and Exhibition, Denver, Oct. 5-8.

Cramer, D., (2004): Analyzing *Well Performance in Hydraulically Fractured Gas Wells: Non-Ideal Cases*, Paper SPE 90777 presented at the SPE Annual Technical Conference and Exhibition in Houston, Texas, U.S.A., September 25-29, 2004.

Cuong T.Q. D., SPE, Nguyen, N. T.B., SPE, and Bae, W., SPE, Sejong University; Byounghi Jung, MKE, Korea; and Jeonghwan Lee, Korea Gas Corporation (2009): *A Precious Achievements Review of Geological Development and IOR Application from 20 Successful Years in High Temperature Fractured Granite Reservoir*, International Petroleum Technology Conference, 7-9 December 2009, Doha, Qatar.

Dandekar, A.Y. (2006): *Petroleum Reservoir Rock and Fluid Properties*, Taylor & Francis Group, New York.

Dal Porto, D.F, and Larson, L.A (1996): *Multiphase Pump Field Trials Demonstrate Practical Applications for the Technology*, SPE paper 36590 presented at the Society of Petroleum Engineers, Annual Technical Meeting, Houston, October 6-9, 1996.

Devegowda D. and S.L. Scott (2003): *An Assessment of Subsea Production Systems*, SPE paper 84045 accepted for presentation at the 2003 SPE Annual Technical Meeting & Exhibition, Denver, Colorado, Oct. 3-6.

Dinwiddie, C. L., Bradbury, K., Ronald, N., McGinnis, R., W. Fedors, and Ferrill, D. A. (2006): *Fault Zone Deformation Overprints Permeability of Nonwelded Ignimbrite: Chalk Cove Fault, Bishop Tuff*, Bishop, California, Published in Vadose Zone Journal 5:610–627 (2006).

Dorenbos, C., Mueller-Link, D. & Jaeschke, A. (2001): *Sand Handling During Multiphase Operations with Twin-Screw Pumps*, SPE Paper No. 69846, Thermal Operations and Heavy Oil Symposium, Venezuela.

ECLIPSE Program Manual (2008), Schlumberger

Elde, J. (2005): *Advantages of Multiphase Boosting, Business Briefing, Exploration & Production*: The Oil & Gas Review, p. 2, 2005.

Falcimaigne, J., Brac, J., Charron, Y., Pagnier, P., Vilagines, R. (2002): *Multiphase Pumping: Achievements and Perspectives*, Oil & Gas Science and Technology - Rev. IFP, Vol. 57 (2002), No. 1, pp. 99-107.

FAST.RTA™ Program (version 3.5+) Manual 2010, Fekete Associates Inc.

Fetkovich, M.J., (1980): *Decline Curve Analysis Using Type Curve*, JPT (June 1980).

Fernø M. A. (2008): *A Study of Capillary Pressure and Capillary Continuity in Fractured Rocks*, a dissertation submitted to the Department of Physics and Technology, University of Bergen, Norway in partial fulfillment of the requirements for the degree philosophiae doctor Bergen, Norway, June, 2008.

Firoozabadi, A. and Hauge, J. (1990): *Capillary Pressure in Fractured Porous Media*, J. Pet. Tech. 42(6):pp.784-791, 1990.

Firoozabadi, A. and Markeset, T. (1994): *Fracture-Liquid Transmissibility in Fractured Porous Media*, SPE Reservoir Eng. 9(3):pp.201-207, 1994.

Framo Engineering As, Technical Bulletin: *Boosting Increased Oil Production and Recovery Utilizing*, Bergen Norway, *www.framoeng.no.*

Gaskari, R., Mohaghegh, S. D. and Jalali, J., West Virginia University (2006): *An Integrated Technique for Production Data Analysis with Application to Mature Fields*, This paper was prepared for presentation at the 2006 SPE Gas Technology Symposium held in Calgary, Alberta, Canada, 15–17 May 2006.

Gang, T. SPE, and M. Kelkar, SPE, U. of Tulsa (2006): *Efficient History Matching in Naturally Fractured Reservoirs*, SPE/DOE Symposium on Improved Oil Recovery, 22-26 April 2006, Tulsa, Oklahoma, USA.

Gautam, P.S. and Mohanty, K.K. (2004): *Matrix-Fracture Transfer through Countercurrent Imbibition in Presence of Fracture Fluid Flow, Transport in Porous Media* 55(3):pp.309-337, 2004.

Geluk, M.C. (2000): *Late Permian (Zechstein) Carbonate Facies Maps, the Netherlands*, Netherlands Journal of Geosciences/Geologie en Mijnbouw 79: 17–27.

Geluk, M.C. (2005): *Stratigraphy and Tectonics of Permo-Triassic Basins in the Netherlands and Surrounding Areas*. – Thesis Univ. Utrecht: 171 pp. ISBN 90-393-3911-2.

Geluk, M.C. (2007): *Permian. In: Geology of the Netherlands*. Royal Netherlands Academy of Arts and Science, Amsterdam: 63-83 pp. ISBN 978-90-6984-481-7.

Giuggioli, A, Villa, M., De Ghetto, G., and Colombi, P. (1999): *Multiphase Pumping for Heavy Oil: Results of a Field Test Campaign*, SPE paper 56464 presented at the 1999 SPE ATCE, Houston (October 3-6, 1999).

Glass, R.J., Nicholl, M.J. and Tidwell, V.C. (1995): *Challenging Models for Flow in Unsaturated, Fractured Rock through Exploration of Small Scale Processes*, Geophysical Research Letters 22(11):pp.1457-1460, 1995.

Glennie, K. W., (1986): *Introduction to the Petroleum Geology of the North Sea, Late Permian-Zechstein*, Blackwell Scientific Publication 1986.

Gonzalez, R. and Guevara, E. (1995): *Economic Field Development in Venezuela Heavy Oil Fields Using Multiphase Pumping Technology*, SPE paper 30262 presented at the 1995 International Oil Symposium, Alberta, Canada (June 19-21, 1995).

Guo, B. and Ghalambor, A. (2005): *Natural Gas Engineering Handbook*, Gulf Publishing Company, Houston, Texas, 2005.

Guo, B. and Ghalambor, A. SPE, U. of Louisiana at Lafayette; Chengcai Xu, CNPC Well Logging Services (2006): *A Systematic Approach to Predicting Liquid Loading in Gas Wells*, Journal SPE Production & Operations, Volume 21, Number 1, pp. 81-88, February 2006.

Hamon, G., Mauduit, D., Bandiziol, D., Massonnat, G (1991): *Recovery Optimization in a Naturally Fractured, Water-Drive Gas Reservoir: Meillon Field*, SPE paper 22915, SPE Annual Technical Conference and Exhibition, 6-9 October 1991, Dallas, Texas.

Heyl, R. F. (2007): *Multiphase Pumping*, Proceeding of the Twenty Third International Pump Users Symposium, Chevron Energy, Research and Technology Company, Houston Texas.

Heng, Li, Chang, H. and Zhang, D., SPE, University of Southern California (2009): *Stochastic Collocation Methods for Efficient and Accurate Quantification of Uncertainty in Multiphase Reservoir Simulations*, SPE Reservoir Simulation Symposium, 2-4 February 2009, the Woodlands, Texas.

Holtz, M.H. The University of Texas, Austin, (2002): *Residual Gas Saturation to Aquifer Influx: A Calculation Method for 3-D Computer Reservoir Model Construction*, SPE Gas Technology Symposium, 30 April-2 May 2002, Calgary, Alberta, Canada.

Horie, T., Firoozabadi, A. and Ishimoto, K. (1990): *Laboratory Studies of Capillary Interaction in Fracture/Matrix Systems*, SPE Reservoir Eng. 5(3):pp.353-360, 1990.

Huttel, P. and Mausfeld, S. (1991): *Digenesis of a Carbonate Member of an Evaporitic Cycle: the Stassfurt Carbonate Formation (Ca2) of South Oldenburg (NW Germany).* Zentralbl. Geol. Palaontol. Teil I, 4, pp. 1073–1090.

International Energy Agency (2004): *Extending the Life of Conventional Fields*. Source: International Energy Agency - Economic Price in 2004.

Jaggernauth, A.J., Brandt, J.U. and Müller-Link, D. (1996): *Offshore Multiphase Pumping Technology Identifying the Problems; Implementing the Solutions-Part 1*, paper presented at the 1996 SPE/NFP European Production Operations Conference, Stavanger (April 16-17, 1996).

Jourde, H. Cornatonb, F. Pistrea S. and Bidauxa, P. (2002): *Flow Behavior in a Dual Fracture Network*, Journal of Hydrology, Volume 266, Issues 1-2, 5 September 2002, Pages 99-119.

Kaiser, R (2001): *Fazies und Sequenzstratigraphie: Das Staßfurtkarbonat (Ca2) am Nördlichen Beckenrand des Südlichen Zechsteinbeckens (NE-Deutschland)*, Hauptdolomit Thesis, 165p, Universität Köln.

Kazemi, H. M.S. Seth, and G.W. Thomas, Atlantic Richfield Co. (1969): *The Interpretation of Interference Tests in Naturally Fractured Reservoirs with Uniform Fracture Distribution*, SPE Journal, Volume 9, Number 4, pages 463-472, December 1969.

Kikani, Jitendra, Stanford U.; Walkup Jr., Gardner W., Chevron Oilfield Research Co.(1991): *Analysis of Pressure-Transient Tests for Composite Naturally Fractured Reservoirs*, SPE Formation Evaluation, Volume 6, Number 2, pages 176 -182, June 1991.

Labastie, A.(1990): *Capillary Continuity between Blocks of a Fractured Reservoir*, SPE ATCE, New Orleans, LA, USA, September 23-28, 1990.

Lawrence Camilleir, Jaime Mendieta (2005): *Artificial Lift*-Schlumberger, Europe-Africa, Technical Manager, Multiphase pumping, Schlumberger, *http://www.slb.com/media/services.*

Lee, J., and Wattenbarger, R.A. (1996): *Gas Reservoir Engineering*, Textbook Series Vol.5, SPE, USA (1996).

Lisigurski, O. and G.C. Rowe, SPE, Oxy U.S.A. Inc. (2006): *Practical Steps To Increase Production and Reserves in Mature Gas Fields: Hugoton and Panoma, Texas County, Oklahoma, USA*, SPE Annual Technical Conference and Exhibition, 24-27 September 2006, San Antonio, Texas, USA.

Lu, B. Alshaalan T.M. and Wheeler M.F. (2007): *Iterative Coupled Reservoir Simulation for Multiphase Flow*, SPE Annual Technical Conference and Exhibition, 11-14 November 2007, Anaheim, California, U.S.A. (SPE 110114).

Martin, A.M. and Scott, S.L. (2002): *Modeling Reservoir/Tubing/Pump Interaction Identifies Best Candidates for Multiphase Pumping*, SPE paper 77500 presented at the SPE Annual Technical Meeting & Exhibition, San Antonio (Sept. 29 - Oct. 2, 2002).

Mattar, L. and Anderson, D.M., (2003): *A Systematic and Comprehensive Methodology for Advanced Analysis of Production Data*, Paper SPE 84472 presented at the SPE Annual Technical Conference and Exhibition in Denver, Colorado. U.S.A., Oct. 5-8, 2003.

MBAL program Manual (2007), Petroleum Experts Ltd., Edinburgh UK.

McCain, WD. Jr (1990): *The Properties of Petroleum Fluids,* Second edition, Penn-Well Publishing Co. Inc.Tulsa, Oklahoma, USA.

McKetta, J.J., and Wehe, A.H., (1958): *Use This Chart for Water Content of Natural Gases,* Petroleum Refiner, August 1958, pp. 153-154.

Mireault R. and Dean, L. Fekete Associates Inc (2008): *Material Balance Analysis, Reservoir Engineering for Geologists,* Part 5A, ISSUE 2 February 2008.

Müller-Link, D., Rohlfing, G. & Spelter, H. (2009): *Twin-Screw Pumps Help Improving Oil Recovery in Mature Fields and Transfer Heavy Crude Oil over Long Distances*, Oil and Gas European Magazine, 3/2009, pp. 127-131, Urban-Verlag, Hamburg – Wien.

Naik, G.C. (2002): *Tight Gas Reservoirs – An Unconventional Natural Energy Source for the Future*.

Nelson, R.A. (2001): *Geologic Analysis of Naturally Fractured Reservoirs,* Gulf Professional Publishing, Woburn, MA, 2001.

Olson, S. Leistritz Corporation (2006): *Multiphase Pumps Solve Liquid Loading*, the American oil & gas reporter, May 2006.

Parsons, R.W. (1966): *Permeability of Idealized Fractured Rock*, Society of Petroleum Engineers Journal (1966), pp. 126–136.

Pershukov, V.A., de Salis, J. and Cordner, M. (2001): *Multiphase Pumps for 250000 bbl/day Field Development*, SPE Annual Technical Conference, Paper 71562, New Orleans, September 30-October 3, 2001.

PETREL^{TM} Program Manual (2007), Schlumberger

Pickard, B., (2003): *Subsea Multiphase Pumps in the Ceiba Field - W. Africa*. Presentation given at the 5th Annual Texas A & M Multiphase Pump User Roundtable, Houston (May 7-8, 2003).

PROSPER Program Manual (2007), Petroleum Experts Ltd., Edinburgh UK.

Räbiger, K., Maskoud, T. M. A. & Ward, J. (2006): *Thermo- and Fluid Dynamic Model of a Multiphase Screw Pump, Operating at Very High Gas Volume Fractions*. University of Glamorgan, School of technology, Wales, UK, ISSN 1616-0762 Sonderdruck Schriftenreihe der Georg-Simon-Ohm-Fachhochschule Nürnberg Nr. 35.

Reitenbach V., Pusch G., Nami P., Meyn R. et al. (2006): *Simulation of the Production Behaviour of Hydraulically Fractured Wells in Tight Gas Reservoirs*, Project 593-9, DGMK research program 593: “Tight Gas Reservoirs”, Final report, 2006.

Richter-Bernburg, G. (1959): *Zur Palaegeographie der Zechsteins. In: I giacimenti gassiferi dell Europa Occidentale 1*, Accad. Nazional die Lincei, Rome. Pp. 88 – 99.

Rushing, J.A., and Blasingame, T.A., (2003): *Integrating Short-Term Pressure Buildup Testing and Long-Term Production Data Analysis to Evaluate Hydraulically- Fractured Gas Well Performance,* Paper SPE 84475 presented at Annual Technical Conference and Exhibition in Denver, Colorado, October 5-8, 2003.

Rückheim, J. and Voigtländer, G., SPE, Erdgas Erdöl GmbH, and M. Stein-Khokhlov, SPE, E.ON Ruhrgas E&P (2005): *The Technical and Economic Challenge of Mature Gas Fields - The Giant Altmark Field: A German Example,* SPE Europec/EAGE Annual Conference, 13-16 June 2005, Madrid, Spain.

Ryazantsev, V.M., Likhman, V.V., and Yakhontov, V.A., (2000): *Twin-Screw Pump for an Oil-Water-Gas Multiphase Liquid,* Chemical and Petroleum Engineering, Vol. 36, No. 78, pp. 432-36.

Saadowi, H., and Olama, S.A., (2003): *Application of Multiphase Pumps in a Remote Oil Field Onshore Abu Dhabi,* SPE Paper No. 81504, 13th SPE Middle East Oil Show and Conference, Bahrain, April 2003.

Sageev, A. Giovanni D. , and Henry J. R. (1985): *Decline Analysis Curve For Infinite Double Porosity Systems Without Wellbore Skin*, Tenth Workshop on Geothermal Reservoir Engineering Stanford University, Stanford, California, January 22-24, 1985

Scott, S.L. and Martin, A.M. (2001): *Multiphase - The Final Pumping Frontier*, Pumps & Systems (July 2001) 8-32.

Scott, S.L. (2001): *Multiphase Production Flows into Industry Mainstream*, the American Oil & Gas Reporter (June 2001) 68-73.

Scott, S.L. and Shippen, M.E. (2002): *Multiphase Pumping as an Alternative to Conventional Separation, Pumping and Compression*, paper PSIG 0210 presented at the 2002 PSIG Conference, Portland, Oregon, Oct 8-9; Offshore Multiphase Production Operations-II, SPE Reprint No. 58 (2004).

Scott, S.L.(2003): *Multiphase Pumping Addresses a Wide Range of Operating Problem*, paper published in the Oil & Gas Journal, pp. 59-71 (Sept. 29, 2003).

Scott, S.L.(2004): *Utilization of Multiphase Pumping Technologies in Oil & Gas Production*, paper presented at the NEL Advances in Multiphase Separation & Multiphase Pumping Technologies Conference, Aberdeen, Scotland (June 30 – July 1, 2004).

Scott, S. L., Devegowda, D., Martin, A. M, Department of Petroleum Engineering Texas A&M University College Station, (2004): *Assessment of Subsea Production & Well Systems*, Final Report Submitted to the U.S. Department of Interior – Minerals Management Service (MMS), Technology Assessment & Research (TA&R) Program,Project Number: 424. October 12, 2004.

Scott, S. L. SPE Texas (2007): Artificial Lift. JPT, MAY 2007.

Stehfest, H. (1970): *Numerical Inversion of Laplace Transforms*, Communications of the ACM, 13, No. 1, 47-49, 1970.

Stones, E.J., Zimmerman, S.A., Chien, C.V. and Marsden, S.S.(1992): *The Effect of Capillary Connectivity Across Horizontal Fractures on Gravity Drainage From Fractured Porous Media*, SPE ATCE, Washington, D.C., USA, October 4-7, 1992.

Strohmenger, C., Rockenbauch, K., Waldmann, R., (1998): *Fazies, Diagenese und Reservoirentwicklung des Zechstein 2_Karbonats (Ober_Perm) in Nordostdeutschland*. Geol. Jahrb., A (149).

Strohmenger, C., Voigt, E., Zimdars, J. (1996 a): *Sequence Stratigraphy and Cyclic Development of Basal Zechstein Carbonate-evaporite Deposits (Upper Permian, northwest Germany).* Sedimentary Geology 102: 33-54.

Tayler, J. C. M., (1986): *Late Permian Zechstein, Introduction to the Petroleum Geology of the North Sea*, Blackwell Scientific Publications, London, pp 87 - 111.

Thomas, F.B, Bennion, O.B., and Hunter, B.E. (1991): *Solid Precipitation from Reservoir Fluids: Experimental and Theoretical Analysis*, Paper presented at 10th SPE Technical Meeting, Port of Spain, Trinidad and Tobago (June 27, 1991).

Tiab D., Restrepo D.P., and Igbokoyi A., SPE, University of Oklahoma (2006): *Fracture Porosity of Naturally Fractured Reservoirs*, First International Oil Conference and Exhibition in Mexico, 31 August-2 September 2006, Cancun, Mexico

Tucker, M. E. (1991): *Sequence Stratigraphy of Carbonate-Evaporite Basins; Models and Application to the Upper Permian (Zechstein) of Northeast England and Adjoining North Sea*, Journal of the Geological Society of London 148: 1019-1036.

Ulmishek, F. Gregory (2003): *Petroleum Geology and Resources of the West Siberian Basin*, U.S. Geological Survey Bulletin 2201-G.

Uvwo, I., B. Adejuyigbe, J. Liu, O. Ejofodomi, S.L. Scott, R. Lansangan and R. Dutton (2004): *Investigation of Three-Phase Flow Measurement Capabilities of a Coriolis Meter*, paper presented at the BHRG Multiphase 04 Conference, Banff, Canada (June 3-4, 2004).

Van de Sande, J.M.M., Reijers, T.J.A., & Casson, N. (1996): *Multidisciplinary Exploration Strategy in the Northeast Netherlands Zechstein 2 Carbonate Play*, Guided by 3D Seismic. In:

Rondeel, H.E., Batjes, D.A.J. & Nieuwenhuijs, W.H. (eds): Geology of Gas and Oil under the Netherlands. Kluwer (Dordrecht): 125-142.

Vena, T. (2003): *Use of Multiphase Pumps at Cold Lake*, presentation given at the 1st Annual Texas A & M Multiphase Pump User Roundtable-CANADA, Calgary (October 27, 2003).

Voig, H.D. (1979): *Berechnung der Erdgasvorräte nach der Druckabfallmethode bei Deformierbaren Porenraum*. Zeitschrift für Angewandte Geologie, 25:15-20, 1979.

Warren, J. E., and Root, P. J. (1963): *The Behavior of Naturally Fractured Reservoirs*, SPEJ, 245–255.

Warren, J. K. (2006): *Evaporites: Sediments, Resources and Hydrocarbons*, Springer-Verlag, ISBN 3-540-26011.

Wattenbarger, R.A and Fraim, M.L (1987): *Gas Reservoir Decline Curve Analysis Using Type Curves with Real Gas Pseudo-pressure and Normalized Time*, SPEFE (December 1987), 671.

Wattenbarger, R.A.; El-Banbi, A.H.; and Villegas, M.E (1998): *Production Analysis of Linear Flow into Fractured Tight Gas Wells*, paper SPE 39931 presented at the 1998 SPE Rocky Mountain Region/Low-Permeability Reservoir Symposium and Exhibition, Denver, 5-8 April.

Webster, M Craig (2007): *Integrating Quantitative and Qualitative Reservoir Data in Sand, Prediction Studies: The Combination of Numerical and Geological Analysis*, SPE 108586-MS, Offshore Europe, 4-7 September 2007, Aberdeen, Scotland, U.K.

Werner, S and Mark, D, BP (2007): *Securing the Future in Mature Gas Fields*, EUROPEC/EAGE Conference and Exhibition, 11-14 June 2007, London, U.K.

Wilkinson, D. (2003): *Use of Multiphase Pumping in a Annulus Vapor Recovery*, presentation given at the 1st Annual Texas A&M Multiphase Pump User Roundtable-CANADA, Calgary (October 27, 2003).

William, C. Lyons, Ph.D., P.E. Gary J. Plisga, B.S. (2005): *Standard Handbook of Petroleum & Natural Gas Engineering*, Second Edition Editors, Gulf Professional Publishing 2005.

7.3 Appendix

7.3.1 Appendix 1: Production History

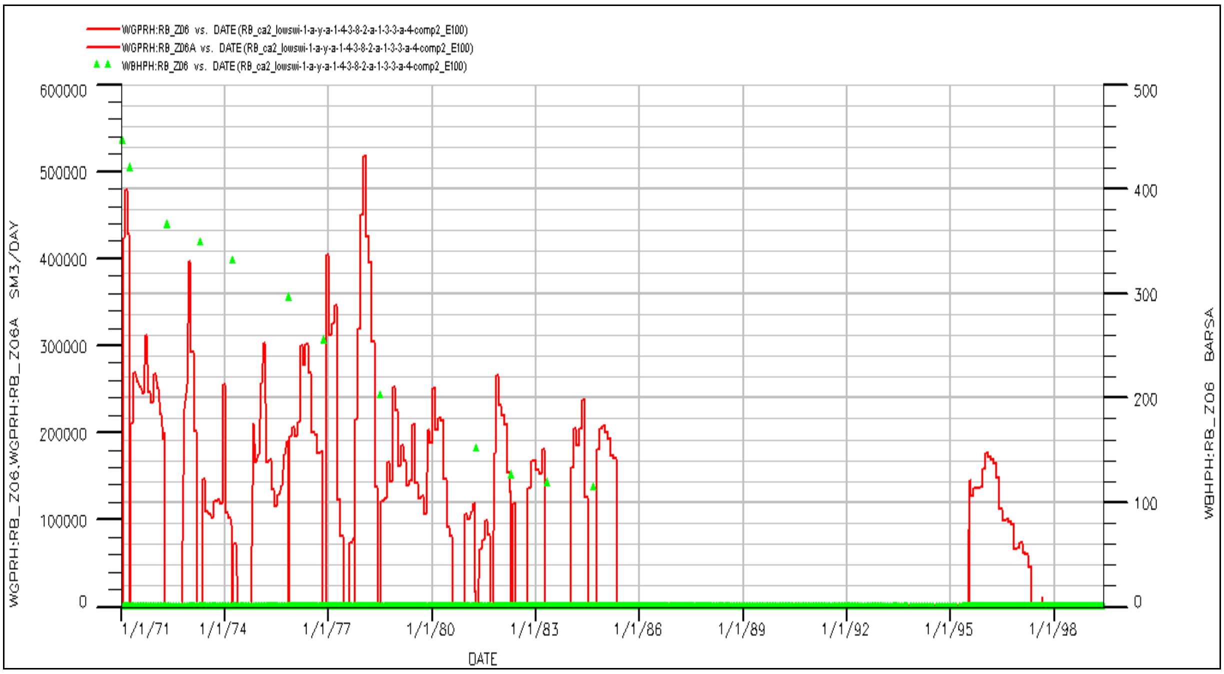

Fig. 1.1: RB_Z06 & RB_Z06a production history (pressure measurements & gas rates vs. time)

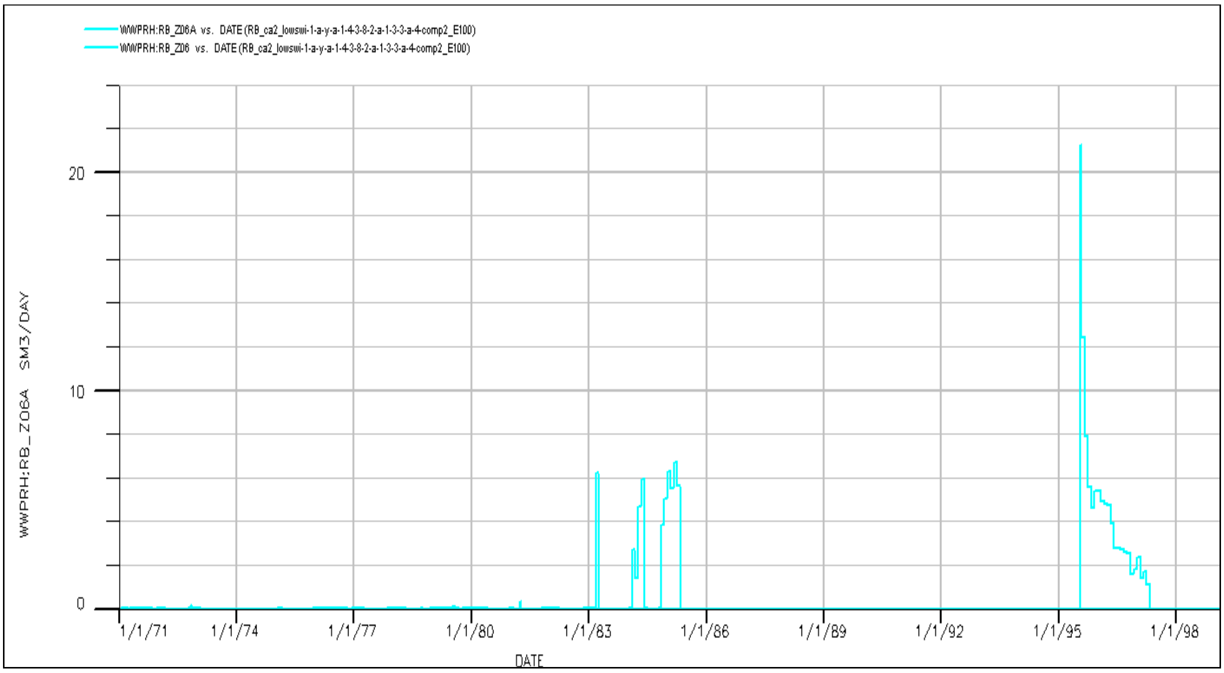

Fig. 1.2: RB_Z06 & RB_Z06a production history (water production vs. time)

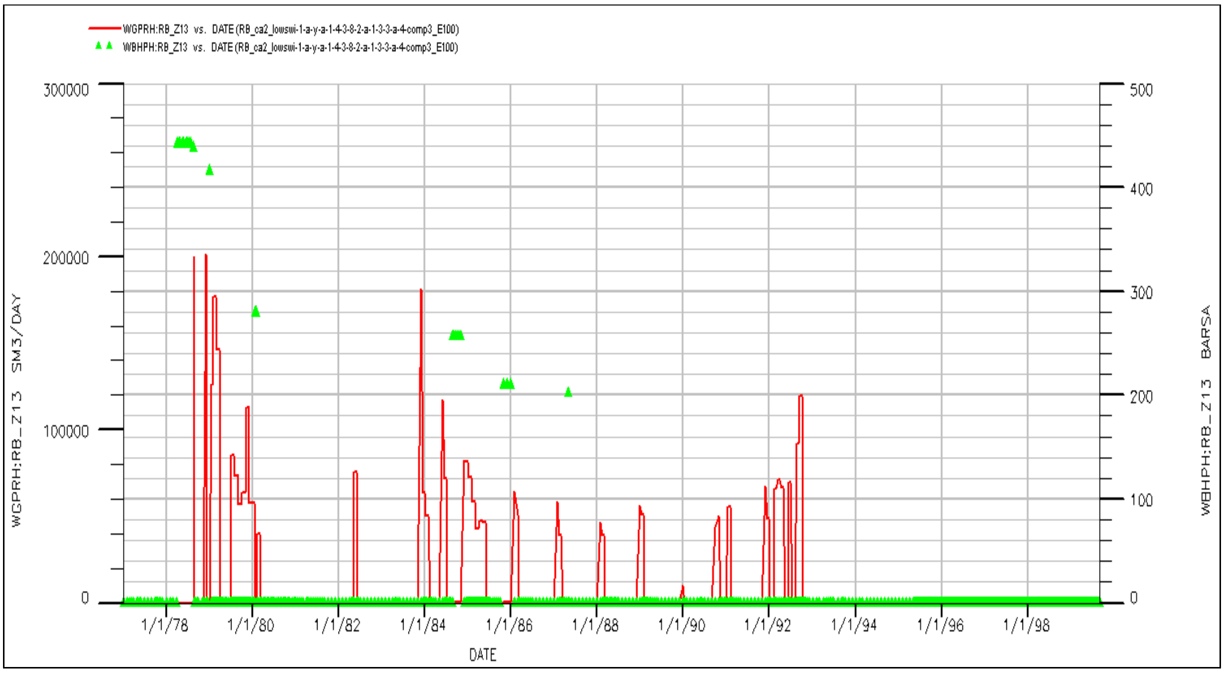

Fig. 1.3: RB_Z13 production history (pressure measurements & gas rates vs. time)

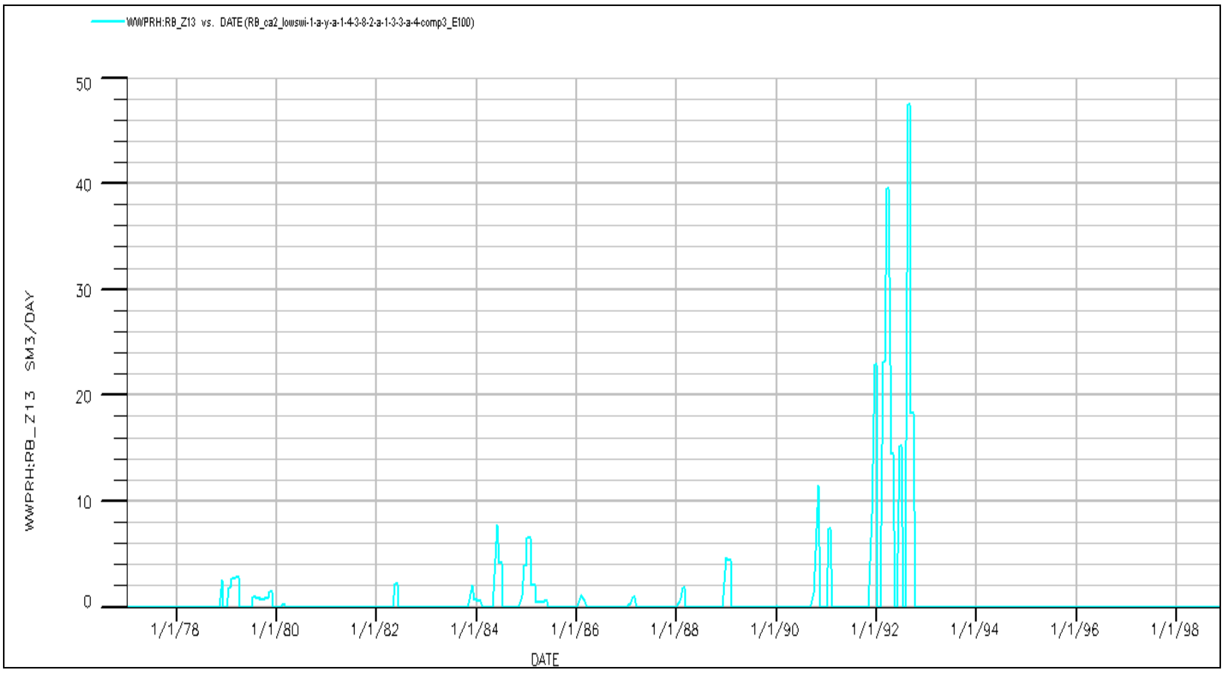

Fig. 1.4: RB_Z13 production history (water production vs. time)

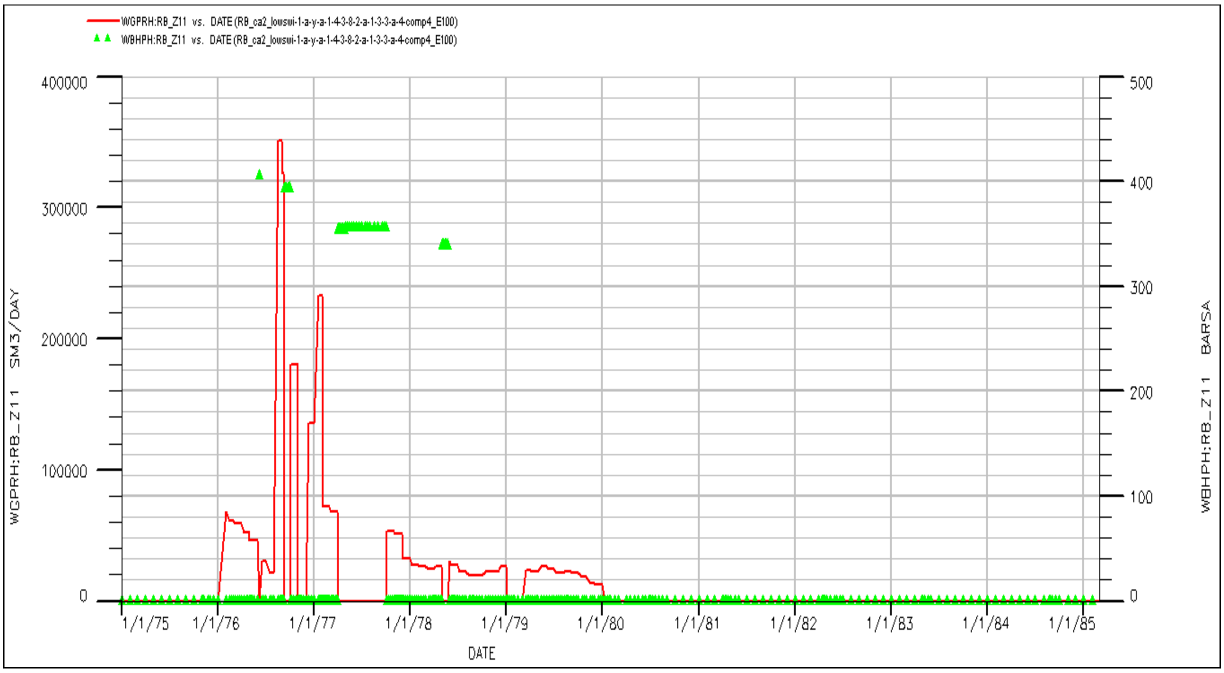

Fig. 1.5: RB_Z11 production history (pressure measurements & gas rates vs. time)

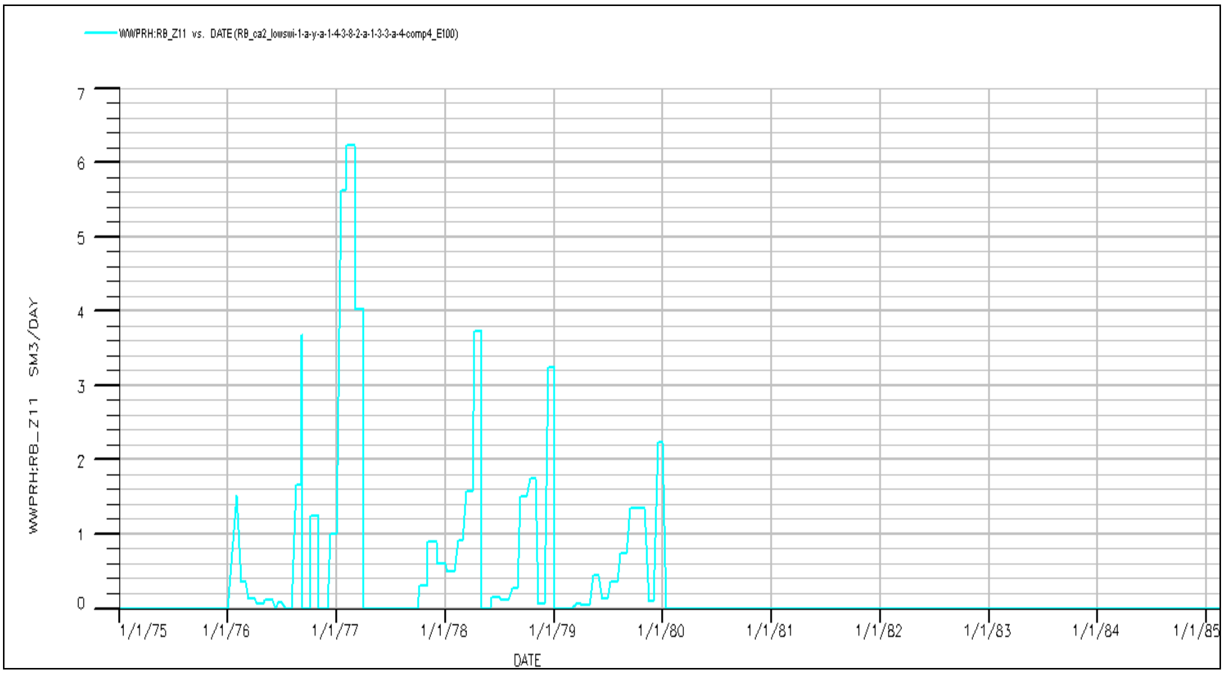

Fig. 1.6: RB_Z11 production history (water production vs. time)

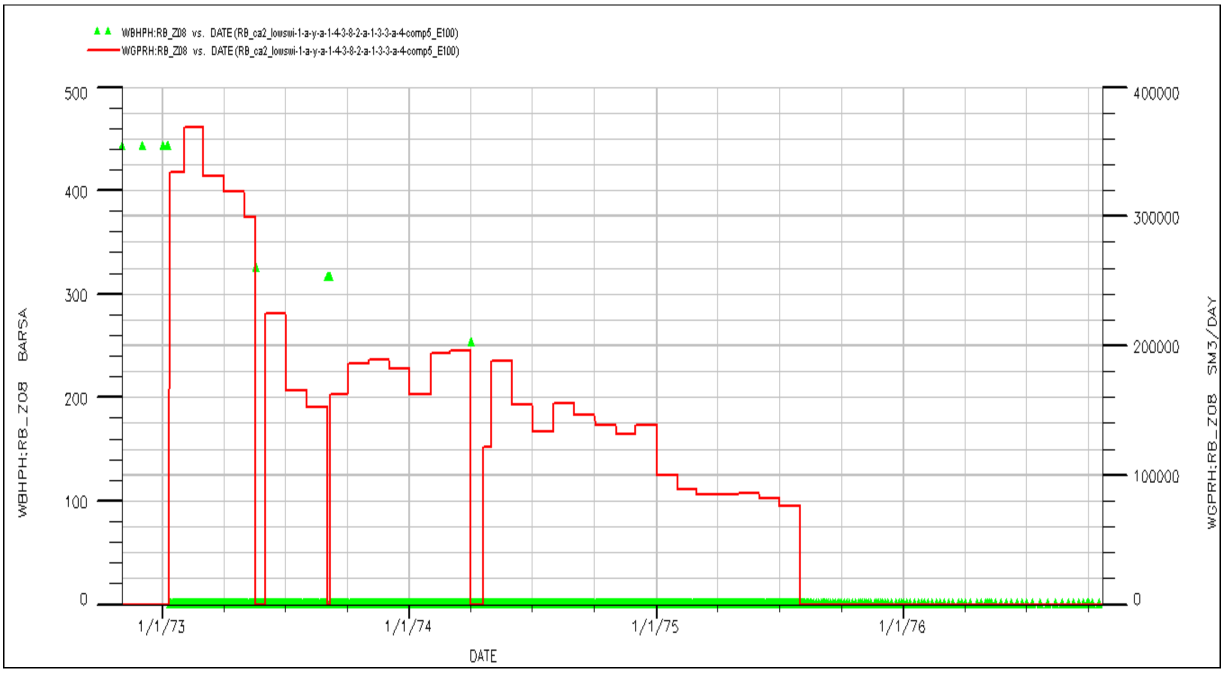

Fig. 1.7: RB_Z08 production history (pressure measurements & gas rates vs. time)

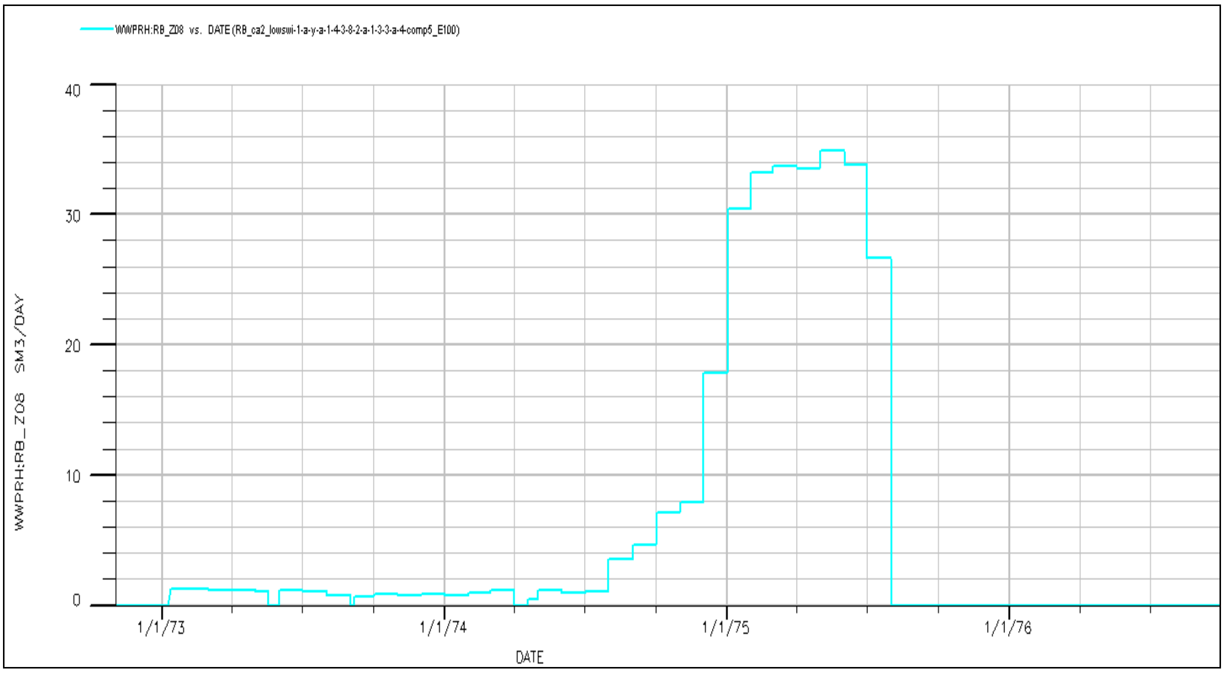

Fig. 1.8: RB_Z11 production history (water production vs. time)

7.3.2 Appendix 2: Decline Curve Analysis

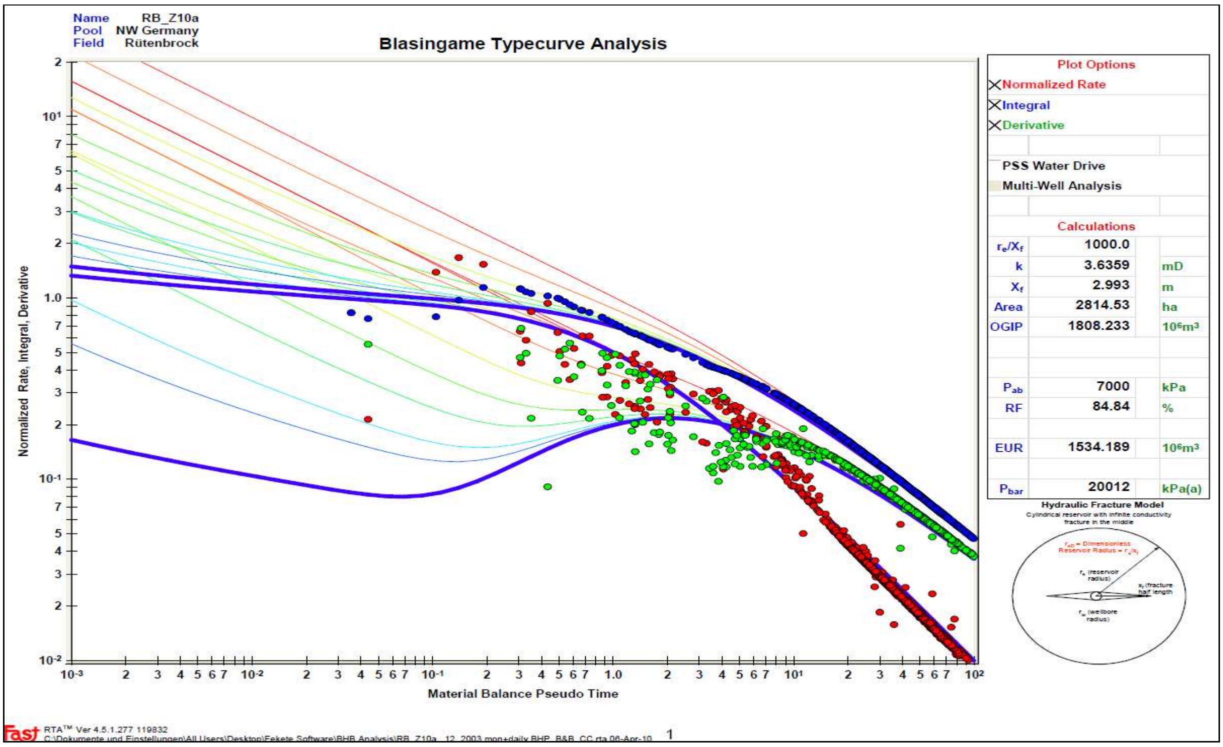

Fig. 2.1: RB_Z10a - Blasingame type curve matching with history production data

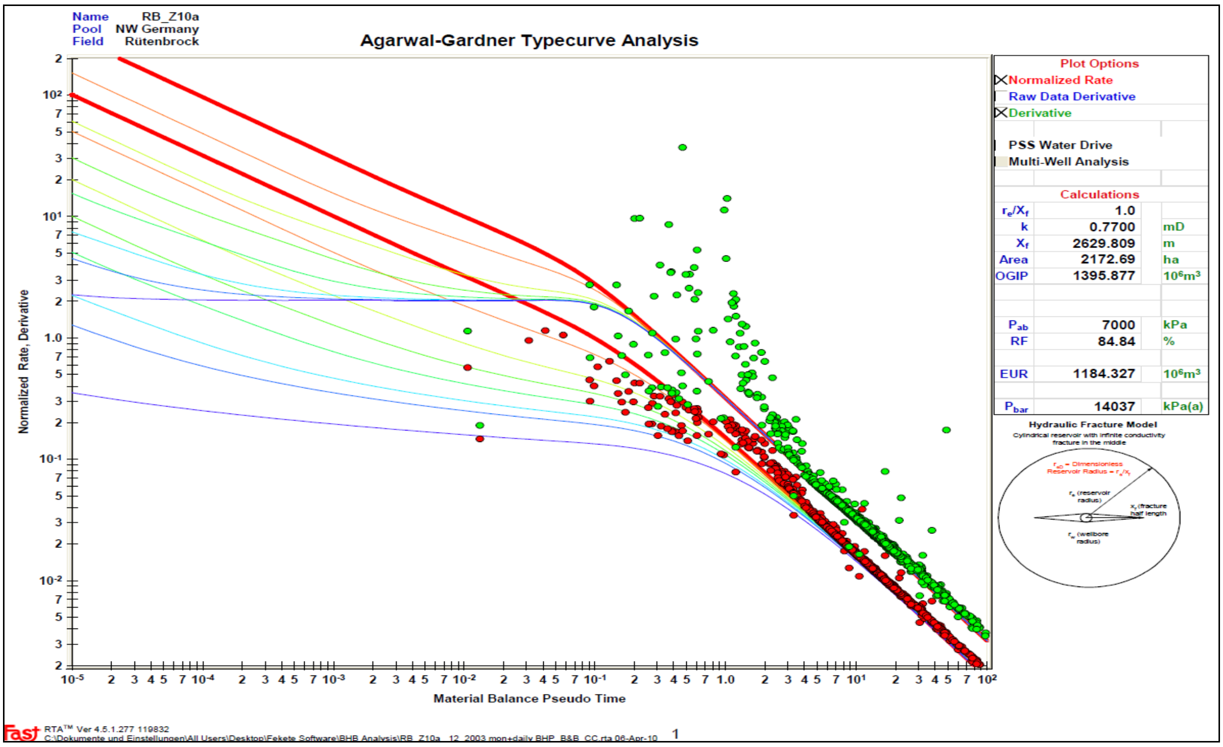

Fig. 2.2: RB_Z10a - Agarwal-Gardner type curve matching with history production data

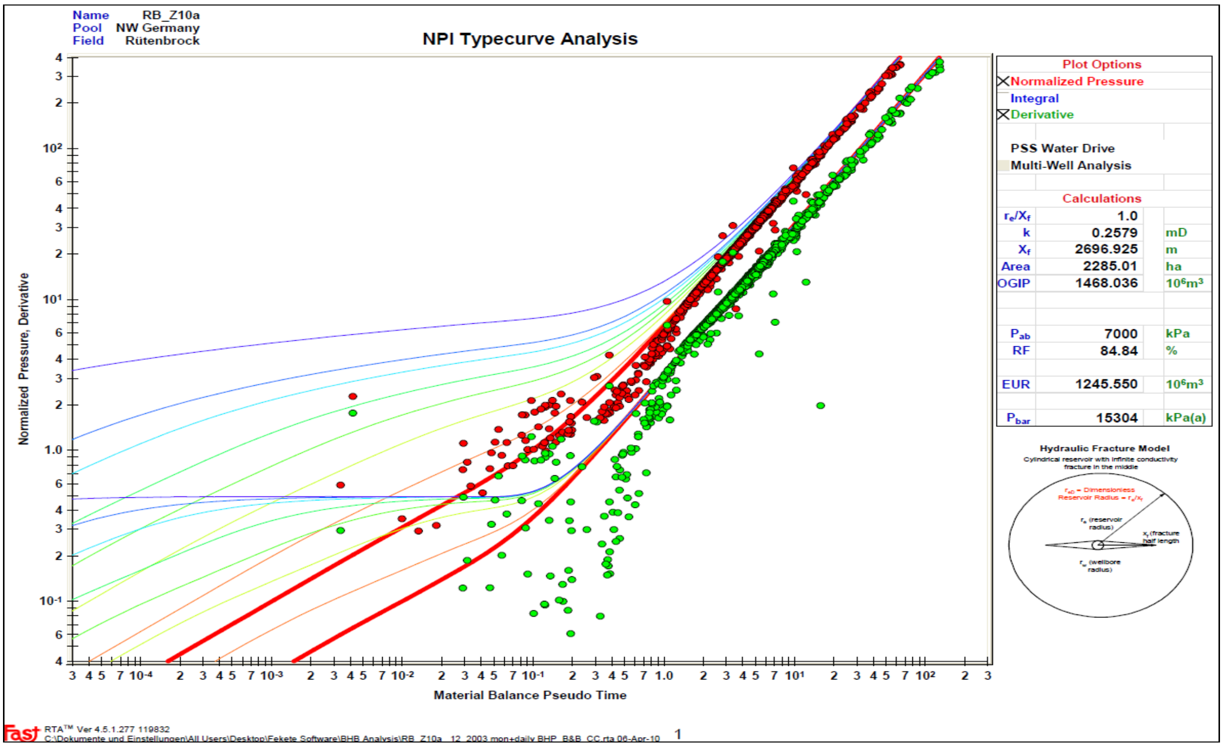
Name RB_Z10a
Pool NW Germany
Field Rütenbrock
NPI Typecurve Analysis
Normalized Pressure, Derivative
Material Balance Pseudo Time
Hydraulic Fracture Model
Cylindrical reservoir with infinite conductivity fracture in the middle
r_{eD} = Dimensionless Reservoir Radius = r_e/x_f
r_e (reservoir radius)
x_f (fracture half length)
r_w (wellbore radius)
RTA™ Ver 4.5.1.277 119832
C:\Dokumente und Einstellungen\All Users\Desktop\Fekete Software\BHB Analysis\RB_Z10a_12_2003 mon+daily BHP_B&B_CC.rta 06-Apr-10
1

Plot Options		
☒ Normalized Pressure		
☐ Integral		
☒ Derivative		
PSS Water Drive		
☐ Multi-Well Analysis		
Calculations		
r_e/X_f	1.0	
k	0.2579	mD
X_f	2696.925	m
Area	2285.01	ha
OGIP	1468.036	$10^6 m^3$
P_{ab}	7000	kPa
RF	84.84	%
EUR	1245.550	$10^6 m^3$
P_{bar}	15304	kPa(a)

Fig. 2.3: RB_Z10a - Normalized Pressure Integral type curve matching with history production data

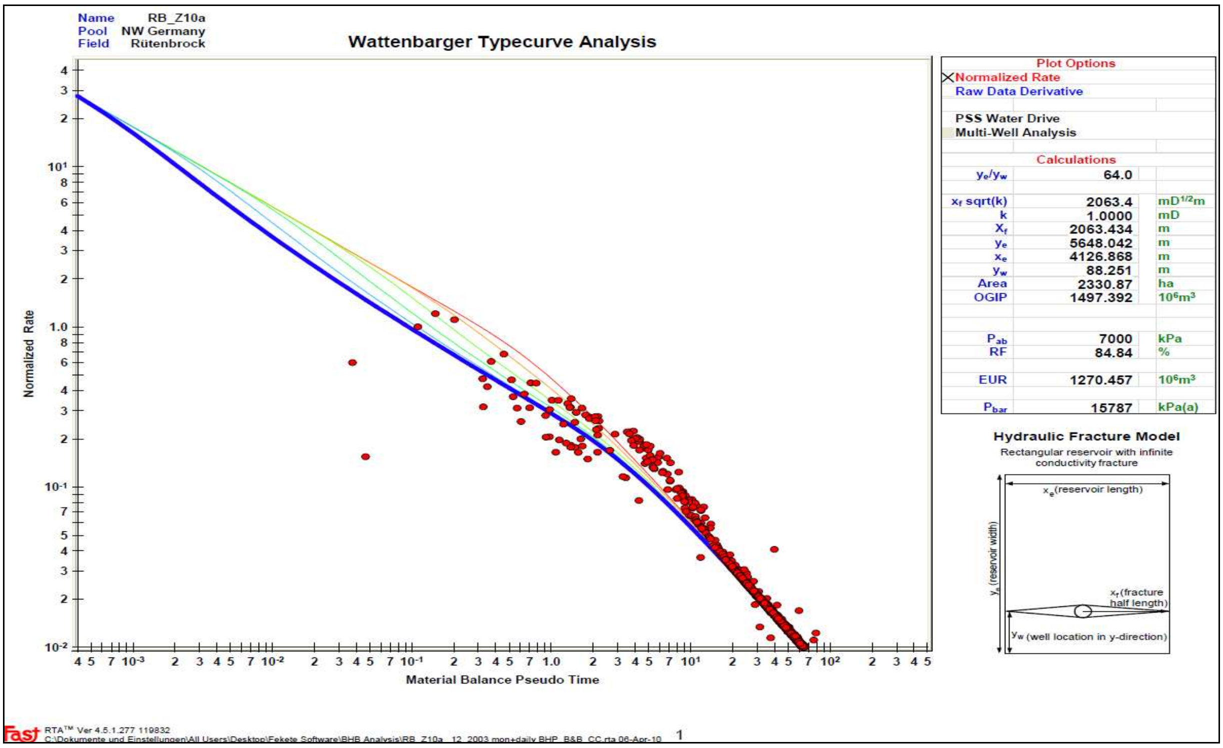
Name RB_Z10a
Pool NW Germany
Field Rütenbrock
Wattenbarger Typecurve Analysis
Normalized Rate
Material Balance Pseudo Time
Hydraulic Fracture Model
Rectangular reservoir with infinite conductivity fracture
x_e(reservoir length)
y_e (reservoir width)
x_f (fracture half length)
y_w (well location in y-direction)
RTA™ Ver 4.5.1.277 119832
C:\Dokumente und Einstellungen\All Users\Desktop\Fekete Software\BHB Analysis\RB_Z10a_12_2003 mon+daily BHP_B&B_CC.rta 06-Apr-10
1

Plot Options		
☒ Normalized Rate		
Raw Data Derivative		
PSS Water Drive		
☐ Multi-Well Analysis		
Calculations		
y_e/y_w	64.0	
x_f sqrt(k)	2063.4	$mD^{1/2}m$
k	1.0000	mD
X_f	2063.434	m
y_e	5648.042	m
x_e	4126.868	m
y_w	88.251	m
Area	2330.87	ha
OGIP	1497.392	$10^6 m^3$
P_{ab}	7000	kPa
RF	84.84	%
EUR	1270.457	$10^6 m^3$
P_{bar}	15787	kPa(a)

Fig. 2.4: RB_Z10a - Wattenbarger type curve matching with history production data

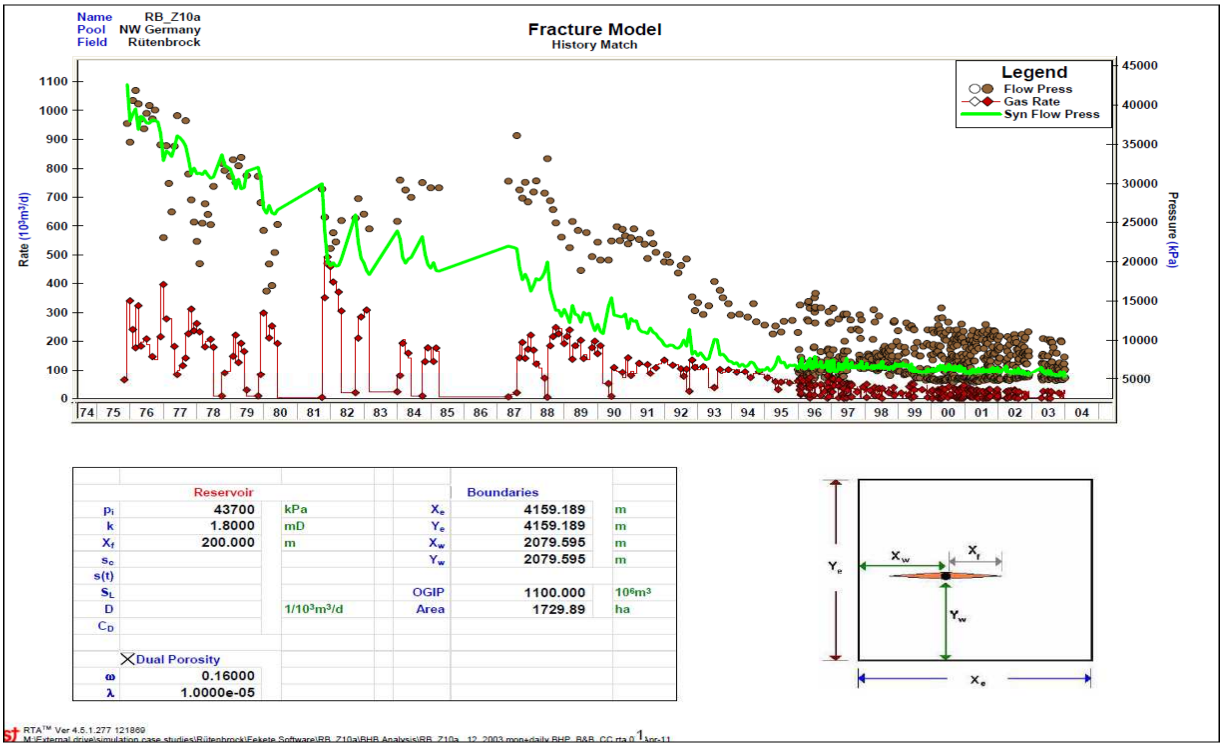

	Reservoir			Boundaries	
p_i	43700	kPa	X_e	4159.189	m
k	1.8000	mD	Y_e	4159.189	m
X_f	200.000	m	X_w	2079.595	m
s_c			Y_w	2079.595	m
s(t)					
S_L			OGIP	1100.000	10⁶m³
D		1/10³m³/d	Area	1729.89	ha
C_D					
	☒ Dual Porosity				
ω	0.16000				
λ	1.0000e-05				

Fig. 2.5: RB_Z10a - Analytical fracture model - bottom hole pressure match

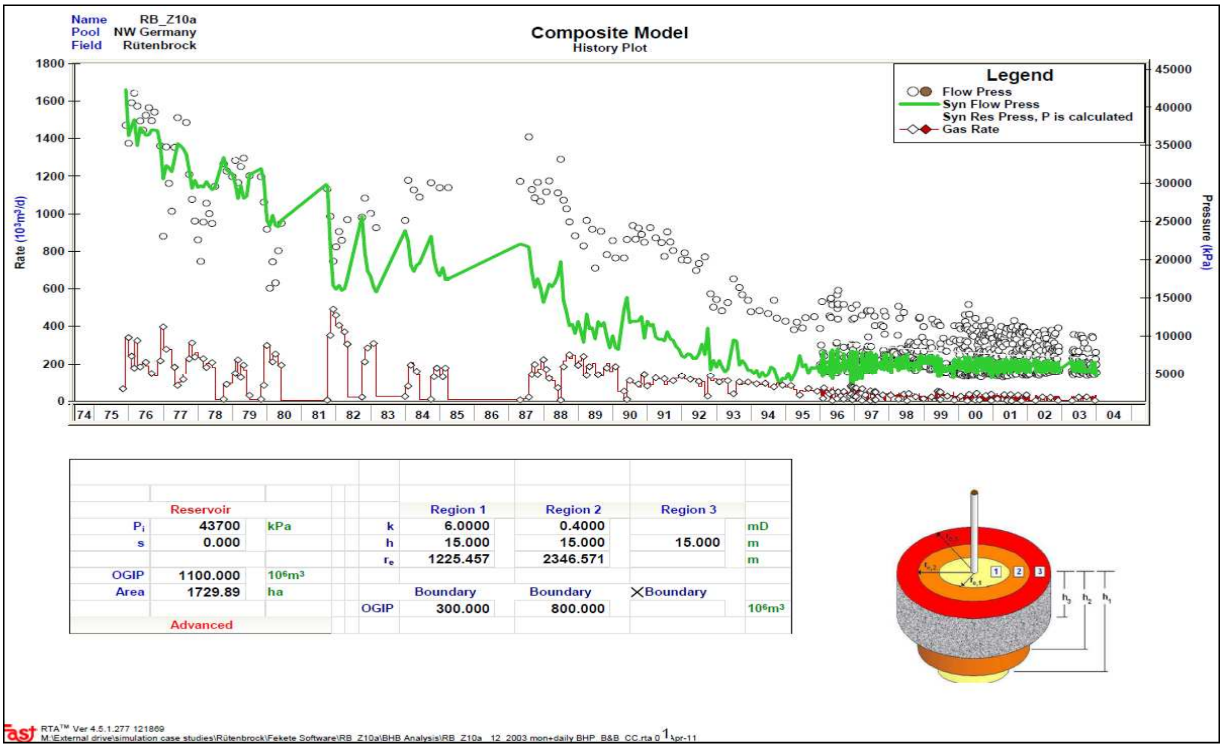

	Reservoir			Region 1	Region 2	Region 3	
P_i	43700	kPa	k	6.0000	0.4000		mD
s	0.000		h	15.000	15.000	15.000	m
			r_e	1225.457	2346.571		m
OGIP	1100.000	10⁶m³					
Area	1729.89	ha		Boundary	Boundary	☒ Boundary	
			OGIP	300.000	800.000		10⁶m³
	Advanced						

Fig. 2.6: RB_Z10a - Analytical composite model - bottom hole pressure match

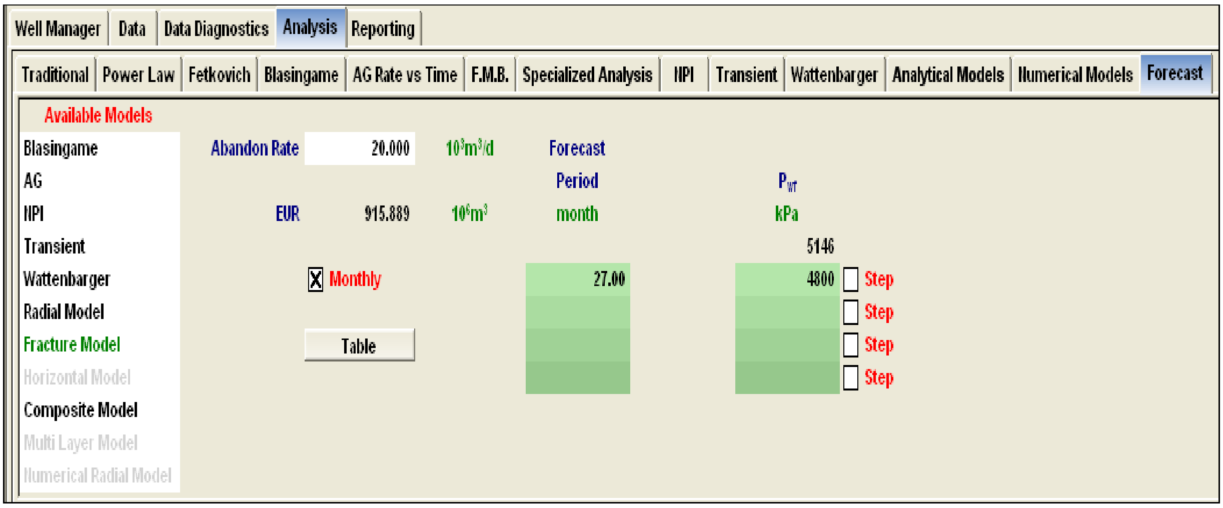
Well Manager | Data | Data Diagnostics | Analysis | Reporting
Traditional | Power Law | Fetkovich | Blasingame | AG Rate vs Time | F.M.B. | Specialized Analysis | NPI | Transient | Wattenbarger | Analytical Models | Numerical Models | Forecast
Available Models
Blasingame
AG
NPI
Transient
Wattenbarger
Radial Model
Fracture Model
Horizontal Model
Composite Model
Multi Layer Model
Numerical Radial Model
Table

Abandon Rate 20.000 $10^3m^3/d$

EUR 915.889 10^6m^3

☒ Monthly

Forecast Period (month): 27.00

P_{wf} (kPa): 5146

4800 ☐ Step

☐ Step

☐ Step

☐ Step

Fig. 2.7: RB_Z10a - conventional compression system prediction (01/2004 -03/2006) results (fracture model)

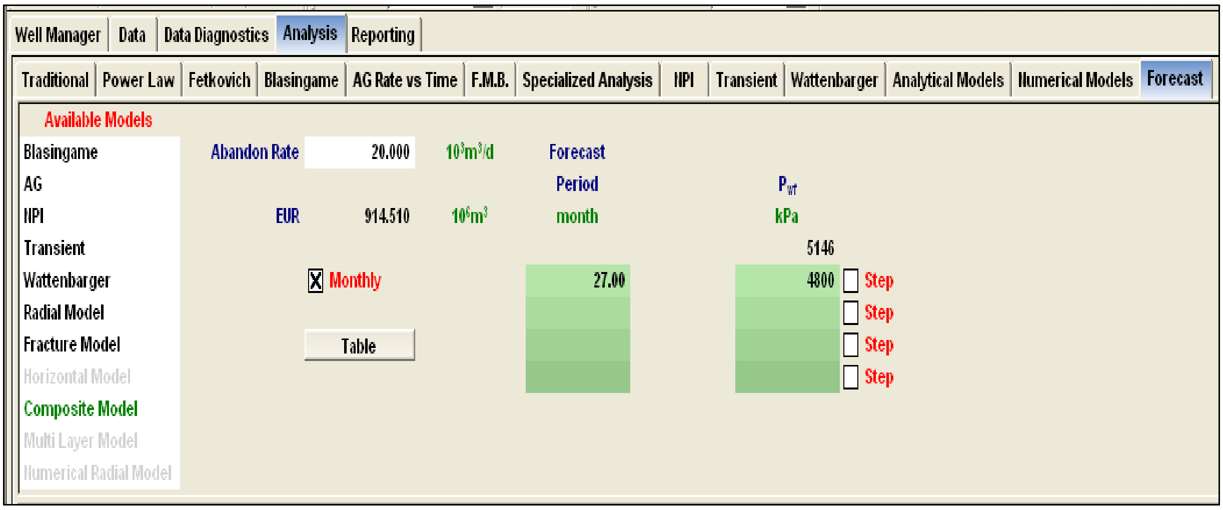
Well Manager | Data | Data Diagnostics | Analysis | Reporting
Traditional | Power Law | Fetkovich | Blasingame | AG Rate vs Time | F.M.B. | Specialized Analysis | NPI | Transient | Wattenbarger | Analytical Models | Numerical Models | Forecast
Available Models
Blasingame
AG
NPI
Transient
Wattenbarger
Radial Model
Fracture Model
Horizontal Model
Composite Model
Multi Layer Model
Numerical Radial Model
Table

Abandon Rate 20.000 $10^3m^3/d$

EUR 914.510 10^6m^3

☒ Monthly

Forecast Period (month): 27.00

P_{wf} (kPa): 5146

4800 ☐ Step

☐ Step

☐ Step

☐ Step

Fig. 2.8: RB_Z10a - conventional compression system prediction (01/2004 -03/2006) results (composite model)

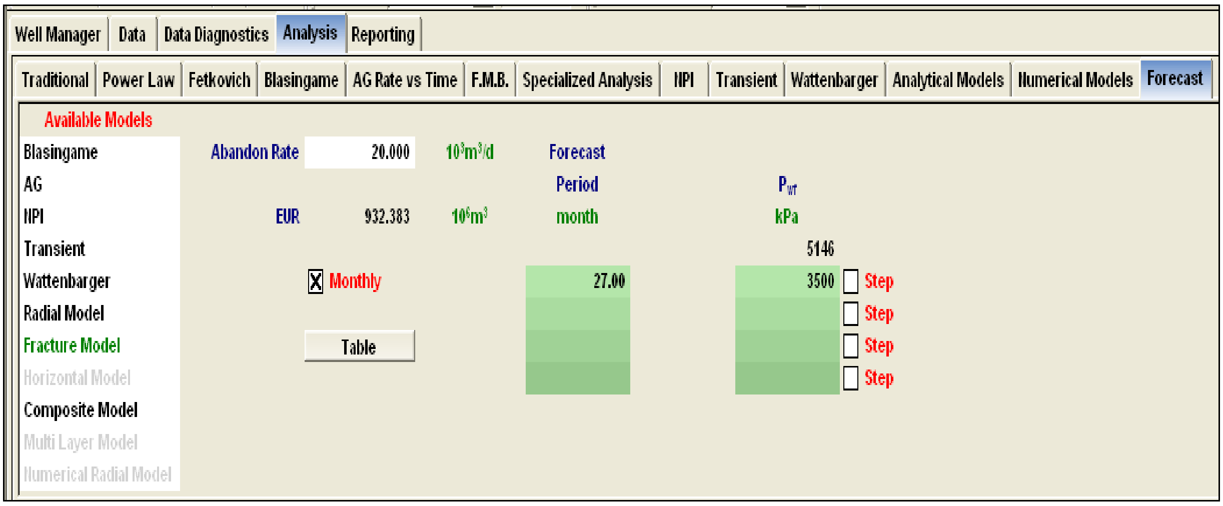
Well Manager | Data | Data Diagnostics | Analysis | Reporting
Traditional | Power Law | Fetkovich | Blasingame | AG Rate vs Time | F.M.B. | Specialized Analysis | NPI | Transient | Wattenbarger | Analytical Models | Numerical Models | Forecast
Available Models
Blasingame
AG
NPI
Transient
Wattenbarger
Radial Model
Fracture Model
Horizontal Model
Composite Model
Multi Layer Model
Numerical Radial Model
Table

Abandon Rate 20.000 $10^3m^3/d$

EUR 932.383 10^6m^3

☒ Monthly

Forecast Period (month): 27.00

P_{wf} (kPa): 5146

3500 ☐ Step

☐ Step

☐ Step

☐ Step

Fig. 2.9: RB_Z10a - Multiphase pump application prediction (01/2004 -03/2006) results (fracture model)

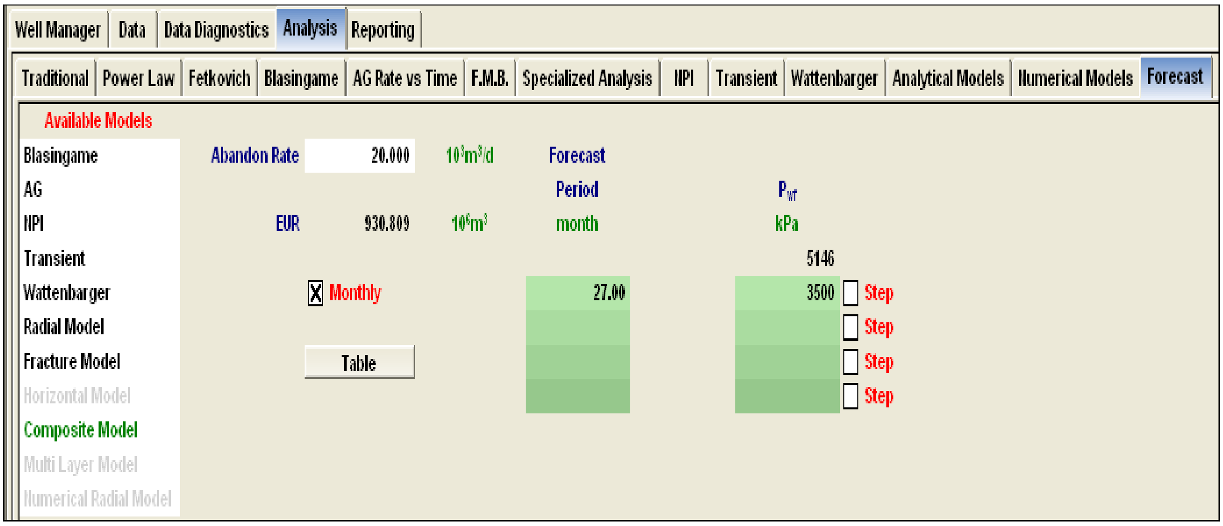
Well Manager
Data
Data Diagnostics
Analysis
Reporting
Traditional
Power Law
Fetkovich
Blasingame
AG Rate vs Time
F.M.B.
Specialized Analysis
NPI
Transient
Wattenbarger
Analytical Models
Numerical Models
Forecast
Available Models
Blasingame
AG
NPI
Transient
Wattenbarger
Radial Model
Fracture Model
Horizontal Model
Composite Model
Multi Layer Model
Numerical Radial Model
Table
☐ Step
☐ Step
☐ Step
☐ Step

Abandon Rate 20.000 $10^3m^3/d$

EUR 930.809 10^6m^3

☒ Monthly

Forecast Period	P_{wf}
month	kPa
	5146
27.00	3500

Fig. 2.10: RB_Z10a -Multiphase pump application prediction (01/2004 -03/2006) results (composite model)

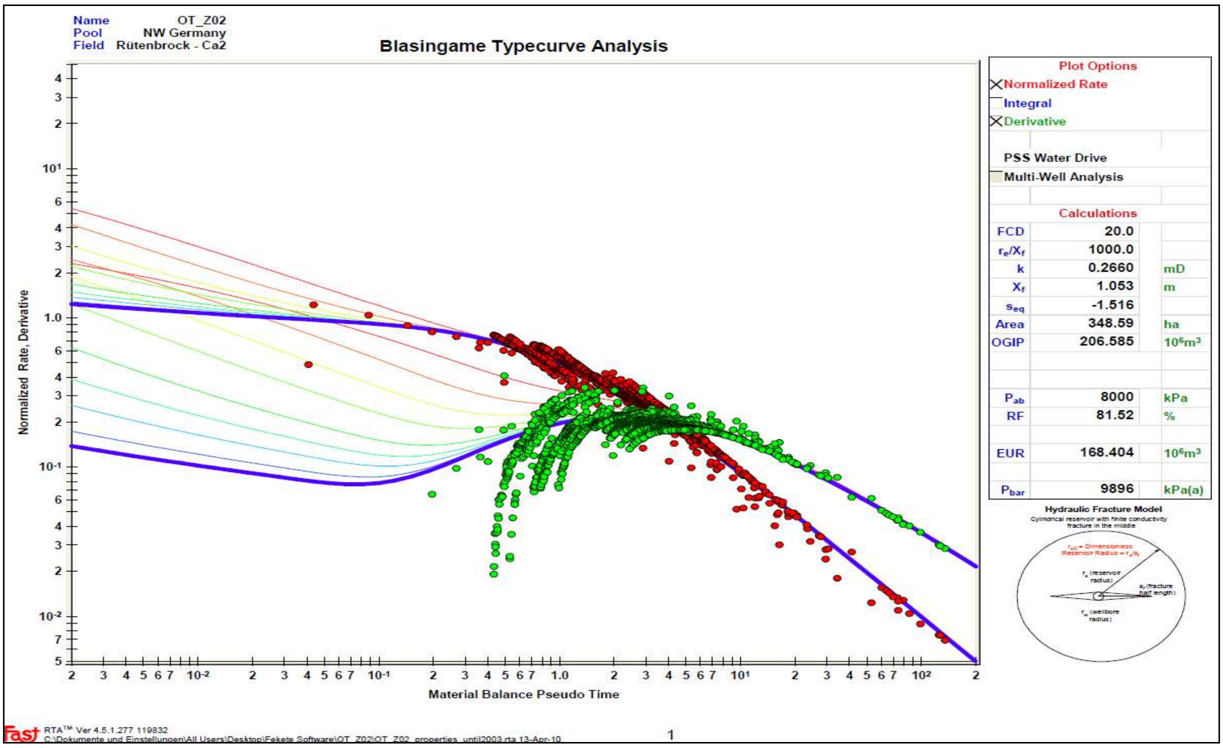
Name OT_Z02
Pool NW Germany
Field Rütenbrock - Ca2

☒ Normalized Rate
☒ Derivative

Calculations

FCD	20.0	
r_e/X_f	1000.0	
k	0.2660	mD
X_f	1.053	m
s_{eq}	-1.516	
Area	348.59	ha
OGIP	206.585	10^6m^3
P_{ab}	8000	kPa
RF	81.52	%
EUR	168.404	10^6m^3
P_{bar}	9896	kPa(a)

RTA™ Ver 4.5.1.277 119832
C:\Dokumente und Einstellungen\All Users\Desktop\Fekete Software\OT_Z02\OT_Z02_properties_until2003.rta 13-Apr-10

Fig. 2.11: OT_Z02 - Blasingame type curve matching with history production data

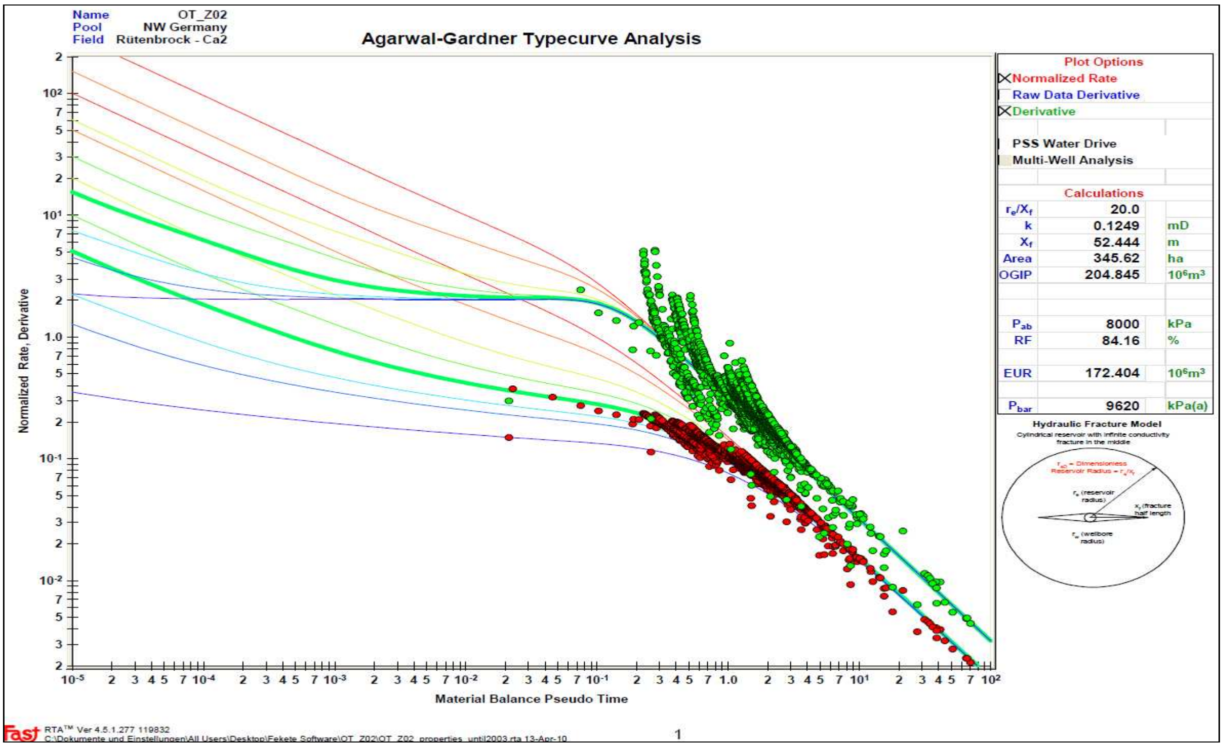

Name OT_Z02
Pool NW Germany
Field Rütenbrock - Ca2

Agarwal-Gardner Typecurve Analysis

Plot Options
☒ Normalized Rate
☐ Raw Data Derivative
☒ Derivative
☐ PSS Water Drive
☐ Multi-Well Analysis

Calculations

r_e/X_f	20.0	
k	0.1249	mD
X_f	52.444	m
Area	345.62	ha
OGIP	204.845	$10^6 m^3$
P_{ab}	8000	kPa
RF	84.16	%
EUR	172.404	$10^6 m^3$
P_{bar}	9620	kPa(a)

RTA™ Ver 4.5.1.277 119832
C:\Dokumente und Einstellungen\All Users\Desktop\Fekete Software\OT_Z02\OT_Z02_properties_until2003.rta 13-Apr-10

Normalized Rate, Derivative
2
10²
7
5
3
2
10¹
7
5
3
2
1.0
7
5
3
2
10⁻¹
7
5
3
2
10⁻²
7
5
3
2
10⁻⁵ 2 3 4 5 7 10⁻⁴ 2 3 4 5 7 10⁻³ 2 3 4 5 7 10⁻² 2 3 4 5 7 10⁻¹ 2 3 4 5 7 1.0 2 3 4 5 7 10¹ 2 3 4 5 7 10²
Material Balance Pseudo Time
Hydraulic Fracture Model
Cylindrical reservoir with infinite conductivity fracture in the middle
r_eD = Dimensionless Reservoir Radius = r_e/X_f
r_e (reservoir radius)
x_f (fracture half length)
r_w (wellbore radius)
Fast
1

Fig. 2.12: OT_Z02 - Agarwal-Gardner type curve matching with history production data

7.3.3 Appendix 3: History Match Results

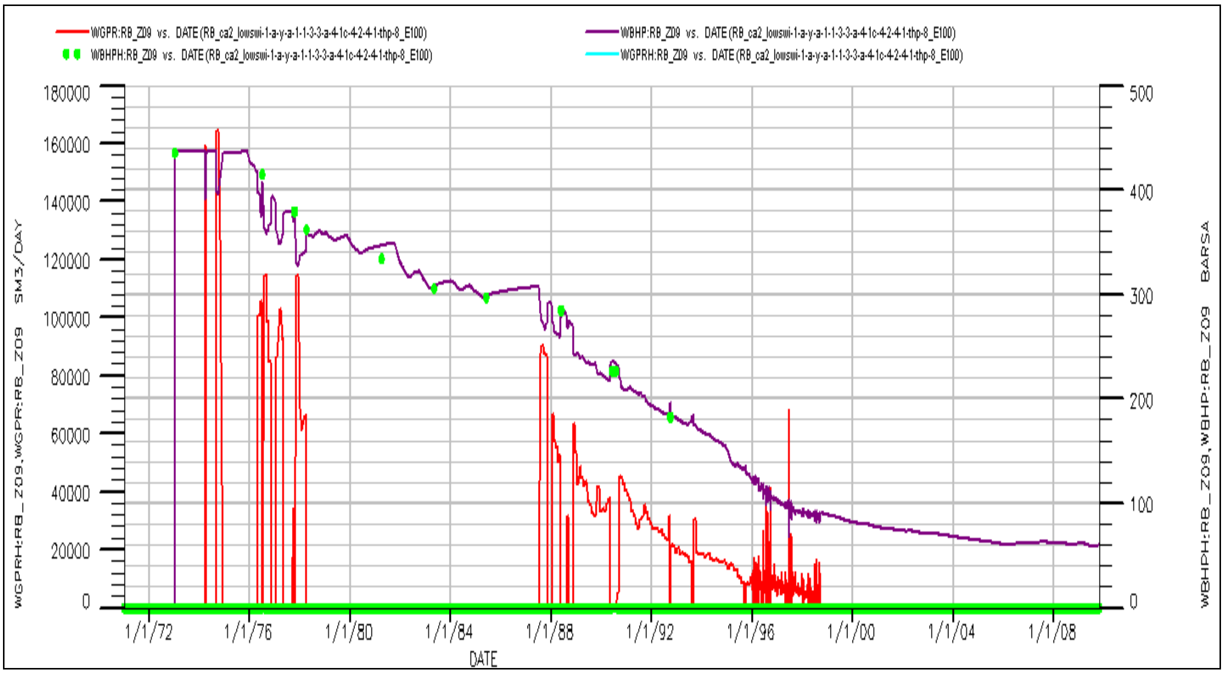

Fig. 3.1: RB_Z09-base case history match (observed bottom hole pressure & gas rate vs. simulation)

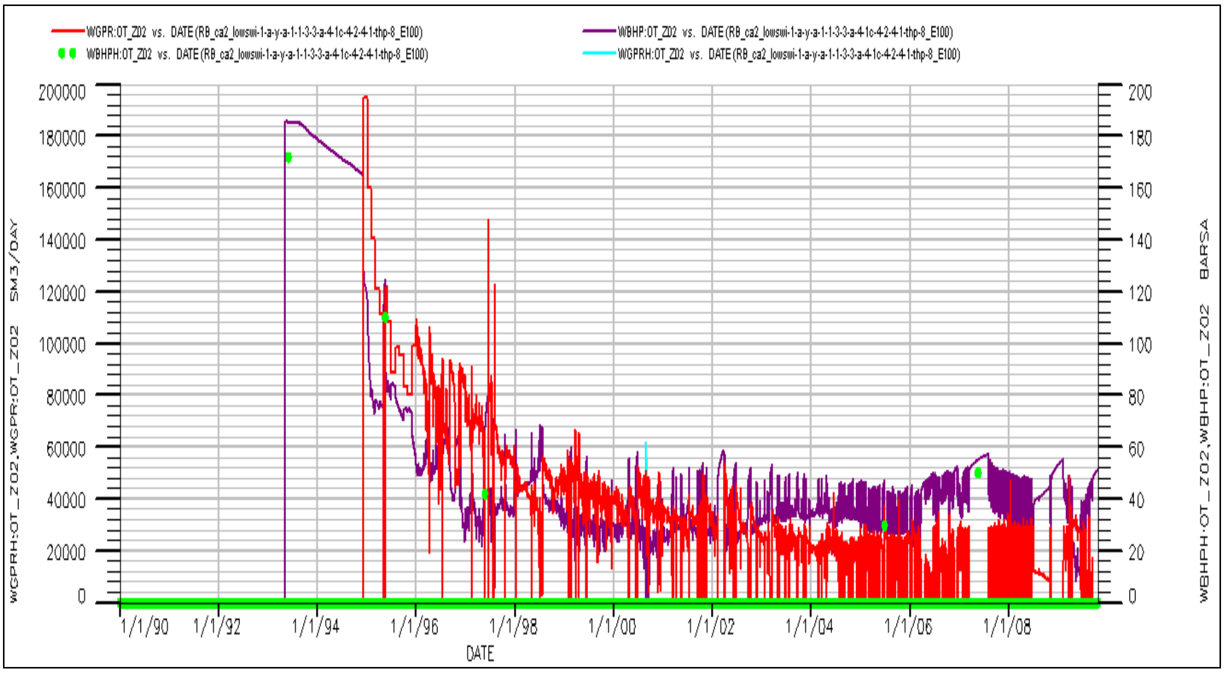

Fig. 3.2: OT_Z02-base case history match (observed bottom hole pressure(green dots) & gas rate (red curve) vs. simulated)

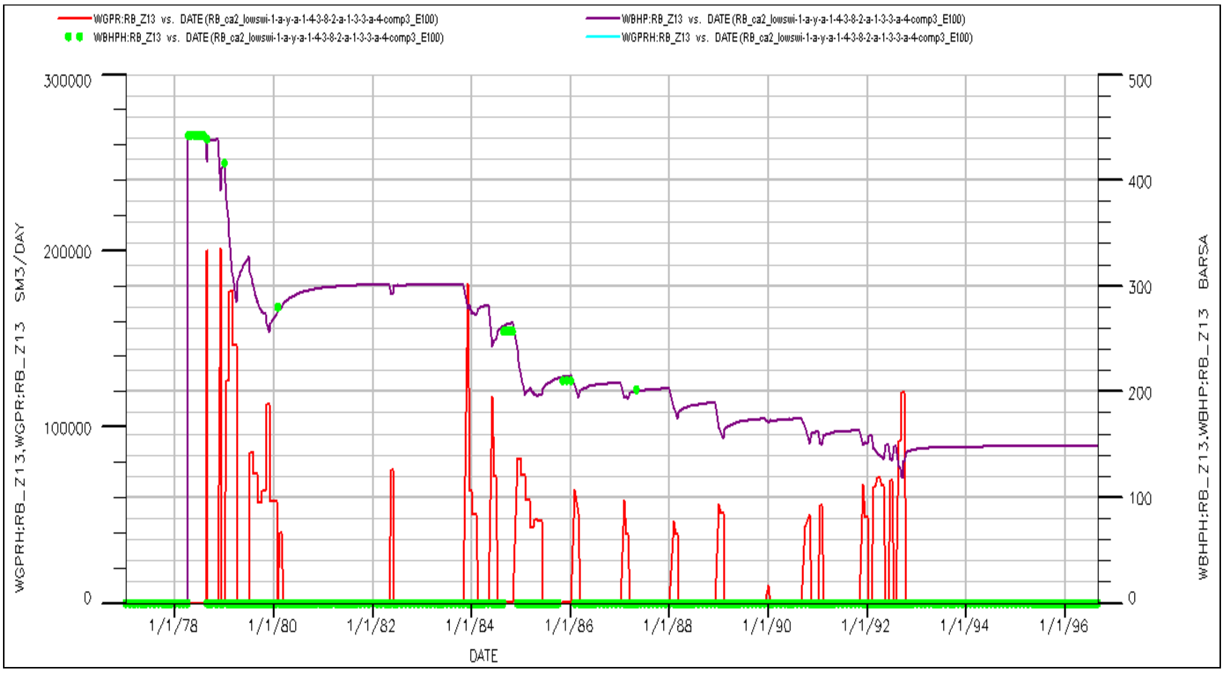

Fig. 3.3: RB_Z13-base case history match (observed bottom hole pressure (green dots) & gas rate (red curve) vs. simulated)

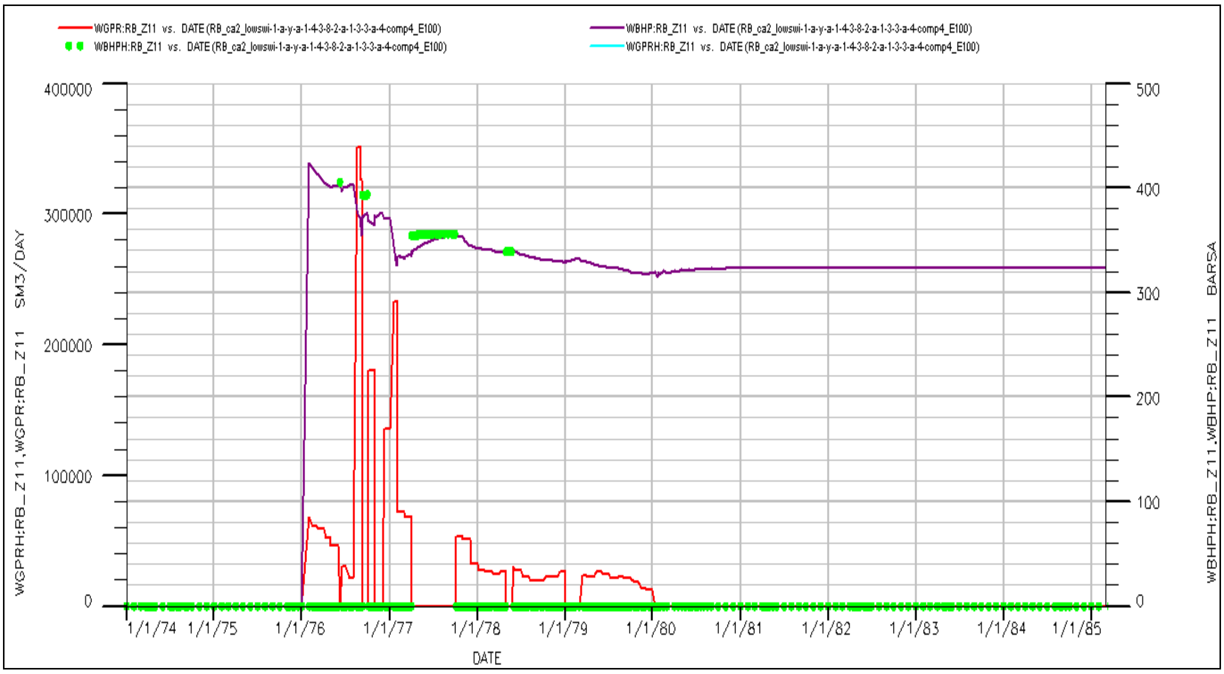

Fig. 3.4: RB_Z11-base case history match (observed bottom hole pressure (green dots) & gas rate (red curve) vs. simulated)

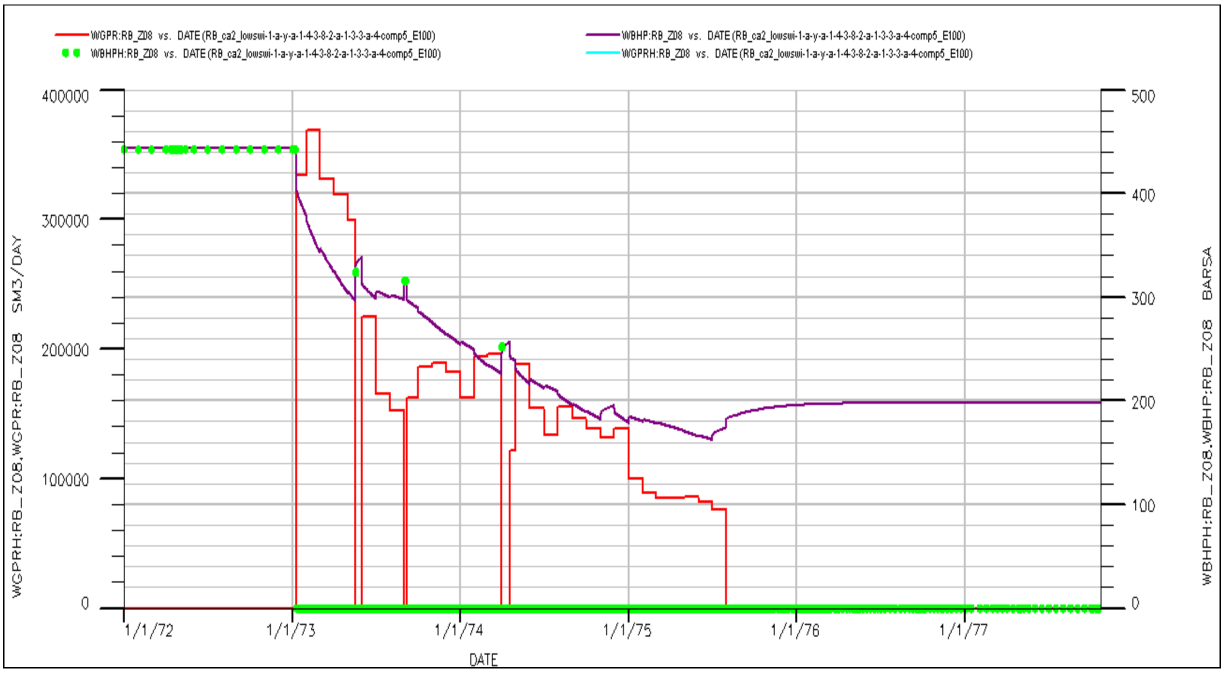

Fig. 3.5: RB_Z08-base case history match (observed bottom hole pressure (green dots) & gas rate (red curve) vs. simulated)

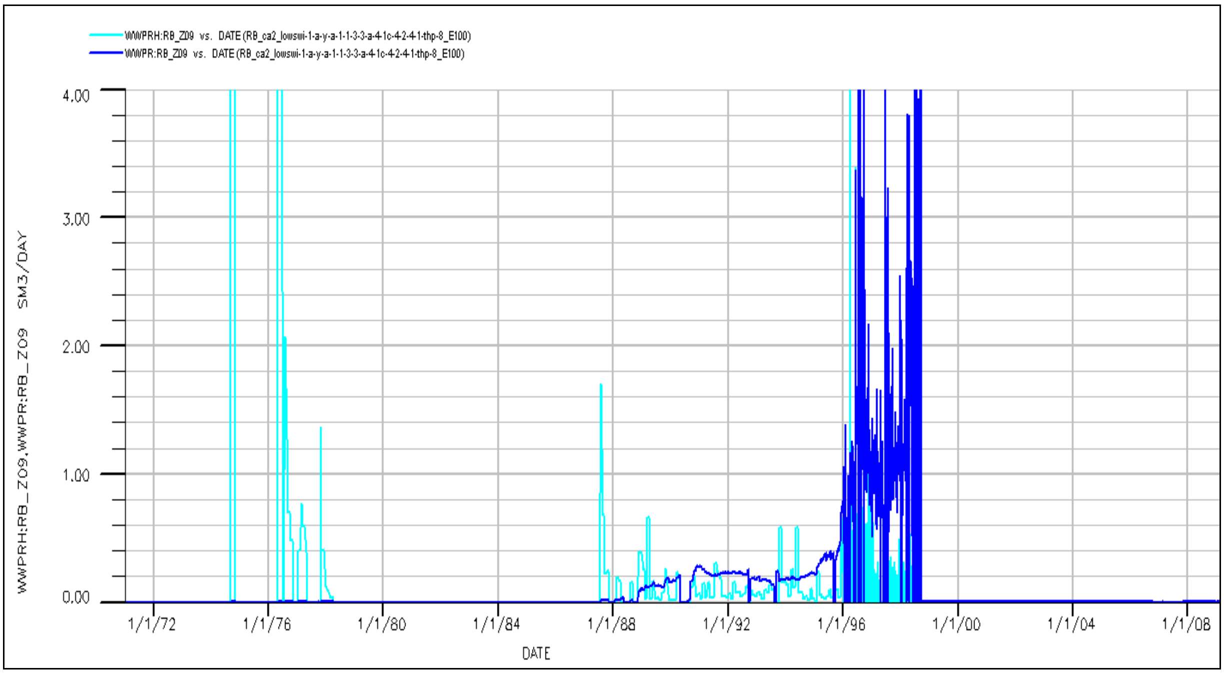

Fig. 3.6: RB_Z09-base case history match (observed water rate (light blue) vs. simulated (dark blue))

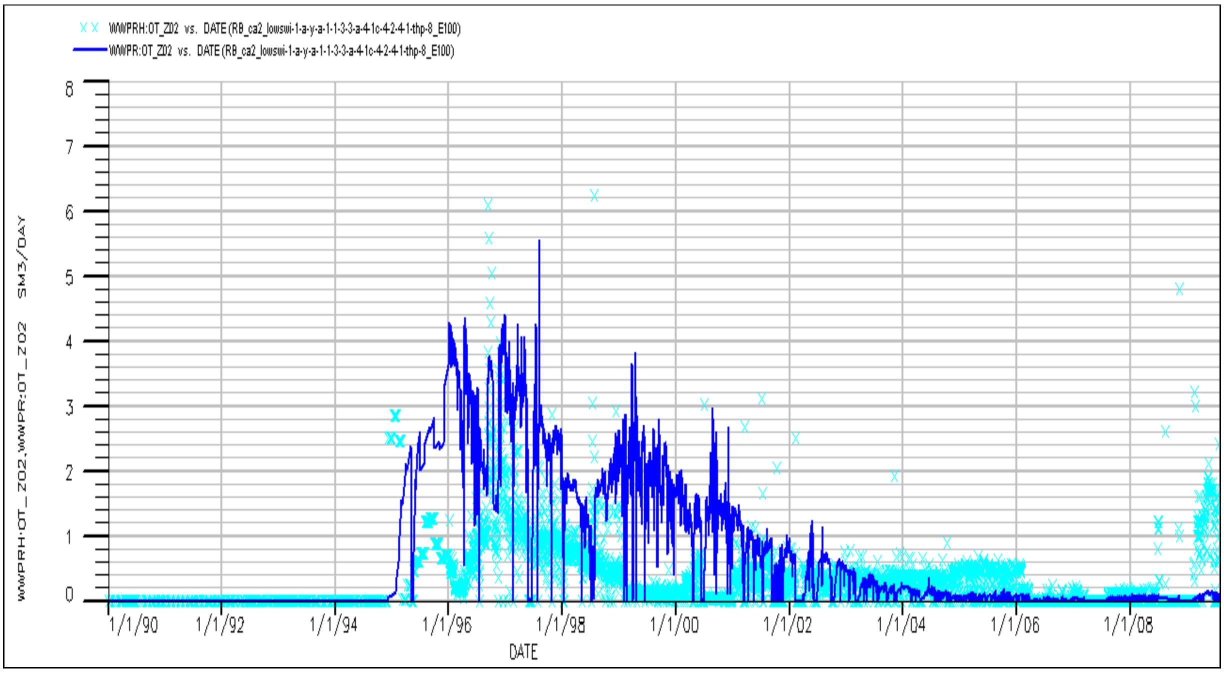

Fig. 3.7: OT_ZO2-base case history match (observed water rate (light blue) vs. simulated (dark blue))

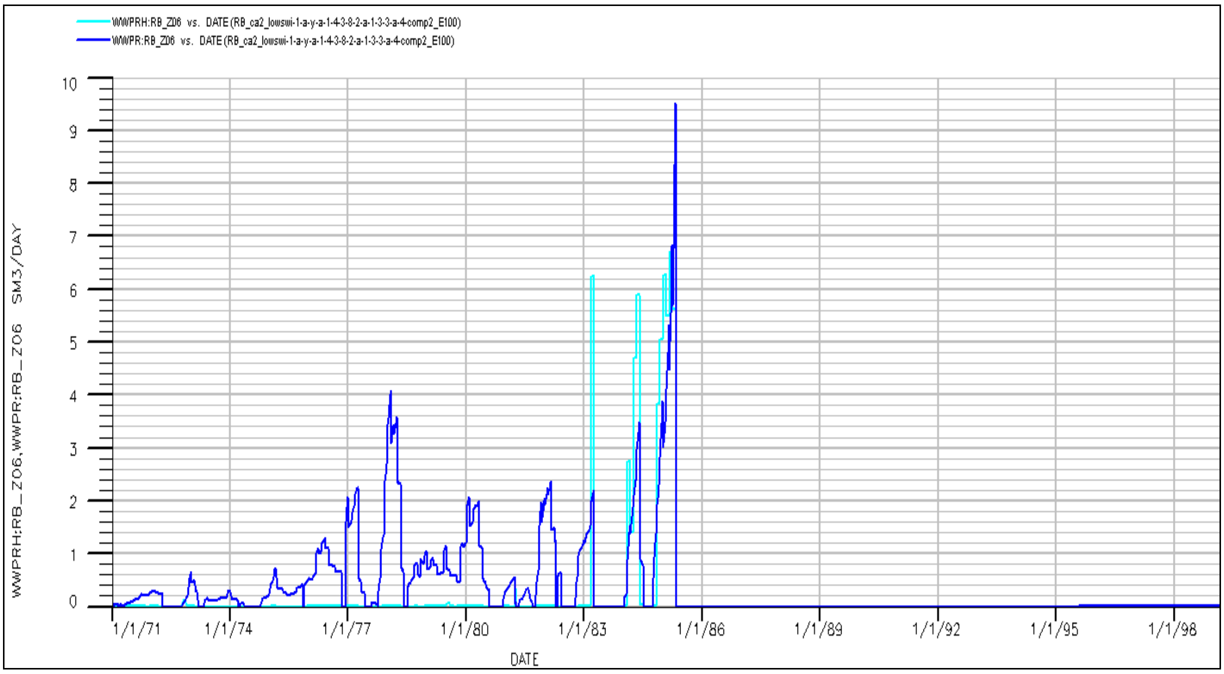

Fig. 3.8: RB_Z06-base case history match (observed water rate (light blue) vs. simulated (dark blue))

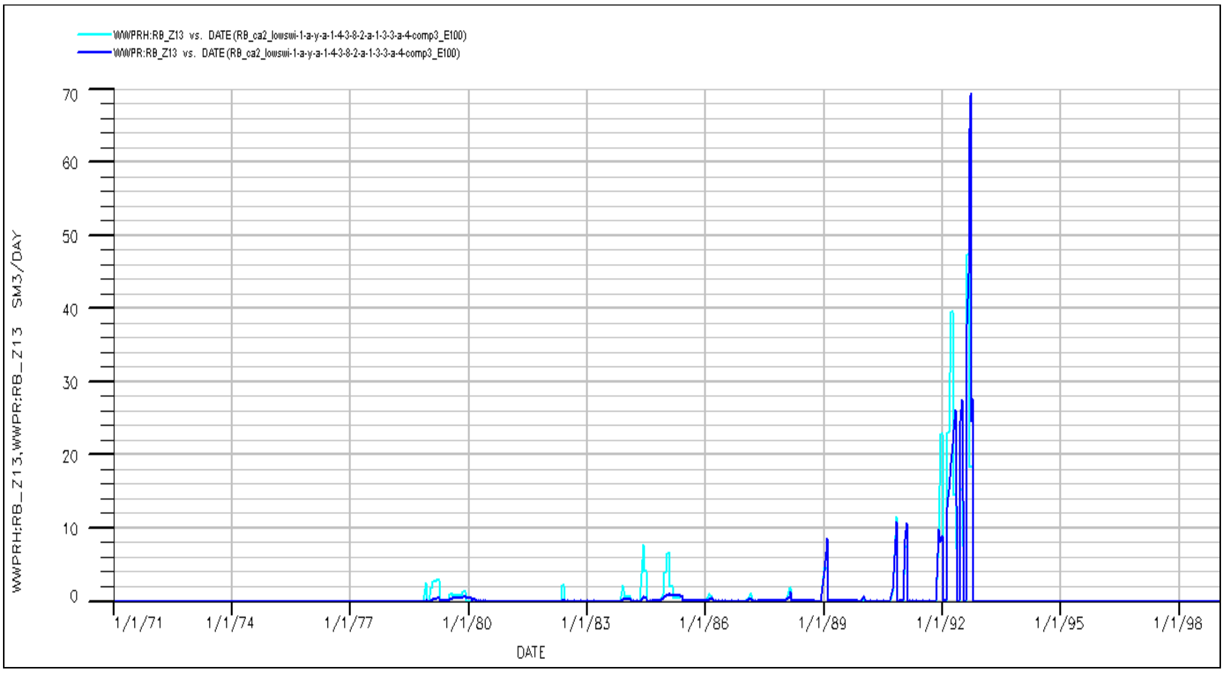

Fig. 3.9: RB_Z13-base case history match (observed water rate (light blue) vs. simulated (dark blue))

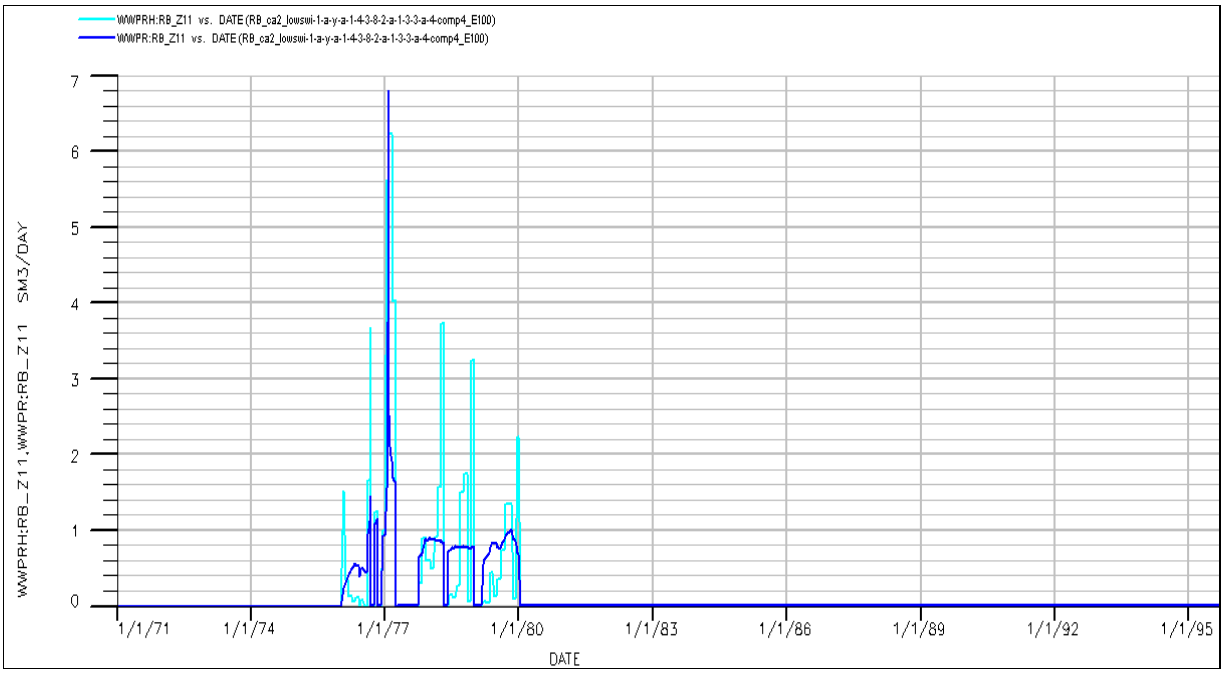

Fig. 3.10: RB_Z11-base case history match (observed water rate (light blue) vs. simulated (dark blue))

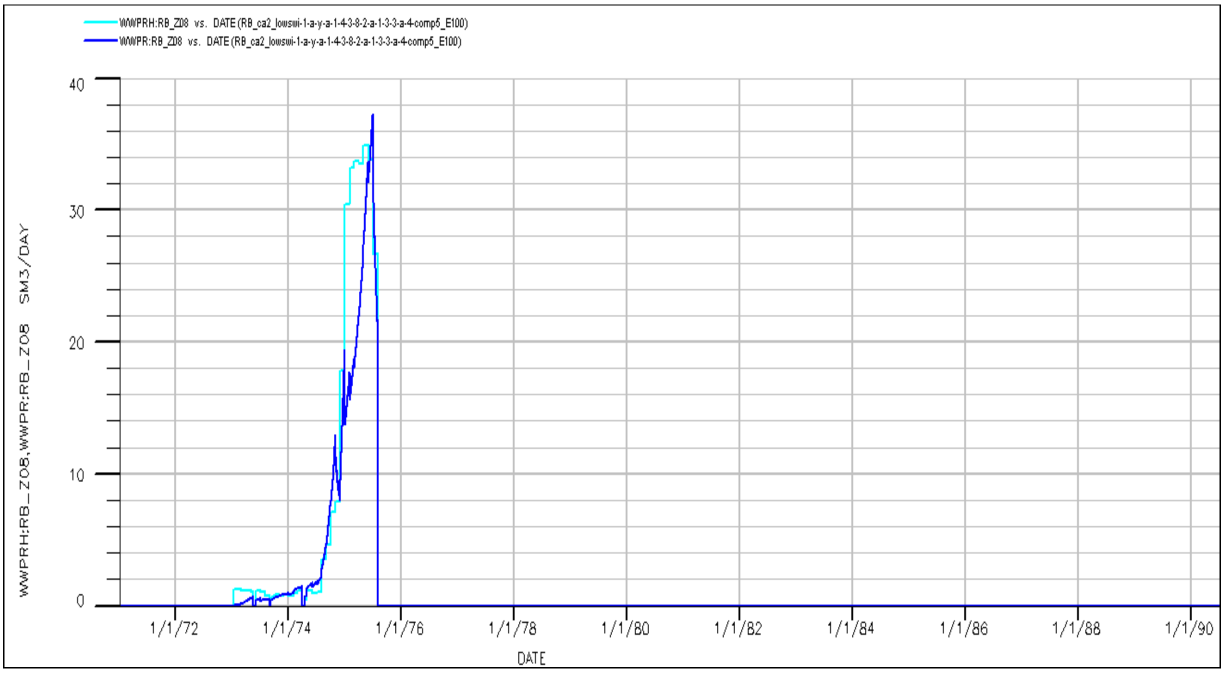

Fig. 3.11: RB_Z08-base case history match (observed water rate (light blue) vs. simulated (dark blue))

Nomenclature

In Chapter IV:

A = drainage area, ha (Hectares)
b = decline exponent
B_g = gas formation volume factor, m^3/ m^3
C_t = total compressibility, bar^{-1}
D_i = initial decline rate, day^{-1}
D = linear Non-Darcy flow coefficient, [m^3/day]-1
F_{CD} = fracture conductivity, mDarcy.m
G = specific gas gravity
h= formation thickness, m
k= permeability, mDarcy
kh = well flow capacity, mDarcy.m
P_i = initial pressure, bar
P_w= well flowing pressure, bar
P_{sc} = pressure at standard condition, bar
q = flow rate, m^3/day
q_i = initial flow rate, m^3/day
q_{Dd} = decline curve dimensionless flow rate
q_D = dimensionless flow rate
Q_{Dd} = decline curve dimensionless cumulative
Q_{DA} = normalized rate cumulative, [m^3/day]/ [bar^2/ mpa.s]
r_w = wellbore radius, m
r_e = effective wellbore radius, m
S = skin, dimensionless
S_w = water saturation
t = time, days
t_D = dimensionless time
t_{Dd} = decline curve dimensionless time
t_{cr} = the constant rate time, days
t_e = pseudo normalized time, days
T = temperature, °C
T_{sc}= temperature at standard condition, °C
w_f = fracture width, m
x_f = fracture half length, m

Z = z-factor, dimensionless

Symbols

ω = storativity ratio

λ = interporosity coefficient

μ = viscosity

Φ = porosity

Subscripts

m = matrix

f = fracture

D = dimensionless

o = oil

w = water

g = gas

r= reservoir

t = total